VNIVERSITAT DE VALÈNCIA

FACULTAT DE GEOGRAFIA I HISTÒRIA

DEPARTAMENT DE PREHISTÒRIA, ARQUEOLOGIA I HISTÒRIA ANTIGA

CHARACTERISATION AND PROVENANCE OF ARCHAEOLOGICAL LITHIC MATERIALS BY CHEMICAL METHODS

TESIS DOCTORAL

PROGRAMA DE DOCTORADO 3157: GEOGRAFÍA E HISTORIA DEL MEDITERRÁNEO DESDE LA PREHISTORIA A LA EDAD MODERNA

Autor: Mirco Ramacciotti

Directores: Oreto García Puchol, Agustín Pastor García, Gianni Gallello

Enero 2022

VNIVERSITAT ⅅ VALÈNCIA

FACULTAT DE GEOGRAFIA I HISTÒRIA

DEPARTAMENT DE PREHISTÒRIA, ARQUEOLOGIA I HISTÒRIA ANTIGA

CHARACTERISATION AND PROVENANCE OF ARCHAEOLOGICAL LITHIC MATERIALS BY CHEMICAL METHODS

TESIS DOCTORAL

PROGRAMA DE DOCTORADO 3157: GEOGRAFÍA E HISTORIA DEL MEDITERRÁNEO DESDE LA PREHISTORIA A LA EDAD MODERNA

Autor: Mirco Ramacciotti

Directores: Oreto García Puchol, Agustín Pastor García, Gianni Gallello

Enero 2022

Agradecimientos

Bueno, hemos llegado al final de este doctorado, así que ha llegado también el momento de los agradecimientos.

En primer lugar, como es apropiado, tengo que agradecer mis directores de tesis: Oreto García Puchol, Agustín Pastor García y, *last but not least*, Gianni Gallello, ya que sin su empuje inicial ni habría venido a Valencia para empezar un doctorado y sin su soporte constante nunca habría podido acabarlo. Os agradezco por haber aceptado ser mis guías en este camino y haberme permitido trabajar sobre casos de estudio interesantes gracias a los cuales he aprendido más de lo que habría podido esperar. Agradezco a todos los coautores de los artículos y a sus instituciones: Dep. de Arqueologia, Prehistoria i Historia Antiga, Dep. de Química Analítica, Institut Universitari de Cièncias dels Materials (Universitat de València), Museo Arqueológico de Sagunto, Dip. di Scienze della Terra (Università di Pisa), Dip. di Scienze Chimiche e Geologiche (Università di Cagliari). Aunque no aparezca en ninguno de los cinco artículos, tengo que agradecer a la profesora María Luisa Cervera Sanz, no tanto por liderar el proyecto gracias al cual estoy contratado - ¡esto ya sería suficiente! - si no por el apoyo humano que me ha dado en los últimos años. Por el mismo motivo agradezco también a los compañeros de camino en Burjassot: estudiantes de grado y master, doctorandos y postdoc todos; en particular, por la cercanía de este último periodo: Andrea DG, Daniel, Ginevra, Kevin y Roberto. Un agradecimiento a los profesores e investigadores del Dep. de Química Analítica con los cuales he compartido los laboratorios en estos años (Angel Morales, Daniel Gallart, Francesc Esteve, Salvador Garrigues, Sergio Armenta, Miguel de la Guardia, Antonio Doménech) y a los compañeros y profesores del Dep. de Prehistòria de las excavaciones de Cueva de la Cocina y Cova de les Cendres (Alfredo, Pilar, Mariel, Joaquín, Salvador, Agustín Diez, Joan Bernabeu).

Un ringraziamento particolare va alla mia compagna Isabella che, nonostante la distanza, continua ad appoggiarmi e a starmi vicina.

Índice

I

Anexos

Ramacciotti et al. (2019a). Chert nucleus and cortex characterization for archaeological provenance study tested in the Prebaetic system region (Valencian community, Spain)

Ramacciotti et al. (2022). Moving to the land: First archaeometric study of chert procurement at Cueva de la Cocina (Eastern Iberia)

Ramacciotti et al (2018). Chronological classification of ancient mortars employing spectroscopy and spectrometry techniques: Sagunto (Valencia, Spain) Case

Ramacciotti et al. (2019b). Chemical and mineralogical analyses on stones from Sagunto Castle (Spain)

Ramacciotti et al. (2020a). An innovative multi-analytical approach based on spectroscopic and electrochemical techniques to study a complex Roman amphorae collection

1. Introducción

1.1. El papel de la química en el estudio de materiales arqueológicos de tipo lítico

Esta tesis de doctorado se ha centrado en la aplicación de metodologías propias de la química con el objetivo de caracterizar materiales líticos, sílex y sillares, o similares a rocas, morteros y cerámicas, y responder a cuestiones arqueológicas concretas sobre aprovisionamiento, circulación y uso. La línea de investigación desarrollada se enmarca en el ámbito de la ciencia arqueológica o, como suele llamarse también, de la "arqueometría" (Wells, 2014), la disciplina que desarrolla y aplica técnicas y conceptos de las ciencias naturales y de la ingeniería para responder a preguntas de interés arqueológico (Martinón-Torres y Killick, 2015).

Los datos obtenidos a través de estas técnicas permiten en muchos casos clarificar diferentes aspectos de la cadena operatoria establecida para abordar el análisis de los artefactos arqueológicos, incluyendo el abastecimiento de las materias primas, la tecnología de producción, la circulación de los mismos y su uso (Tite, 1991). El análisis de la información resulta por tanto de gran interés para investigar cuestiones como, por ejemplo, la movilidad y la relación de los grupos humanos con su entorno, interacciones e intercambios/comercio, división del trabajo y organización social.

El desarrollo de esta tesis doctoral incide en esta línea de investigación e intenta aportar una contribución a la ciencia arqueológica desde el punto de vista metodológico, mediante el desarrollo y optimización de protocolos metodológicos específicos sobre varios tipos de materiales. Para ello se han testado potencialidades y limitaciones de diferentes instrumentaciones y enfoques, confrontando los datos obtenidos por técnicas diversas sobre los mismos materiales, y analizando como estos datos se comportan, o si pueden complementarse para apoyar explicaciones más precisas y robustas. Este propósito resulta particularmente evidente en el trabajo llevado a cabo sobre la caracterización de afloramiento naturales de sílex del valle del Serpis (Ramacciotti et al., 2019a), y sobre el conjunto de ánforas del Museo Arqueológico de Sagunto (Ramacciotti et al., 2020a). En el primer caso el objetivo de la investigación ha sido comprobar la efectividad del empleo de determinados marcadores elementales para diferenciar entre afloramientos y observar problemáticas relativas al análisis sobre diferentes partes de la roca distinguidas macroscópicamente y las posibles

implicaciones en el análisis multielemental. En el segundo caso se propone una aproximación multianalítica para el estudio de cerámicas arqueológicas con el objetivo de discriminar ánforas de diferentes procedencias. De otro lado, aunque una contribución metodológica a la ciencia arqueológica sea en sí mismo también una contribución a la arqueología, que adquiere nuevos métodos de investigación o permite refinar aquellos utilizados, esta tesis trata de incidir también en un enfoque más propiamente arqueológico. En este sentido, se han utilizado por primera vez resultados analíticos en morteros[1] y sillares de roca carbonatada del Castillo de Sagunto (Sagunto, Valencia) y de sus alrededores, en el análisis de edificios que presentan complejas historias constructivas desde la época romano-republicana a la modernidad. El objetivo reside en aclarar cuestiones abiertas relacionadas con las fases constructivas y la procedencia de los materiales (Ramacciotti et al., 2018; 2019b). Finalmente, se ha procedido a la caracterización de potenciales materias primas silíceas empleadas en la manufactura de la industria lítica del yacimiento de Cueva de la Cocina (Dos Aguas, Valencia), cuya secuencia arqueológica remite a niveles del Mesolítico y del Neolítico (Ramacciotti et al., 2022).

El trabajo llevado a cabo se ha centrado en la aplicación de técnicas espectroscópicas sobre muestras de materiales geológicos y arqueológicos. La espectroscopía estudia la radiación electromagnética (de la cual la luz visible es una parte) y su interacción con la materia (Kakkar, 2015). Las técnicas de espectroscopía utilizan para la caracterización de las muestras las radiaciones emitidas, dispersadas y absorbidas por los átomos y por las moléculas mientras experimentan transiciones de estado energético (Stuart, 2007). En arqueología se emplean diferentes técnicas de espectroscopía atómica para determinar la composición de una muestra, desde el punto de vista de la estructura electrónica de los átomos, frecuentemente para obtener datos semicuantitativos o cuantitativos sobre el contenido elemental. Las técnicas de espectroscopía molecular son especialmente útiles para determinar las estructuras químicas presentes en un material.

---

[1] En cuanto a los morteros, hay que destacar que un primer trabajo analítico sobre las estructuras del Castillo de Sagunto, en el cual participó el autor de esta tesis, se había publicado previamente (Gallello et al., 2017).

Por lo que concierne al análisis elemental, las técnicas espectroscópicas se han utilizado de manera rutinaria desde los años 50 (Pollard y Heron, 2008). La espectroscopía de emisión óptica (OES) fue una técnica de referencia para el análisis de cerámica, metal y materiales líticos durante tres décadas. Se basa en el análisis de la luz emitida por una muestra pulverizada que se volatiliza a través de una chispa eléctrica, ya que cada elemento emite radiaciones características y cuyas intensidades están relacionadas con su cantidad. La OES fue progresivamente remplazada por la absorción atómica[2] (AAS) y, en los años 80, por la espectroscopía de emisión atómica con plasma acoplado inductivamente (ICP-OES). La ICP-OES permitió llevar a cabo análisis multielementales con límites de detección más bajos que la OES de chispa eléctrica (y en algunos casos también que la AAS[3]), gracias al empleo de una antorcha que puede mantener un plasma de argón a temperaturas de aproximadamente 8000 K y a otros avances técnicos.

Las técnicas basadas en rayos X se utilizan también de forma amplia, especialmente la espectroscopía de fluorescencia de rayos X por energía dispersiva[4] (ED-XRF), basado en la emisión de la radiación emitida por átomos irradiados con rayos X, cuyo empleo resulta rutinario para la determinación de elementos mayoritarios (Pollard et al., 2007). Esta técnica se ha empleado desde los años 60 en prácticamente todos los tipos de materiales arqueológicos inorgánicos (Musílek et al., 2012), teniendo la ventaja de rápida y económica comparada con otras, y no destructiva. También tiene algunas limitaciones relacionadas con los límites de detección relativamente elevados,

---

[2] En este caso, la medida está basada en la cantidad de radiación absorbida por una muestra irradiada por una lámpara de cátodo hueco que emite una luz de longitud de onda característica para cada analito. La muestra, previamente digerida por ataque ácido y en disolución liquida, es aspirada en una llama.

[3] El ICP-OES o la AAS necesitan una muestra en disolución liquida que se puede obtener digiriendo por ácido un sólido previamente pulverizado y homogenizado. La mayor desventaja de la AAS comparada con la ICP-OES es que la primera es más lenta, ya que cada elemento necesita de una medida por separado y que requiere una lampara específica para cada elemento.

[4] La espectroscopía de fluorescencia de rayos X de dispersión por longitud de onda (WD-XRF) es menos utilizada en arqueometría porque es menos económica, y porque necesita más tiempo de medida (Pollard y Heron, 2008).

especialmente para los elementos ligeros[5], y dificultad para la caracterización de muestras heterogéneas o meteorizadas, ya que consigue obtener solo datos superficiales[6] (Musílek et al., 2012; Shackley, 2011).

En el análisis multielemental tienen especial relevancia también la activación neutrónica (NAA) y la espectrometría de masas con plasma acoplado inductivamente (ICP-MS), dos técnicas muy efectivas para la determinación de elementos trazas. El NAA ha sido un método de referencia durante muchos años desde los años 50, debido al tratamiento sencillo de muestras y estándares, por ser una técnica no destructiva, su alta precisión, y a la comparabilidad de resultados obtenidos en diferentes laboratorios (Speakman y Glascock, 2007). El análisis por NAA consiste en la irradiación de la muestra con neutrones para convertir sus elementos en isótopos radioactivos y, en consecuencia, poder medir las concentraciones mediante la emisión de radiaciones de desintegración (Pollard y Heron, 2008). La ICP-MS reemplazó el análisis por NAA como técnica rutinaria ya que no necesita de grandes fuentes de neutrones y tiene niveles de efectividad similares (Pollard et al., 2007). La aplicación de esta técnica en materiales arqueológicos se realizó por primera vez en los años 80 y su uso aumentó en las décadas siguientes (Dussubieux, 2020).

La espectroscopía de infrarrojo (IR) y la de Raman, en cambio, son dos técnicas que permiten investigar las estructuras moleculares en restos arqueológicos orgánicos e inorgánicos. La radiación de IR (de 14285 a 100 cm^{-1}) corresponde esencialmente al calor y se origina por transiciones de baja energía entre estados moleculares acompañadas por vibraciones de estiramiento y de flexión de los enlaces (Pollard y Heron, 2008). En los espectros de IR, las diversas bandas corresponden a modos vibracionales característicos de grupos funcionales o aniones en moléculas o minerales identificados por transmisión de una radiación IR a través de una muestra o por reflexión[7]. La región del IR medio (de 4000 a 400 cm^{-1}) ha sido la más usada en

---

[5] Además, los elementos más ligeros del Na no se pueden detectar ni siquiera con los modelos mejores de espectrómetro ED-XRF.

[6] De hecho, con muestras sacrificables, para hacer análisis representativos se utilizan frecuentemente pastillas o perlas de fusión obtenida a partir de muestras previamente pulverizadas y homogenizadas.

[7] La medida por trasmisión necesita de un tratamiento previo de la muestra que prevé su destrucción, mientras que la por reflexión puede ser efectuada también sobre una muestra íntegra.

aplicaciones arqueológicas, aunque hay trabajos que emplean también el IR cercano (de 14285 a 4000 cm^{-1}) y el lejano (de 400 a 100 cm^{-1}). Se ha utilizado para diferentes alcances como, por ejemplo, el análisis de estructuras en rocas, cerámicas y morteros, la detección de alteraciones térmicas en huesos incinerados o quemados, el proceso de diagénesis de los mismos, y el estudio de residuos orgánicos (Monnier, 2018). En la espectroscopía Raman, en cambio, se irradia la muestra empleando un láser y se identifican los compuestos presentes por medio de las radiaciones dispersas de longitudes de onda diferentes a las de la radiación incidente (Pollard et al., 2007). Como en el caso de la de IR, el análisis por espectroscopía Raman se emplea para la identificación de compuestos tanto orgánicos como inorgánicos, habiéndose aplicado con particular éxito en la identificación de pigmentos y aglutinantes en pinturas (Caravá et al., 2020; Bersani y Lottici, 2016; Bersani y Madariaga, 2012). Ambas técnicas permiten una caracterización rápida y potencialmente no destructiva de las muestras, y son además complementarias ya que, en algunos casos, modos vibracionales inactivos o poco intensos por IR están activos en Raman y viceversa (Pollard et al., 2007). Para concluir, hay que hacer una mención de la difractometría de rayos X (XRD), una técnica clásica de la química arqueológica. En este caso se irradia una muestra, normalmente pulverizada y homogenizada con un haz de rayos X monocromático y los diferentes ángulos de difracción permiten reconocer las estructuras (Pollard et al., 2007).

En los últimos años se ha ido imponiendo el uso de instrumentación portátil y el desarrollo de métodos de estudio no destructivos o microdestructivos. De hecho, la portabilidad de los equipos permite efectuar análisis en campo o en museos, evitando el transporte al laboratorio de las muestras. Además, en muchos casos las piezas arqueológicas son únicas y no pueden ser sacrificadas para los análisis. Muchos trabajos prevén la medida directa a través de espectrómetros Raman e IR portátiles (Arrizabalaga et al., 2014; Rousaki y Vandenabeele, 2021), así como el empleo de espectroscopía de plasma inducido por láser (LIBS; Botto et al., 2019), o de la ablación laser (LA) para el muestreo[8] en los análisis de ICP-OES y, sobre todo, ICP-MS

---

[8] En este sentido, hay que apuntar que se han desarrollado muestreadores basados en ablación láser para el muestreo directo en campo (Glaus et al., 2012).

(Fricker y Günther, 2016). Sin embargo, los equipos que en gran medida han revolucionado la ciencia arqueológica son seguramente los modelos portátiles de espectrómetro ED-XRF (pED-XRF) que se han ido difundiendo no solo en los departamentos de ciencias naturales, sino también en los de arqueología para casos de estudios diferentes (Frahm y Doonan, 2013).

Uno de los hilos conductores de esta tesis es el rol central del análisis multielemental. Para obtener las concentraciones de los elementos mayoritarios, minoritarios y traza, incluidas las tierras raras, se han utilizado en todos los estudios la espectroscopía ED-XRF[9] y el ICP-MS (Ramacciotti et al., 2018; 2019a; 2019b, 2020a; 2022), y en Ramacciotti et al., 2019a también la ICP-OES. Sin embargo, la gama de técnicas empleadas no se reduce a las citadas. Para caracterizar estructuras se ha recurrido a la espectroscopía de IR cercano de transformada de Fourier (FT-NIR; Ramacciotti et al., 2020a), la cual, como ya se ha indicado, en arqueología no se ha empleado de modo tan amplio como el IR medio. Además, se han utilizado también datos obtenidos por XRD (Ramacciotti et al., 2019b) y por voltamperometría de partículas inmovilizadas (VIMP; Ramacciotti et al., 2020a), una técnica propia de la electroquímica[10].

Un caso paradigmático de caracterización y estudio de procedencia de artefactos líticos es el de la obsidiana en el Mediterráneo. La obsidiana es una roca félsica de textura vidriosa empleada para la manufactura de herramientas. Desde los años 60, para caracterizar las fuentes de materia prima se han empleado las técnicas analíticas más variadas. En su discriminación se consideran particularmente eficaces los elementos traza como marcadores de procedencia, ya que tienen la capacidad de distinguir diferentes condiciones de formación de las rocas (Pollard y Heron, 2008; Tykot, 2021). Debido a los particulares procesos implicados en su formación, se trata de una roca localizada en un limitado número de afloramientos relativamente bien identificados (Pollard y Heron, 2008), a diferencia de lo que sucede por ejemplo con el sílex. Esto

---

[9] En casi todos los artículos se utilizó el pED-XRF del Departament de Química Analítica de la Universitat de València, mientras que en Ramacciotti et al. 2019b se utilizaron los resultados obtenidos por el espectrómetro ED-XRF de bancada del Departamento de Ciencias de la Tierra de la Universidad de Pisa en colaboración con el cual se llevó a cabo la investigación.

[10] Los análisis electroquímicos de VIMP fueron llevados a cabo por el equipo del Prof. Doménech-Carbó del Departament de Química Analítica de la Universitat de València.

hace que sea un marcador excelente para trazar interacciones entre diferentes asentamientos también a larga distancia (Terradas et al., 2014).

Más allá del análisis multielemental, en el trabajo desarrollado en esta tesis, la caracterización del contenido en elementos traza de las muestras tiene un rol central, sobre todo el empleo de los elementos de las tierras raras[11] (REE) como marcadores para discriminar materiales de diferente procedencia. Los REE son un grupo de elementos metálicos que comprende el lantano (La), los lantanoides o lantánidos (Ce, Pr, Nd, Pm[12], Sm, Eu, Gd, Tb, Dy, Ho, Er, Tm, Yb, Lu), y el escandio (Sc) y el itrio (Y). En algunos casos, se dividen en ligeros (LREE, de La a Nd), medios (MREE, de Sm a Dy) y pesados (HREE, de Ho a Lu incluyendo el Y; Voncken, 2016). Debido a las propiedades de estos elementos, sus concentraciones e índices de fraccionamiento[13] son marcadores muy efectivos de fenómenos geoquímicos relacionados con la formación de rocas y sedimentos (e.g.: Laveuf y Cornu, 2009; Murray, 1994; Sugahara et al., 2010; Tostevin et al., 2016). El empleo de estos elementos en arqueología es una de las líneas fundamentales de ArchaeChemis, la unidad de investigación de ciencia arqueológica de la Universidad de Valencia en la cual se ha realizado esta tesis. De hecho, la unidad está desarrollando y aplicando métodos basados en el uso de los REE para evaluar el impacto de la diagénesis en huesos (Gallello, 2014a; Gallello et al., 2013a; 2015), como marcadores de actividades antrópica en sedimentos arqueológicos (Gallello et al., 2013b; 2014b; 2019; 2020a; 2021), de procedencia en rocas ígneas (Gallello et al., 2016a; Orozco Köhler y Gallello, 2017) y para el estudio de morteros, ocres y cerámicas (Aura Tortosa et al., 2020; Gallello et al., 2017; Vega Maeso et al., 2020). La investigación llevada a cabo sigue esta trayectoria volviendo a testar métodos ya utilizados para otros casos de estudio (Ramacciotti et al., 2018). De este modo se ha ampliado su aplicación a otros tipos de materiales y para finalidades diferentes como la caracterización de sillares de rocas carbonatadas, incluyendo la

---

[11] Para una introducción general sobre el tema de los elementos de las tierras raras, sus propriedades físico-químicas, y su descubrimiento y empleos se puede ver Voncken (2016).

[12] Desde aquí, cuando se hable de REE no se considerará el prometio (Pm) ya que es un elemento inestable que no se encuentra en la corteza terrestre.

[13] "*Separation of a mixture in successive stages, each stage removing from the mixture some proportion of one of the substances, as by differential solubility in water-solvent mixtures*" (Licker, 2003: 159).

procedencia (Ramacciotti et al., 2019b), la discriminación de cerámicas de orígenes diversos y la identificación de piezas no identificables por su morfología (Ramacciotti et al., 2020a), o la caracterización de sílex de afloramientos diversos para identificar el origen de los artefactos y evaluar los efectos de la meteorización sobre los REE (Ramacciotti et al., 2019a; 2022).

1.2. Algunas cuestiones abiertas

Diferentes cuestiones metodológicas han sido discutidas y desarrolladas gracias a la colaboración y al trabajo interdisciplinar entre las comunidades de arqueólogos y de las ciencias naturales.

Desde el punto de vista técnico y metodológico, Killick (2015) señala un cierto descuido en cuanto a la calidad de los datos, sea por cuestiones conectadas con el control de la conservación de los materiales, sea por lo que respecta al protocolo de preparación de las muestras y de los análisis. A este respecto, en el desarrollo de nuestro trabajo y por lo que concierne a los materiales de construcción (Ramacciotti et al., 2018, 2019b) se evitó muestrear y analizar las zonas superficiales o evidentemente degradadas, dada su mayor exposición a fenómenos de meteorización y contaminaciones[14]. En cuanto a las ánforas (Ramacciotti et al., 2020a) se han evitado también las superficies que presentaban incrustaciones superficiales. Por lo que se refiere al sílex, como hemos comentado, Ramacciotti et al. (2019a) se han tenido en cuenta los posibles efectos de la meteorización en los niveles elementales de esta roca de forma que los resultados han contribuido a evaluar el protocolo para el estudio de muestras arqueológicas (Ramacciotti et al., 2022). Los protocolos analíticos de los trabajos reunidos en esta tesis presentan su optimización empleando muestras certificadas, cuando ha sido posible, o muestras de control para verificar la reproducibilidad de los resultados en las diferentes medidas. En algunos casos, como en la selección de la mayoría de los isótopos medidos por ICP-MS o la digestión de muestras de materiales como las rocas carbonatadas y los morteros, se sigue el camino trazado (Gallello, 2014a). Sin embargo, los métodos de digestión tuvieron que ser optimizados para matrices como sílex y cerámica.

---

[14] Aunque cuestiones de conservación de los monumentos limitaron los muestreos.

Una discusión aparte merece la aplicación del pED-XRF. La introducción masiva de estos espectrómetros no ha dejado de plantear cuestiones relativas a la calidad de los datos: el empleo del análisis cuantitativo es problemático debido a que los diferentes modelos ofrecen distintas calibraciones internas que limitan la reproducibilidad de los resultados y la comparabilidad de los datos entre laboratorios. Frahm (2013) cree que la coherencia de los resultados garantiza la fiabilidad de los datos y de las conclusiones que de estos se pueden sacar, por lo menos a nivel del estudio presentado y de los análisis efectuados por el mismo modelo de espectrómetro. Otros investigadores opinan en cambio que esta conclusión no es aceptable ya que la investigación es una empresa colectiva, y la reproducibilidad y contrastación de los resultados es esencial para el avance del conocimiento científico. De este modo ven problemático el empleo de este instrumento cuando no sea posible aplicar una calibración externa[15] (Killick, 2015; Speakman y Shackley, 2013). En esta tesis el pED-XRF tiene un rol central, sobre todo para la medida de las concentraciones de elementos mayoritarios, y se ha empleado en muestras previamente pulverizadas y homogenizadas. A lo largo del trabajo, para optimizar el método y verificar la fiabilidad y reproducibilidad de los resultados cuantitativos se emplearon muestras certificadas de referencia (CRM) y muestras de control de origen geológico tratadas de la misma forma que las muestras (i.e., pulverizadas y homogenizadas) y que tenían matrices similares.

En cuanto al tema del desarrollo de métodos destructivos, en esta tesis no hemos empleado técnicas que prevén la medida directa sobre la muestra intacta por motivos que se explicarán en el siguiente capítulo. Sin embargo, si entendemos la destructividad en un sentido más amplio, sí que hemos utilizado técnicas que permiten la reutilización de la muestra pulverizada (pED-XRF, XRD). Además, en el caso de

---

[15] La posibilidad de comparar resultados sería obviamente óptima, también para generar bases de datos a disposición de todos los científicos. Hay que añadir que, igual que se utilizan técnicas no cuantitativas o semicuantitativas de manera rutinaria, no se entiende porque no se podría utilizar de la misma manera la fluorescencia de rayos X, ya que las relaciones entre las concentraciones de las muestras proporcionadas normalmente respetan las reales y son en este sentido reproducibles, garantizando la coherencia interna en un estudio, como es anotado por Frahm (2013), y la robustez de los resultados y de las conclusiones. Sin embargo, no parece que esta controversia haya detenido de alguna manera el empleo de estos equipos.

las cerámicas (Ramacciotti et al., 2020a) y de los sillares de Sagunto (Ramacciotti et al., 2019b), el método de muestreo y el protocolo analítico llevados a cabo fueron calibrados para emplear una cantidad de muestra reducida y pueden ser considerados, en nuestra opinión, mínimamente invasivos.

Finalmente, hay que hacer una mención del tratamiento estadístico de los datos. Aunque se hayan utilizado aplicaciones quimiométricas que, a esta fecha, son relativamente comunes en los trabajos arqueométricos, la manera en la cual se han tratado los analitos discriminadores de procedencia, los REE en particular, muestra que estos elementos pueden ser procesados de manera diferente respeto a los modos tradicionales que no explotan totalmente su potencial informativo, como a través de diagramas de araña, de comparaciones por diagramas binarios o, también, procesándolos con grandes conjuntos de variables que pueden enmascarar su capacidad como marcadores[16].

1.3. Principios de las técnicas analíticas y estadísticas empleadas

1.3.1. Espectroscopía de fluorescencia de rayos X por energía dispersiva

El pED-XRF S1 Titan de Bruker fue empleado en todos los casos sobre muestras pulverizadas.

La técnica está basada en la medición de la radiación de fluorescencia emitida por una muestra irradiada por un haz de rayos X, una radiación electromagnética caracterizada por longitudes de onda entre 10^{-9} y 10^{-15} m. Un espectrómetro XRF está compuesto por tres partes fundamentales: una fuente de rayos X, un detector que convierte la radiación emitida en una señal electrónica y un procesador que convierte esta señal en una concentración elemental (Gutiérrez-Ginés y Ranz, 2010).

---

[16] Por ejemplo, estos tipos de procesado de datos de REE se pueden encontrar en los estudios de sílex de Olofsson y Rodushkin (2011) y de Chatzimpaloglou (2020), o en lo de morteros efectuado por Sanjurjo-Sánchez et al. (2010).
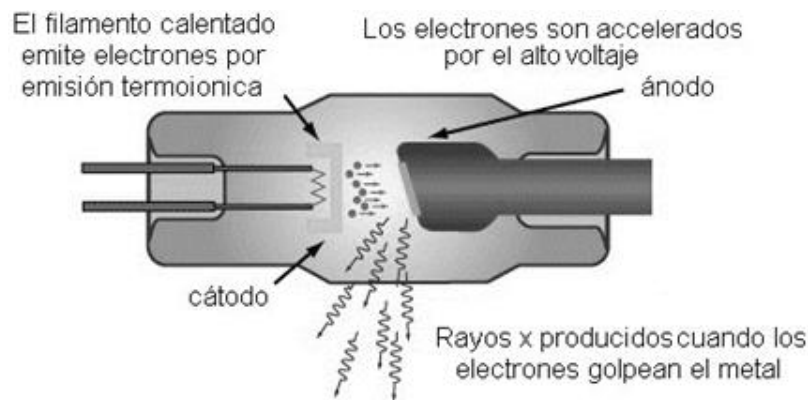
Fig. 1 - Esquema del funcionamiento del tubo de rayos X[17].

En el caso del espectrómetro S1 Titan, la fuente consiste en un tubo de rayos X. Este tubo tiene un filamento calentado como fuente de electrones y un ánodo enfriado de rodio (Rh). Los electrones son acelerados por un alto potencial positivo del cátodo hacia el ánodo que, debido a este bombardeo, emite rayos X (Fig. 1; Pollard et al., 2007). El principio fundamental de la espectroscopía XRF es que estos rayos X primarios pueden ionizar los átomos de la muestra sobre la cual impactan, expulsando electrones de los orbitales más internos que son reemplazados por electrones de los niveles energéticos superiores que en este salto emiten rayos X secundarios. Estas radiaciones tienen una energía igual a la diferencia entre la de los dos orbitales, y son características de cada átomo (Fig. 2).
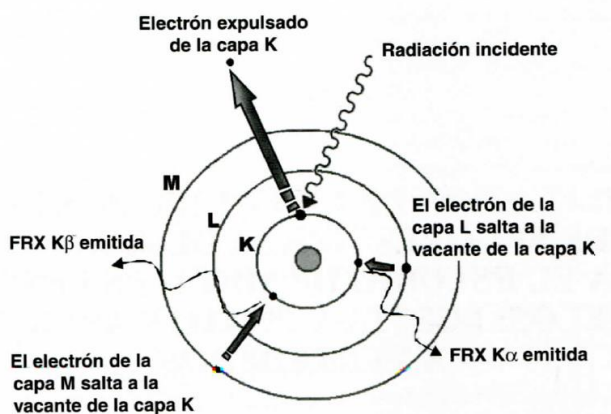
Fig. 2 - Esquema de la emisión de la radiación de fluorescencia en la espectroscopía XRF (de Gutiérrez-Ginés y Ranz, 2010).

---

[17] Imagen modificada de https://www.arpansa.gov.au/understanding-radiation/what-is-radiation/ionising-radiation/x-ray.

Los rayos X emitidos por la muestra son convertidos en impulsos eléctricos por un detector de deriva de silicio (SDD) que permite una discriminación cualitativa de los componentes de la radiación y cuantitativa desde el punto de vista de la intensidad. Los resultados de un análisis ED-XRF pueden ser resumidos en espectros: en las abscisas está el voltaje (keV), proporcional a la energía de la radiación, mientras que la intensidad del impulso está en las ordenadas. Como se puede por ejemplo observar en la Figura 3, el espectro de sílex tiene bandas poco intensas, debido a que su componente principal, el Si, se caracteriza por una radiación de fluorescencia relativamente débil y los otros elementos se encuentran a niveles muy bajos. El espectro de caliza está dominado por las bandas del Ca. La muestra de cerámica tiene un perfil elemental más variado. Para obtener resultados cuantitativos se pueden construir calibrados para diferentes matrices a través del empleo de muestras que tienen concentraciones conocidas de los diversos analitos y la identificación de las líneas más adecuadas para extraer las intensidades de la señal relativa a los elementos que se quiere medir. Como se ha indicado previamente, los espectrómetros pED-XRF tienen normalmente una calibración interna cuya calidad hay que evaluar con atención.
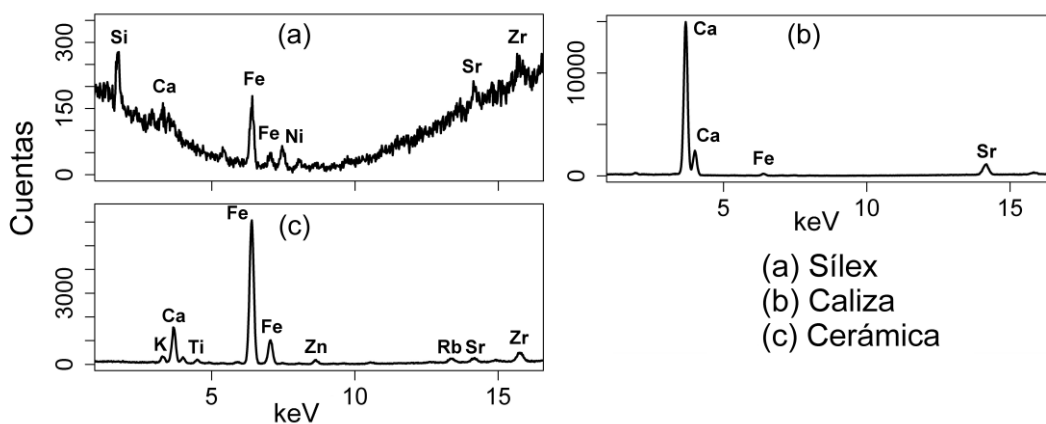
Fig. 3 - Espectros de pED-XRF de sílex (a), caliza (b) y cerámica (c).

1.3.2. Espectrometría de masas con plasma acoplado inductivamente (ICP-MS)

El ICP-MS fue utilizado en todos los estudios para la medida de las concentraciones de elementos traza, incluidos los elementos de las tierras raras (REE), debido a que sus concentraciones en la mayoría de los casos son inferiores a los límites de detección del pED-XRF. El espectrómetro empleado es un Elan DRCII de Perkin Elmer.

Informaciones detalladas sobre el funcionamiento de un ICP-MS se pueden encontrar, por ejemplo, en el manual de Thomas (2013). Resumiendo (Fig. 4), cada disolución es aspirada por una bomba peristáltica y llevada a una cámara de nebulización de cuarzo, donde es transformada en aerosol, y sucesivamente transportada a la antorcha por medio de un flujo continuo de argón. La antorcha está formada por tres tubos concéntricos de cuarzo y la extremidad opuesta al lugar de ingreso de la muestra está envuelta en un solenoide de cobre conectado a un generador de radiofrecuencias (RF). La potencia de las RF produce en el solenoide una corriente alternada que causa un campo electromagnético. Una chispa eléctrica aplicada al gas causa la perdida de electrones que son capturados y acelerados por el campo magnético, causando la perdida de otros electrones. De esta manera se forma un plasma de alta temperatura (6000 - 8000 K) de átomos de argón, iones de argón y electrones libres. El aerosol se ioniza gracias a este mismo proceso cuando llega a esta zona de la antorcha a través del tubo inyector. Debido a la diferencia de presión entre el plasma y el área interior del espectrómetro, la muestra ionizada pasa a la interfase, donde dos conos de platino recogen el haz, y seguidamente al área de vacío, producido por bombas turbomoleculares. Una serie de lentes iónicas aceleran y coliman el haz y descartan las especies neutras. Antes de llegar al detector, el flujo de iones tiene que pasar por un analizador de masas, en nuestro caso un sistema de cuadrupolo compuesto por cuatro varas metálicas que a través de una corriente directa y una corriente alternada de RF crea un campo magnético que permite el descarte de los iones caracterizados por una relación masa/carga diferente a la del analito. Las condiciones para esta selección cambian en el tiempo para dejar que lleguen en secuencia al detector solo los iones de cada isótopo seleccionado para medir.
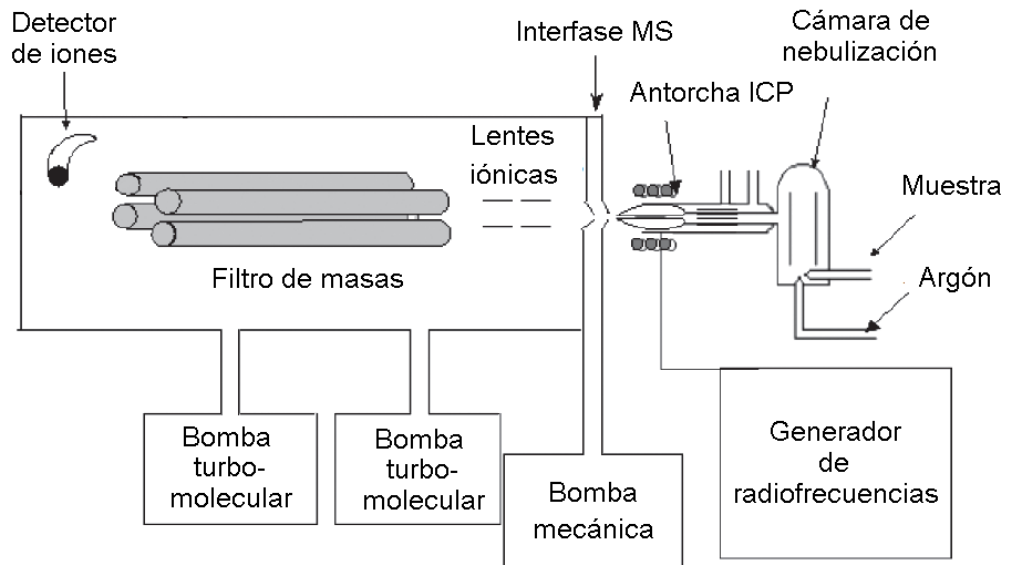
Fig. 4 - Esquema representativo de los componentes principales de un ICP-MS (imagen modificada de Thomas, 2013).

El análisis cuantitativo requiere analizar una serie de patrones, o sea disoluciones con contenido de ácidos similares a las muestras, y cantidades conocidas de los analitos en diferentes concentraciones. Para el control de la atenuación de la señal debida el efecto matriz, que puede variar según la composición de las muestras, es necesario también añadir un estándar interno a cada disolución, o sea una cantidad conocida de un cierto elemento que se supone presente en cantidad despreciable en las muestras, en nuestro caso el Rh. Finalmente, cada diez muestras fueron insertadas disoluciones estándares a fin de controlar la deriva instrumental.

1.3.3. Las otras técnicas analíticas

Aunque el ICP-MS y el pED-XRF hayan sido las técnicas más utilizadas a lo largo de los trabajos de esta tesis, como ya se ha mencionado, ocasionalmente se emplearon otras.

Para la medida de las concentraciones de Na, Mg y Al en las muestras de sílex del valle del Serpis (Ramacciotti et al., 2019a) se empleó un espectrómetro de emisión atómica con plasma acoplado inductivamente (ICP-OES) Optima 5300 DV de Perkin Elmer. La motivación que llevó a elegir esta técnica fue que estos elementos no se podían medir por pED-XRF por falta de sensibilidad del equipo, y se encuentran en

14

concentraciones muy altas para el ICP-MS y se quería evitar diluir demasiado las muestras. Así que el ICP-OES parecía la elección más adecuada dado que se podían emplear las disoluciones de partida usadas para preparar el ICP-MS. La manera de producir el plasma y de insertar la disolución en el sistema es similar a la del ICP-MS. Sin embargo, el espectrómetro mide la intensidad de la luz emitida por los átomos/iones excitados en el plasma a longitudes de ondas características. La luz emitida puede ser medida en sentido axial, o sea paralelamente respeto a la antorcha, o radial, o sea perpendicularmente (Fig. 5). Los analitos considerados fueron medidos por el sentido radial.
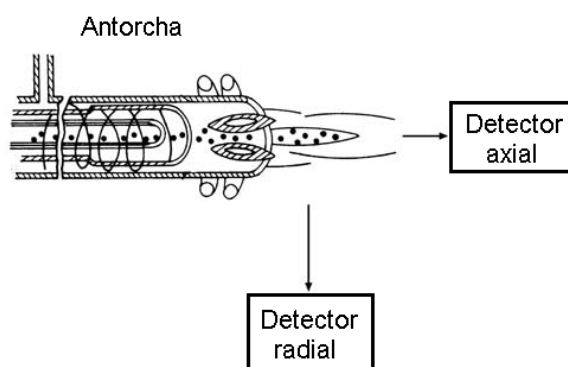
Fig. 5 - Esquema de antorcha y detectores del ICP-OES (imagen modificada de Pollard et al., 2007).

La última técnica usada es la espectroscopía de IR cercano (14285 - 4000 cm^{-1}) de trasformada de Fourier (FT-NIR). El espectrómetro utilizado es un Multipurpose Analyzer (MPA) de Bruker. Antes de las medidas, una pequeña cantidad de cada muestra pulverizada fue puesta en viales de vidrio (transparente en el NIR), colocados en estufa a 110 °C durante 48 h para que las muestras perdiesen el agua adsorbida. Las medidas fueron llevadas a cabo por reflectancia difusa. La radiación incidente en un cuerpo puede reflejarse de tres maneras (Fig. 6): la primera es la reflexión en la superficie de la muestra que tiene un ángulo igual al de incidencia de la radiación (reflexión de Fresnel o especular) y la segunda es la reflexión superficial que tiene un ángulo diferente debido a la disposición de las partículas. Ambas reflexiones no tienen información sobre la composición de la muestra y mientras que la primera puede ser excluida, la segunda puede ser atenuada reduciendo la muestra a un polvo muy fino y diluyéndola. El tercer tipo ocurre cuando una parte de la radiación será en cambio absorbida por lo menos por una partícula de la muestra y la radiación reflejada tendrá

bandas características dependientes de la radiación absorbida por estas partículas (reflexión difusa o de Kubelka-Munk; Mitchell, 1993).
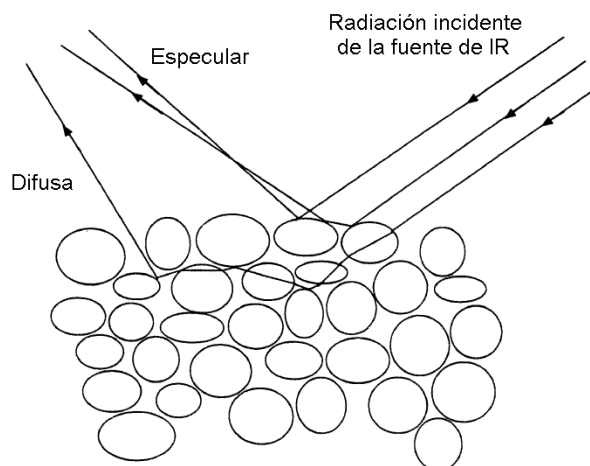
Fig. 6 - Tipos de radiación reflejada en la espectroscopía IR (imagen modificada de Mitchell, 1993).

De otro lado, necesitan por lo menos una mención las técnicas analíticas que no fueron empleadas personalmente por el autor de esta tesis.

Los análisis de difractometría de rayos X (XRD) de los sillares del Castillo de Sagunto (Ramacciotti et al., 2019b) fueron llevados a cabo sobre muestras pulverizadas. Esta técnica está basada en el hecho de que la radiación incidente en los cristales no se dispersa uniformemente en todas las direcciones y, a determinados ángulos tiene una mayor intensidad debido a interferencias constructivas entre los planos cristalográficos cercanos según la ley de Bragg. Los resultados pueden ser resumidos en espectros (difractogramas) que presentan picos en ángulos característicos para los diferentes minerales y cuya anchura depende también de la cristalinidad de los mismos (Stanjek y Häusler, 2004).

Para el análisis electroquímico en las ánforas (Ramacciotti et al., 2020a) fue empleado un potenciostato CH I660C de Cambria Scientific. La técnica en cuestión es la voltamperometría de micropartículas inmovilizadas (VIMP) en la cual una mínima cantidad de muestra se transfiere por abrasión en un electrodo inerte que se sumerge en un electrolito para registrar la respuesta voltamperométrica, que corresponde a reducciones y oxidaciones características del material sólido (Doménech-Carbó et al. 2009).

1.3.4. Análisis de datos

El análisis de los datos por técnicas de estadística multivariada fue llevado a cabo empleando dos *softwares* diferentes. En los primeros trabajos (Ramacciotti et al., 2018; 2019a; 2019b) se empleó la PLS_Toolbox de Eigenvector, un paquete con una interfaz muy intuitiva que automatiza unos procedimientos para efectuar el análisis quimiométrico y su visualización a través de MATLAB (MathWorks; Wise et al., 2006). Sin embargo, en los trabajos más recientes (Ramacciotti et al., 2020a; 2022) se ha utilizado R (R Core Team, 2020) que es más versátil, comparado con la *toolbox* citada, y tiene un ambiente de programación más abierto. Además, es un *software* libre, hay muchos paquetes con rutinas automatizadas y disponibles gratuitamente en red, y numerosos recursos para el aprendizaje, incluyendo una comunidad de usuarios muy activa.

En general, a lo largo de los artículos de la tesis se ha utilizado de forma constante el análisis de los componentes principales (PCA). Esta técnica de aprendizaje no supervisado se utiliza frecuentemente para el análisis estadístico exploratorio en los estudios arqueométricos y permite una reducción de la dimensionalidad a través del empleo de nuevas variables llamadas componentes principales (PC) que son combinaciones lineales de las variables originarias. El primer PC es la combinación lineal de las variables que explica la mayor variancia en el conjunto de datos (i.e. la recta que minimiza los residuales), mientras que el segundo PC es la combinación lineal que explica la mayor variancia entre las que no están correlacionadas con el primero[18] y así sucesivamente. En muchos casos, empleando unos de estos PC se pueden resumir las características fundamentales de conjuntos de datos con un gran número de variables como las de los resultados del análisis multielemental o de espectroscopía de IR haciéndolas más interpretables y visuales a través de diagramas de puntuaciones (James et al., 2013). Antes de llevar a cabo el PCA, los datos de análisis multielemental fueron estandarizados, o sea se emplearon las unidades tipificadas, para eliminar las diferencias debida a la presencia de diversos ordenes de magnitud, mientras que los de FT-NIR fueron solo centrados en el promedio para

---

[18] Así que el plano basado en los dos primeros PC es el más cercano a todas las observaciones y así sucesivamente añadiendo dimensiones o sea PC.

evitar que el ruido tuviese demasiado peso en el modelo. Además de esto, los datos de absorbancia entre 7350 and 4000 cm^{-1} fueron previamente procesados por el filtro Savitzky-Golay que suaviza la señal a través de una regresión polinomial (orden: 2; ventana: 31 puntos) y calcula sucesivamente la derivada (orden: 2), para quitar las líneas de bases y resaltar algunos aspectos como la presencia de características enmascaradas por las bandas principales (Rinnan et al., 2009). El PCA fue usado principalmente como técnica de exploración de los datos, para observar si había dimensiones en el espacio multivariado en las cuales se pudiesen discriminar muestras de diferentes clases y que variables eran responsables de las diferencias entre los grupos. En un sentido similar, se empleó para estimar las ventajas que habrían podido darse entre el empleo de todos los elementos y la selección de elementos marcadores, en particular los REE, en el momento de discriminar entre grupos. En el caso del sílex del Serpis (Ramacciotti et al., 2019a) se empleó también el análisis de grupos (o *cluster*) jerárquico para identificar las posibles aglomeraciones de muestras basado en parámetros de fraccionamiento de los REE. El algoritmo de *clustering* calcula en primer lugar la distancia (en nuestro caso la euclídea) entre cada observación, consideradas en principio como si cada una fuese un grupo distinguido, y asocia las dos más cercanas; en un segundo paso recalcula las distancias y asocia los otros dos *cluster* más cercanos y así sucesivamente. Para calcular la distancia entre grupos con más de una observación hay diferentes métodos, en nuestro caso se empleó uno de los clásicos, el de encadenamiento completo (o vecinos más lejanos) que utiliza la distancia máxima entre los diferentes elementos de dos grupos (James et al., 2013).

En el artículo sobre los morteros de Sagunto (Ramacciotti et al., 2018) y en el del sílex de Cueva de la Cocina (Ramacciotti et al., 2022) se usaron también dos técnicas clasificatorias diferentes o sea el análisis discriminante de mínimos cuadrados parciales (PLS-DA) y el análisis discriminante cuadrático (QDA). Tanto el PLS-DA como el QDA son técnicas de aprendizaje supervisado en las cuales se utiliza un *training set* compuesto de observaciones clasificadas *a priori* para encontrar los limites más eficientes para separar esas clases en el espacio multivariado y, sucesivamente, clasificar observaciones no identificadas. El PLS-DA puede ser considerado como una versión supervisada del PCA en el cual la computación de las nuevas dimensiones (variables latentes, LV) busca el mejor hiperplano de separación, que tiene en cuenta

también la clasificación de las observaciones del *training set* (Ruiz-Perez et al., 2020; Wise et al., 2006). Esta técnica fue utilizada para clasificar morteros de época Islámica y morteros de época romana. El QDA encuentra en cambio una hipersuperficie cuadrática discriminante entre las clases y permite computar la probabilidad de pertenencia a estas de observaciones no clasificadas; esta técnica no tiene entre las asunciones la de trabajar con clases que tengan matrices de covariancia iguales como en el DA lineal, siendo además más robusta en caso de distribuciones no normales de los datos (Finch y Schneider, 2006; James et al., 2013). Esta técnica se utilizó para evaluar la posible procedencia de los artefactos de Cueva de la Cocina entre diferentes afloramientos. Para evitar que las variables tuviesen demasiada colinealidad, se emplearon los componentes principales para llevar a cabo el QDA. En ambos los caso, las variables originales fueron los REE, debido a la capacidad observada previamente en los PCA de marcar las diferencias entre las clases consideradas. Para evaluar los modelos, y elegir el número de LV y PC sobre los cuales llevar a cabo el QDA, se utilizó la validación cruzada dejando uno fuera (*leave-one-out*).

2. Materiales y métodos

Durante estos años de tesis nos hemos enfrentado con materiales y problemáticas diferentes. A este respecto, el trabajo se ha centrado en el desarrollo o perfeccionamiento de enfoques metodológicos para estudiar artefactos tallados en sílex, materiales de construcción (morteros y sillares de roca carbonatada), y ánforas antiguas, tratando de solucionar a través de métodos propios de la química analítica cuestiones arqueológicas relacionadas con la identificación de materias primas, la discriminación de materiales diferentes para averiguar la presencia de fases constructivas en mamposterías, y la clasificación de fragmentos cerámicos no determinados tipológicamente por análisis morfológicos.

A lo largo de este capítulo se ofrecerá una introducción a los materiales objeto de estudio y se indicarán el cómo y por qué se han desarrollado los trabajos[19], y cuál es su contribución a nuestro campo de estudio.

---

[19] E.g.: ¿cuál es la cuestión?, ¿cómo se plantearon el muestreo y el protocolo analítico, y por qué?, ¿cómo se utilizaron los datos arqueométricos?

2.1. El sílex: entre desarrollo metodológico y arqueología

2.1.1. Qué es el sílex y porque lo estudiamos

El sílex (Fig. 7), también conocido como pedernal[20], es una roca sedimentaria compuesta principalmente de cuarzo y otros polimorfos del dióxido de silicio (SiO_2) en forma cripto- y microcristalina que en la mayoría de los casos superan el 90% de la masa total. Se encuentra en forma de nódulos (Fig. 7a) o estratificaciones en niveles sedimentarios de rocas carbonatadas de origen tanto lacustre como pelágica, y su ocurrencia se debe a sucesivas precipitaciones de SiO_2, en muchos casos de origen biogénico y causadas por variaciones locales de pH, desde minerales metaestables como el ópalo, a estructuras más estables (Sen, 2014).
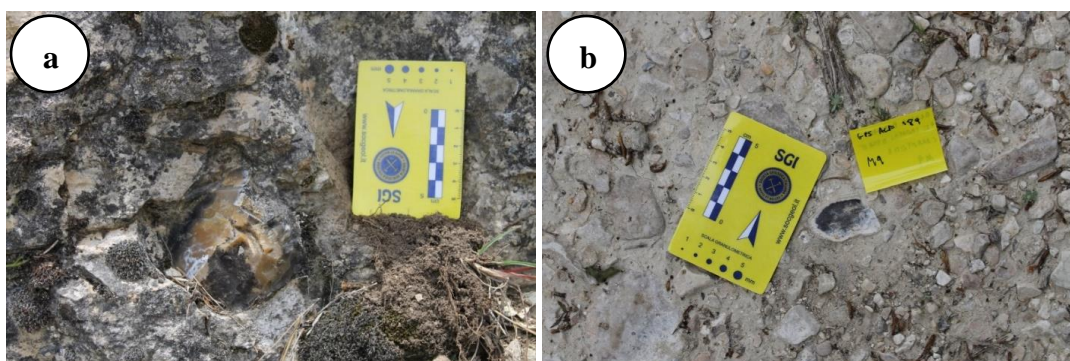
Fig. 7 - Nódulo de sílex encajado en un nivel de caliza (a, Font del Barxell) y fragmento de sílex en depósito coluvial (b, Barranc de les Coves) (Alcoy, Alicante, España).

Por lo que concierne al aspecto arqueológico, hay que destacar que el sílex fue por varios motivos una de las rocas más empleadas, sobre todo en la Prehistoria, para la producción de herramientas. En primer lugar, al contrario de rocas como la obsidiana, es relativamente frecuente en las formaciones sedimentarias; debido a su composición, al ser una roca de grano fino, bastante homogénea y caracterizada por fractura concoidea, el sílex reúne buenas condiciones para la talla y es al mismo tiempo una roca tenaz y dura, por lo que se trata de un material muy versátil para la producción de instrumentos de diferentes tamaños y funciones (Luedtke, 1992).

---

[20] En la literatura arqueológica de idioma inglés se emplean prevalentemente "*chert*" y "*flint*", aunque *chert* se está afirmando cada vez más como término científico (Herz, 2001).

El estudio de la industria lítica puede ser abordado desde diferentes puntos de vistas. Los arqueólogos se enfrentan desde hace décadas a cuestiones diversas a propósito de la tecnología de manufactura, la fabricación y la función de los artefactos líticos con implicaciones sobre las actividades llevadas a cabo en los asentamientos y las modalidades y las fases de ocupación de los mismos, así como sobre aspectos relacionados con las capacidades cognitivas, las dinámicas ecológico-adaptativas, y los procesos de trasmisión y de evolución cultural (Clarkson, 2008; Mahaney, 2014; Odell, 2000; 2001; 2004; Shennan, 2020). Dos de los trabajos de esta tesis conciernen a un tema clásico relacionado con los artefactos líticos: el abastecimiento de materia prima, incluyendo cuestiones metodológicas acerca del empleo de las técnicas analíticas para llevar a cabo estudios de procedencia.

La identificación del origen de las fuentes de aprovisionamiento de materia prima aporta información sobre las dinámicas socio-ecológicas de las poblaciones prehistóricas relacionadas con la movilidad de los grupos humanos, y las modalidades de explotación y empleo de estos recursos (Odell, 2000; Tarriño-Vinagre y Terradas, 2013). La presencia de rocas procedentes de territorios lejanos puede ser marcador de patrones de movilidad estacionales, largos desplazamientos poblacionales, de contactos e intercambios entre grupos de diferentes áreas, y pueden ser evidencia del rol de un asentamiento en un contexto territorial más amplio (e.g.: Boulanger et al., 2015; Hess y Riede, 2020; Landry et al., 2018; Milne et al., 2009; O'Leary et al., 2017; Speer, 2014; Terradas et al., 2012). Un enfoque de tipo diacrónico sobre el abastecimiento de sílex resulta también de interés. Por ejemplo, diferentes trabajos han señalado estrategias de abastecimiento coincidentes con la neolitización dirigidas a la explotación de materia prima de mejor calidad (Parow-Souchon y Purschwitz, 2020; Robb y Farr, 2008). En algunos casos, la intensidad de la explotación y la difusión sobre amplias áreas de materiales de particular calidad como el sílex "chocolate" polaco (Werra y Kerneder-Gubała, 2021) o el *silex blond* provenzal (Francia; Binder, 2000; Borrell et al., 2019) sugiere la existencia de redes de contactos muy desarrolladas y de dinámicas socio-económicas complejas.

Los estudios de procedencia más tradicionales se han basado en una caracterización de los artefactos desde el punto de vista macroscópico, es decir observando características como el color, la translucidez, la textura y el tamaño de grano, la

presencia de pátina o córtex y sus características, y de carbonataciones u oxidaciones superficiales. En algunos casos se han apoyado también en la microscopía óptica para identificar la presencia de impurezas, de fósiles, y mediante la confrontación de estas cualidades con las del sílex procedente de los afloramientos naturales reconocidos (Delluniversità, 2019). Un enfoque de este tipo sigue siendo muy empleado en arqueología ya que permite llevar a cabo el estudio de grandes cantidades de muestras rápidamente, de manera económica y no destructiva, y puede ser un primer paso que en muchos casos permite una identificación de los tipos de sílex presentes en un sitio arqueológico, información esencial para abordar una investigación (Bustillo et al., 2009; Machado et al., 2017; McElrath y Emerson, 2000; Milne et al., 2009). Basarse solo en estos datos, que dependen también de la sensibilidad y de la experiencia subjetiva del investigador, puede no ser suficiente[21], ya que a menudo el mismo afloramiento presenta una marcada variabilidad a nivel macroscópico. De este modo, resulta difícil encontrar características determinantes para diferenciarlo de otros y, de la misma manera, no es raro que rocas de afloramientos o también formaciones distintas parezcan idénticas. Diferentes investigadores han señalado como este enfoque resulta frecuentemente inadecuado (e.g.: Chatzimpaloglou, 2020; Hess, 1996; Luedtke, 1993; Newlander y Lin, 2017; Sánchez de la Torre et al., 2019; Terradas, 1998).

2.1.2. El rol de las técnicas analíticas en los estudios de procedencia

El empleo de las técnicas analíticas ha contribuido de manera determinante en el campo de los estudios de procedencia a través de la caracterización de rocas de diferentes orígenes[22]. La lógica detrás de este tipo de investigación está explicitada en el "postulado de procedencia" (*provenience*[23] *postulate;* Weigand et al., 1977) según

---

[21] Hay que destacar que la clasificación por color en rocas translúcidas como el sílex tiene su problemática intrínseca, debido a la dependencia con el espesor de la pieza.

[22] Sin embargo, el estudio de las estructuras mineralógicas se ha llevado a cabo también para investigar la cuestión de la alteración del sílex por calentamiento, que puede causar un cambio de color hacía el rojo y tiene también implicaciones sobre el trabajo de la roca (Schmidt et al., 2015).

[23] En el debate teórico, algunos autores de lengua inglesa distinguen entre "*provenience*" y "*provenance*": la "*provenience*" de un artefacto lítico sería el afloramiento donde se recoge la materia prima de un lado y su lugar de descubrimiento del otro ("*archaeological provenience*"), mientras que

el cual, para distinguir dos fuentes de materia prima, la diferencia de una o más características químicas entre las piezas procedentes de la primera fuente y las procedentes de la segunda tiene que ser mayor a la diferencia entre las piezas de cada afloramiento. Una vez este principio es respetado, identificado este marcador se podría teóricamente establecer si una muestra de procedencia desconocida tiene su origen en un afloramiento. Otros autores (Shackley, 1998; Wilson y Pollard, 2001) han mostrado algunas de las problemáticas de los estudios de abastecimiento debido a la variación de las características químicas de muchos depósitos de sílex, a la naturaleza probabilística de las atribuciones y a la imposibilidad de excluir la existencia de fuentes de materia prima desconocidas presentes o pasadas.

Para enfrentarse a un estudio de procedencia de artefactos silíceos, el primer aspecto que hay que tener en cuenta es el de la estrategia de muestreo. La identificación de fuentes de materia prima es una cuestión evidentemente complicada y requiere un trabajo geoarqueológico complejo que incluye el estudio en profundidad de la geología del área. En cambio, de forma general encontramos una escasa literatura sobre este tipo de roca, suplida a partir de la recopilación de información entre la población local y de prospecciones en lugares a menudo no fácilmente accesibles. Otro aspecto problemático concierne a la relación entre fuentes primarias y secundarias (Luedtke, 1979): en las primeras (Fig. 7a) el sílex aparece en conexión con la roca caja o en sus inmediaciones, y puede encontrarse en territorios muy amplios apareciendo en diferentes afloramientos de una misma formación geológica; mientras que en las segundas (Fig. 7b) el sílex aparece desplazado en depósitos naturales de diferentes tipos y orígenes como las terrazas aluviales. Estas últimas pueden encontrarse a distancias considerables de los afloramientos originarios e incorporar rocas de varias formaciones, así que es necesario tenerlas en consideración para evitar hipótesis erróneas sobre el aprovisionamiento de materias primas alóctonas (Delage, 2003).

En cuanto a los métodos de análisis, a lo largo de los años, se han testado y aplicado diferentes enfoques para el estudio de la procedencia de artefactos basados en la

---

la "*provenance*" comprendería también lo que se encuentra en el medio de estos dos puntos extremos de la vida de una pieza arqueológica (una síntesis de la discusión se puede leer, por ejemplo, en Zipkin et al., 2017).

comparación de las características químicas. Sin embargo, la discriminación de muestras de sílex desde este punto de vista es un reto para los arqueólogos ya que esta roca está esencialmente compuesta por dióxido de silicio. Por este motivo, desde los años 70 se entendió la relevancia de los elementos traza que se encuentran en la roca a niveles de pocas partes por millón o menos. En sus trabajos de referencia en este ámbito, Luedtke (1978; 1979) mostró la efectividad de un enfoque basado en elementos traza y técnicas de estadística multivariada, ya que los niveles de estos elementos se ven afectados por las diferentes condiciones medioambientales que distinguen las formaciones, o por las características de los microambientes en el interior de una misma cuenca sedimentaria. Para la determinación de los niveles elementales se han empleado numerosas técnicas, sobre todo NAA, ICP-MS y ED-XRF. La primera, como ya se ha comentado, ha sido la técnica de referencia para la determinación de elementos traza; se ha utilizado también en los estudios citados de Luedtke (1978; 1979) y sigue siendo empleada (Boulanger et al., 2015; Prudêncio et al., 2016). La ICP-MS, y en menor medida la ICP-OES, se usan también regularmente para la determinación de los elementos traza (Skarpelis et al., 2017; ten Bruggencate et al., 2017). Sin embargo, estas técnicas presentan problemas relacionados con la conservación de las muestras y otros propiamente técnicos: de hecho, de un lado necesitan que las piezas puedan ser destruidas, de otro el trabajo de pulverización y digestión por medio de ácido resulta bastante dificultoso debido a la elevada dureza de la roca y al hecho de que la matriz silícea requiere el empleo de ataques por ácidos como el fluorhídrico (HF), lo cual comporta un cierto riesgo para el analista, y precauciones particulares. Estas cuestiones se han superado en parte gracias al empleo de la ablación laser que es microdestructiva y no necesita de más preparación de la muestra que la remoción de las contaminaciones superficiales, si bien tiene menor sensibilidad y necesita de más medidas para obtener concentraciones representativas (Bradley et al., 2020; Chatzimpaloglou, 2020). La ED-XRF se utiliza comúnmente para el análisis multielemental, siendo un método rápido, económico y potencialmente no destructivo (Sánchez de la Torre et al., 2019). Sin embargo, en el análisis multielemental de sílex muchos elementos marcadores se encuentran por debajo del límite de detección para esta técnica; además, los análisis son superficiales y necesariamente relativos a unos puntos de medición de pocos milímetros de rayo,

haciendo difícil obtener resultados representativos en muestras con zonas meteorizadas. En caso de análisis no destructivo, la muestra tiene también que ofrecer una superficie lisa y regular respeto a la fuente de rayos X, condición no siempre presente, sobre todo en los artefactos (Gauthier et al., 2012). Estos aspectos negativos empeoran cuando se utiliza un espectrómetro portátil debido a la sensibilidad todavía más baja del detector, aunque a pesar de esto los pED-XRF se están empleando cada vez más y con buenos resultados (Newlander y Lin, 2017; Delluniversità et al., 2019). A menudo se lleva a cabo el análisis petrográfico en láminas delgadas y la caracterización de las estructuras presentes en las muestras por XRD, Raman o FT-IR. Aunque, como ya se ha indicado, el sílex sea una roca bastante homogénea y prevalentemente compuesta por un solo mineral, la presencia de impurezas como minerales accesorios y materia orgánica, o de polimorfos del dióxido de silicio característicos, así como diferencias en el grado de cristalinidad del cuarzo, pueden servir de apoyo para la discriminación de diferentes fuentes de materia prima (Moscone et al., 2020; Parish et al., 2013; Roldán et al., 2015). En muchos de los trabajos citados (e.g.: Bradley et al., 2020; Luedtke, 1979; Parish et al., 2013), los datos obtenidos por las diferentes analíticas son tratados mediante varias técnicas de estadística multivariada como el análisis de componentes principales (PCA), el análisis de grupos o el discriminante (DA) para observar las relaciones entre las variables y las muestras, identificar agrupaciones, y clasificar artefactos de procedencia desconocida. En general, las propuestas metodológicas prevén frecuentemente enfoques multianalíticos que van de la caracterización macroscópica hasta el análisis multielemental, con una atención particular en la actualidad a la no destructividad o la micro destructividad (Chatzimpaloglou, 2020; Delluniversità et al., 2019).

Un aspecto muy característico de los artefactos en sílex es la presencia frecuente de una típica corteza opaca alrededor de un núcleo central a menudo más translúcido (Fig. 8). Esta corteza puede derivar del nivel entre la roca caja y el núcleo silíceo (Fig. 8a), o puede originarse por meteorización pasando de ser una sutil patina a un estrato de unos milímetros de espesor[24] (Fig. 8b), de color blanquecino o rojizo dependiendo del

---

[24] Esta corteza exterior, cuando es producida por la meteorización, se encuentra definida también como neocórtex (Fernandes et al., 2007).

ambiente de desarrollo (Hurst y Kelly, 1961). El número de trabajos enfocados a la caracterización química de esta parte del sílex es relativamente limitado, sobre todo por lo que concierne al contenido elemental. A pesar de eso, no todos los estudios arqueométricos especifican como se trató el córtex durante la preparación de las muestras para llevar a cabo los análisis (e.g.: Evans et al., 2007; Herrero-Alonso et al., 2016; Nazaroff et al., 2013).
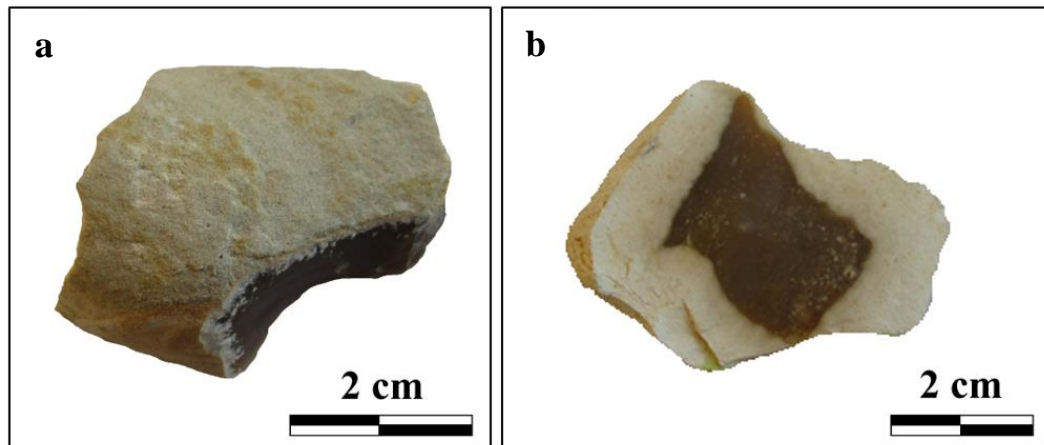
Fig. 8 - Fragmento de sílex con estratificación intra rocas (a, S14) y fragmento de sílex con evidente presencia de corteza blanquecina (b, S43; muestras de Ramacciotti et al., 2019a).

En un trabajo de revisión sobre el tema, Thiry et al. (2014) observaron que los mecanismos de meteorización que llevan a la formación del córtex consisten esencialmente en la lixiviación de los cristales de sílice menos estables, y en el progresivo aumento de la porosidad de los estratos exteriores de la roca que desarrolla un típico aspecto desconchado. Thacker y Ellwood (2002) confrontaron la susceptibilidad magnética del área cortical y de la roca fresca encontrando niveles menores en la primera, debido probablemente a la perdida de minerales ferromagnéticos. Al revés, los análisis por XRD de Graetsch y Grünberg (2012) evidenciaron que la corteza que se encuentra en el estrato de contacto entre sílex y roca caja, comparada con el núcleo central, está caracterizada por una mayor cantidad de polimorfos de la sílice diferentes del cuarzo, que además se encuentran en cristales de menor tamaño. Fernandes et al. (2007) estudiaron por SEM las relaciones entre la morfología del córtex desarrollado en piezas silíceas y los depósitos secundarios en los cuales se habían muestreado para emplear ese dato como marcador de procedencia. Tienen interés también los resultados de microanálisis elemental obtenidos por SEM de Bustillo et al. (2009) que observaron niveles más altos de Mg, Ca, Al y Fe en la

superficie porosa de las áreas meteorizadas. Moreau et al. (2016) llevaron a cabo como test la caracterización multielemental por LA-ICP-MS de áreas de roca fresca y alterada durante un estudio de procedencia sobre sílex de Bélgica y Alemania. El comentario ocupa solo un breve párrafo del artículo y los resultados no son presentados de manera extensa, y se resumen en que no hay diferencias significativas entre las dos partes.

2.1.3. Las estrategias de muestreo

Se han empleado estrategias diferentes de muestreo adaptadas a cada caso de estudio. Por lo que concierne el sílex del valle del Serpis (Ramacciotti et al., 2019a), hay que notar que la identificación de fuentes de materia prima contaba con un trabajo previamente desarrollado. Destaca el excelente trabajo de mapeo de potenciales fuentes de materia prima, tanto primarias como secundarias, y caracterización macroscópica[25] de las rocas de toda esta área del sistema Prebético llevado a cabo por Molina Hernández (2016). Previamente, Villaverde et al. (1999) efectuaron prospecciones para identificar los depósitos silíceos relacionados con la Cova de les Cendres. La elección de los puntos de muestreo partió de la caracterización realizada por Molina Hernández y del reconocimiento previo de la zona en relación con los trabajos arqueológicos sistemáticos realizados sobre las industrias líticas talladas del Mesolítico y del Neolítico (García Puchol, 2005). La elección de los puntos de muestreo siguió dos lógicas. Desde un punto de vista de desarrollo metodológico era de interés muestrear sílex de diferentes niveles geológicos y en diferentes posiciones respecto a la roca caja, así que se muestrearon nódulos y fragmentos de sílex Serrat (Paleoceno), Mariola (Cretácico) y Serreta (Eoceno). Además, se diferenció también del tipo de afloramiento para disponer de sílex procedente de posiciones primarias (Mariola) y de posiciones secundarias (Serrat y Serreta). Finalmente, del sílex Serreta se consideró oportuno muestrear en tres afloramientos secundarios distintos en los cuales las piezas habían sido supuestamente expuestas a condiciones de meteorización diversas. De esta manera se pudo observar la variabilidad de las características en depósitos que tienen diferentes relaciones entre ellos. Una cuestión de interés es que en algunas zonas de la Península Ibérica como el área de la cuenca del rio Ebro, de los

---

[25] De algunas muestras fue efectuado también el análisis petrográfico.

Pirineos sur-orientales y de la Cordillera Catalana(e.g.: Ortega et al., 2016; 2018; Sánchez de la Torre et al., 2021 y referencias citadas; Terradas et al., 2017) o el área septentrional de la Cordillera Cantábrica, de la cuenca Vasco-Cantábrica y de los Pirineos norte-occidentales (e.g.: Herrero-Alonso et al., 2016; 2021; Olivares et al., 2009; 2013; Tarriño-Vinagre et al., 2015; 2016), a lo largo de los años, se han censado las posibles fuentes de materia prima silícea, acumulando también una cantidad relevante de datos arqueométricos. En cambio, a pesar de la importancia del área estudiada para la Prehistoria del este peninsular[26], hay pocos trabajos que desarrollan el estudio arqueométrico de materias primas locales, y los que lo hacen tienen limitaciones evidentes desde el punto de vista del tamaño de muestra (Eixea et al., 2014; 2016; Prudêncio et al., 2016; Roldán et al., 2015; Schmich y Wilkens, 2006). Ramacciotti et al. (2019a) es el primer estudio que incluye un muestreo de diferentes tipologías de sílex de esta zona del Prebético, sobre todo del tipo Serreta, el sílex melado[27] del Serpis. La explotación de sílex melado tiene un papel remarcable en el área Mediterránea durante el Neolítico, especialmente en conexión con contextos cardiales (Fig. 9; García Puchol, 2005; 2009). Este tipo de sílex resulta recurrente en los asentamientos Neolítico del Valle del Serpis y puede haber sido empleado más allá de la zona del Prebético (García Puchol, 2009), también en épocas anteriores al Neolítico (Eixea et al., 2014).

Fig. 9 - Esquirlas de sílex Serreta (S39 en Ramacciotti et al. 2019a).

---

[26] En Ramacciotti et al. (2019a) se ofrece un breve cuadro de la cuestión desde el Paleolítico hasta el Neolítico.

[27] El sílex melado es un tipo de sílex de grano fino, translúcido y caracterizado por un color entre amarillo y marrón.

El segundo trabajo (Ramacciotti et al., 2022) es el primer estudio arqueométrico de procedencia de los artefactos silíceos de Cueva de la Cocina (Dos Aguas, Valencia), un yacimiento paradigmático para el estudio de los últimos cazadores-recolectores del área mediterránea peninsular y de su neolitización. Gracias al descubrimiento y a las primeras excavaciones de Luis Pericot (1946), y después a través de los estudios y las campañas de excavaciones llevadas a cabo por Javier Fortea (1973), la secuencia estratigráfica de Cueva de la Cocina y análisis diacrónico de la industria lítica han contribuido a su consideración como referencia para el estudio del Mesolítico Geométrico (Martí Oliver et al., 2009). A pesar de la importancia del sitio, no se había llevado a cabo un estudio de procedencia de los artefactos silíceos de Cueva de la Cocina, incluyendo la caracterización por métodos químicos de muestras arqueológicas y muestras de depósitos naturales localizados a su alrededor. Nuestra investigación se incluye en los trabajos de excavación, prospección y estudio de materiales más recientes llevados a cabo por el Departament de Prehistòria, Arqueologia i Història Antiga de la Universitat de València y del Museu de Prehistòria de València (e.g.: Gallello et al., 2021; García Puchol et al., 2015; 2016; 2018a; 2018b; Pardo-Gordó et al., 2016; 2017). En este caso, el muestreo tuvo como fin principal identificar las potenciales fuentes de materia prima relacionadas con el yacimiento confrontando los perfiles elementales de las rocas y de las piezas arqueológicas. En cuanto a estas últimas, siendo el primer test realizado, y utilizando un método destructivo, se seleccionaron artefactos procedentes de limpiezas de perfiles y por tanto desprovistos de un claro contexto arqueológico que abren el camino al desarrollo de algunas primeras hipótesis. En cuanto a los depósitos naturales, hay que destacar que no consta que existan trabajos de caracterización de las fuentes de materia prima relacionadas con el entorno inmediato de Cocina. En esta zona de la cordillera Ibérica aflora un sílex cretácico señalado también en el mapa geológico (García Velez et al., 1980a) que tiene características macroscópicas muy variadas y es similar a muchos de los artefactos hallados en la cueva. Muestras de este sílex se recogieron en tres afloramientos distintos: el afloramiento de La Canal y el de La Paridera, encontrados durante prospecciones recientes (Pardo-Gordó et al., 2016; 2017) y distantes de la cueva unos cientos metros el primero y aproximadamente 6 km en línea recta el segundo. Recientemente fue posible identificar la roca caja en este segundo. Un tercer

29

afloramiento fue localizado en Real de Montroy, a unos 15 km de Cocina, durante una prospección conectada con el presente trabajo. De esta manera hemos podido observar también la variación de las características macroscópicas y químicas de la roca a lo largo de la misma formación. Además, se recogieron fragmentos de sílex de tipo Domeño en un afloramiento coluvial relacionado con el asentamiento mesolítico de Mangranera (Andilla; García Puchol, 2005), distante cerca 65 km de Cueva de la Cocina. De hecho, algunos artefactos encontrados en la cueva y algunos de los analizados en nuestro trabajo tenían características macroscópicas similares, como la superficie opaca de color gris. Esta roca aparece en niveles sedimentarios jurásicos de la cordillera Ibérica y se encuentra en numerosos sitios arqueológicos entre la provincia de Valencia y la de Castellón. Este sílex ha sido estudiado también desde el punto de vista arqueométrico en algunos trabajos, relacionados sobre todo con el Abrigo de la Quebrada (Eixea et al. 2014; 2016; Prudencio et al., 2016; Roldán et al., 2015). De este modo, en Ramacciotti et al. (2022) se aportan de un lado datos sobre el citado afloramiento y, además, por primera vez se proporciona el perfil completo de los REE de muestras de sílex Domeño. Finalmente, debido a la ocurrencia de sílex melado en Cueva de la Cocina, los datos de sílex Serreta obtenidos en Ramacciotti et al. (2019a) fueron empleados para verificar la posible presencia de material alóctono.

2.1.4. Preparación de las muestras y protocolos analíticos

Para llevar a cabo la preparación de las muestras del valle del Serpis se eligió un método destructivo (Ramacciotti et al., 2019a). A este respecto, las muestras fueron pulverizadas antes de los análisis químicos. Sobre este aspecto hay que hacer algunas consideraciones. En primer lugar, ya que se trabajaba con muestras de depósitos naturales, la cuestión de la conservación era segundaria. Además, la pulverización de una cantidad significativa de cada muestra es la manera más apropiada para obtener datos representativos sobre una roca, ya que por homogénea que ésta sea, los análisis no destructivos o micro destructivos proporcionan distribuciones de concentraciones que pueden resultar no del todo representativos de la roca.

A nuestro parecer, conocer la diferencia en cuanto a los niveles elementales de córtex y núcleo central de una pieza de sílex resulta de interés para una interpretación más precisa de los resultados de análisis multielemental. De este modo, previamente a

valorar cuestiones de procedencia de los artefactos, estimamos necesario llevar a cabo un estudio específico para optimizar el método e investigar sobre este tema a través de un amplio conjunto de elementos, sobre todo de los elementos trazas que, como ya se ha indicado, tienen un papel fundamental en los estudios de procedencia. Por este motivo, en el trabajo analítico sobre el sílex del Valle del Serpis este aspecto se ha desarrollado ampliamente. Las piezas de sílex fueron limpiadas con un cepillo y agua ultrapura y trituradas con un triturador de mandíbula equipado con placas de carburo de wolframio (WC) para obtener pequeñas esquirlas de pocos milímetros. Después de la trituración, se separaron cuidadosamente de cada fragmento o nódulo de sílex las esquirlas del núcleo, o sea de la parte interior, y las de la corteza. De este modo obtuvimos dos muestras de cada pieza para el análisis multielemental. Las esquirlas fueron pulverizadas y homogenizadas por mortero de ágata.

Para llevar a cabo los análisis fueron elegidas las técnicas pED-XRF, ICP-MS y ICP-OES porque permitían cubrir un rango de elementos muy amplio, desde los mayoritarios a los traza, con escasas limitaciones relacionadas con los límites de detección. Los equipos utilizados son complementarios siendo cada uno más adecuado en diferentes intervalos de concentraciones y también para diferentes analitos. Por ejemplo, la medida de Si, Ti y Zr después de digestión ácida es muy problemática debido a la dificultad de disolver estos elementos; por esta causa, los tres elementos citados se midieron por fluorescencia de rayos X. En cambio, Mg, Al y Na estaban debajo de los límites de detección del pED-XRF, así que para medirlos se empleó el ICP-OES.

Para efectuar el análisis multielemental por pED-XRF, se colocó la muestra pulverizada directamente encima de la ventana de medida del espectrómetro (Fig. 10).

Fig. 10 - Espectrómetro pED-XRF S1 Titan en condiciones de medida.

Para los análisis de ICP-MS y ICP-OES tuvimos que desarrollar un método apropiado con digestión por ataque ácido que incluyese el empleo de ácido fluorhídrico (HF), necesario para destruir la matriz de sílice de la roca. El empleo del HF añade problemas de seguridad para el operador y también sobre los materiales de laboratorio que se emplean. De hecho, se necesitan contenedores de politetrafluoroetileno[28] (PTFE) para llevar a cabo la digestión, y el HF residual tiene que ser neutralizado o dejado evaporar para que no quede en la disolución final, ya que podría dañar el espectrómetro. El método se desarrolló a partir de Segal et al. (2005), añadiendo una predigestión en agua regía para mejorar la disolución de las impurezas del sílex.

Gracias a la propuesta metodológica desarrollada y publicada con anterioridad, el estudio sobre el sílex de Cueva de la Cocina (Ramacciotti et al., 2022) ha podido llevarse a cabo de manera más eficaz controlando mejor las variables que pueden afectar a la interpretación de los resultados obtenidos. Las muestras fueron preparadas siguiendo el protocolo desarrollado, aunque después de la trituración se pulverizaron y analizaron solo las esquirlas que no presentaban huellas evidentes de meteorización. Cada muestra fue analizada en polvo por pED-XRF y en disolución ácida por ICP-MS.

---

[28] Conocido también con el nombre comercial de teflón.

2.1.5. Control de la calidad de los análisis

Como se ha indicado en el primer capítulo, la cuestión de la calidad de los resultados de pED-XRF es objeto de debate en arqueometría. El espectrómetro S1 Titan de Bruker empleado en nuestros trabajos tiene un sistema integrado de calibración para la medida de materiales geológicos (*GeoChem Trace application*) que tuvo que ser perfeccionado para los análisis cuantitativos de muestras en polvo a través del empleo de muestras de referencia certificadas (CRM) y muestras de control.

La muestra certificada más adecuada para el análisis de sílex es sin duda JCh-1, una CRM producida con sílex por el Servicio Geológico de Japón (Terashima et al., 1990). Su empleo se encuentra ocasionalmente también en trabajos arqueométricos (e.g.: Högberg et al., 2016; Hughes et al., 2012). En el momento de llevar a cabo la tesis, esta muestra ya no estaba disponible. Por lo tanto, en el caso del sílex hemos empleado muestras certificada no de referencia (CNRM) de la empresa AMIS[29]. Estas muestras de control son AMIS0484, constituida por arena de sílice pulverizada a través de un molino, y AMIS0439, constituida por fragmentos de cuarcita de aproximadamente 7 g. De estos últimos fueron seleccionados diez fragmentos que pulverizamos con un mortero de ágata. En la tabla de la hoja informativa están reportadas las concentraciones promedio y las desviaciones estándar obtenidas en los análisis efectuadas en laboratorios independientes y comisionadas por la empresa. Para valorar la precisión de los análisis sobre una muestra de sílex, se elaboró una muestra propia que llamamos "MixSil" empleando fragmentos de diferentes tipos de sílex muestreados durante la prospección del valle del Serpis (Ramacciotti et al., 2019a). Se pulverizaron con un mortero de ágata aproximadamente 200 g de esquirlas de sílex obtenidas por trituración de fragmentos más grandes a través de un triturador equipado con mandíbulas de carburo de wolframio (WC).

En la Tabla 1 se presentan los resultados obtenidos en las muestras empleadas para la evaluación de los resultados de pED-XRF sobre sílex. Las concentraciones certificadas del CNRM fueron medidas por ED-XRF, excepto donde queda expresamente indicado. Para la comparación entre las concentraciones obtenidas y los valores

---

[29] La página web de la empresa es https://amis.co.za/ .

certificados se emplearon pruebas de significación de medias experimentales (Miller y Miller, 2002) considerando un p-valor de 0.05 como umbral.

Tabla 1 - Valores certificados y concentraciones obtenidas por pED-XRF en AMIS0484, AMIS0439 y en la muestra MixSil.

Elemento	AMIS0484				Elemento	AMIS0439				MixSil	
	Valor certificado		Concentración obtenida (n = 15)			Valor certificado		Concentración obtenida (n = 15)		Concentración obtenida (n = 10)	
	Promedio	DS	Promedio	DS		Promedio	DS	Promedio	DS	Promedio	DS
Si	46.35	0.02	46.30	1.10	Si	45.39	0.20	45.43	0.67	44.99	0.99
P	< 0.01		0.04	< 0.01	P	< 0.01		0.03	< 0.01	0.03	< 0.01
K	0.12	< 0.01	0.13	< 0.01	K	0.29	0.02	0.40	0.03	0.04	< 0.01
Ca	< 1		0.02	< 0.01	Ca	0.05	0.04	0.03	< 0.01	1.14	0.05
Ca*	0.02	0.01			Ti	0.05	0.01	0.06	0.01	0.01	< 0.01
Ti	0.02	< 0.01	0.02	< 0.01	Fe	0.24	0.19	0.22	< 0.01	0.08	< 0.01
Fe	0.02	< 0.01	0.06	< 0.01	Zr	-		-		9	2
Fe*	0.05	0.01									
Zr*	21	1	24	2							

Nota: Concentraciones expresadas como porcentaje masa/masa, excepto Zr (mg/kg). (*): valores certificados obtenidos por ICP-MS (Zr) o ICP-OES (Ca, Fe). DS: desviación estándar; ND: no determinado.

Por lo que concierne AMIS0484, las concentraciones de Si y Ti obtenidas resultan estadísticamente semejantes de las del CNRM. La concentración de Ca está dentro del límite indicado respeto a la certificada medida con ED-XRF y no es significativamente diferente respeto a la certificada medida con ICP-OES. La concentración de Fe obtenida se encuentra entre una desviación estándar respeto a la certificada medida con ICP-OES y la de K queda entre un ±10% respeto a la del CNRM. En cuanto a AMIS0439, las pruebas de significación sugieren que la diferencia entre las concentraciones promedio no son significativas para Si y Fe. Las concentraciones promedio de Ca y Ti obtenidas quedan entre una desviación estándar respeto a las certificadas. La desviación estándar relativa (RSD) es menor o igual al 10% para casi todos los elementos excepto Ti y P en AMIS0439 (25% y 19%), Ca (11% en AMIS0484 y 13% en AMIS0439). En la muestra de control MixSil, la RSD es menor o igual a 10% en Si, K, Ca y Fe, y más alta en P (15%), Ti (12%) y Zr (17%).

En la Tabla 2 se pueden observar los resultados de ICP-MS de las mismas muestras. Al respeto de AMIS0484, las pruebas de significación sugieren que los valores certificados y las concentraciones obtenidas son estadísticamente semejantes para Ce, Sm, Tb, Dy, Ho, Er, Pb y U. En cuanto a los otros analitos, las concentraciones

promedio obtenidas se quedan entre una desviación estándar respecto a las certificadas para Yb, Lu, Ni, Sr. Las concentraciones obtenidas se encuentran en los límites certificados para Sc, Bi, Cd, Co, Cr, Cu, Li, Mo, Tl y V. En cuanto a AMIS0439, las diferencias no son significativas para La, Ce, Pr, Nd, Eu, Gd, Ba, Li, Pb, Th y U. Los valores obtenidos quedan entre una desviación estándar respecto a los certificados para Mn y entre los límites indicados para Bi, Co, Cr, Mo, Tl y Zn. La RSD es menor o igual a 10% para todos los REE en AMIS0484, excepto Tm (14%), Lu (13%) y Sc (15%), y en todos menos Nd (20%) y Sc (21%) en AMIS0439. En cuanto a MixSil, se puede observar que la RSD es menor o igual a 10% en todos los REE excepto Dy (12%), Er (16%) y Lu (11%). En los otros elementos traza, la RSD es menor de 10% en Ba, Co y Sr en AMIS0484, y en Ba, Cu, Mn, Pb, Tl, V, Th y U en AMIS0439. En MixSil, la RSD es menor de 10% en Ba, Cd, Co, Cr, Cu, Mn, Ni, V y Zn.

Tabla 2 - Valores certificados y concentraciones obtenidas por ICP-MS en AMIS0484, AMIS0439 y en la muestra MixSil.

Elemento	Masa (Da)	AMIS0484 Valor certificado		AMIS0484 Conc. obtenida (n = 6)		AMIS0439 Valor certificado		AMIS0439 Conc. obtenida (n = 2)		MixSil Conc. obtenida (n = 4)	
		M	DS	M	DS	M	DS	M	DS	M	DS
La	139	3.32	0.11	3.16	0.15	4.90	0.74	5.27	0.18	0.949	0.016
Ce	140	5.52	0.16	5.6	0.2	9.2	2.2	8.8	0.2	1.30	0.03
Pr	141	0.67	0.02	0.63	0.03	1.1	0.1	0.974	0.011	0.212	0.009
Nd	142	2.35	0.08	2.54	0.14	4.10	0.46	3.9	0.8	0.86	0.07
Sm	152	0.37	0.02	0.39	0.02	0.84	0.05	0.748	0.013	0.178	0.018
Eu	151	< 0.02		0.058	0.004	0.16	0.02	0.144	0.002	0.038	0.004
Gd	158	0.21		0.32	0.02	0.63	0.07	0.67	0.03	0.166	0.015
Tb	159	0.06	0.08	0.044	0.004	0.10	0.01	0.084	0.002	0.021	0.001
Dy	162	0.25	0.02	0.25	0.016	0.59	0.04	0.523	0.008	0.127	0.015
Ho	165	0.05	0.01	0.048	0.005	0.12	0.01	0.086	0.001	0.022	0.002
Er	166	0.15	0.01	0.152	0.013	0.39	0.03	0.29	0.03	0.066	0.010
Tm	169	0.02		0.023	0.003	0.06	0.01	0.036	0.001	0.008	0.001
Yb	172	0.18	0.03	0.153	0.013	0.41	0.03	0.258	0.004	0.050	0.005
Lu	175	0.02	0.01	0.025	0.003	0.06	0.01	0.038	0.002	0.007	0.001
Sc	45	< 1		0.49	0.07	1.0		0.81	0.17	0.22	0.01
Y	89	1.39	0.07	1.25	0.06	3.10	0.17	2.579	0.003	0.84	0.02
Ba	138	15.60	0.99	12.3	0.8	48.0	3.6	47.0	0.9	12.8	1.1
Bi	209	< 0.1		0.019	0.009	< 0.1		0.015	0.004	0.008	0.003
Cd	111	< 0.5		0.025	0.008	< 0.5		0.051	0.018	0.021	0.002
Co	59	< 5		0.35	0.02	< 5		0.337	0.012	42.2	0.6
Cr	52	< 50		25	5	< 50		11.8	1.4	21.6	1.6
Cu	63	< 2.5		1.7	0.5	6.7	2.4	1.68	0.11	1.15	0.06
Li	7	< 0.5		0.47	0.08	16.4	0.35	12	3	16	2
Mn	55	15.40	1.60	10.7	1.6	23.1	24.8	11.5	1.0	4.6	0.2
Mo	95	< 0.5		0.21	0.03	< 0.5		0.023	0.015	0.49	0.08
Ni	60	8.50	2.35	6.7	0.8	< 1		1.5	0.4	8.4	0.8
Pb	207	1.20	0.89	1.06	0.17	2.9	4.0	1.635	0.007	0.34	0.07
Sr	88	2.15	0.24	2.35	0.09	4.8	0.60	3.8	0.5	18	2
Tl	205	< 0.1		0.044	0.011	< 0.1		0.083	0.007	0.012	0.004
V	51	< 5		2.3	0.3	11.0	2.0	5.59	0.13	2.71	0.09
Zn	64	< 1		1.63	0.7	< 5		4.6	1.8	5.2	0.2
Th	232	1.62	0.07	1.81	0.18	2.0	0.12	2.04	0.13	0.26	0.03
U	238	0.41	0.03	0.44	0.06	0.48	0.06	0.45	0.03	0.71	0.08

Nota: Concentraciones expresadas como mg/kg. M: promedio; DS: desviación estándar; Conc.: concentración.

En la Tabla 3 se reportan los valores de referencia y los que hemos obtenidos por ICP-OES en las muestras de control relacionadas con el sílex.

Tabla 3 - Valores certificados y concentraciones obtenidas por ICP-OES en AMIS0484, AMIS0439 y en la muestra de control MixSil.

Elemento	AMIS0484 Valor certificado			AMIS0484 Conc. obtenida (n = 3)		AMIS0439 Valor certificado			AMIS0439 Conc. obtenida (n = 3)		MixSil Conc. obtenida (n = 3)	
	Equipo	M	DS	M	DS	Equipo	M	DS	M	DS	M	DS
Na	ICP-OES	0.02	< 0.01	0.02	< 0.01	ICP-OES	0.02	0.01	0.01	< 0.01	0.01	< 0.01
	ED-XRF	0.02	< 0.01			ED-XRF	0.01	0.01				
Mg	ICP-OES	< 1	-	0.01	< 0.01	ICP-OES	0.03	0.01	0.02	< 0.01	0.02	< 0.01
	ED-XRF	0.01	< 0.01			ED-XRF	0.03	0.01				
Al	ICP-OES	0.24	0.01	0.13	< 0.01	ICP-OES	0.78	0.05	0.56	0.01	0.02	< 0.01
	ED-XRF	0.23	< 0.01			ED-XRF	0.78	0.05				

Nota: Concentraciones expresadas como porcentaje masa/masa. M: promedio; DS: desviación estandar; Conc: concentración.

La diferencia no se considera significativa para el valor obtenido de Mg y el certificado por ED-XRF en AMIS0484 y para los obtenidos de Na y los certificados por ED-XRF en AMIS0439. Las concentraciones promedio obtenidas para estos elementos quedan entre una desviación estándar respeto a las certificadas. En ningún caso la RSD supera el 10%.

2.1.6. Procesado de datos y análisis estadístico

El trabajo realizado proporciona una serie de parámetros procesados por diferentes técnicas de estadística multivariada. Luedtke (1979) ya se había dado cuenta de la importancia de la selección de elementos diagnósticos para llevar a cabo estudios de procedencia. En nuestro caso, los elementos de las tierras raras (REE) y sus índices de fraccionamiento (Lawrence et al., 2006) ocupan un lugar central como marcadores, debido a su capacidad de discriminar entre rocas caracterizadas por diferentes ambientes de sedimentación. El empleo de estos elementos ha sido esporádico en el estudio de sílex (ver por ejemplo Murray, 1994) y para estudios arqueológicos de procedencia de artefactos hechos con esta materia prima (e.g.: Chatzimpaloglou, 2020; Elefanti et al., 2021; Olofsson y Rodushkin, 2011; Ortega et al., 2018;). Del mismo modo, es inusual la interpretación de los datos de REE como marcadores de

procedencia a través del empleo de la estadística multivariada. En el trabajo sobre el sílex del Serpis (Ramacciotti et al., 2019a) se utilizaron el análisis de componentes principales (PCA) y el análisis de grupos como técnicas de estadística exploratoria para interpretar un conjunto de datos compuestos por muchas variables. La finalidad de estas técnicas estadísticas era, por un lado, identificar las tendencias principales (e.g.: ¿qué diferencia hay entre los niveles elementales de la corteza y de la parte interior?) y, por otro, evaluar la efectividad de conjuntos particulares de variables para discriminar rocas diferentes. La estadística multivariada y los REE tienen un rol central también en el estudio de procedencia del sílex de Cueva de la Cocina (Ramacciotti et al., 2022). En este caso, después de haber comprobado el papel de este grupo de elementos como marcadores de procedencia, se empleó el análisis discriminante cuadrático (QDA) para interpretar más en profundidad los datos analíticos y efectuar hipótesis más robustas de procedencia de los artefactos.

2.2. Materiales de construcción en la antigua ciudad de Sagunto

Los materiales de construcción antiguos son un tema de estudio abordado por numerosas disciplinas, dado su interés histórico-arqueológico, artístico y arquitectónico, así como por parte de la ingeniería, y de las ciencias de los materiales y de la conservación. Por lo tanto, no sorprende que las técnicas analíticas desarrolladas por las ciencias naturales sean utilizadas de manera extensiva como complemento a la investigación arqueológica de un lado, así como para caracterizar los materiales y sus formas de deterioro, y evaluar el estado de conservación y programar intervenciones de restauración en los monumentos (e.g.: Barca et al., 2010; Berthonneau et al., 2016; Siedel y Siegesmund, 2014;).

Por lo que concierne a la arqueología, los materiales de construcción tienen un particular interés en el ámbito de la arqueología de la arquitectura. Esta rama investiga los procesos constructivos relacionados con monumentos y estructuras, y se desarrolló sobre todo a partir de los años '70 y '80 del siglo XX, en un primer momento, dentro de la arqueología medieval (Dessales, 2017). Los objetivos principales de este tipo de investigación están relacionados con el conocimiento de los procesos de construcción de estructuras, incluyendo la datación y la identificación de las diferentes fases constructivas, el análisis tecno-tipológico y estratigráfico de las mamposterías, la

procedencia de las materias primas y las tecnologías de producción de los materiales empleados (Azkarate, 2020). Estos datos son fundamentales para entender la transformación de un monumento o de un complejo arqueológico en el tiempo, la función de los espacios, las modalidades del trabajo, el desarrollo y la transmisión de las técnicas constructivas, la movilidad de los grupos de trabajadores, y la explotación, la difusión y el procesamiento de los recursos naturales desde los lugares de cantera a los de obra, incluyendo, en algunos casos, la reutilización (Brogiolo, 2007; Ferris, 1989; Francovich y Bianchi, 2002).

Los dos artículos sobre materiales de construcción presentados en esta tesis (Ramacciotti et al., 2018; 2019b) están relacionados con las estructuras del Castillo de Sagunto y sus inmediaciones, y se incluyen en una serie de trabajos arqueométricos llevados a cabo en los últimos cinco años sobre el riquísimo patrimonio cultural saguntino (Gallello et al., 2020b). La ocupación de esta área remonta a la época Íbera, al menos desde el VI siglo a.C. Tanto el Castillo como la ciudad reflejan una serie de fases constructivas y de destrucciones. Entre estas últimas anotaremos la cartaginense en el 218 a.C., o las más recientes relacionadas con la Guerra Napoleónica y la Guerra Civil. Sobre las fases constructivas más destacadas debemos mencionar la propiciada por el empuje de la urbanización de matriz Romana, la ocupación Islámica y la Reconquista (Aranegui Gascó, 2012; 2014; Melchor Monserrat, 2007).

2.2.1. Morteros históricos y arqueometría

El estudio de los morteros antiguos constituye un campo donde la aplicación de los métodos arqueométricos ha tenido un relieve particular ya que las características macroscópicas aportan datos relativamente escasos. Se puede abordar el estudio de este tipo de material desde diferentes puntos de vista. De hecho, dos aspectos importantes son los relativos a las materias primas y la tecnología de producción, que pueden a su vez estar relacionados con la función del mortero mismo. Los morteros son materiales compuestos formados por un aglutinante (e.g.: cal o arcilla) y un agregado (normalmente una arena) que pueden tener función cohesiva entre los elementos de un muro, como en los morteros de junta para atar sillares y ladrillos o en el relleno de la mampostería de escombros, o de protección y decoración, como en los revestimientos de enlucido (Miriello, 2018). En el caso de la cal, la materia prima para

39

producir el aglutinante, una roca carbonatada como la caliza o la dolomía, tiene que pasar también a través de un procesado de cocción a temperaturas de aproximadamente 900 °C para que del carbonato de calcio ($CaCO_3$) se obtenga la cal viva[30] (CaO). Una vez hidratada pasa al estado de hidróxido de calcio ($Ca(OH)_2$) y está lista para ser mezclada con un agregado y empleada en la obra. Para conferir características hidráulicas a la cal, se añadían materiales puzolánicos tales como arenas volcánicas particulares o cerámica triturada que, al reaccionar con el hidróxido de calcio provocan la formación de silicatos y aluminatos de calcio hidratos[31], un aglutinante que se endurece también en agua y resulta particularmente resistente a la lixiviación. A lo largo de los años, para estudiar las características de agregados y aglutinantes se han desarrollado métodos multianalíticos basados en el análisis petrográfico por microscopía óptica y electrónica, y en el análisis químico por XRD, SEM-EDS, ED-XRF y de determinación de los volátiles (CO_2 y H_2O) por ignición y gasometría que permiten obtener datos sobre las dos fracciones de los morteros, deducir la presencia de características hidráulicas y en algunos casos identificar las materias primas empleadas (Crisci et al., 2004). Para determinar las fases mineralógicas en morteros antiguos, así como la posible presencia de aditivos orgánicos, se ha utilizado también la espectroscopía de infrarrojo (Al Sekhaneh et al., 2020; Rao et al., 2015). En cuanto a la identificación de las fases del aglutinante y de las propiedades hidráulicas, se han confirmado con el tiempo métodos basados en la separación de las dos fracciones que componen los morteros y el sucesivo análisis de la cal a través de termogravimetría y calorimetría diferencial de barrido (TG-DSC) (Cantisani et al., 2021; Lezzerini et al., 2014a; 2016). La identificación de las rocas empleadas como materia prima para la producción de la cal se puede efectuar a través del análisis multielemental por SEM-EDS o LA-ICP-MS de pequeños restos de fragmentos de caliza intactos no totalmente quemados. También a partir de los grumos de cal que se encuentran comúnmente en los morteros antiguos, formados durante el amasijo de la cal viva, ya que se supone la

---

[30] $CaCO_3 \rightarrow CaO + CO_2$. La cocción de la cal magnesiana pasa por dos fases con una primera disociación de la dolomita según la siguiente reacción endotérmica: $CaMg(CO_3)_2 \rightarrow CaCO_3 + MgO + 2CO_2$.

[31] En muchos artículos sobre morteros antiguos los compuestos hidráulicos están indicados como fases CSH, que es la nomenclatura utilizada en la química de los cementos (Lezzerini et al., 2016).

conservación de las propiedades elementales de la roca (Fichera et al., 2015; Miriello et al., 2015). Normalmente los materiales empleados para la producción de morteros son locales, pero hay ejemplos de importación de materias primas, sobre todo por lo que concierne a los materiales puzolánicos, dado que los afloramientos son menos comunes (Hohfelder et al., 2007; Marra y D'Ambrosio, 2012). Estos datos sobre las tecnologías y las materias primas empleadas son por sí mismo de interés arqueológico y pueden ser útiles también para elegir materiales para restauraciones. Además, en muchos casos se hacen trabajos arqueométricos sobre morteros con el fin de proporcionar cronologías relativas[32] de las estructuras de un complejo monumental o arqueológico. De hecho, la identificación de morteros que tienen características distintas puede ser de apoyo para el análisis tipológico-estratigráfico de las mamposterías, o para a la identificación de diferentes fases de aplicación del enlucido (Chiarelli et al., 2015; Corti et al., 2013; Ergenç y Fort, 2019; Lezzerini et al., 2018; Ortega et al., 2008; Sanjurjo-Sánchez et al., 2010).

2.2.2. Estudio de fases constructivas en los morteros antiguos de Sagunto

En Ramacciotti et al. (2018) se han analizado morteros de cal[33] procedentes de dos excavaciones en Sagunto: la primera estaba relacionada con la recualificación del área del circo romano (Fig. 11a) y de los restos del sitio del solar de Quevedo (Calle de los Huertos, Fig. 11b), y la valorización de los restos arqueológicos allí presentes, y la segunda se efectuó en una intervención de urgencia en la zona de la estación de tren en Sagunto (ver figura 1 en Ramacciotti et al., 2018).

En cuanto a los objetivos, nuestro trabajo se centra en los estudios de las fases constructivas. Desde el punto de vista metodológico supone una continuación de los trabajos desarrollados con anterioridad (Gallello et al., 2017). En el último trabajo citado se caracterizaron por análisis multielemental morteros enteros[34] procedentes del

---

[32] Hay que destacar que se utiliza también el análisis de radiocarbono para efectuar dataciones absolutas de morteros (Daugbjerg et al., 2021).

[33] Se analizaron también seis muestras de mortero de tierra encontradas en dos estructuras del sitio del Solar de Quevedo, pero el trabajo está enfocado en las de cal.

[34] Con enteros se entiende que no se separaron agregado y aglutinante. Los morteros fueron pulverizados para los análisis de pED-XRF y el polvo fue digerido por ataque ácido para los de ICP-MS.

41

Castillo de Sagunto empleando espectroscopía pED-XRF e ICP-MS. Los morteros pertenecían a varias estructuras datadas en diferentes fases (romano republicana, romano imperial, islámica y moderna), y la finalidad consistía en testar la efectividad de los datos de REE para observar diferencias entre morteros de diferentes periodos de construcción y poder clasificar morteros pertenecientes a estructuras de cronología. A partir de los resultados positivos de esta primera aproximación, en Ramacciotti et al. (2018) se llevó a cabo el mismo tipo de análisis, o sea la espectroscopía pED-XRF de muestras pulverizadas con mortero de ágata y el análisis por ICP-MS de muestras digeridas por ataque ácido con agua regia. Se empleó el mismo enfoque permitiendo así verificar la reproducibilidad del método en un segundo caso de estudio.

Fig. 11 - Puerta meridional del circo romano de Sagunto (a) y estructuras del sitio del Solar del Quevedo (b).

En ambos casos, las muestras fueron proporcionadas por los arqueólogos que estaban llevando a cabo las excavaciones y que efectuaron también las primeras interpretaciones de la cronología de algunas de las mamposterías. No habiendo criterios de conservación muy estrictos, pudieron cogerse dos muestras de cada estructura para tener bajo control la variabilidad interna de los niveles elementales. Algunas muestras fueron extraídas de las mamposterías relacionadas con la puerta meridional del circo y su tribuna. Los restos cerámicos encontrados durante las excavaciones anteriores en este monumento y el estudio de las estructuras sugieren una datación al final de la primera mitad del II siglo d.C., coherente con las fechas de los circos de otras ciudades menores de las provincias hispanas (Hernández Hervás et al., 1995). Por esta razón, los morteros muestreados en el circo podían ser utilizados

como referencia cronológica para los de otras estructuras localizadas en el inmediato sur-este. En esta área, que había sido incorporada a los huertos del Convento de la Trinidad (XIII d.C.), se encontraba una plaza pública de época imperial probablemente contemporánea al circo y, de acuerdo con estudios anteriores, relacionada quizás con un edificio monumental. De la misma quedan los restos de un pórtico, una entrada con dos pilares monumentales y una cloaca (Ferrer-Maestro et al., 2020; Melchor Monserrat et al., 2017). Sobre las estructuras del pórtico se apoyaban los restos de dos habitaciones (*Room 1* y *Room 2* en Ramacciotti et al., 2018), construidas con sillares ligados con morteros de tierra, que los arqueólogos habían relacionado con ocupaciones de época Islámica. En la excavación de la estación se han encontrado alzados que según una primera interpretación arqueológica podrían estar relacionados con estructuras monumentales de época romana[35]. Además, se emplearon como referencia cronológica también los datos de los morteros del castillo y, entre estos, los de las muestras que podían servir de referencia para la fase de ocupación islámica de la ciudad de Sagunto. Hay que destacar que los estudios arqueométricos sobre morteros están normalmente relacionados con un único monumento o con restos de edificios de una misma excavación arqueológica. Por ello, este trabajo resulta original desde un punto de vista metodológico en la manera de solucionar cuestiones cronológicas a través de datos arqueométricos para un horizonte más amplio, y añade datos que podrán ser utilizados como referencia para la datación de otras estructuras históricas en el área de Sagunto. Para explorar los datos, evaluar la efectividad de los REE como marcadores de morteros perteneciente a cronologías distintas se utilizó la técnica del PCA, procesando también los datos de los morteros del castillo como referencia. Además del PCA, se construyó un modelo clasificatorio de análisis discriminante por mínimos cuadrados parciales (PLS-DA) empleando como conjunto de contraste los morteros de la fase islámica y los de la fase romano-imperial del castillo.

2.2.3. Arqueología y ciencia arqueológica en el estudio de las mamposterías

La aportación de la arqueología de la arquitectura sobre rocas consiste en la observación de las características macroscópicas de los sillares que indican la

---

[35] Comunicación personal de los arqueólogos responsables de la excavación.

presencia de materiales diferentes, la forma, el tamaño y la disposición de los elementos que componen las mamposterías, además de las huellas de mano de obra que pueden también mostrar el uso de las diferentes herramientas para trabajar la materia prima y disponer los elementos constructivos en su lugar (Adam, 2002; Cagnana, 2000). Estos detalles forman parte de la información necesaria también para reconstruir la estratigrafía muraria de un edificio. Los métodos de las ciencias naturales aportan una contribución fundamental para reconstruir la procedencia de las rocas utilizadas en edificios históricos y caracterizar su degradación para fines de conservación. El análisis de microfacies a través de microscopio petrográfico, que permite observar las características de los ambientes sedimentarios, es un método clásico y todavía muy utilizado para distinguir entre rocas carbonatadas procedentes de diferentes canteras (Flügel, 2010). Se han utilizado también técnicas de análisis multielemental para obtener datos cuantitativos sobre los contenidos de elementos mayoritarios y traza con el fin llevar de a cabo clasificaciones más robustas (Emami et al., 2018; Lecuit et al., 2018). En algunas áreas, y para algunos materiales de particular valor y de amplia circulación, este tipo de estudio ha tenido a lo largo de los años un carácter sistemático. En Toscana (Italia), por ejemplo, los métodos arqueométricos se han utilizado ampliamente en la caracterización de rocas de canteras y de sillares relacionados con los principales materiales lapídeos empleados en la construcción de edificios desde la Antigüedad hacía la Edad Moderna sobre todo por las universidades y los centros de investigación de Pisa y Florencia (e.g.: Aquino et al., 2020; Franzini et al., 2010; Fratini et al., 2020; Pecchioni et al., 2016). De manera similar, disponemos en la actualidad de una base de datos químicos, isotópicos y petrográficos sobre los principales mármoles blancos que circularon desde la época Romana en todo el Mediterráneo (Antonelli y Lazzarini, 2015). Recientemente, es cada vez más frecuente el empleo de aparatos portátiles como pED-XRF, y espectrómetros Raman e IR, y el desarrollo de métodos no destructivos para el estudio arqueométrico *in situ* y la detección directa de productos de meteorización química (Gallello et al., 2016b; Morillas et al., 2016; Pecchioni, 2019; Sciuto et al., 2019).

2.2.4. Los sillares de roca carbonatada del Castillo de Sagunto

El segundo trabajo (Ramacciotti et al, 2019b) tiene como objeto los sillares de las estructuras del Castillo de Sagunto y, en particular, los de roca carbonatada.

Fig. 12 - Torre de la Moneda (MT en Ramacciotti et al., 2019b)

Al mismo tiempo se ha hecho también un estudio arqueométrico sobre algunos sillares de arenisca para evaluar su compatibilidad con los afloramientos del Monte Picayo, no incluido en la presente tesis (Ramacciotti et al., 2020b). El trabajo ha tenido como objetivo discriminar las fuentes de materia prima para la producción de los sillares. De hecho, todavía no se habían llevado a cabo trabajos arqueométricos para verificar, por ejemplo, el empleo efectivo de las dos canteras presentes en la colina del castillo, donde afloran dolomías y calizas dolomíticas (Goy et al., 1972). Sus características macroscópicas y, obviamente, la cercanía al complejo, hacían factible su utilización en la Antigüedad para la fabricación de sillares ya desde época pre romana (Aranegui Gascó, 2014; Rouillard, 1979). Además, el empleo de diferentes materias primas podía ser útil para el estudio de las fases constructivas de las estructuras del monumento (Fig. 12). De hecho, a lo largo de los años se han realizado diferentes estudios arqueológicos sobre los edificios del castillo que evidencian la complejidad de la historia de este complejo. Los restos de estructuras más antiguas han sido atribuidos a la época ibérica (IV a.C.; Rouillard, 1979). Una primera e importante fase constructiva estuvo relacionada con el periodo sucesivo a la destrucción por parte de los Cartagineses (219 a.C.), cuando se construyen las bases de algunos de los edificios muestreados (ver el mapa en la figura 1 de Ramacciotti et al., 2019b) como la Torre Central de Plaza de los Estudiantes (Pascual Buyé y Aranegui Gascó, 1993), o algunas estructuras del foro

y de su alrededor, lugar en el que se superponen importantes intervenciones de época romano imperial a partir del final del I a.C. y el inicio del siguiente siglo, incluyendo la edificación de la basílica y la curia (Aranegui Gascó, 1984; Aranegui Gascó et al., 1986; Hernández y Aranegui, 1989). De hecho, este periodo se caracteriza por un fuerte empuje edilicio de forma que muchos edificios públicos y monumentales saguntinos pertenecen a esta fase (Benedito Nuez, 2015); entre estos se incluye también el teatro, cuya construcción data del I siglo d.C. (Hernández et al., 1993). Sin embargo, la historia de este gran conjunto histórico y arquitectónico no acaba con el Imperio Romano; de hecho, el foro y otras áreas del castillo fueron objeto de numerosas intervenciones relacionadas sobre todo con obras de fortificación militar llevadas a cabo durante la ocupación islámica, como es el caso de la Torre de la Moneda (Fig. 12; Moliner Cantos et al., 2014), después de la Reconquista, y durante la Edad Moderna (Cebrián Fernández, 2017; Pascual Buyé y Aranegui Gascó, 1993; Peruga Ayete y Carbonell Rubio, 2019). Esta sucesión de intervenciones constructivas en las mismas áreas y edificios ya se había señalado a través del estudio de los morteros (Gallello et al., 2017).

Aunque en nuestros trabajos se hayan practicado análisis destructivos, tuvimos también que enfrentarnos con limitaciones a la hora de la toma de muestra, con protocolos muy estrictos debido a cuestiones de conservación. Así que planteamos un protocolo analítico y de muestreo mínimamente invasivo, gracias al cual se pudieran extraer cuantos más datos posibles a partir de una cantidad de roca muy pequeña. El muestreo fue llevado a cabo con el apoyo de los arqueólogos del Museo Arqueológico de Sagunto. Se rascó ligeramente una pequeña área de la superficie de los sillares seleccionados para eliminar el estrato más externo, alterado por la meteorización, y con un cincel se cogió una pequeña esquirla de roca fresca que fue pulverizada. Se llevó a cabo el análisis por ICP-MS de los elementos traza incluidos los REE ya que, al igual que con el sílex, estos elementos pueden ser buenos marcadores de procedencia debido a la capacidad de distinguir entre diferentes ambientes de sedimentación en rocas carbonatadas (e.g.: Franchi et al., 2015; Zhang et al., 2017). De todas formas, para distinguir entre los litotipos era importante tener datos sobre las fases mineralógicas presentes en las rocas y, ya que en el área se encuentran rocas carbonatadas de la serie calcita-dolomita (Goy et al., 1972), se consideró necesario

poder medir las concentraciones de Mg, un elemento ligero que el espectrómetro pED-XRF no consigue en muchos casos detectar por límites de sensibilidad. Una parte de cada muestra pulverizada fue enviada al Departamento de Ciencias de la Tierra de la Universidad de Pisa para efectuar los análisis de XRD y caracterizar las fases mineralógicas, y los de ED-XRF para obtener las concentraciones de los elementos mayoritarios incluyendo el Mg. Finalmente, la agrupación de las muestras fue llevada a cabo empleando el análisis estadístico multivariado (PCA), después de haber evaluado el papel de los elementos mayoritarios y traza en la discriminación entre los diferentes tipos de roca.

2.2.5. Control de la calidad de los análisis

La calibración del pED-XRF tuvo que ser optimizada para el análisis de muestras pulverizadas. En este apartado se presentan los datos obtenidos en los CRM NIM-GBW07408 (Soil) (GBW), un suelo rico en Si y Al, y NCS DC73375 (Limestone) (DC73), un sedimento rico en Ca, ya que los morteros tienen concentraciones elementales que pueden oscilar entre estos dos CRM (Tabla 4).

Tabla 4 - Valores certificados y concentraciones obtenidas por pED-XRF en las CRM NIM-GBW07408 (Soil) y NCS DC73375 (Limestone).

Elemento	NIM-GBW07408				NCS DC73375			
	Valor certificado		Conc. obtenida (n = 30)		Valor certificado		Conc. obtenida (n = 30)	
	Promedio	DS	Promedio	DS	Promedio	DS	Promedio	DS
Al	6.31	0.08	5.32	0.32	0.36	0.03	0.50	0.10
Si	27.4	0.06	24.82	0.98	3.11	0.07	3.09	0.16
K	2.01	0.03	1.99	0.09	0.12	0.02	ND	
Ca	5.91	0.09	5.80	0.23	36.52	0.29	33.44	1.02
Ti	0.38	0.10	0.36	0.01	0.02	< 0.01	0.02	< 0.01
Fe	3.13	0.03	3.10	0.06	0.15	0.01	0.18	0.01

Nota: Concentraciones expresadas como porcentaje masa/masa. DS: desviación estándar; ND: no determinado; Conc.: concentración.

Las pruebas estadísticas sugieren que la diferencia entre las concentraciones obtenidas y los valores certificados no son significativas para K, Ca, Ti y Fe en GBW, y para el Si en DC73. Las concentraciones de Si en GBW y de Ca en DC73 quedan entre un

±10% respeto a las certificadas. La RSD está en todos los casos menor de 10% excepto para el Al (20%) y para el Ti (20%) en DC73.

Los protocolos de preparación de las muestras y de análisis, así como el control de la calidad de los análisis de ED-XRF para Ramacciotti et al. (2019b) pueden encontrarse en Lezzerini et al. (2013; 2014b). En cuanto al ICP-MS, los niveles de exactitud y la reproducibilidad de los datos sobre la muestra GBW se habían testado previamente en la tesis doctoral de Gallello (2014a). La Tabla 5 muestra en cambio las concentraciones certificadas y medidas por ICP-MS en DC73.

Las pruebas de significación sugieren que la concentración certificada y la obtenida son estadísticamente diferentes para Ba, Cr, Cu, Pb y Zn. En cuanto a los valores de referencia, los de Ho, Er y Tm se encuentran a menos que una desviación estándar respecto a las que hemos obtenido. La RSD es menor de 10% por el Sc.

Tabla 5 - Valores certificados y concentraciones obtenidas por ICP-MS en la CRM NCS DC73375 (Limestone).

Elemento	Masa (Da)	Valor certificado		Conc. obtenida (n = 4)		Elemento	Masa (Da)	Valor certificado		Conc. obtenida (n = 4)	
		M	DS	M	DS			M	DS	M	DS
La	139	2.3	0.2	2.3	0.4	Ba	138	9	2	6	4
Ce	140	4.6	0.4	4.5	0.8	Bi	209	0.03	0.01	0.03	0.02
Pr	141	0.60	0.14	0.50	0.07	Cd	111	0.02	0.01	0.027	0.016
Nd	142	1.96	0.14	2.1	0.3	Co	59	0.8	0.3	1.0	0.2
Sm	152	0.40	0.05	0.33	0.06	Cr	52	3.4	0.4	1.4	1.1
Eu	151	0.08	0.02	0.075	0.011	Cu	63	2.2	0.3	1.1	0.3
Gd	158	0.36	0.08	0.33	0.05	Li	7	4.8	1.0	4.0	1.1
Tb	159	0.05	0.010	0.052	0.011	Mn	55	28	4	26	11
Dy	162	0.28	0.07	0.26	0.07	Mo	95	0.18	0.06	0.18	0.08
Ho	165	[0.045]		0.055	0.016	Ni	60	[4]		14	3
Er	166	[0.17]		0.14	0.04	Pb	207	5	2	1.4	0.4
Tm	169	[0.024]		0.022	0.005	Sr	88	107	9	108	13
Yb	172	0.15	0.05	0.12	0.05	Tl	205	[0.03]		0.045	0.008
Lu	175	0.02	0.01	0.021	0.006	V	51	5.4	1.6	5	3
Sc	45	[0.7]		1.34	0.07	Zn	64	7	2	3.4	1.4
Y	89	1.9	0.4	1.2	0.9						

Nota: Las concentraciones están expresadas como mg/kg. Los valores entre corchetes solo sirven como referencia. M: promedio; DS: desviación estándar; Conc: concentración.

2.3. Las ánforas del Museo Arqueológico de Sagunto

En el último artículo presentado en esta tesis se expone un trabajo de desarrollo metodológico para la caracterización y el estudio de procedencia de ánforas a través de un enfoque multianalítico.

2.3.1. Arqueología y aplicaciones analíticas en materiales cerámicos

Los fragmentos de cerámica están entre los restos más comunes que pueden encontrarse durante las excavaciones y prospecciones arqueológicas. Después de haber sido durante siglos objeto de interés por parte de anticuarios y por su valor histórico artístico, posteriormente, el estudio de los tipos cerámicos antiguos ha permitido desarrollar secuencias cronológicas y determinar áreas de influencia cultural. Además, el interés se ha ampliado a aspectos relacionados con la tecnología de producción y la organización del trabajo, la función de las diferentes formas, o la difusión desde los centros productivos a través del comercio. Del mismo modo, se han empleado los datos cualitativos y cuantitativos relacionados con las piezas cerámicas también para la interpretación de dinámicas de exportación/importación, y producción local o interregional (Orton y Hughes, 2013). Las ánforas fueron los contenedores por excelencia durante la Antigüedad, principalmente de bebidas y alimentos, empleadas en particular para el transporte de media y larga distancia. Por ello, tienen un rol central en el estudio del comercio de épocas históricas entre poblaciones sobre todo en el Mediterráneo, siendo no solo una evidencia de la existencia de intercambios, si no marcadores del transporte de productos particulares (Theodore Peña, 2007; Peacock y Williams, 1991). Por este motivo los arqueólogos, empezando por los trabajos pioneros de Heinrich Dressel en el siglo XIX, han llevado a cabo exhaustivos estudios tipológicos basados en las morfologías y en las inscripciones para la identificación de las piezas (e.g.: Öniz, 2016; Opaiţ y Tsaravopoulos, 2011; Villa, 1994). Sin embargo, el límite evidente de un enfoque de tipo macroscópico es el grado de fragmentación de los restos recuperados en una excavación; además, algunos tipos de ánforas tuvieron imitaciones locales (Baklouti et al., 2018; Franco y Capelli, 2014), así que en este ejemplo concreto los métodos arqueométricos de procedencia pueden contribuir a la discriminación de las diferentes tipologías mediante las características químicas.

El análisis petrográfico y multielemental, especialmente de elementos traza, son métodos empleados ampliamente en los estudios de cerámica antigua para la identificación de inclusiones minerales características y de marcadores químicos para relacionar las producciones con determinadas regiones (Raneri et al., 2019; Vega Maeso et al., 2020; Whitbread, 2001). Además de la procedencia y la materia prima, la caracterización de la textura, de los clastos y de los minerales presentes en el cuerpo cerámico, llevada a cabo por microscopía óptica y electrónica, XRD, FT-IR o espectroscopía Raman, resulta de interés para entender la tecnología de producción de las piezas. Esto incluye el empleo de desgrasantes, y la temperatura y la atmosfera de cocción (Ceccarelli et al., 2018; Fantuzzi et al., 2016; Ostrooumov y Gogichaishvili, 2013), así como la caracterización de los revestimientos que pueden cubrir las superficies de las piezas cerámicas como engobe, vitrina y esmalte, y los pigmentos que las decoraban (Aquilia et al., 2013; Krishnan et al., 2005; Tanevska et al., 2009). Métodos basados en cromatografía se han empleados también para investigar los materiales transportados por las ánforas y los revestimientos interiores analizando los residuos orgánicos presentes (Dimitrakoudi et al., 2011; Pecci et al., 2017).

2.3.2. Desarrollo de un método multianalítico para el estudio de cerámicas antiguas

Nuestro estudio se llevó a cabo empleando fragmentos de la colección de ánforas de época Romana del Museo Arqueológico de Sagunto (Fig. 13). La colección es muy amplia y recoge restos procedentes de las muchas excavaciones efectuadas en Sagunto y su entorno, incluyendo el antiguo puerto del Grau Vell, de relevancia en las rutas comerciales de esta área del Mediterráneo ya en la época ibérica (Aranegui Gascó, 2012). De hecho, las excavaciones llevadas a cabo en este sitio han evidenciado la presencia de piezas cerámica de importación fenicia, ática, púnica y masaliota ya del VI siglo a.C. (Albelda Borrás, 2015), y alrededor de Sagunto se han localizado talleres de ánforas (Aranegui Gascó, 2010), sugiriendo el importante papel de este puerto en la costa central valenciana y su relación con la economía del área. Se eligieron unos fragmentos identificables para ser utilizados como referencias y una serie de fragmentos no clasificables. Los materiales identificados procedían de ánforas Adriáticas, Campanas, Ibero-Romanas, Marsellesas, Púnicas, Saguntinas y Tarraconenses. Hay que destacar que los fragmentos púnicos pueden ser identificados tipológicamente como originarios del estrecho de Gibraltar, o de las islas Baleares, no

habiendo sido estos últimos caracterizados químicamente antes del presente estudio. El empleo de muestras clasificadas como referencias en vez de potenciales materias primas es particularmente indicado en el caso de estudio de artefactos cerámicos. De hecho, al ser en muchos casos resultado de mezclas de materiales de diferentes orígenes, las piezas cerámicas pueden haber perdido las características químicas típicas de la materia prima (Wilson y Pollard, 2001).

Fig. 13 - Ánforas expuestas en el Museo Arqueológico de Sagunto.

El desarrollo del ensayo metodológico tenía como objetivo principal implementar un método de clasificación de fragmentos desconocidos de ánforas antiguas empleando una cantidad mínima de muestra y analizando las muestras con diferentes técnicas analíticas. Los resultados obtenidos indican que el empleo de una única técnica no es suficiente para formular hipótesis de procedencia y en algunos casos puede llegar a formular hipótesis imprecisas. De hecho, las cerámicas son materiales complejos (Wilson y Pollard, 2001) y la posibilidad de cruzar datos relacionados con las materias primas y la tecnología de producción aumenta la probabilidad de llegar a identificaciones más precisas. Las muestras fueron pulverizadas y homogenizadas por mortero de ágata antes de los análisis. Para evitar resultados erróneos, se obvió pulverizar las superficies que presentaban huellas evidentes de degradado como carbonataciones e incrustaciones. El análisis multielemental fue llevado a cabo por pED-XRF e ICP-MS, y fue utilizado para una primera clasificación de las muestras, siendo una manera relativamente eficaz de efectuar estudios de procedencia. Sin

embargo, fue también la ocasión para confrontar los resultados obtenidos por una clasificación empleando todos los elementos como marcadores de procedencia y los REE, siendo estos últimos elementos buenos marcadores de las materias primas utilizadas en las cerámicas (Baklouti et al., 2014; 2016). Para llevar a cabo los análisis de ICP-MS se empleó un método de digestión por ataque ácido similar al del sílex, dado que la matriz rica en aluminosilicatos de la cerámica requería también del empleo del HF. Además, se añadió un ataque ácido previo mediante ácido clorhídrico (HCl).

Las muestras se analizaron también por técnicas raramente empleadas para análisis de cerámica como la espectroscopía FT-IR en la región del infrarrojo cercano (FT-NIR) y la voltamperometría de partículas inmovilizadas (VIMP). Al contrario de la espectroscopía del IR medio, utilizada de manera bastante rutinaria para determinar las estructuras moleculares presentes en las cerámicas e identificar minerales marcadores de la temperatura de cocción de las materias primas, la región del NIR ha sido hasta ahora infrautilizada. Esto quizás se debe a la mayor dificultad en la identificación de los minerales debido a una resolución espectral relativamente limitada. Sin embargo, dos estudios precedentes habían revelado como la intensidad de las bandas de NIR relacionadas con agua en muestras cerámicas tiene una correlación negativa respecto a la temperatura de cocción (Bruni et al., 2001; 2018); además, algunos minerales como carbonatos y filosilicatos tienen bandas diagnósticas también en la región del NIR (Bishop et al., 2002; 2008; Clark et al., 1990). En cuanto a los análisis electroquímicos de VIMP, esta técnica aplicada a las cerámicas proporciona información relacionada con la materia prima, la atmosfera y la temperatura de cocción; sin embargo, aunque se haya utilizado en algunos trabajos para la caracterización de cerámica histórica (e.g.: Fabrizi et al., 2020; La-Torre-Riveros et al., 2019), nunca se había empleado en estudios de procedencia de ánforas.

2.3.3. Control de la calidad de los análisis

La muestra GBW07408 (Soil) puede considerarse una buena CRM para ser utilizada en el control de la exactitud y de la reproducibilidad de los datos de los protocolos analíticos empleados en los análisis de las ánforas de Sagunto, ya que en ambos los casos las matrices son ricas en aluminosilicatos, aunque tienen una cantidad en algunos casos no despreciable de calcio.

Por lo que concierne a los datos de pED-XRF, se pueden consultar la Tabla 4 y las consideraciones hechas con anterioridad[36].

En la Tabla 6 se muestran los resultados de los análisis de ICP-MS realizados en la sesión de medidas de las ánforas.

Las concentraciones promedio obtenidas y las certificadas son significativamente semejantes para La, Ce, Pr, Nd, Sm, Eu, Gd, Sc, Ba, Bi, Co, Cr, Mn, Mo, Ni, Pb, Sr, Tl, V y Zn, mientras que el valor obtenido de Li se queda entre un ±10% respeto al certificado. La RSD es menor de 10% en La, Ce, Pr, Sm, Eu, Gd, Dy, Er, Yb, Y, Ba, Bi, Cr, Li, Mn, Ni, Pb, Sr y Zn.

Tabla 6 - Valores certificados y concentraciones obtenidas por ICP-MS en la CRM NIM-GBW07408 (Soil).

Elemento	Masa (Da)	Valor certificado		Conc. obtenida (n = 2)		Elemento	Masa (Da)	Valor certificado		Conc. obtenida (n = 2)	
		M	DS	M	DS			M	DS	M	DS
La	139	36	3	33.0	1.4	Ba	138	480	23	499	17
Ce	140	66	7	64.4	1.1	Bi	209	0.3	0.04	0.32	0.02
Pr	141	8.3	0.8	7.3	0.7	Cd	111	0.13	0.02	0.32	0.17
Nd	142	32	2	31	4	Co	59	12.7	1.1	14	2
Sm	152	5.9	0.4	5.68	0.09	Cr	52	68	6	66	3
Eu	151	1.2	0.1	1.25	0.08	Cu	63	24.3	1.2	33	8
Gd	158	5.4	0.5	4.99	0.16	Li	7	35	2	31.5	0.7
Tb	159	0.89	0.08	0.73	0.09	Mn	55	650	23	689	67
Dy	162	4.8	0.4	3.84	0.13	Mo	95	1.16	0.10	2.3	0.9
Ho	165	0.97	0.08	0.72	0.10	Ni	60	31.5	1.8	33.1	0.7
Er	166	2.8	0.2	1.93	0.10	Pb	207	21	2	16.9	1.0
Tm	169	0.46	0.07	0.29	0.06	Sr	88	236	13	268	4
Yb	172	2.8	0.2	1.68	0.07	Tl	205	0.58	0.06	0.6	0.2
Lu	175	0.43	0.04	0.28	0.06	V	51	81	5	108	23
Sc	45	11.7	0.7	13	2	Zn	64	68	4	72	7
Y	89	26	2	17.9	1.2						

Nota: Concentraciones expresadas como mg/kg. Conc.: concentración; M: promedio; DS: desviación estándar.

2.3.4. Análisis de datos e identificación de las muestras no clasificadas

La estadística multivariada ha sido empleada para la evaluación de los datos de análisis multielemental y de espectroscopía FT-NIR. En ambos casos se utilizó el PCA para

---

[36] Cfr. pp. 39-40.

evaluar diferencias entre las muestras de referencia y observar cómo se agrupaban aquellas que no habían podido ser identificadas por análisis morfológico. En cuanto al estudio de los datos de análisis multielemental, los resultados de PCA fueron de interés también para evaluar el rol de los REE como marcadores de procedencia. El empleo de la estadística multivariada fue particularmente relevante en los datos de FT-IR, ya que la simple comparación de los espectros brutos no llevó a conclusiones particularmente relevantes, así que fue determinante gracias a la identificación de la región del NIR diagnóstica y a la selección de los parámetros de procesamiento de los espectros más apropiados para proporcionar datos informativos.

Al final, se realizaron una serie de pasos a través de la comparación entre las posibles clasificaciones obtenidas por las diferentes técnicas, llegando a discriminar la clase o las posibles clases de pertenencia de una pieza desconocida o a descartar clasificaciones engañosas (ver la figura 8 en Ramacciotti et al., 2020a).

3. Resultados obtenidos y posibles avances futuros

3.1. Resultados y conclusiones

El trabajo llevado a cabo en los años de doctorado ha permitido desarrollar y perfeccionar métodos para solucionar problemáticas arqueológicas a través de las técnicas propias de la química, centrándose sobre todo en el análisis multielemental y en el empleo de los elementos de las tierras raras como marcadores de procedencia. En todos los estudios los resultados obtenidos contemplan objetivos metodológicos arqueométricos y arqueológicos. Desde un punto de vista metodológico hay que destacar el papel central de los elementos de las tierras raras como marcadores de procedencia y para la discriminación entre materiales diferentes. En cada trabajo se han explorado las potencialidades de este grupo de elementos para solucionar cuestiones arqueológicas, proponiendo métodos para procesar los resultados analíticos empleando técnicas de estadística multivariada.

3.1.1. El sílex

Considerados como un conjunto, los trabajos de caracterización sobre sílex (Ramacciotti et al., 2019a; 2022) han demostrado la posibilidad de discriminar diferentes fuentes de materia prima de la Comunidad Valenciana a través del análisis

multielemental, y ofrecen datos que pueden ser utilizados en estudios de procedencia sobre una gran cantidad de elementos relacionados con afloramientos que, hasta la fecha, o no se habían caracterizado arqueometricamente o lo habían sido mediante criterios de muestreo metodológicamente cuestionables.

Desde este punto de vista, en el trabajo sobre el sílex del valle del Serpis (Ramacciotti et al., 2019a) se ha caracterizado un conjunto de muestras numéricamente relevante de sílex del sistema Prebético perteneciente a diferentes formaciones y relacionado con un área que reúne yacimientos importantes del Paleolítico Medio (Cova del Salt, Abric del Pastor, Cova Beneito), del Paleolítico Superior (Cova Beneito), del Mesolítico (Abric de la Falguera, Benámer), y del Neolítico (Abric de la Falguera, Cova de la Sarsa, Cova de l'Or, Mas d'Is, Benámer). El trabajo propone un enfoque metodológico para llevar a cabo estudios de procedencia a través del análisis multielemental. Un aspecto central del trabajo es la separación entre el córtex y la parte interna que ha evidenciado las diferencias en los niveles elementales de las dos partes en las muestras de sílex analizadas. Por lo que concierne a los elementos mayoritarios, en los tres tipos de sílex el córtex ha resultado tener concentraciones menores de Si, quizás debido a diferentes niveles de substitución de la sílice en el sedimento original en las áreas más exteriores de la roca o a la lixiviación de los polimorfos del dióxido de silicio menos estables, y mayores de otros, en particular del Ca. En cambio, el Na se encuentra en concentraciones más altas en el núcleo, posiblemente por fenómenos de diagénesis (Murray, 1994). En cuanto a los elementos traza, las partes corticales tienen concentraciones superiores de la mayoría de estos elementos. En particular, el córtex parece tener niveles más altos de Sr y Ba, probablemente debido a la mayor presencia de carbonatos. Por lo que concierne los REE, los análisis han evidenciado diferentes concentraciones de estos elementos y, en algunos casos, fenómenos de fraccionamiento que podrían ser explicados por procesos geoquímicos ocurridos durante la formación de la roca o por la meteorización. La diferencia de niveles elementales entre las dos partes de las muestras ha sido confirmada también a través de la estadística multivariada empleando el PCA. Como consecuencia se han señalado posibles problemas de fiabilidad de los resultados del análisis multielemental debido al modo de proceder a la hora de analizar este tipo de material. Una atención particular debe prestarse en el momento de interpretar los datos de análisis directos que incluyan

porciones de roca limitadas y superficiales como los de pED-XRF o de LA-ICP-MS sobre materiales arqueológicos, un enfoque que en los últimos años se ha ido afirmando cada vez más. En el artículo se ha propuesto también un conjunto de variables (concentraciones de Al, Ti, Fe y REE, y índices de fraccionamiento de los REE) para llevar a cabo la discriminación entre los tres diferentes tipos de sílex muestreados en el valle del Serpis utilizando PCA y análisis de *cluster*, y los datos obtenidos procesando las concentraciones del núcleo de la roca se han revelado buenos marcadores de procedencia, mientras que la discriminación resulta más problemática empleando los de córtex.

En el segundo trabajo (Ramacciotti et al., 2022) se ha llevado a cabo el primer estudio de procedencia sobre artefactos líticos del yacimiento prehistórico de Cueva de la Cocina (Dos Aguas, Valencia), Con ocupaciones del Mesolítico Geométrico, el Neolítico y la Edad del Bronce. Como hemos comentado previamente, entre las piezas arqueológicas seleccionadas como muestras se habían identificado algunas que tenían características macroscópicas que sugerían la posible presencia de tipos de sílex no locales como el sílex Domeño y de sílex Serreta melado procedente del Valle del Serpis. De este modo, la caracterización química del sílex procedente de las diferentes fuentes de materia prima ha sido fundamental para poder abordar una primera aproximación a los estudios de procedencia. En un primer PCA se han confrontado las rocas de los afloramientos locales, las muestras de sílex Domeño muestreadas en Andilla y los artefactos. Este PCA ha mostrado que hay diferencias en los niveles elementales de las rocas de los afloramientos más cercanos a la cueva, aunque pertenezcan a la misma formación geológica: en particular entre el afloramiento inmediato de La Canal, a unos cientos metros de la cueva, y los dos afloramientos locales de La Paridera (~6 km) y de Real de Montroy (~15 km). Además, este tipo de sílex ha podido ser diferenciado del de Domeño. Los REE, incluyendo Sc e Y, se han revelado entre las variables más importantes para poder discriminar entre las diversas materias primas. Este primer análisis estadístico exploratorio ha permitido observar también que algunos de los artefactos analizados tenían características químicas diferentes de la roca local. Un segundo PCA ha sido llevado a cabo empleando solo los marcadores más efectivos (i.e., REE incluyendo Y e Sc) e introduciendo también las muestras de sílex Serreta analizadas en el trabajo precedente (Ramacciotti et al.,

2019a). Este segundo PCA ha evidenciado que, basado en los niveles de tierras raras, se podían distinguir por lo menos tres grupos de materias primas: proximal (La Canal), local (La Paridera y Real de Montroy) y no local (sílex Domeño y sílex Serreta). Para explorar de manera más detallada estos resultados, y la relación entre los artefactos y las diferentes fuentes potenciales de abastecimiento se empleó un modelo clasificatorio basado en las puntuaciones del PCA como variables y los tres grupos citados como clases. A través de la validación cruzada se verificó la oportunidad de emplear un modelo de QDA ya que estimaba una mayor exactitud empleando un modelo más sencillo (o sea con un menor número de variables) respeto al análisis discriminante lineal. Los resultados del QDA han confirmado que la mayoría de los artefactos arqueológicos tenía niveles de REE compatibles con las muestras de los depósitos más cercanos a la cueva y, sobre todo, con el sílex de La Canal. Aunque las inferencias hayan sido limitadas por el empleo de piezas arqueológicas de las cuales no se conocían las unidades estratigráficas de procedencia, una presencia más notable de material local es coherente con lo que se ha observado en otros asentamientos Mesolíticos de la Comunidad Valenciana (Martí Oliver et al., 2009) y con lo que sugiere el análisis macroscópico del sílex de Cueva de la Cocina (García Puchol, 2005). La presencia de sílex procedente de afloramientos alóctonos situados hacia el sur (Serreta) y el norte (Domeño) resulta de interés para explorar hipótesis iniciales sobre los patrones de movilidad que puede tener también una lectura distinta en relación con la amplia diacronía de las ocupaciones de la cueva (Martí Oliver et al., 2009).

3.1.2. Los materiales de construcción

Los análisis de los morteros de Sagunto (Ramacciotti et al., 2018) han confirmado la fiabilidad del método basado en análisis de REE para identificar fases constructivas pertenecientes a diferentes épocas históricas y así desarrollar un método de cronología indirecta testado por primera vez en el Castillo de Sagunto (Gallello et al., 2017). Se ha también demostrado la posibilidad de utilizar los morteros para llevar a cabo estudios de fases constructivas en un área más amplia que incluya diferentes monumentos o sitios arqueológicos. Más en detalle, el análisis de los datos ha evidenciado que por las muestras del área del circo romano los niveles de tierras raras están correlacionado positivamente con la concentración de aluminio y negativamente

con la de calcio, sugiriendo que la contribución de REE en los morteros está probablemente conectada con las impuridades de la caliza empleada para la producción de la cal o con la fracción de agregado. De todas formas, los resultados obtenidos de los morteros de la excavación de emergencia cerca de la estación de trenes de Sagunto no han evidenciado correlaciones claras para efectuar interpretaciones de este tipo, quizás debido a alguna diferencia en la receta empleada para su manufacturación. El estudio quimiométrico para llevar a cabo la reconstrucción de las fases constructivas ha mostrado que los morteros de cal de ambos contextos de excavación tienen niveles de tierras raras similares a los de las mamposterías de época romano imperial del castillo y del circo, sugiriendo la pertenencia de estas estructuras a este periodo histórico y, por lo que concierne las estructuras de la plaza porticada, confirmando la datación sugerida por los datos arqueológicos y las fuentes epigráficas (Ferrer-Maestro et al., 2020). Esta conclusión está corroborada también por el análisis estadístico llevado a cabo por PLS-DA que excluye la presencia de morteros de cal de la fase islámica en las dos áreas de excavación.

En cuanto a los sillares de roca carbonatada del Castillo de Sagunto (Ramacciotti et al., 2019b), desde un punto de vista metodológico, los resultados obtenidos han validado el protocolo analítico mínimamente invasivo que se había planteado debido a las condiciones de conservación del conjunto monumental. Los análisis de XRD y de XRF muestran la presencia de diferentes tipos de rocas en la serie calcita-dolomita que van de la caliza pura a la dolomía ligeramente calcítica. En cambio, las rocas de las dos canteras localizadas en la colina del castillo fueron clasificadas entre la caliza dolomítica y la dolomía ligeramente calcítica. El empleo del PCA utilizando como variables una serie de marcadores geoquímicos que incluyen las tierras raras ha confirmado las observaciones precedentes poniendo en evidencia la presencia de dos grupos principales de materiales: de un lado los sillares de caliza dolomítica y dolomía, cuyas características químicas son compatibles con las de las rocas que afloran en las dos canteras, del otro los sillares de caliza, procedentes de una o más canteras diferentes de las primeras, aunque posiblemente locales. Los datos obtenidos gracias a los análisis de los sillares han mostrado que en muchas estructuras se pueden encontrar las rocas de los dos grupos. Si comparamos los mismos con los de los morteros de Gallello et al. (2017), se confirma la complejidad de la historia

constructiva del Castillo de Sagunto. Sin embargo, se ha podido observar que los sillares de caliza aparecen sobre todo en los edificios de época romano imperial, así como en edificios de época romano republicana. Su presencia en edificios posteriores como la estructura islámica llamada "Puerta Islámica" y otra cercana "Muro Moderno" podría explicarse por la reutilización de materiales, o por la explotación de las mismas canteras en periodos diferentes. Rocas similares a las que afloran en las canteras de la colina se han encontrado en mamposterías que parecían pertenecer a la época republicana, como la de una estructura perteneciente a un alzado del foro republicano llamada "Muro Republicano", sugiriendo una posible explotación también en esta fase o intervenciones en las estructuras que no se habían detectado en el trabajo sobre los morteros. El empleo de una cantera ciudadana en época romana se ha observado también en otros centros (Gutiérrez García-M., 2011); sin embargo, estas rocas parecen más frecuentes en muros cuyos morteros habían evidenciado la presencia de fases posteriores, como los de la Torre de Plaza de los Estudiantes o de la Torre de la Moneda, quizás debido a una mayor explotación de esta materia prima en épocas posteriores a la romana.

3.1.3. Las ánforas

El trabajo realizado sobre las ánforas del Museo de Sagunto (Ramacciotti et al., 2020a) está más orientado al desarrollo metodológico y a la prueba de técnicas para caracterizar pastas cerámicas como el FT-NIR y la VIMP y la comparación de los resultados con el análisis multielemental que es un enfoque más utilizado.

Los niveles de tierras raras procesados por PCA han permitido definir agrupaciones relacionadas con la concentración total de estos elementos, más alta en las ánforas campanas coherentemente con investigaciones anteriores (Grifa et al., 2019) y quizás debido al empleo de fragmentos de rocas volcánicas como desgrasante observado en otras cerámicas procedente de la zona (Belfiore et al., 2014), y también con el fraccionamiento de LREE y HREE. Además, los resultados de análisis multielemental han definido la presencia de elementos marcadores de procedencia, en particular para la distinción de las ánforas púnicas producidas en la Baleares y las del estrecho de Gibraltar, ricas en Sr y Ca quizás relacionados con el uso de materiales calcáreos como desgrasante (Maniatis et al., 1984). Un número mayor de muestras tendría que ser

analizado para confirmar este dato. Los resultados de FT-NIR procesados por PCA han señalado la presencia de temperaturas de cocción variables también en las mismas tipologías de ánforas, así como diferencias conectadas probablemente con los minerales presentes en el cuerpo cerámico, aunque la interpretación de este dato resulte difícil debido a la resolución de la técnica empleada y a la complejidad del material. Tanto la espectroscopía de infrarrojo como los análisis electroquímicos han puesto en evidencia agrupaciones entre tipologías de ánforas que pueden complementar los resultados del análisis multielemental.

La clasificación de los fragmentos de procedencia desconocida se llevó a cabo cruzando los resultados de los tres tipos de analíticas. En particular, se ha podido observar que en algunos casos la clasificación efectuada por el análisis multielemental podía ser refinada a través de las obtenidas FT-NIR y por VIMP, confirmando la efectividad y utilidad de las dos técnicas para este tipo de estudio, mientras que en otros las diferentes técnicas han proporcionado clasificaciones incoherentes. Este hecho sugiere la inconsistencia de un enfoque basado en un solo método en el momento de efectuar estudios de procedencia sobre conjuntos cerámicos complejos como el de las ánforas de Sagunto, ya que podría proporcionar datos que lleven a desarrollar interpretaciones poco fiables.

3.2. Propuestas de futuro

Los estudios llevados a cabo y los resultados obtenidos han ofrecido herramientas complementarias para seguir avanzando en la investigación sobre la caracterización de materiales líticos.

Uno de los objetivos futuros consiste en dar continuidad a la línea iniciada en relación con la caracterización de los recursos silíceos en las comarcas centrales y meridionales valencianas. De hecho, el trabajo de Molina Hernández (2016) ha evidenciado una riqueza de depósitos de materias primas y de tipos de sílex que no han sido cubiertos en los análisis de Ramacciotti et al. (2019a). De manera similar, los resultados de los análisis del sitio de la Cueva de la Cocina señalan la presencia de rocas procedentes de fuentes todavía desconocidas y los mapas geológicos de esta área de la Cordillera

Ibérica indican la existencia de sílex del Triásico, del Jurásico Inferior[37] y del Tardo Cretácico - Paleoceno (García Velez et al., 1980b; Lendínez González y Tena-Dávilaz Ruiz, 1980) cuyos afloramientos no pudieron ser identificados y muestreados. Prospecciones de campo futuras deberían contemplar el objetivo de encontrar y muestrear afloramientos de cada tipología de sílex para proceder a su caracterización. Otro aspecto que será abordado es el análisis de piezas arqueológica de Cueva de la Cocina procedentes de unidades estratigráficas conocidas y representativas de las diferentes fases de ocupación. De hecho, aunque el empleo de piezas descontextualizadas constituye un paso necesario para una primera aproximación al problema, ha limitado la posibilidad de formular conclusiones arqueológicas significativas dejando abiertas muchas cuestiones.

En cuanto a los materiales de construcción, continúan abiertas cuestiones de tecnología de producción y de materia prima. Por lo que concierne a los morteros, el método empleado en Gallello et al. (2017) y Ramacciotti et al. (2018), aunque se haya revelado eficaz para solucionar cuestiones relativas a las fases constructivas, no es adecuado para entender los procesos de producción y tendrían que llevarse a cabo analíticas para la caracterización por separados de las fracciones de aglutinante y de agregado. En cuanto a los sillares, aunque se haya identificado la probable fuente de las rocas carbonatadas magnesiana, no se ha podido identificar la fuente de la caliza. Será probablemente necesario llevar a cabo prospecciones para buscar canteras en el entorno inmediato de Sagunto y muestrear por lo menos los diferentes tipos de caliza que afloran en el entorno. Además, dados los resultados alentadores del test sobre los morteros (Ramacciotti et al., 2018), podría ser útil montar una base de datos relacionados con los materiales del castillo para apoyar el estudio de estructuras encontradas durante las excavaciones en la ciudad. Por lo que concierne a las ánforas, la propuesta metodológica que se hizo en Ramacciotti et al. (2020a) tendría que ser probada a través del análisis de un conjunto de muestras más amplio. Además, podría ser de interés arqueológico llevar a cabo la caracterización de las ánforas púnicas de diferente origen, ya que parece que se puedan distinguir debido a concentraciones elementales.

---

[37] El sílex Domeño pertenece a niveles sedimentarios del Jurásico Medio (Eixea et al., 2014).

La cuestión de la caracterización de un número de muestras significativo es necesaria para llevar a cabo análisis de datos más robustos, por esto es importante desarrollar métodos eficaces con análisis directos no destructivos o microdestructivos sobre muestras intactas de interés arqueológico. Por lo que concierne el sílex, sería oportuno probar la LA-ICP-MS para desarrollar un método basado en los REE como el que se ha utilizado en los dos trabajos de esta tesis; en particular, sería de interés efectuar mapeos elementales para profundizar en los límites de la técnica de manera similar a lo que se ha realizado con el sílex del valle del Serpis (Ramacciotti et al., 2019b). Ya se está trabajando sobre el tema de los métodos no destructivo experimentando enfoques multianalíticos con pED-XRF, y espectrómetros Raman y FT-IR portátiles tanto en laboratorio (Lezzerini et al., 2021; Ramacciotti et al., 2021) como en museo (Vadillo Conesa et al., 2021). De particular interés resulta el empleo de datos de colorimetría obtenidos por espectrofotometría en la región de la luz visible y por análisis de imagen empleando fotos de smartphone. De hecho, el empleo de los smartphones como herramientas analíticas ha demostrado resultados relevantes en varias ramas de la química (Rezazadeh et al., 2019), pero su potencialidad en la ciencia arqueológica queda todavía por explorar. Creemos que se trata de un campo novedoso que merece ser desarrollado, siendo el smartphone un instrumento potencialmente muy rápido, económico y al alcance de cualquier laboratorio de arqueología. Enfoques de este tipo se están probando por primera vez sobre pinturas experimentales para ver las interacciones entre diferentes cantidades de pigmento, aglutinantes y soportes de roca carbonatadas, en los artefactos silíceos procedentes del Abrigo de la Calvera (Camaleño) para diferenciar entre materias primas (Ramacciotti et al., 2021) y también con muestras de morteros de la Torre Islámica de Silla (Valencia) y del Castillo de Fuengirola (Malaga) para discriminar entre fases constructivas (Lezzerini et al., 2021). En todos los casos los enfoques propuestos, en particular los resultados de *imaging*, están dando resultados muy prometedores que serán publicados en breve.

Referencias bibliográficas

Adam, J.-P. (2002). *La construcción romana: materiales y técnicas*. Editorial de los Oficios.

Al Sekhaneh, W., Shiyyab, A., Arinat, M., y Gharaibeh, N. (2020). Use of FTIR and thermogravimetric analysis of ancient mortar from The Church of the Cross in Gerasa (Jordan) for conservation purposes. *Mediterranean Archaeology and Archaeometry*, 20(3), 159-174. doi:10.5281/zenodo.4016073

Albelda Borrás, V. (2015). El Grau Vell (Sagunt). Una salida al mar en el norte de la Edetania. *SAGVNTVM*, No. Extra 17, 89-98.

Antonelli, F., y Lazzarini, L. (2015). An updated petrographic and isotopic reference database for white marbles used in antiquity. *Rendiconti Lincei*, 26(4), 399-413. doi:10.1007/s12210-015-0423-4

Aquilia, E., Barbera, G., Barone, G., Crupi, V., Longo, F., Majolino, D., Mazzoleni, P., y Venuti, V. (2013). Combined XRF-SEM analysis of varnished pottery: the case of Syracuse and Adrano (Sicily) archaeological finds. *X-Ray Spectrometry*, 42(1), 38-44. doi:10.1002/xrs.2432

Aquino, A., Pagnotta, S., Polese, S., Tamponi, M., y Lezzerini, M. (2020). Panchina Calcarenite: A Building Material from Tuscany Coast. *IOP Conference Series: Earth and Environmental Science*, 609, 012077. doi:10.1088/1755-1315/609/1/012077

Aranegui Gascó, C. (1984). La cisterna del flanco septentrional del foro de Saguntum. *SAGVNTVM*, 18, 195-203. doi:10.7203/SAGVNTVM.18.5300

Aranegui Gascó, C. (2010). Ocupación económica, ritual y estratégica del litoral valenciano. *Mainake*, 32, 689-704.

Aranegui Gascó, C. (2012). Saguntum (Sagunto). In Bagnall, R.S., Brodersen, K., Champion, C.B., Erskine, A., y Huebner, S.R. (Eds.), *The Encyclopedia of Ancient History* (2 pp.). Wiley. doi:10.1002/9781444338386.wbeah16130

Aranegui Gascó, C. (2014). Saguntum. In Olcina Domènech, M.H. (Ed.), *Ciudades Romanas Valencianas* (pp. 107-122). MARQ-Museo Arqueológico de Alicante.

Aranegui Gascó, C., Hernández, E., López Piñol, M., Mantilla, A., y Olcina, M. (1986). El edificio NE del foro de Sagunto. *Archivo Español de Arqueología*, 59(153), 47-66.

Arrizabalaga, I., Gómez-Laserna, O., Aramendia, J., Arana, G., y Madariaga, J.M. (2014). Applicability of a diffuse reflectance infrared Fourier transform handheld spectrometer to perform in situ analyses on cultural heritage materials. *Spectrochimica Acta Part A: Molecular and Biomolecular Spectroscopy*, 129, 259-267. doi:10.1016/j.saa.2014.03.096

Aura Tortosa, J.E., Gallello, G., Roldán, C., Cavallo, G., Pastor, A., y Murcia-Mascarós, S. (2020). Characterization and sources of Paleolithic–Mesolithic ochre from Coves de Santa Maira (Valencian Region, Spain). *Geoarchaeology - An International Journal*, 36(1), 72-91. doi:10.1002/gea.21821

Azkarate, A. (2020). Archaeology of architecture: buildings archaeology. En Orser Jr., C.E., Zarankin, A., Funari, P.P.A., Lawrence, S., y Symonds, J. (Eds.), *The Routledge Handbook of Global Historical Archaeology* (pp. 517-536). Routledge.

Baklouti, S., Maritan, L., Ouazaa, N.L., Casas, L., Joron, J.L., Kassaa, S.L., y Moutte, J. (2014). Provenance and reference groups of African Red Slip ware based on statistical analysis of chemical data and REE. *Journal of Archaeological Science*, 50, 524-538. doi:10.1016/j.jas.2014.08.003

Baklouti, S., Maritan, L., Casas, L., Ouazaa, N.L., Jàrrega, R., Prevosti, M., Mazzoli, C., Fouzaï, B., Larabi Kassaa, S., y Fantar, M. (2016). Establishing a new reference group of Keay 25.2 amphorae from Sidi Zahruni (Nabeul, Tunisia). *Applied Clay Science*, 132, 140-154. doi:10.1016/j.clay.2016.05.027

Baklouti, S., Maritan, L., Duocastella, L.C., Járrega, R., Prevosti, M., Mazzoli, C., y Ouazaa, N.L. (2018). Archaeometric study of African Keay 25.2 amphorae in Catalonia (Spain): a history of importation and imitation. *European Journal of Mineralogy*, 30(4), 759-772. doi:10.1127/ejm/2018/0030-2754

Barca, D., Belfiore, C.M., Crisci, G.M., La Russa, M.F., Pezzino, A., y Ruffolo, S.A. (2010). Application of laser ablation ICP-MS and traditional techniques to the study

of black crusts on building stones: a new methodological approach. *Environmental Science and Pollution Research*, 17(8), 1433-1447. doi:10.1007/s11356-010-0329-8

Belfiore, C.M., La Russa, M.F., Barca, D., Galli, G., Pezzino, A., Ruffolo, S.A., Viccaro, M., y Fichera, G.V. (2014). A trace element study for the provenance attribution of ceramic artefacts: the case of Dressel 1 amphorae from a late-republican ship. *Journal of Archaeological Science*, 43, 91-104. doi:10.1016/j.jas.2013.12.015

Benedito Nuez, J. (2015). Las infraestructuras viarias de Saguntum en época imperial. *Potestas: Religión, poder y monarquía. Revista del Grupo Europeo de Investigación Histórica*, 8, 9-35. doi: 10.6035/Potestas.2015.8.1

Bersani, D., y Lottici, P.P. (2016). Raman spectroscopy of minerals and mineral pigments in archaeometry. *Journal of Raman Spectroscopy*, 47(5), 499-530. doi:10.1002/jrs.4914

Bersani, D., y Madariaga, J.M. (2012). Applications of Raman spectroscopy in art and archaeology. *Journal of Raman Spectroscopy*, 43(11), 1523-1528. doi:10.1002/jrs.4219

Berthonneau, J., Bromblet, P., Cherblanc, F., Ferrage, E., Vallet, J. M., y Grauby, O. (2016). The spalling decay of building bioclastic limestones of Provence (South East of France): From clay minerals swelling to hydric dilation. *Journal of Cultural Heritage*, 17, 53-60. doi:10.1016/j.culher.2015.05.004

Binder, D. (2000). Mesolithic and Neolithic interaction in southern France and northern Italy: new data and current hypotheses. En Douglas Price, T. (Ed.), *Europe's First Farmers* (pp. 117-143). Cambridge University Press. doi:10.1017/CBO9780511607851.006

Bishop, J.L., Lane, M.D., Dyar, M.D., y Brown, A.J. (2008). Reflectance and emission spectroscopy study of four groups of phyllosilicates: smectites, kaolinite-serpentines, chlorites and micas. *Clay Minerals*, 43, 35-54. doi:10.1180/claymin.2008.043.1.03

Bishop, J.L., Murad, E., y Dyar, M.D. (2002). The influence of octahedral and tetrahedral cation substitution on the structure of smectites and serpentines as observed

through infrared spectroscopy. *Clay Minerals*, 37(4), 617-628. doi:10.1180/0009855023740064

Borrell, F., Bosch, J., Gibaja, J.F., Schmidt, P., y Terradas, X. (2019). The status of imported Barremian-Bedoulian flint in north-eastern Iberia during the Middle Neolithic. Insights from the variscite mines of Gavà (Barcelona). *PLOS ONE*, 14(11), e0224238. doi: 10.1371/journal.pone.0224238

Botto, A., Campanella, B., Legnaioli, S., Lezzerini, M., Lorenzetti, G., Pagnotta, S., Poggialini, F., y Palleschi, V. (2019). Applications of laser-induced breakdown spectroscopy in cultural heritage and archaeology: a critical review. *Journal of Analytical Atomic Spectrometry*, 34(1), 81-103. doi:10.1039/C8JA00319J

Boulanger, M.T., Buchanan, B., O'Brien, M.J., Redmond, B.G., Glascock, M.D., y Eren, M.I. (2015). Neutron activation analysis of 12,900-year-old stone artifacts confirms 450–510+ km Clovis tool-stone acquisition at Paleo Crossing (33ME274), northeast Ohio, U.S.A. *Journal of Archaeological Science*, 53, 550-558. doi:10.1016/j.jas.2014.11.005

Bradley, S., Cummings, V., y Baker, M.J. (2020). Sources of flint in Britain and Ireland: A quantitative assessment of geochemical characterisation using acid digestion inductively coupled plasma-mass spectrometry (ICP-MS). *Journal of Archaeological Science: Reports*, 31, 102281. doi:10.1016/j.jasrep.2020.102281

Brogiolo, G.P. (2007). Dall'Archeologia dell'architettura all'Archeologia della complessità. *Pyrenae*, 38(1), 7-38.

Bruni, S., Cariati, F., Bagnasco Gianni, G., Bonghi Jovino, M., Artioli, G., y Russo, U. (2001). Spectroscopic characterization of Etruscan depurata and impasto pottery from the excavation at Pian di Civita in Tarquinia (Italy): A comparison with local clay. En Druc, I.C. (Ed.), *Archaeology and Clays*, 942. British Archaeological Reports Ltd.

Bruni, S., Guglielmi, V., Della Foglia, E., Castoldi, M., y Gianni, G.B. (2018). A non-destructive spectroscopic study of the decoration of archaeological pottery: from matt-painted bichrome ceramic sherds (southern Italy, VIII-VII BC) to an intact Etruscan

cinerary urn. *Spectrochimica Acta Part A: Molecular and Biomolecular Spectroscopy*, 191, 88-97. doi:10.1016/j.saa.2017.10.010

Bustillo, M.A., Castañeda, N., Capote, M., Consuegra, S., Criado, C., Díaz-Del-Río, P., Orozco, T., Pérez-Jiménez, L., y Terradas, X. (2009). Is the macroscopic classification of flint useful? A petroarchaeological analysis and characterization of flint raw materials from the Iberian Neolithic mine of Casa Montero. *Archaeometry*, 51(2), 175-196. doi:10.1111/j.1475-4754.2008.00403.x

Cagnana, A. (2000). *Archeologia dei materiali da costruzione*. Editrice S.A.P.

Cantisani, E., Calandra, S., Barone, S., Caciagli, S., Fedi, M., Garzonio, C.A., Liccioli, L., Salvadori, B., Salvatici, T., y Vettori, S. (2021). The mortars of Giotto's Bell Tower (Florence, Italy): raw materials and technologies. *Construction and Building Materials*, 267, 120801. doi:10.1016/j.conbuildmat.2020.120801

Caravá, S., Roldán García, C., Vázquez de Agredos-Pascual, M.L, Murcia Mascarós, S., y Izzo, F.C. (2020). Investigation of modern oil paints through a physico-chemical integrated approach. Emblematic cases from Valencia, Spain. *Spectrochimica Acta Part A: Molecular and Biomolecular Spectroscopy*, 240, 118633. doi:10.1016/j.saa.2020.118633

Cebrián Fernández, R. (2017). Nuevas aportaciones al estudio del foro de Saguntum. Las excavaciones de W.B. Conyngham en 1784. *SAGVNTVM*, 49, 123-143. doi:10.7203/SAGVNTVM.49.10389

Ceccarelli, L., Bellotto, M.P., Caruso, M., Cristiani, C., Dotelli, G., Stampino, P.G., Gasti, G., y Primavesi, L. (2018). Characterization of clays and the technology of Roman ceramics production. *Clay Minerals*, 53(3), 413-429. doi:10.1180/clm.2018.30

Chatzimpaloglou, P. (2020). A geoarchaeological methodology for sourcing chert artefacts in the Mediterranean region: A case study from Neolithic Skorba on Malta. *Geoarchaeology - An International Journal*, 35(6), 897-920. doi:10.1002/gea.21813

Chiarelli, N., Miriello, D., Bianchi, G., Fichera, G., Giamello, M., y Turbanti Memmi, I. (2015). Characterisation of ancient mortars from the S. Niccolò archaeological

complex in Montieri (Tuscany – Italy). *Construction and Building Materials*, 96, 442-460. doi:10.1016/j.conbuildmat.2015.08.023

Clark, R.N., King, T.V., Klejwa, M., Swayze, G.A., y Vergo, N. (1990). High spectral resolution reflectance spectroscopy of minerals. *Journal of Geophysical Research: Solid Earth*, 95(B8), 12653-12680. doi:10.1029/JB095iB08p12653

Clarkson, C. (2008). Lithics and Landscape Archaeology. En David, B., y Thomas, J. (Eds.), *Handbook of Landscape Archaeology* (pp. 490-501). Routledge. doi:10.4324/9781315427737

Corti, C., Rampazzi, L., Bugini, R., Sansonetti, A., Biraghi, M., Castelletti, L., Nobile, I., y Orsenigo, C. (2013). Thermal analysis and archaeological chronology: The ancient mortars of the site of Baradello (Como, Italy). *Thermochimica Acta*, 570, 71-84. doi:10.1016/j.tca.2013.08.015

Crisci, G.M., Franzini, M., Lezzerini, M., Mannoni, T., y Riccardi, M.P. (2004). Ancient mortars and their binder. *Periodico di Mineralogia*, 73(3), 259-268.

Daugbjerg, T.S., Lindroos, A., Heinemeier, J., Ringbom, Å., Barrett, G., Michalska, D., Hajdas, I., Raja, R., y Olsen, J. (2021). A field guide to mortar sampling for radiocarbon dating. *Archaeometry*, 63(5), 1121-1140. doi:10.1111/arcm.12648

Delage, C. (2003). *Siliceous Rocks and Prehistory: Bibliography on Geo-Archaeological Approaches to Chert Sourcing and Prehistoric Exploitation*. John and Erica Hedges. doi:10.30861/9781841713427

Delluniversità, E., Muntoni, I.M., Allegretta, I., Tarantini, M., Monno, A., Maiorano, P., Girone, A., Morsilli, M., Terzano, R., y Eramo, G. (2019). Development of a multiparametric characterisation protocol for chert investigation and application on the Gargano Promontory mines. *Archaeological and Anthropological Sciences*, 11, 6037-6063. doi:10.1007/s12520-019-00875-8

Dessales, H. (2017). The archaeology of construction: a new approach to Roman architecture. Annales. *Histoire, Sciences Sociales - English Edition*, 72(1), 69-86. doi:10.1017/ahsse.2019.6

Dimitrakoudi, E.A., Mitkidou, S.A., Urem-Kotsou, D., Kotsakis, K., Stephanidou-Stephanatou, J., y Stratis, J.A. (2011). Characterization by Gas Chromatography—Mass Spectrometry of Diterpenoid Resinous Materials in Roman-Age Amphorae from Northern Greece. *European Journal of Mass Spectrometry*, 17(6), 581-591. doi:10.1255/ejms.1155

Doménech-Carbó, A., Doménech-Carbó, M.T., y Costa, V. (2009). *Electrochemical methods in archaeometry, conservation and restoration*. Springer. doi:10.1007/978-3-540-92868-3

Dussubieux, L. (2020). Inductively Coupled Plasma-Mass Spectrometry (ICP-MS): Applications in Archaeology. En Smith, C. (Ed.), *Encyclopedia of Global Archaeology* (II ed.) (pp. 5729-5734). Springer. doi:10.1007/978-3-030-30018-0_338

Eixea, A., Roldán, C., Villaverde, V., y Zilhão, J. (2014). Middle Palaeolithic flint procurement in Central Mediterranean Iberia: Implications for human mobility. *Journal of Lithic Studies*, 1(1), 103-115. doi: 10.2218/jls.v1i1.783

Eixea, A., Roldán, C., Villaverde, V., y Zilhão, J. (2016). Caracterización del sílex del Abrigo de la Quebrada (Chelva, Valencia). Resultados y valoración en el contexto Paleolítico Medio de la región central del Mediterráneo ibérico. *Cuadernos de Prehistoria Y Arqueología de la Universidad de Granada*, 26, 313-326. doi:10.30827/cpag.v26i0.7404

Elefanti, P., Marshall, G., Stergiou, C.L., y Kotjabopoulou, E. (2021). Raw material procurement at Boila Rockshelter, Epirus, as an indicator of hunter-gatherer mobility in Greece during the Late Upper Palaeolithic and Early Mesolithic. *Journal of Archaeological Science: Reports*, 35, 102719. doi:10.1016/j.jasrep.2020.102719

Emami, M., Eslami, M., Fadaei, H., Karami, H.R., y Ahmadi, K. (2018). Mineralogical-Geochemical Characterization and Provenance of the Stones Used at the Pasargadae Complex in Iran: A New Perspective. *Archaeometry*, 60(6), 1184-1201. doi:10.1111/arcm.12395

Ergenç, D., y Fort, R. (2019). Multi-technical characterization of Roman mortars from Complutum, Spain. *Measurement*, 147, 106876. doi:10.1016/j.measurement.2019.106876

Evans, A.A., Wolframm, Y.B., Donahue, R.E., y Lovis, W.A. (2007). A pilot study of "black chert" sourcing and implications for assessing hunter-gatherer mobility strategies in northern England. *Journal of Archaeological Science*, 34, 2161-2169. doi:10.1016/j.jas.2007.03.007

Fabrizi, L., Nigro, L., Cappella, F., Spagnoli, F., Guirguis, M., Niveau de Villedary y Mariñas, A.M., Doménech-Carbó, M.T., De Vito, M., y Doménech-Carbó, A. (2020). Discrimination and provenances of Phoenician Red Slip Ware using both the solid state electrochemistry and petrographic analyses. *Electroanalysis*, 32(2), 258-270. doi:10.1002/elan.201900515

Fantuzzi, L., Cau Ontiveros, M.A., y Aquilué, X. (2016). Archaeometric characterization of amphorae from the late antique city of Emporiae (Catalonia, Spain). *Archaeometry*, 58, 1-22. doi:10.1111/arcm.12176

Fernandes, P., Le Bourdonnec, F.X., Raynal, J.P., Poupeau, G., Piboule, M., y Moncel, M.H. (2007). Origins of prehistoric flints: The neocortex memory revealed by scanning electron microscopy. *Comptes Rendus Palevol*, 6(8), 557-568. doi:10.1016/j.crpv.2007.09.015

Ferrer-Maestro, J., Benedito-Nuez, J., y Melchor-Monserrat, J.M. (2020). Saguntum: The Remains of an Honorary Arch and Urban Planning Outside the City Walls. *European Journal of Archaeology*, 23(1), 43-63. doi:10.1017/eaa.2019.43

Ferris, I.M. (1989). The Archaeological Investigation of Standing Buildings. *Vernacular Architecture*, 20(1), 12-17. doi:10.1179/vea.1989.20.1.12

Fichera, G.V., Belfiore, C.M., La Russa, M.F., Ruffolo, S.A., Barca, D, Frontoni, R., Galli, G., y Pezzino, A. (2015). Limestone Provenance in Roman Lime-Volcanic Ash Mortars from the Villa dei Quintili, Rome. *Geoarchaeology - An International Journal*, 30(2), 79-99. doi:10.1002/gea.21504

Finch, W.H., y Schneider, M.K. (2006). Misclassification rates for four methods of group classification: Impact of predictor distribution, covariance inequality, effect size, sample size, and group size ratio. *Educational and Psychological Measurement*, 66(2), 240-257. doi:10.1177/0013164405278579

Flügel, E. (2010) Microfacies and Archaeology. In Flügel, E. (Ed.), *Microfacies of Carbonate Rocks*. Springer. doi:10.1007/978-3-642-03796-2_19

Fortea, J. (1973). *Los complejos microlaminares y geométricos del Epipaleolítico mediterráneo español* (Tesis doctoral). Universidad de Salamanca.

Frahm, E. (2013). Validity of "off-the-shelf" handheld portable XRF for sourcing Near Eastern obsidian chip debris. *Journal of Archaeological Science*, 40(2), 1080-1092. doi:10.1016/j.jas.2012.06.038

Frahm, E., y Doonan, R.C.P. (2013). The technological versus methodological revolution of portable XRF in archaeology. *Journal of Archaeological Science*, 40(2), 1425-1434. doi:10.1016/j.jas.2012.10.013

Franchi, F., Hofmann, A., Cavalazzi, B., Wilson, A., y Barbieri, R. (2015). Differentiating marine vs hydrothermal processes in Devonian carbonatemounds using rare earth elements (Kess Kess mounds, Anti-Atlas, Morocco). *Chemical Geology*, 409, 69-86. doi:10.1016/j.chemgeo.2015.05.006

Franco, C., y Capelli, C. (2014). New archaeological and archaeometric data on Sicilian wine amphorae in the Roman period (1st to 6th century AD). Typology, origin and distribution in selected western Mediterranean contexts. *Rei Cretariae Romanae Fautorum Acta*, 43, 547-555.

Francovich, R., y Bianchi, G. (2002). L'archeologia dell'elevato come archeologia. *Arquelogía de la arquitectura*, 1, 101-111.

Franzini, M., Lezzerini, M., y Origlia, F. (2010). Marbles from the Campiglia Marittima area (Tuscany, Italy). *European Journal of Mineralogy*, 22(6), 881-893. doi:10.1127/0935-1221/2010/0022-2056

Fratini, F., Cantisani, E., Pecchioni, E., Pandeli, E., y Vettori, S. (2020). Pietra Alberese: Building Material and Stone for Lime in the Florentine Territory (Tuscany, Italy). *Heritage*, 3(4), 1520-1538. doi:10.3390/heritage3040084

Fricker, M.B., y Günther, D. (2016). Instrumentation, Fundamentals, and Application of Laser Ablation- Inductively Coupled Plasma-Mass Spectrometry. En Dussubieux,

L., Golitko, M., y Gratuza, B. (Eds.), *Recent Advances in Laser Ablation ICP-MS for Archaeology* (pp. 1-19). Springer. doi:10.1007/978-3-662-49894-1_1

Gallello, G. (2014a). *Western Mediterranean Archaeology: chemical element levels in archaeological materials as a methodological tool* (Tesis doctoral). Universitat de València.

Gallello, G., Bernabeu, J., Díez Castillo, A., Escribá Ruiz, P., Pastor, A., Lezzerini, M., Chenery, S., Hodson, M., y Stump, D. (2020a). Developing REE parameters for soil and sediment profile analysis to identify Neolithic anthropogenic signatures at Serpis Valley (Spain). *Atti della Societa Toscana di Scienze Naturali - Memorie (Serie A)*, 126, 13-32. doi:10.2424/ASTSN.M.2019.09

Gallello, G., Ferro-Vázquez, C., Chenery, S., Lang, C., Thornton-Barnett, S., Kabora, T., Hodson, M.E., y Stump, D. (2019). The capability of rare earth elements geochemistry to interpret complex archaeological stratigraphy. *Microchemical Journal*, 148, 691-701. doi:10.1016/j.microc.2019.05.050

Gallello, G., Ghorbani, S., Pastor, A., y de la Guardia, M. (2016b). Non-destructive analytical methods to study the conservation state of Apadana Hall of Persepolis. *Science of the Total Environment*, 544, 291-298. doi:10.1016/j.scitotenv.2015.11.156

Gallello, G., Kuligowski, J., Pastor, A., Diez, A., y Bernabeu, J. (2013a). Biological mineral content in Iberian skeletal cremains for control of diagenetic factors employing multivariate statistics. *Journal of Archaeological Science*, 40(5), 2477-2484. doi:10.1016/j.jas.2013.01.022

Gallello, G., Kuligowski, G., Pastor, A., Diez, A., y Bernabeu, J. (2015). Chemical Element Levels as a Methodological Tool in Forensic Science. *Journal of Forensic Research*, 6(1), 264. doi:10.4172/2157-7145.1000264

Gallello, G., Orozco, T., Pastor, A., de la Guardia, M., y Bernabeu, J. (2016a). Regional provenance of dolerite prehistoric objects through mineral analysis. *Microchemical Journal*, 124, 167-174. doi:10.1016/j.microc.2015.08.018

Gallello, G., Pastor, A., Diez, A., y Bernabeu, J. (2014b). Lanthanides revealing anthropogenic impact within a stratigraphic sequence. *Journal of Archaeology*, Volume 2014, 767085. doi:10.1155/2014/767085

Gallello, G., Pastor, A., Diez, A., La Roca, N., y Bernabeu, J. (2013b). Anthropogenic units fingerprinted by REE in archaeological stratigraphy: Mas d'Is (Spain) case. *Journal of Archaeological Science*, 40(2), 799-809. doi:10.1016/j.jas.2012.10.005

Gallello, G., Pastor, A., y Hernández, E. (2020b). El proyecto de ArchaeChemis en el Castillo de Sagunto. *Arse*, 54, 15-32.

Gallello, G., Ramacciotti, M., García Puchol, O., Chenery, S., Cortell-Nicolau, A., Cervera, M.L., Diez-Castillo, A., Pastor, A., y McClure, S. B. (2021). Analysis of stratigraphical sequences at Cocina Cave (Spain) using rare earth elements geochemistry. *Boreas*, 50(4), 1190-1208. doi:10.1111/bor.12530

Gallello, G., Ramacciotti, M., Lezzerini, M., Hernandez, E., Calvo, M., Morales, A., Pastor, A., y de la Guardia, M. (2017). Indirect chronology method employing rare earth elements to identify Sagunto Castle mortar construction periods. *Microchemical Journal*, 132, 251-261. doi:10.1016/j.microc.2017.02.009

García Puchol, O. (2005). *El Proceso de Neolitización en la fachada mediterránea de la Península Ibérica: Tecnología y Tipología de la Piedra Tallada*. British Archaeological Reports.

García Puchol, O. (2009). La piedra tallada del neolítico en Cendres. En J. Bernabeu, y L., Molina (Eds.), *La Cova de les Cendres (Moraira-Teulada, Alicante)* (pp. 85-104). Museo Arqueológico de Alicante – MARQ

García Puchol, O., Diez Castillo, A., McClure, S.B., Juan Cabanilles, J., Pardo Gordó, S., Cortell Nicolau, A., y Escribá Ruiz, P. (2016). Cueva de la Cocina (Dos Aguas, Valencia) 2016: Intervención, metodología, resultados. *SAGVNTUM*, 48, 191-195. doi:10.7203/SAGVNTVM.48.9203

García Puchol, O., Juan Cabanilles, J., McClure, S.B., Diez Castillo, A.,y Pardo Gordó, S. (2015). Avance de resultados de los nuevos trabajos arqueológicos en Cueva

de la Cocina (Dos Aguas, Valencia): campaña de 2015. *SAGVNTUM*, 47, 251-255. doi:10.7203/SAGVNTVM.47.7195

García Puchol, O., McClure, S.B., Juan-Cabanilles, J., Diez-Castillo, A., Bernabeu, J., Martí-Oliver, B., Pardo-Gordó, S., Pascual-Benito, J.L., Pérez-Ripoll, M., Molina-Balaguer, Ll., y Kennet, D.J. (2018a). Cocina Cave revisited: Bayesian radiocarbon chronology for the last hunter-gatherers and first farmers in Eastern Iberia. *Quaternary International*, 472, 259-271. doi:10.1016/j.quaint.2016.10.037

García Puchol, O., Pardo Gordó, S., Diez Castillo, A., Cortell Nicolau, A., Juan Cabanilles, J., McClure, S. B., y Ramacciotti, M. (2018b). Actuación arqueológica en los depósitos mesolíticos de Cueva de la Cocina (Dos Aguas, Valencia): valoración preliminar. *SAGVNTVM*, 50, 249-254. doi:10.7203/SAGVNTVM.50.13273

García Velez, A., Goy Goy, J.L., Zazo Cardeña, C., y García Ruz, L. (1980a). *Memoria de la hoja no. 746 (Llombay), Mapa geológico de España E. 1:50.000. Segunda serie (MAGNA)* (I ed.). Instituto Geológico y Minero de España (IGME).

García Velez, A., Soubrier González, J., Muelas Peña, A., Goy Goy, J.L., Zazo Cardeña, C., y García Ruz, L. (1980b). *Memoria de la hoja no. 721 (Cheste), Mapa geológico de España E. 1:50.000. Segunda serie (MAGNA)* (I ed.). Instituto Geológico y Minero de España (IGME).

Gauthier, G., Burke, A.L., y Leclerc, M. (2012). Assessing XRF for the geochemical characterization of radiolarian chert artifacts from northeastern North America. *Journal of Archaeological Science*, 39(7), 2436-2451. doi:10.1016/j.jas.2012.02.019

Glaus, R., Koch, J., y Günther, D. (2012). Portable Laser Ablation Sampling Device for Elemental Fingerprinting of Objects Outside the Laboratory with Laser Ablation Inductively Coupled Plasma Mass Spectrometry. *Analytical Chemistry*, 84(12), 5358-5364. doi:10.1021/ac3008626

Goy, J.L., Gutiérrez, M., Pedraza, J., Vegas, R., y Zazo, C. (1972). *Mapa geológico de la Hoja n° 668 (Sagunto). Mapa Geológico de España E. 1:50.000, Segunda Serie (MAGNA)* (I ed.). Instituto Geológico y Minero de España.

Graetsch, H.A., y Grünberg, J.M. (2012). Microstructure of flint and other chert raw materials. *Archaeometry*, 54(1), 18-36. doi:10.1111/j.1475-4754.2011.00610.x

Grifa, C., Germinario, C., De Bonis, A., Langella, A., Mercurio, M., Izzo, F., Smiljanic, D., Guarino, V., Di Mauro, S., y Soricelli, G. (2019). Comparing ceramic technologies: the production of Terra Sigillata in Puteoli and in the Bay of Naples. *Journal of Archaeological Science: Reports*, 23, 291-303. doi:10.1016/j.jasrep.2018.10.014

Gutiérrez García-M., A. (2011). The exploitation of local stone in Roman times: the case of north-eastern Spain. *World Archaeology*, 43(2), 318-341. doi:10.1080/00438243.2011.586201

Gutiérrez Ginés, M.J.G., y Ranz, I. (2010). Utilización de un equipo portátil de fluorescencia de rayos X para el estudio de metales pesados en suelos: puesta a punto y aplicación en vertederos. En Bartolomé Esteban, C., y Hernández Sánchez, A.J. (Eds.), *Estudio multidisciplinar de vertederos sellados: caracterización y pautas de recuperación* (pp. 109-120). Editorial Universidad de Alcalá.

Hernández, E., y Aranegui, C. (1989). Estudio de las fases constructivas del foro de Saguntum. En Conselleria de Cultura, Educació i Ciència (Ed.), *Homenaje A. Chabret 1888-1988* (pp. 143-153). Generalitat Valenciana.

Hernández Hervás, E., López Piñol, M., y Pascual Buyé, I. (1995). La implantación del Circo en el área suburbana de Saguntum. *SAGVNTVM*, 29, 221-230.

Hernández, E., López, M., Pascual, I., y Aranegui, C. (1993). El teatro romano de Sagunto. En Ramallo Asensio, S.F., y Santiuste de Pablos, F. (Eds.), *Teatros romanos de Hispania* (Vol. 2, pp. 25-42). Universidad de Murcia.

Herrero-Alonso, D., Tarriño-Vinagre, A., Fernández-Martínez, E., Fuertes-Prieto, N., y Neira-Campos, A. (2021). Black chert and radiolarite: knappable lithic raw materials in the prehistory of the Cantabrian Mountains (North Spain). *Archaeological and Anthropological Sciences*, 13(7), 1-24. doi:10.1007/s12520-021-01340-1

Herrero-Alonso, D., Tarriño-Vinagre, A., Neira-Campos, A., y Fuertes-Prieto, N. (2016). Chert from the Vegamián formation: A new raw-material supply source in the

Cantabrian Mountains (NW Spain) during prehistory. *Journal of Lithic Studies*, 3(2), 1-21. doi:10.2218/jls.v3i2.1449

Herz, N. (2001). Sourcing Lithic Artifacts by Instrumental Analysis. En Goldberg, P., Holliday, V.T., y Ferring, C.R. (Eds.), *Earth Sciences and Archaeology* (pp. 449-472). Springer. doi:10.1007/978-1-4615-1183-0

Hess, S.C. (1996). Chert provenance analysis at the Mack Canyon Site, Sherman County, Oregon: An evaluative study. *Geoarchaeology - An International Journal*, 11, 51-81. doi:10.1002/(SICI)1520-6548(199601)11:1<51::AID-GEA3>3.0.CO;2-9

Hess, T., y Riede, F. (2020). The use of lithic raw materials at the Early Mesolithic open-air site Feuersteinacker (Vogelsbergkreis, Germany). *Geoarchaeology - An International Journal*, 36, 252-265. doi:10.1002/gea.21828

Högberg, A., Hughes, R.E., y Olausson, D. (2016). Chemical and visual analysis of flint from Gotland and Öland. *Fornvännen*, 3(111), 145-152.

Hohfelder, R.L., Brandon, C., y Oleson, J.P. (2007). Constructing the Harbour of Caesarea Palaestina, Israel: New Evidence from the ROMACONS Field Campaign of October 2005. *International Journal of Nautical Archaeology*, 36(2), 409-415. doi:10.1111/j.1095-9270.2007.00156.x

Hughes, R. E., Högberg, A., y Olausson, D. (2012). The chemical composition of some archaeologically significant flint from Denmark and Sweden. *Archaeometry*, 54(5), 779-795. doi:10.1111/j.1475-4754.2011.00655.x

Hurst, V.J., y Kelly, A.R. (1961). Patination of cultural flints: Flint artifacts can be dated by cortical changes in mineralogy and texture. *Science*, 134(3474), 251-256. doi:10.1126/science.134.3474.251

James, G., Witten, D., Hastie, T., y Tibshirani, R. (2013). *An introduction to statistical learning*. Springer. doi:10.1007/978-1-4614-7138-7

Kakkar, R. (2015). *Atomic and Molecular Spectroscopy: Basic Concepts and Applications*. Cambridge University Press. doi:10.1017/CBO9781107479999

Killick, D. (2015). The awkward adolescence of archaeological science. *Journal of Archaeological Science*, 56, 242-247. doi:10.1016/j.jas.2015.01.010

Krishnan, K., Freestone, I.C., y Middleton, A.P. (2005). The Technology of 'Glazed' Reserved Slip Ware–A Fine Ceramic of the Harappan Period. *Archaeometry*, 47(4), 691-703. doi:10.1111/j.1475-4754.2005.00227.x

Landry, D.B., Milne, B., y Rachel, E. (2018). Combining remote sensing, geophysics, and lithic provenance and reduction to understand long-term continuity in Paleo-Inuit chert quarrying and seasonal inland travels on southern Baffin Island, NU. *Quaternary International*, 549, 155-162. doi:10.1016/j.quaint.2018.04.021

La-Torre-Riveros, L., Doménech-Carbó, A., Cabrera, C.R., Doménech-Carbó, M.T., Huahuasoncco-Condori, W., Guzmán, D.Q., Gutíerrez-Castillo, M., Carmona-Ochoa, K., y Pérez-Trujillo, A. (2019). Solid-state electrochemical analysis of Inka pottery from Qotakalli archeological site in the Cusco (Perú) area. *Journal of Solid State Electrochemistry*, 23(5), 1541-1552. doi:10.1007/s10008-019-04243-3

Laveuf, C., y Cornu, S. (2009). A review on the potentiality of rare earth elements to trace pedogenetic processes. *Geoderma*, 154(1–2), 1-12. doi:10.1016/j.geoderma.2009.10.002

Lawrence, M.G., Greig, A., Collerson, K.D., y Kamber, B.S. (2006). Rare earth element and yttrium variability in South East Queensland waterways. *Aquatic Geochemistry*, 12(1), 39-72. doi:10.1007/s10498-005-4471-8

Lecuit, M., Fronteau, G., Boulvain, F., Dechamps, S., Eyssautier-Chuine, S., Piavaux, M., y Yans, J. (2018). Geochemical characterization of "Lorraine limestones" from the Saint-Paul Cathedral of Liège (Belgium): Assumptions for the true provenance of the building stones. *Environmental Earth Sciences*, 77, 361. doi:10.1007/s12665-018-7554-8

Lendínez González, A., y de Tena-Dávila Ruiz, M. (1980). *Mapa geológico de la Hoja n° 745 (Jalance). Mapa Geológico de España E. 1:50.000, Segunda Serie (MAGNA)* (I ed.). Instituto Geológico y Minero de España.

Lezzerini, M., Legnaioli, S., Lorenzetti, G., Palleschi, V., y Tamponi, M. (2014a). Characterization of historical mortars from the bell tower of St. Nicholas church (Pisa, Italy). *Construction and Building Materials*, 69, 203-212. doi:10.1016/j.conbuildmat.2014.07.051

Lezzerini, M., Ramacciotti, M., Cantini, F., Fatighenti, B., Antonelli, F., Pecchioni, E., Fratini, F., Cantisani, E., y Giamello, M. (2016). Archaeometric study of natural hydraulic mortars: the case of the Late Roman Villa dell'Oratorio (Florence, Italy). *Archaeological and Anthropological Sciences*, 9, 603-615. doi:10.1007/s12520-016-0404-2

Lezzerini, M., Ramacciotti, M., Gallello, G., Pagnotta, S., Aquino, A., Martín Ruiz, J.A., Perez-Malumbre Landa, A., Hiraldo Aguilera, R., Godoy Ruiz, D., Alapont Martín, Ll., Cervera Sanz, M.L., y Pastor, A. (2021). Archaeometric study of ancient mortars from Silla Islamic Tower and Fuengirola Castle (Spain) cultural heritages. En *XI congresso nazionale AIAr (Napoli 28-29-30 Luglio 2021) Abstract Book* (p. 32). Associazione Italiana di Archeometria.

Lezzerini, M., Raneri, S., Pagnotta, S., Columbu, S., y Gallello, G. (2018). Archaeometric study of mortars from the Pisa's Cathedral Square (Italy). *Measurement*, 126, 322-331. doi:10.1016/j.measurement.2018.05.057

Lezzerini, M., Tamponi, M., y Bertoli, M. (2013). Reproducibility, precision and trueness of X-ray fluorescence data for mineralogical and/or petrographic purposes. *Atti della Società Toscana di Scienze Naturali - Memorie (Serie A)*, 120, 67-73. doi:10.2424/ASTSN.M.2013.15

Lezzerini, M., Tamponi, M., y Bertoli, M. (2014b). Calibration of XRF data on silicate rocks using chemicals as in-house standards. *Atti della Società Toscana di Scienze Naturali - Memorie (Serie A)*, 121, 65-70. doi:10.24.24/ASTSN.M.2014.16

Licker, M.D. (2003). *Dictionary of Chemistry* (II ed.). McGraw-Hill.

Luedtke, B.E. (1978). Chert Sources and Trace-Element Analysis. *American Antiquity*, 43(3), 413-423. doi:10.2307/279398

Luedtke, B.E. (1979). The identification of Sources of Chert Artifacts. *American Antiquity*, 44(4), 744-757. doi:10.2307/279116

Luedtke, B.E. (1992). *An Archaeologist's Guide to Chert and Flint*. Cotsen Institute of Archaeology Press.

Luedtke, B.E. (1993). Lithic Source Analysis in New England. Bulletin of the Massachusetts. *Archaeological Society*, 54(2), 56-60.

Machado, J., Molina, F.J., Hernández, C.M., Tarriño, A., y Galván, B. (2017). Using lithic assemblage formation to approach Middle Palaeolithic settlement dynamics: El Salt Stratigraphic Unit X (Alicante, Spain). *Archaeological and Anthropological Science*, 9, 1715-1743. doi:10.1007/s12520-016-0318-z

Mahaney, R.A. (2014). Lithic Analysis as a Cognitive Science: A Framework. *Lithic Technology*, 39(3), pp. 173-189. doi:10.1179/2051618514Y.0000000005

Maniatis, Y., Jones, R.E., Whitbread, I.K., Kostikas, A., Simopoulos, A., Karakalos, C., y Williams, C.K. (1984). Punic amphoras found at Corinth, Greece: an investigation of their origin and technology. *Journal of Field Archaeology*, 11(2), 205-222. doi:10.1179/jfa.1984.11.2.205

Marra, F., y D'Ambrosio, E. (2012). Trace Element Classification Diagrams of Pyroclastic Rocks from the Volcanic Districts of Central Italy: the Case Study of the Ancient Roman Ships of Pisa. *Archaeometry*, 55(6), 993-1019. doi:10.1111/j.1475-4754.2012.00725.x

Martinón-Torres, M., y Killick, D. (2015). Archaeological theories and archaeological sciences. En Gardner, A., Lake, M., y Sommer, U. (Eds., 2013). *The Oxford Handbook of Archaeological Theory*. Oxford Handbooks Online. doi:10.1093/oxfordhb/9780199567942.013.004

Martí Oliver, B., Aura Tortosa, J.E., Juan Cabanilles, J., García Puchol, O., y Fernández López de Pablo, J. (2009). El Mesolítico geométrico de tipo" Cocina" en el País Valenciano. En Utrilla Miranda, M.P., y Montes Ramírez, L. (Eds.), *El mesolítico geométrico en la Península Ibérica* (pp. 205-258). Universidad de Zaragoza.

McElrath, D.L., y Emerson, T.E. (2000). Toward an "Intrinsic Characteristics" Approach to Chert Raw Material Classification: An American Bottom Example. *Midcontinental Journal of Archaeology*, 25(2), 215-244.

Melchor Monserrat, J.M. (2007). Dos siglos de destrucción de patrimonio histórico de Sagunto (1807–2007). *Arse*, 41, 231-262.

Melchor Monserrat, J.M., Benedito Nuez, J., Ferrer Maestro, J.J., García García, F., y Buchón Moragues, F.F. (2017). Nuevas aportaciones al conocimiento del circo romano de Sagunto y su entorno monumental. En López Vilar, J. (Ed.), *La glòria del circ: curses de carros i competicions circenses: Tarraco Biennal, actes. 3r Congrés Internacional d'Arqueologia i Món Antic. In memoriam Xavier Dupré i Raventós. Tarragona, 16-19 de novembre de 2016* (pp. 155-160). Fundació Privada Mútua Catalana.

Miller, J.N., y Miller, J.C. (2002). *Estadística y Quimiometría para Química Analítica* (IV ed.). Pearson Education Limited.

Milne, S.B., Hamilton, A., y Fayek, M. (2009). Combining Visual and Geochemical Analyses to Source Chert on Southern Baffin Island, Arctic Canada. *Geoarchaeology - An International Journal*, 24(4), 429-449. doi:10.1002/gea.2027

Miriello, D. (2018). Ancient Mortars and Plaster. En López Varela, S.L. (Ed.), The Encyclopedia of Archaeological Sciences (pp. 6). Wiley. doi:10.1002/9781119188230.saseas0382

Miriello, D., Barca, D., Pecci, A., De Luca, R., Crisci, G.M., López Luján, L., y Barba, L. (2015). Plasters from Different Buildings of the Sacred Precinct of Tenochtitlan (Mexico City): Characterization And Provenance. *Archaeometry*, 57(1), 100-127. doi:10.1111/arcm.12074

Mitchell, M.B. (1993). Fundamentals and Applications of Diffuse Reflectance Infrared Fourier Transform (DRIFT) Spectroscopy. En Urban, M.W., y Craver, C.D. (Eds.), *Structure-Property Relations in Polymers* (pp. 351-357). ACS Publications. doi:10.1021/ba-1993-0236.ch013

Molina Hernández, F.J. (2016). *El sílex del Prebético y cuencas neógenas en Alicante y Sur de Valencia: su caracterización y estudio aplicado al Paleolítico Medio* (Tesis Doctoral). Universidad de Alicante.

Moliner Cantos, M.E., Gil, L.M.A., García, C.C., y Esteve, S.T. (2014). Restauración de tres sectores de la muralla del castillo de Sagunto. *Papeles del Partal: revista de restauración monumental*, 6, 191-204.

Monnier, G.F. (2018). A review of infrared spectroscopy in microarchaeology: Methods, applications, and recent trends. *Journal of Archaeological Science: Reports*, 18, 806-823. doi:10.1016/j.jasrep.2017.12.029

Moreau, L., Brandl, M., Filzmoser, P., Hauzenberger, C., Goemaere, É., Jadin, I., Collet, H., Hauzeur, A., y Schmitz, R.W. (2016). Geochemical sourcing of flint artifacts from Western Belgium and the German Rhineland: Testing hypotheses on Gravettian period mobility and raw material economy. *Geoarchaeology - An International Journal*, 31(3), 229-243. doi:10.1002/gea.21564

Morillas, H., Garcia-Galan, J., Maguregui, M., Garcia-Florentino, C., Marcaida, I., Carrero, J.A., y Madariaga, J.M. (2016). In-situ multianalytical methodology to evaluate the conservation state of the entrance arch of La Galea Fortress (Getxo, north of Spain). *Microchemical Journal*, 128, 288-296. doi:10.1016/j.microc.2016.05.010

Moscone, D., Eramo, G., Caggiani, M.C., Morandi Bonacossi, D., y Conati Barbaro, C. (2020). Compositional features of cherts from the Jebel Zawa mines (Dohuk, Kurdistan Region of Iraq) and implications for exploitation strategies during the Late Chalcolithic/Early Bronze Age. *Journal of Archaeological Science: Reports*, 29, 102086. doi:10.1016/j.jasrep.2019.102086

Murray, R.W. (1994). Chemical criteria to identify the depositional environment of chert: General principles and applications. *Sedimentary Geology*, 90(3-4), 213-232. doi:10.1016/0037-0738(94)90039-6

Musílek, L., Čechák, T., y Trojek, T. (2012). X-ray fluorescence in investigations of cultural relics and archaeological finds. *Applied Radiation and Isotopes*, 70(7), 1193-1202. doi:10.1016/j.apradiso.2011.10.014

Nazaroff, A.J., Baysal, A., y Çiftçi, Y. (2013). The importance of chert in Central Anatolia: Lessons from the neolithic assemblage at Çatalhöyük, Turkey. *Geoarchaeology - An International Journal*, 28, 340-362. doi:10.1002/gea.21446

Newlander, K., y Lin, Y. (2017). Integrating visual and chemical data to source chert artifacts in the North American Great Basin. *Journal of Archaeological Science: Reports*, 11, 578-591. doi:10.1016/j.jasrep.2016.12.037

Odell, G.H. (2000). Stone tool research at the end of the millennium: procurement and technology. *Journal of Archaeological Research*, 8(4), 269-331. doi:10.1023/A:1009439725979

Odell, G.H. (2001). Stone tool research at the end of the millennium: classification, function, and behavior. *Journal of Archaeological Research*, 9(1), 45-100. doi:10.1023/A:1009445104085

Odell, G.H. (2004). *Lithic Analysis*. Springer. doi:10.1007/978-1-4419-9009-9

O'Leary, M.J., Ward, I., Key, M.M., Burkhart, M.S., Rawson, C., y Evans, N. (2017). Challenging the 'offshore hypothesis' for fossiliferous chert artefacts in southwestern Australia and consideration of inland trade routes. *Quaternary Science Reviews*, 156, 36-46. doi:10.1016/j.quascirev.2016.11.016

Olivares, M., Irazola, M., Murelaga, X., Baceta, J.I., Tarriño, A., Castro, K., y Etxebarria, N. (2013). Sourcing sedimentary cherts with archaeological use through the combination of chromatographic and spectroscopic techniques. *Applied Geochemistry*, 33, 252-259. doi:10.1016/j.apgeochem.2013.02.020

Olivares, M., Tarriño, A., Murelaga, X., Baceta, J.I., Castro, K., y Etxebarria, N. (2009). Non-destructive spectrometry methods to study the distribution of archaeological and geological chert samples. *Spectrochimica Acta Part A: Molecular and Biomolecular Spectroscopy*, 73(3), 492-497. doi:10.1016/j.saa.2008.12.036

Olofsson, A., y Rodushkin, I. (2011). Provenancing flint artefacts with ICP-MS using REE signatures and Pb isotopes as discriminants: preliminary results of a case study from northern Sweden. *Archaeometry*, 53(6), 1142-1170. doi:10.1111/j.1475-4754.2011.00605.x

Öniz, H. (2016). *Amphorae in the Eastern Mediterranean*. Archaeopress.

Opaiţ, A., y Tsaravopoulos, A. (2011). Amphorae of Dressel 24 similis type in the central Aegean area (Chios–Erythrai–Kyme). *Annual of the British School at Athens*, 106, 275-323. doi:10.1017/S0068245411000050

Orozco Köhler, T., y Gallello, G. (2017). Testing a new methodological approach to define the use of dolerite outcrops for prehistoric tool production in Mediterranean Iberia. En Pereira, T., Terradas, X., y Bicho, N. (Eds.), *Raw materials exploitation in Prehistory: Sourcing, processing and distribution* (pp. 193-205). Cambridge Scholars Publishing.

Ortega, D., Roqué, C., Ibáñez, J., Beamud, E., Larrasoaña, J.C., Sáez, A., y Terradas, X. (2018). The chert from the Castelltallat Formation (south-central Pyrenees): archaeometric characterisation and archaeological implications. *Archaeological and Anthropological Sciences*, 10, 1329-1346. doi:10.1007/s12520-016-0458-1

Ortega, D., Roqué, C., y Terradas, X. (2016). Disponibilidad de rocas silíceas en el noreste peninsular: resultados del proyecto LITOcat. *Cuadernos de Prehistoria y Arqueología de la Universidad de Granada*, 26, 245-282. doi:10.30827/cpag.v26i0.7402

Ortega, L.A., Zuluaga, M.C., Alonso-Olazabal, A., Insausti, M., y Ibañez, A. (2008). Geochemical characterization of archaeological lime mortars: provenance inputs. *Archaeometry*, 50(3), 387-408. doi:10.1111/j.1475-4754.2007.00360.x

Orton, C., y Hughes, M. (2013). *Pottery in Archaeology* (II ed.). Cambridge University Press.

Ostrooumov, M., y Gogichaishvili, A. (2013). Raman and Infrared reflection spectroscopic study of pre-Columbian Mesoamerican pottery. *European Journal of Mineralogy*, 25(5), 895-905. doi:10.1127/0935-1221/2013/0025-2304

Pardo-Gordó, S., García Puchol, O., Diez Castillo, A., Cortell, A., y Molina, L. (2016). Prospección arqueológica en la Canal de Dos Aguas (València). El territorio inmediato a Cueva de la Cocina. *SAGVNTUM*, 48, 197-200. doi:10.7203/SAGVNTVM.48.90

Pardo-Gordó, S., García Puchol, O., Nicolau, A.C., y Balaguer, L.M. (2017). Segunda campaña de prospección en el territorio inmediato a Cueva de la Cocina: el Valle del Magre. *SAGVNTUM*, 49, 187-190. doi:10.7203/SAGVNTVM.49.10976

Parish, R.M., Swihart, G.H., y Li, Y.S. (2013). Evaluating Fourier Transform Infrared Spectroscopy as a Non-Destructive Chert Sourcing Technique. *Geoarchaeology - An International Journal*, 28(3), 289-307. doi:10.1002/gea.21437

Parow-Souchon, H., y Purschwitz, C. (2020). Variability in chert raw material procurement and use during the Upper Paleolithic and Early Neolithic of the southern Levant: A regional perspective from the Greater Petra area. *Journal of Archaeological Science: Reports*, 29, 102087. doi:10.1016/j.jasrep.2019.102087

Pascual Buyé, I., y Aranegui Gascó, C. (1993). Una torre defensiva de época republicana en el Castell de Sagunt. *SAGVNTVM*, 26, 189-204. doi:10.7203/SAGVNTVM..2689

Peacock, D.P.S., y Williams, D.F. (1991). *Amphorae and the Roman Economy: an introductory guide*. Longman.

Pecci, A., Clarke, J., Thomas, M., Muslin, J., van der Graaff, I., Toniolo, L., Miriello, D., Crisci, G.M., Buonincontri, M., y Di Pasquale, G. (2017). Use and reuse of amphorae. Wine residues in Dressel 2–4 amphorae from Oplontis Villa B (Torre Annunziata, Italy). *Journal of Archaeological Science: Reports*, 12, 515-521. doi:10.1016/j.jasrep.2017.02.025

Pecchioni, E., Magrini, D., Cantisani, E., Fratini, F., Garzonio, C.A., Nosengo, C., Santo, A.P., y Vettori, S. (2019). A Non-Invasive Approach for the Identification of "Red Marbles" from Santa Maria Del Fiore Cathedral (Firenze, Italy). *International Journal of Architectural Heritage*, 15(3), 494-504. doi:10.1080/15583058.2019.1629045

Pecchioni, E., Vettori, S., Cantisani, E., Fratini, F., Ricci, M., y Garzonio, C.A. (2016). Chemical and mineralogical studies of the red chromatic alteration of Florentine Pietra Serena sandstone. *European Journal of Mineralogy*, 28(2), 449-458. doi:10.1127/ejm/2015/0027-2504

Pericot, L. (1946). La Cueva de "La Cocina" (Dos Aguas): Nota preliminar. *Archivo de prehistoria levantina*, 2, 39-72.

Peruga Ayete, S., y Carbonell Rubio, R. (2019). Histórico de obras en el Castillo de Sagunto (784-2019). *Arse*, 53, 111-128.

Pollard, A.M., Batt, C., Stern, B., y Young, S.M.M. (2007). *Analytical Chemistry in Archaeology*. Cambridge University Press. doi: 10.1017/CBO9780511607431

Pollard, A.M., y Heron, C. (2008). *Archaeological Chemistry* (II ed.). The Royal Society of Chemistry. doi:10.1039/9781847558299

Prudêncio, M.I., Roldán, C., Dias, M.I., Marques, R., Eixea, A., y Villaverde, V. (2016). A micro-invasive approach using INAA for new insights into Palaeolithic flint archaeological artefacts. *Journal of Radioanalytical Nuclear Chemistry*, 308, 195-203. doi:10.1007/s10967-015-4294-z

R Core Team (2020). R: A language and environment for statistical computing. R Foundation for Statistical Computing. https://www.R-project.org/

Ramacciotti, M., Gallello, G., Aranegui Gascó, C., Hernández, E., y Pastor, A. (2020b). Análisis químicos de los sillares de arenisca del Castillo de Sagunto. *Archivo de Prehistoria Levantina*, 33, 231-242.

Ramacciotti, M., Gallello, G., Diez Castillo, A., y Cervera, M.L. (2021). A non-destructive archaeometric approach for the characterisation and provenance study of the siliceous lithic assemblage from La Calvera rock-shelter (Camaleño, Spain). In Gómez De Soler, B., Soto, M., Chacón, M.G., y Soares Remiseiro, M. (Eds.), *Rock and Roll: 13th International Symposium on Knappable Materials: Multi-scalar Characterization of Raw Materials (Tarragona, Spain, 4th-7th October, 2021)* (p. 60). Recurso digital.

Ramacciotti, M., Gallello, G., Navarro-Martos, D., Doménech-Carbó, A., Roldán, C., Hernández, E., Garrigues, S., y Pastor, A. (2020a). An innovative multi-analytical approach based on spectroscopic and electrochemical techniques to study a complex Roman amphorae collection. *Applied Clay Science*, 198, 105857. doi:10.1016/j.clay.2020.105857

Ramacciotti, M., Gallello, G., Pastor, A., Diez Castillo, A., y García Puchol, O. (2019a). Chert Nucleus and Cortex Characterization for Archaeological Provenance Study Tested in the Prebaetic System Region (Valencian Community, Spain). *Lithic Technology*, 44(3), 166-180. doi:10.1080/01977261.2019.1618043

Ramacciotti, M., García-Puchol, O., Cortell-Nicolau, A., Gallello, G., Morales, A., y Pastor, A. (2022). Moving to the land: First archaeometric study of chert procurement at Cueva de la Cocina (Eastern Iberia). *Geoarchaeology - An International Journal*. (En prensa) doi:10.1002/gea.21903

Ramacciotti, M., Rubio, S., Gallello, G., Lezzerini, M., Columbu, S., Hernandez, E., Morales-Rubio, A., Pastor, A., y de la Guardia, M. (2018). Chronological Classification of Ancient Mortars Employing Spectroscopy and Spectrometry Techniques: Sagunto (Valencia, Spain). *Journal of Spectroscopy*, Vol. 2018, 9736547. doi:10.1155/2018/9736547

Ramacciotti, M., Rubio, S., Gallello, G., Lezzerini, M., Raneri, S., Hernandez, E., Calvo, M., Columbu, S., Morales, A., Pastor, A., y de la Guardia, M. (2019b). Chemical and mineralogical analyses on stones from Sagunto Castle (Spain). *Journal of Archaeological Science: Reports*, 24, 931-938. doi:10.1016/j.jasrep.2019.03.017

Raneri, S., Venturi, F., Palleschi, V., Legnaioli, S., Lezzerini, M., Pagnotta, S., Ramacciotti, M., y Gallello, G. (2019). Social and technological changes in the ceramic production of the Northern Levant during the LBA/IA transition: New evidence about the Sea People issue through archaeometry. *Journal of Anthropological Archaeology*, 56, 101087. doi:10.1016/j.jaa.2019.101087

Rao, H., Li, B., Yang, Y., Ma, Q., y Wang, C. (2015). Proteomic identification of organic additives in the mortars of ancient Chinese wooden buildings. *Analytical Methods*, 7(1), 143-149. doi:10.1039/C4AY01766H

Rezazadeh, M., Seidi, S., Lid, M., Pedersen-Bjergaard, S., y Yamini, Y. (2019). The modern role of smartphones in analytical chemistry. *TrAC Trends in Analytical Chemistry*, 118, 548-555. doi:10.1016/j.trac.2019.06.019

Rinnan, Å., Van Den Berg, F., y Engelsen, S.B. (2009). Review of the most common pre-processing techniques for near-infrared spectra. *TrAC Trends in Analytical Chemistry*, 28(10), 1201-1222. doi:10.1016/j.trac.2009.07.007

Robb, J.E., y Farr, R.H. (2008). Substances in Motion: Neolithic Mediterranean "Trade". In Blake, E., y Knapp, A.B. (Eds.), *The Archaeology of Mediterranean Prehistory* (pp. 24-45). Blackwell Publishing. doi:10.1002/9780470773536.ch2

Roldán, C., Carballo, J., Murcia, S., Eixea, A., Villaverde, V., y Zilhão, J. (2015). Identification of local and allochthonous flint artefacts from the Middle Palaeolithica site 'Abrigo de la Quebrada' (Chelva, Valencia, Spain) by macroscopic and physicochemical methods. *X-ray Spectrometry*, 44(4), 209-216. doi:10.1002/xrs.2602

Rouillard, P. (1979). *Investigaciones sobre la muralla ibérica de Sagunto (Valencia)*. Servicio de Investigación Prehistórica.

Rousaki, A., y Vandenabeele, P. (2021). In situ Raman spectroscopy for cultural heritage studies. *Journal of Raman Spectroscopy*, 52(12), 2178-2189. doi:10.1002/jrs.6166

Ruiz-Perez, D., Guan, H., Madhivanan, P., Mathee, K., y Narasimhan, G. (2020). So you think you can PLS-DA? *BMC Bioinformatics*, 21(2), 2. doi: 10.1186/s12859-019-3310-7

Sánchez De La Torre, M., García-Simón, L.M., Le Bourdonnec, F.-X., y Domingo, R. (2019). Geochemical fingerprinting of Monegros cherts: Redefining the origin of a prehistoric tracer. *Archaeometry*, 61(6), 1233-1245. doi:10.1111/arcm.12494

Sánchez de la Torre, M., Utrilla, P., Montes, L., Domigo, R., Le Bourdonnec, F.-X., y Gratuze, B. (2021). Characterizing the lithic raw materials from Fuente del Trucho (Asque-Colungo, Huesca): New data about Palaeolithic human mobility in north-east Iberia. *Archaeometry*, 63(2), 247-265. doi:10.1111/arcm.12612

Sanjurjo-Sánchez, J., Trindade, M.J., Blanco-Rotea, R., Garcia, R.B., Mosquera, D.F., Burbidge, C., Prudêncio, M.I., y Dias, M.I. (2010). Chemical and mineralogical characterization of historic mortars from the Santa Eulalia de Bóveda temple, NW

Spain. *Journal of Archaeological Science*, 37(9), 2346-2351. doi:10.1016/j.jas.2010.04.008

Schmich, S., y Wilkens, B. (2006). Non-destructive identification and characterization of lithics from the Polop Alto: A preliminary assessment using proton induced X-ray emission (PIXE). In O. García Puchol, y J.E. Aura Tortosa (Eds.), *El abric de la Falguera (Alcoi, Alacant): 8.000 años de ocupación humana en la cabecera del río de Alcoi* (pp. 164-170). Museo Arqueológico de Alicante-MARQ.

Schmidt, P., Paris, C., y Bellot-Gurlet, L. (2015). The investment in time needed for heat treatment of flint and chert. *Archaeological and Anthropological Sciences*, 8, 839-848. doi:10.1007/s12520-015-0259-y

Sciuto, C., Allios, D., Bendoula, R., Cocoual, A., Gardel, M.E., Geladi, P., Gobrecht, A., Gorretta, N., Guermeur, N., Jay, S., Linderholm, J., y Thyrel, M. (2019). Characterization of building materials by means of spectral remote sensing: The example of Carcassonne's defensive wall (Aude, France). *Journal of Archaeological Science: Reports*, 23, 396-405. doi:10.1016/j.jasrep.2018.10.030

Segal, I., Nathan, Y., Zbenovich, V., y Barzilay, E. (2005). Geochemical characterization of cherts and flint artifacts from the Modi'in area. *Israel Journal of Earth Sciences*, 54(4), 229-236.

Sen, G. (2014). *Petrology: Principles and Practice*. Springer. doi:10.1007/978-3-642-38800-2

Shackley, M.S. (1998). Gamma Rays, X-Rays and Stone Tools: Some Recent Advances in Archaeological Geochemistry. *Journal of Archaeological Science*, 25, 259-270. doi:10.1006/jasc.1997.0247

Shackley, M.S. (2011). An Introduction to X-Ray Fluorescence (XRF) Analysis in Archaeology. En Shackley, M.S. (Ed.), *X-Ray Fluorescence Spectrometry (XRF) in Geoarchaeology* (pp. 7-44). Springer. doi:10.1007/978-1-4419-6886-9_2

Shennan, S. (2020). Style, function and cultural transmission. In Culture History and Convergent Evolution. En Groucutt, H.S. (Ed.), *Culture History and Convergent*

Evolution. Vertebrate Paleobiology and Paleoanthropology (pp. 291-298). Springer. doi:10.1007/978-3-030-46126-3_15

Siedel, H., y Siegesmund, S. (2014). Characterization of Stone Deterioration on Buildings. En Siegesmund S., y Snethlage R. (Eds.) *Stone in Architecture* (V ed.) (pp. 349-414). Springer. doi:10.1007/978-3-642-45155-3_6

Skarpelis, N., Carter, T., Contreras, D.A., y Mihailović, D.D. (2017). Characterization of the siliceous rocks at Stélida, an early prehistoric lithic quarry (Northwest Naxos, Greece), by petrography and geochemistry: A first step towards chert sourcing. *Journal of Archaeological Science: Reports*, 12, 819-833. doi:10.1016/j.jasrep.2016.11.015

Speakman, R.J., y Glascock, M.D. (2007). Acknowledging fifty years of neutron activation analysis in archaeology. *Archaeometry*, 49(2), 179-183. doi:10.1111/j.1475-4754.2007.00294.x

Speakman, R.J., y Shackley, M.S. (2013). Silo science and portable XRF in archaeology: a response to Frahm. *Journal of Archaeological Science*, 40(2), 1435-1443. doi:10.1016/j.jas.2012.09.033

Speer, C.A. (2014). LA-ICP-MS analysis of Clovis period projectile points from the Gault Site. *Journal of Archaeological Science*, 52, 1-11. doi:10.1016/j.jas.2014.08.014

Stanjek, H., y Häusler, W. (2004). Basics of X-ray Diffraction. *Hyperfine Interactions*, 154, 107-119. doi:10.1023/B:HYPE.0000032028.60546.38

Stuart, B.H. (2007). *Analytical Techniques in Materials Conservation*. Wiley. doi:10.1002/9780470060520

Sugahara, H., Sugitani, K., Mimura, K., Yamashita, F., y Yamamoto, K. (2010). A systematic rare-earth elements and yttrium study of Archean cherts at the Mount Goldsworthy greenstone belt in the Pilbara Craton: Implications for the origin of microfossil-bearing black cherts. *Precambrian Research*, 177, 73–87. doi:10.1016/j.precamres.2009.10.005

Tanevska, V., Colomban, P., Minčeva-Šukarova, B., y Grupče, O. (2009). Characterization of pottery from the Republic of Macedonia I: Raman analyses of

Byzantine glazed pottery excavated from Prilep and Skopje (12th–14th century). *Journal of Raman Spectroscopy*, 40(9), 1240-1248. doi:10.1002/jrs.2273

Tarriño-Vinagre, A., Elorrieta, I., y García-Rojas, M. (2015). Flint as raw material in prehistoric times: Cantabrian Mountain and Western Pyrenees data. *Quaternary International*, 364, 94-108. doi: 10.1016/j.quaint.2014.10.061

Tarriño-Vinagre, A., Muñoz-Fernández, E., Baigorri, I.E., Normand, C., del Río, P.R., García-Rojas, M., y Pérez-Bartolomé, M. (2016). El sílex en la cuenca Vasco-Cantábrica y el Pirineo occidental: materia prima lítica en la Prehistoria. *Cuadernos de Prehistoria y Arqueología de la Universidad de Granada*, 26, 191-228. doi:10.30827/cpag.v26i0.7400

Tarriño-Vinagre, A., y Terradas, X. (2013). Materias primas líticas. In García-Diez, M., y Zapata, L. (Eds.), *Métodos y técnicas de análisis y estudio en la arqueología prehistórica. De lo técnico a la reconstrucción de los grupos humanos* (pp. 439-452). Servicio Editorial de la Universidad del País Vasco.

Ten Bruggencate, R.E., Milne, S.B., Park, R.W., Fayek, M., y Stenton, D.R. (2017). Combining chert provenance and least-cost pathway analyses to reconstruct Pre-Dorset and Dorset mobility on southern Baffin Island. *Journal of Archaeological Science: Reports*, 14, 651-661. doi:10.1016/j.jasrep.2017.06.030

Terashima, S., Ando, A., Okai, T., Kanai, Y., Taniguchi, M., Takizawa, F., y Itoh, S. (1990). Elemental concentrations in nine new GSJ rock reference samples "sedimentary rock series". *Geostandards Newsletter*, 14(1), 1-5. doi:10.1111/j.1751-908X.1990.tb00062.x

Terradas, X. (1998). Estado actual de las investigaciones sobre el aprovisionamiento de materias primas líticas entre grupos cazadores-recolectores prehistóricos en el estado español. En Bernabeu, J., Orozco, T., y Terradas, X. (Eds.) *Los recursos abióticos en la prehistoria: Caracterización, aprovisionamiento e intercambio* (pp. 73-82). Universitat de València.

Terradas, X., Antolín, F., Bosch, Á., Buxó, R., Chinchilla, J., Clop, X., Gibaja, J.F., Oliva, M., Palomo, A., Piqué, R., Saña, M., y Tarrús, J. (2012). Áreas de

aprovisionamiento, territorios de subsistencia y producciones técnicas en el Neolítico antiguo de la Draga. *Rubricatum: revista del Museu de Gavà*, 5, 441-448.

Terradas, X., Gratuze, B., Bosch, J., Enrich, R., Esteve, X., Xavier Oms, F., y Ribé, G. (2014). Neolithic difusión of obsidian in the wester Mediterranean: new data from Iberia. *Journal of Archaeological Science*, 41, 69-78. doi:10.1016/j.jas.2013.07.023

Terradas, X., Ortega, D., Marín, D., y Alba, M. (2017). Neolithic Flint quarries on Montvell (Catalan Pre-Pyrenees, NE Iberia). En Pereira, T., Terradas, X., y Bicho, N. (Eds.), *Raw materials exploitation in Prehistory: Sourcing, processing and distribution* (pp. 77-89). Cambridge Scholars Publishing.

Thacker, P.T., y Ellwood, B.B. (2002). The Magnetic Susceptibility of Cherts: Archaeological and Geochemical Implications of Source Variation. *Geoarchaeology - An International Journal*, 17(5), 465-482. doi:10.1002/gea.10023

Theodore Peña, J. (2007). *Roman Pottery in the Archaeological Record*. Cambridge University Press. doi:10.1017/CBO9780511499685

Thiry, M., Fernandes, P., Milnes, A., y Raynal, J.P. (2014). Driving forces for the weathering and alteration of silica in the regolith: Implications for studies of prehistoric flint tools. *Earth-Science Reviews*, 136, 141-154. doi:10.1016/j.earscirev.2014.05.008

Thomas, R. (2013). *Practical Guide to ICP-MS: A Tutorial for Beginners* (III ed.). CRC Press.

Tite, M.S. (1991). Archaeological Science – Past Achievements and Future Prospects. *Archaeometry*, 33(2), 139-151. doi:10.1111/j.1475-4754.1991.tb00695.x

Tostevin, R., Shields, G.A., Tarbuck, G.M., He, T., Clarkson, M.O., y Wood, R.A. (2016). Effective use of cerium anomalies as redox proxy in carbonate-dominated marine settings. *Chemical Geology*, 438, 146-162. doi:10.1016/j.chemgeo.2016.06.027.

Tykot, R.H. (2021). Obsidian in Prehistory. En Richet, P., Conradt, R., Takada, A., y Dyon, J. (Eds.), *Encyclopedia of Glass Science, Technology, History, and Culture* (pp. 1237-1248). Wiley. doi:10.1002/9781118801017.ch10.1

Vadillo Conesa, M., Ramacciotti, M., Gallello, G., Jardón Giner, P., Soler Mayor, B., Pastor, A., y Aura Tortosa, E.J. (2021). Non-destructive chemical analysis and use-wear of a Palaeolithic "lissoir" from Hort de Cortés-Volcán del Faro (Cullera, València). En Gómez De Soler, B., Soto, M., Chacón, M.G., Soares Remiseiro, M. (Eds.), *Rock and Roll: 13th International Symposium on Knappable Materials: Multi-scalar Characterization of Raw Materials (Tarragona, Spain, 4th-7th October, 2021)* (p. 62). Recurso digital.

Vega Maeso, C., Gallello, G., Palmero, S., Ferrari, B., Sánchez Carro, M.Á., González Morales, M.R., Gutiérrez Zugasti, I., Ramacciotti, M., y Pastor, A. (2020). Ceramic productions and human interactions during the Early Bronze Age in northern Iberia. *Archaeometry*, 63(1), 68-87. doi:10.1111/arcm.12605

Villa, L. (1994). Le anfore tra tardoantico e medioevo. En Lusuardi Siena, S. (Ed.), *Ad mensam: Manufatti d'uso da contesti archeologici fra tarda antichità e medioevo* (pp. 335-431). Del Bianco Editore.

Villaverde, V., Martínez Valle, R., Badal, E., Guillem, P.M., García, R., y Menargues, J. (1999). El Paleolítico superior de la Cova de les Cendres (Teulada-Moraira, Alicante). Datos proporcionados por el sondeo efectuado en los cuadros A/B-17. *Archivo de Prehistoria Levantina*, 23, 9-65.

Voncken, J.H.L. (2016). *The Rare Earth Elements: An Introduction*. Springer. doi:10.1007/978-3-319-26809-5

Weigand, P.C., Harbottle, G., y Sayre, E.V. (1977). Turquoise Sources and Source Analysis: Mesoamerica and the Southwestern U.S.A. En Earle, T.K., y Ericson, J.E. (Eds.), *Exchange Systems in Prehistory* (pp. 15-34). Academic Press. doi:10.1016/C2009-0-22080-0

Wells, E.C. (2014). Archaeometry: Definition. En Smith C. (Ed.), *Encyclopedia of Global Archaeology* (pp. 468-470). Springer. doi:10.1007/978-1-4419-0465-2_360

Werra, D.H., y Kerneder-Gubała, K. (2021). 'Chocolate' flint mining from Final Palaeolithic up to Early Iron Age–a review. En Françoise Bostyn, F., Giligny, F, y Topping, P. (Eds.), *From Mine to User: Production and Procurement Systems of*

Siliceous Rocks in the European Neolithic and Bronze Age. Proceedings of the XVIII UISPP World Congress (4-9 June 2018, Paris, France) (pp. 42-56). Archaeopress.

Whitbread, I.K. (2001). Ceramic Petrology, Clay Geochemistry and Ceramic Production – from Technology to the Mind of the Potter. In Brothwell, D.R., y Pollard, A.M. (Eds.), *Handbook of Archaeological Sciences* (pp. 449-459). Wiley.

Wilson, L., y Pollard, A.M. (2001). The Provenance Hypothesis. In Brothwell, D.R., y Pollard, A.M. (Eds.), *Handbook of Archaeological Sciences* (pp. 507-517). Wiley.

Wise, B.M., Gallagher, N.B., Bro, R., Shaver, J.M., Windig, W., y Koch, R.S. (2006). *PLS_Toolbox 4.0 for use with MATLAB^{TM}*. Eigenvector Research.

Zhang, K.J., Li, Q.H., Yan, L.L., Zeng, L., Lu, L., Zhang, Y.X., Hui, J., Jin, X., y Tang, X.C. (2017). Geochemistry of limestones deposited in various plate tectonic settings. *Earth-Science Reviews*, 167, 27-46. doi:10.1016/j.earscirev.2017.02.003

Zipkin, A.M., Ambrose, S.H., Hanchar, J.M., Piccoli, P.M., Brooks, A.S., y Anthony, E.Y. (2017). Elemental fingerprinting of Kenya Rift Valley ochre deposits for provenance studies of rock art and archaeological pigments. *Quaternary International*, 430(A), 42-59. doi:10.1016/j.quaint.2016.08.032

Abreviaturas

AAS: espectroscopía de absorción atómica

CRM: material de referencia certificado

CNRM: material certificado no de referencia

DA: análisis discriminante

DS: desviación estándar

ED-XRF: espectroscopía de fluorescencia de rayos X por energía dispersiva

FT-IR: espectroscopía de infrarrojo de transformada de Fourier

HREE: elementos de las tierras raras pesados (Ho, Er, Tm, Yb, Lu)

ICP-OES: espectroscopía de emisión óptica con plasma acoplado inductivamente

ICP-MS: espectrometría de masas con plasma acoplado inductivamente

IR: infrarrojo/infrarroja

LA: ablación láser

LIBS: espectroscopía de plasma inducido por láser

LV: variable latente

LREE: elementos de las tierras raras ligeros (La, Ce, Pr, Nd)

M: promedio

MREE: elementos de las tierras raras medios (Sm, Eu, Gd, Tb, Dy)

NAA: análisis de activación neutrónica

NIR: infrarrojo cercano

OES: espectroscopía de emisión óptica

PC: componente principal

PCA: análisis de los componentes principales

pED-XRF: espectrómetro portátil de fluorescencia de rayos X por energía dispersiva

PLS-DA: análisis de discriminante por mínimos cuadrados parciales

QDA: análisis de discriminante cuadrático

RDS: desviación estándar relativa

REE: elementos de las tierras raras

RF: radiofrecuencia

SDD: detector de deriva de silicio

SEM-EDS: microscopio electrónico de barrido equipado con espectroscopía de energía dispersiva

TG-DSC: termogravimetría y calorimetría diferencial de barrido

VIMP: voltamperometría de partículas inmovilizadas

WD-XRF: espectroscopía de fluorescencia de rayos X por dispersión de longitud de onda

XRD: difractometría de rayos X

Índice de figuras

Índice de tablas

Anexos

Anexo A

Ramacciotti et al. (2019a). Chert nucleus and cortex characterization for archaeological provenance study tested in the Prebaetic system region (Valencian community, Spain)

Routledge
Taylor & Francis Group

Check for updates

Chert Nucleus and Cortex Characterization for Archaeological Provenance Study Tested in the Prebaetic System Region (Valencian Community, Spain)

Mirco Ramacciotti [a,b], Gianni Gallello [b,c], Agustín Pastor [b], Agustín Diez Castillo [d] and Oreto García Puchol [e]

[a]Department of Prehistory, Archaeology and Ancient History, Faculty of Geography, History University of Valencia, Valencia, Spain; [b]Department of Analytical Chemistry, University of Valencia, Valencia, Spain; [c]Department of Archaeology, University of York, York, UK; [d]GRAM Research Group, Department of Prehistory, Archaeology and Ancient History, Faculty of Geography and History, University of Valencia, Valencia, Spain; [e]PREMEDOC Research Group, Department of Prehistory, Archaeology and Ancient History, Faculty of Geography and History, University of Valencia Valencia, Spain

ABSTRACT

The characterization of chert artifacts and the identification of their raw material is a pivotal issue in archaeology for the comprehension of economic and territorial patterns related to prehistoric populations. In the last years, several analytical techniques have been employed to characterize chert and discriminate among different provenances. In this study, cherts collected from different outcrops exploited since the Prehistory in the area of Alcoi (Alacant, Spain) were analyzed. Nucleus and cortex of each sample were divided and separately analyzed to determine their concentrations of major, minor and trace elements. The analyses revealed the elemental difference between both the parts of the chert and pointed out the importance of separation during sample preparation. Eventually, only the results of the nucleus analysis allowed discriminate among the different outcrops.
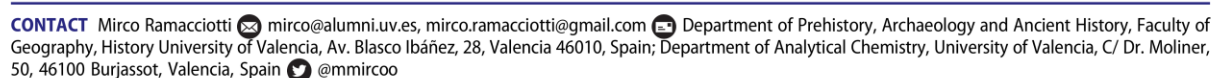
Introduction

Chert is a sedimentary rock mainly composed of micro- and cryptocrystalline quartz (SiO_2 concentration is usually higher than 90 wt%). Its formation involves different stages of solubilization and precipitation of metastable silica minerals (i.e. opal-A and opal-CT), frequently of biogenic origin, in marine and lacustrine environments, and it occurs in sedimentary sequences as beds or as replacement nodules and lenses in different host sediments (Bustillo, 2010; DeMaster, 2003; Hesse, 1989a, 1989b). Chert is macroscopically characterized by an inner nucleus and an external cortex, this last is often whitish and coarser due to weathering and silica leaching (Thiry, Fernandes, Milnes, & Raynal, 2014) and in some cases shows a reddish surface because of iron impurities (Graetsch & Grünberg, 2012).

Among the numerous lithotypes used by humans since the Prehistory to fabricate tools, chert is certainly one of the most recurring due to its mechanical properties that make it durable and suitable for producing very sharp and small in size tools (Luedtke, 1992). The identification of raw material provenance for chert

artifacts is a key evidence for better understanding trade, territorial control, and mobility of human groups. For example, the chemical characterization by trace elements analysis of raw material chert quarries was fundamental to reconstruct settlement dynamics, mobility and patterns of raw material exploitation of the Baffin Island (Canada) populations (Landry, Milne, & ten Bruggencate, 2018; Ten Bruggencate, Milne, Park, Fayek, & Stenton, 2017, 2018). In some cases, a naked-eye examination is enough for a preliminary discrimination of different cherts. However, weathering phenomena can severely alter chert surfaces and, due to the translucidity of most chert varieties, the color strictly depends on the thickness of the piece since small and thin fragments can appear almost colorless. Multielement analysis is widely employed to characterize chert from archaeological sites and potential quarries. For example, Bustillo et al. (2009) classified seven groups of chert samples from the Neolithic mine of Casa Montero (Madrid) according to their macroscopic features, which were later reduced to four groups according to petrographic, mineralogical and chemical

analyses performed through optical microscopy, X-ray diffraction (XRD) and scanning electron microscopy with X-ray microanalysis (SEM-EDS) that evidenced similar diagenetic processes of macroscopically different cherts and point out weathering processes suffered by the samples resulting in different macroscopic features. Analytical methods for chert discrimination have been tested by using X-ray fluorescence (XRF) through portable (Newlander & Linb, 2017) and non-portable spectrometers (Nazaroff, Baysal, & Çiftçi, 2013) which permit to carry out non-destructive analyses of the samples; instead, inductively coupled plasma optical emission spectrometry (ICP-OES) (Herrero-Alonso, Tarriño-Vinagre, Neira-Campos, & Fuertes-Prieto, 2016; Ten Bruggencate et al., 2017) and inductively coupled plasma mass spectrometry (ICP-MS) (Skarpelis, Carter, Contreras, & Mihailović, 2017; Ten Bruggencate et al., 2018) have been employed to detect elements at very low concentrations. Many studies used techniques from multivariate statistics like principal component analysis (PCA) (e.g.: Ten Bruggencate et al., 2017) or discriminant analysis (Moreau et al., 2016) to process the chemical database and group chert samples coming from different outcrops.

ICP-OES and ICP-MS analyses require more complex preparation of samples which include lithium-borate fusion (Ortega et al., 2017) or pulverization through hard grinding devices such as an agate mortar (Ten Bruggencate et al., 2017), a zirconium tray (Herrero-Alonso et al., 2016) or a tungsten carbide (WC) ball mill (Skarpelis et al., 2017), and total wet digestion with multiple acids (i.e. HCl, HNO_3 and HF) to bring samples in solution (Segal, Nathan, Zbenovich, & Barzilay, 2005). However, in the last years, micro-destructive techniques involving laser ablation sampler have been used (Sánchez de la Torre et al., 2017).

Among the different provenance markers, a special focus must be given to rare earth elements (REE). Applied to archaeological materials, REE have proven their effectiveness for igneous rock provenance study (Gallello, Orozco, Pastor, de la Guardia, & Bernabeu, 2016), for detecting anthropic activities in archaeological sediments (Gallello, Pastor, Diez Castillo, La Roca, & Bernabeu, 2013, 2014) and to establish relative chronologies in some architectonic features (Gallello et al., 2017; Ramacciotti et al., 2018) due to their coherent behavior during weathering, erosion and fluvial transportation and their high resistance to chemical mobilization (Arena, Ortega, García-Martínez, Querol, & Llamas, 2011; Munksgaard, Lim, & Livingstone, 2003; Zhangdog, Fuchun, Junji, Sumin, & Jimin, 2006). In sedimentary rocks like chert, REE have shown to be particularly effective proxy of the depositional environment

conditions because less affected by diagenetic and post-diagenetic processes (Murray, 1994).

Many archaeometric studies that carry out chemical analysis on chert do not indicate how they deal with cortex during sample preparation (Evans, Wolframm, Donahue, & Lovis, 2007; Herrero-Alonso et al., 2016; Nazaroff et al., 2013) and only few studies have dealt with its composition showing differences from the mineralogical point of view (Graetsch & Grünberg, 2012; Thacker & Ellwood, 2002). Moreover, semiquantitative chemical analyses through SEM-EDS indicate that the alteration of the external area can cause an enrichment or depletion in certain major elements and possible variabilities in physical, mineralogical and chemical characteristics within the cortical part of a single sample caused by weathering degree (Bustillo et al., 2009; Pawlikowki & Wasilewski, 2002).

The present study wants to push forward the methodological boundaries of chert provenance research by analyzing both nucleus and cortex samples previously separated from the same chert nodules and fragments. In fact, the aforementioned works suggest substantial differences between cortex and nucleus, thus, an analytical approach involving a wide set of elements could consistently contribute with new data to better understand the role of both chert parts for provenance issues. The proportion between cortex and nucleus can vary in each stone due to weathering conditions, surface scraping by rolling and in the case of chipped artifacts. Therefore, the investigation of the elemental contribution of cortex and nucleus becomes necessary to evaluate the effects of mixing both parts during the sample preparation and to consider if they are suitable for chert characterization. This study could improve the quality criteria used to select samples for chemical analysis and our ability to interpret the analytical results.

Moreover, the presence and amount of cortex in archaeological chert is used as an indicator for problems related to material curation and use, quarries exploitation and site function (Dibble, Schurmans, Iovita, & McLaughlin, 2005) and the discrimination of cortex on the basis of objective criteria could be also useful to solve these issues.

In this study, thirty-four chert samples were collected from five sites, exploited during the Prehistory, located in the valley of the Serpis river (Alcoi, Alacant, Spain), in the northernmost area of the Prebaetic System (Figure 1). Cortex and nucleus were analyzed to determine their contents in major, minor and trace elements. Multivariate statistics techniques were also employed to observe possible elemental differences between these two chert parts and finally to evaluate raw materials provenance.
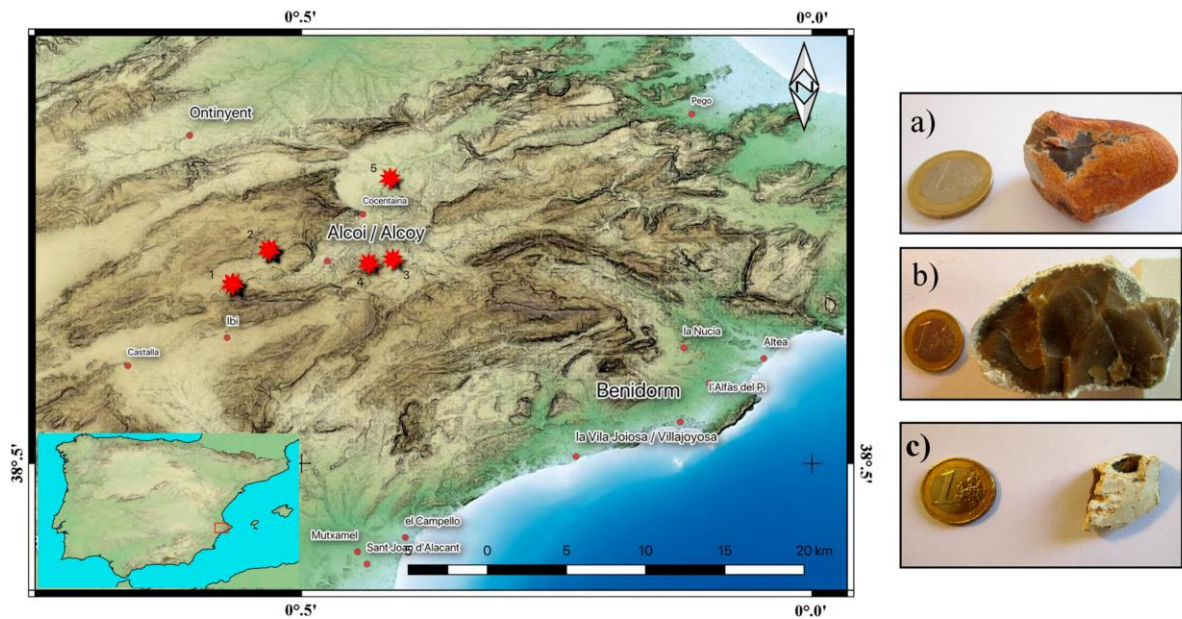
Figure 1. Map of the area with sampling points: (1) Barranc de les Coves (Serrat chert), (2) Font del Barxell (Mariola chert), (3) Penella (Serreta chert), (4) Forminyà (Serreta chert), (5) Muro d'Alcoi (Serreta chert); on the right, three samples of the three chert types: (a) S3 from Barranc de les Coves, (b) S15 from Font del Barxell, (c) S38 from Forminyà.

Geographic and archaeological background

The area of sampling is located in the Prebaetic System, corresponding to the north end of the Baetic System. The Prebaetic System extends from the provinces of Jaén and Granada to Alacant. The studied area is defined by the Vinalopó river on the west and by the Iberian System on the north, it consists of relieves which correspond with anticline standing out in direction SW-NE and is characterized by the prevalent outcropping of cretaceous levels (Vera, 2004). Mariola chert nodules are present in the upper part of the Early Maastrichtian sequence, characterized by 70 m thick grayish limestone strata (Lendínez Gonzalez, Muñoz del Real, & Pascual Muñoz, 2008). Serrat chert outcrops as beds and nodules, hosted by carbonate rocks levels in Selandian and Thanetian (Paleocene) levels (Martínez del Olmo & Benzaquen, 1975). Although the geologic maps do not mention the presence of Serreta chert in the local Eocene sequence, Molina Hernández (2015) identified the host limestone, whose strata reach a thickness of 150 m in the area south of Alcoi.

The central and southern territories of Eastern Iberia where the valley of Serpis is located offer one of the best-known prehistoric sequence in the Western Mediterranean encompassing Upper Pleistocene and Holocene human occupations. El Salt and Abric del Pastor (Alcoi, Alacant), and Cova Beneito (Muro, Alacant) represent key sites regarding the Middle Paleolithic in the

region showing developed stratigraphic sequences covering the Upper Pleistocene (MIS 3) and including the transition between Middle and Upper Paleolithic (Galván et al., 2014; Iturbe et al., 1993). Molina Hernández (2015) shows the importance of local outcrops and carried out a deep and exhaustive geoarchaeological characterization of the area. This study is the outcome of an extensive field survey in which the main outcrops and the secondary sources of chert were individuated and the different rocks classified according to the geological framework of the area, and characterized from the macroscopic and microscopic point of views. Nevertheless, studies attempting to deal with the chemical characterization of chert in the region are still scarce (Eixea, Roldán, Villaverde, & Zilhão, 2014, 2016; Prudêncio et al., 2016; Schmich & Wilkens, 2006).

The Upper Paleolithic is also well-known from different sites located in the Serpis valley and the surroundings corridors (Aura, 2014; Aura & Villaverde, 2014; Cacho et al., 1995; Domènech et al., 2014; Iturbe et al., 1993; Villaverde et al., 2014). The region offers remarkable archaeological evidences also of the late Pleistocene/Early Holocene human settlement (Cacho et al., 1995; García Puchol & Aura Tortosa, 2006; Molina Hernández, Tarriño Vinagre, Galván Santos, & Hernández Gómez, 2011). Despite the scarcity of specific raw materials studies, some papers including lithic analysis (Cacho et al., 1995; Molina Hernández et al., 2011)

reveal the importance of local raw materials. Furthermore, the studied area constitutes one of the most remarkable territories for understanding the beginning of agriculture and husbandry practices in the Western Mediterranean (García Puchol & Salazar García, 2017). In fact, the Serpis Valley, from the inner territories to the coastal ones, has been highlighted as one of the pioneer areas related to the Neolithic spread in Iberian Peninsula according with current radiocarbon dataset from direct domestic samples (Bernabeu Aubán, García Puchol, & Orozco-Köhler, 2018; García Puchol, Diez Castillo, & Pardo-Gordó, 2018; Zilhao, 2001). The relevance of specific local chert types (as Serreta chert), together with the recurrent presence (although scarce) of jasper and rock crystal (quartz) were indicative to start investigating the first Neolithic occupation: Cova de l'Or (Beniarrés, Alacant), Mas d'Is (Penàguila, Alacant), Falguera (Alcoi, Alacant) and Cova de les Cendres (Moraira-Teulada, Alacant) (Bernabeu & Molina, 2009; Bernabeu, Orozco, Diez Castillo, Gómez, & Molina, 2003; García Puchol & Aura Tortosa, 2006). The abundance and wide distribution of chert outcrops, including some high-quality varieties (Serreta type) reinforces the interest for developing specific techniques to characterize and discriminate potential quarries exploited during the Prehistory in order to understand economic and territorial patterns for exploring prehistoric long-term socio-ecological dynamics considering mobility patterns and distribution networks.

Materials and methods

Sampling

Thirty-four samples of chert were collected from five natural outcrops (Figure 1 and Table 1). Seven samples

of Serrat chert (also known as Font Roja) were collected in sedimented colluvial deposit in Barranc de les Coves (S1-4, S7, S9, S10). These samples are characterized by dark brown nucleus or brownish gray one (S1) and whitish to light gray cortex whose thickness is up to 3 mm and that in some cases shows reddish surface (S2-4). Eight samples of Mariola chert were collected in Font del Barxell (S11-18). These samples were collected directly from the host rock except for S11 and S16 which were found close to it. The samples were characterized by whitish cortex about 2 mm thick and dull brown nucleus except for S17 and S18 which have darker brown nucleus. Nineteen samples of Serreta chert were collected in three different secondary outcrops: eleven samples (S19, S22, S24-26, S30-34, S36) were collected in a colluvial sedimented deposit in the area of Penella, few kilometers northern of Sierra de la Serreta, six samples were collected from Forminyà (S37-42), in the foothill of Sierra de la Serreta, in a not sedimented colluvial deposit, and two samples were collected in an alluvial deposit close to Muro d'Alcoi (S43-44). The samples of Serreta chert are characterized by whitish cortex whose thickness range between 2 and 5 mm except for S22, S37 and S42-44 ones, whose cortex goes up to 1 cm. Most of the samples have nucleus of different hues of brown (S19, S22, S24-26, S30-32, S36, S38-44), S22 has a light gray nucleus, S33-34 a light yellow one, while S37 has a brownish gray one.

Separation of cortex and nucleus

All the samples were cleaned and brushed with deionized water to remove materials from their surfaces (carbonate encrustations, earth, etc.), then, each one was reduced to very small chips through a tungsten carbide

Table 1. List of samples with sampling point, chert type and nucleus color according to Munsell color system.

Sample	Outcrop	Outcrop	Chert	Nucleus color	Code	Sample	Outcrop	Outcrop	Chert	Nucleus color	Code
S1	Barranc de les Coves	Colluvium	Serrat	Brownish gray	7.5 YR 4/1	S24	Penella	Colluvium	Serreta	Grayish brown	7.5 YR 6/2
S2	Barranc de les Coves	Colluvium	Serrat	Dark brown	7.5 YR 3/3	S25	Penella	Colluvium	Serreta	Reddish brown	10 R 5/3
S3	Barranc de les Coves	Colluvium	Serrat	Dark brown	7.5 YR 3/3	S26	Penella	Colluvium	Serreta	Dull brown	7.5 YR 5/3
S4	Barranc de les Coves	Colluvium	Serrat	Dark brown	7.5 YR 3/3	S30	Penella	Colluvium	Serreta	Dull brown	7.5 YR 6/3
S7	Barranc de les Coves	Colluvium	Serrat	Grayish brown	7.5 YR 4/2	S31	Penella	Colluvium	Serreta	Dull brown	7.5 YR 6/3
S9	Barranc de les Coves	Colluvium	Serrat	Dark brown	7.5 YR 3/3	S32	Penella	Colluvium	Serreta	Brown	7.5 YR 4/3
S10	Barranc de les Coves	Colluvium	Serrat	Dark brown	7.5 YR 3/3	S33	Penella	Colluvium	Serreta	Light yellow	2.5 Y 7/3
S11	Font del Barxell	Host rock[+]	Mariola	Dull brown	7.5 YR 6/3	S34	Penella	Colluvium	Serreta	Light yellow	2.5 Y 7/3
S12	Font del Barxell	Host rock	Mariola	Dull brown	7.5 YR 5/4	S36	Penella	Colluvium	Serreta	Dull brown	7.5 YR 5/3
S13	Font del Barxell	Host rock	Mariola	Dull brown	7.5 YR 5/4	S37	Forminyà	Colluvium	Serreta	Brownish gray	7.5 YR 6/1
S14	Font del Barxell	Host rock	Mariola	Dull brown	7.5 YR 5/4	S38	Forminyà	Colluvium	Serreta	Dull brown	7.5 YR 5/3
S15	Font del Barxell	Host rock	Mariola	Dull brown	7.5 YR 5/4	S39	Forminyà	Colluvium	Serreta	Dull brown	7.5 YR 5/4
S16	Font del Barxell	Host rock[+]	Mariola	Dull brown	7.5 YR 5/4	S40	Forminyà	Colluvium	Serreta	Dull brown	7.5 YR 5/3
S17	Font del Barxell	Host rock	Mariola	Brown	7.5 YR 4/4	S41	Forminyà	Colluvium	Serreta	Grayish brown	7.5 YR4/2
S18	Font del Barxell	Host rock	Mariola	Brown	7.5 YR 4/4	S42	Forminyà	Colluvium	Serreta	Dull brown	7.5 YR 6/3
S19	Penella	Colluvium	Serreta	Dull brown	7.5 YR 5/3	S43	Muro d'Alcoi	Alluvium	Serreta	Brown	7.5 YR 4/4
S22	Penella	Colluvium	Serreta	Light gray	5 Y 8/2	S44	Muro d'Alcoi	Alluvium	Serreta	Brown	7.5 YR 4/4

Note: Nucleus color and related codes are given according to Munsell Soil Color Chart. The samples marked with a plus sign ([+]) were collected in close proximity to the host rock.

(WC) jaw crusher (Retsch, BB 50) whose high strength and hardness permitted to prepare small fragments avoiding high contamination of the samples. Then, pieces of nucleus and cortex were carefully separated and selected. Finally, both nucleus and cortex samples were pulverized and homogenized through an agate mortar. The original samples are indicated with S (Table 1) while N and C (Table 2) indicate nucleus and cortex respectively (e.g.: sample S1; N1: nucleus of sample S1; C1: cortex of sample S1).

Portable X-ray fluorescence spectroscopy (pXRF)

Powdered samples of nucleus and cortex were analyzed by a portable model S1 Titan energy dispersive X-ray fluorescence spectrometer from Bruker (Kennewick, Washington DC, USA) equipped with a Rhodium X-ray tube and X-Flash®SDD detector (50 keV,15 µA). S1RemoteCtrl (Geochem-trace application) and S1Sync software from Bruker for controlling the instrument were employed to measure concentrations of Si, P, K, Ca, Ti, Fe and Zr. The instruments permitted to obtain reliable data for the concentrations of these elements through fast (60 s) and cheap analyses with minimal sample treatment. However, for Zr measurement, pXRF was preferred to ICP-MS due to the difficulty of dissolving the Zr compounds during samples preparation. Since certified reference materials made up of chert are not available for sale, Blank silica powder (AMIS0484) and quartzite chips (AMIS0439) previously ground through an agate mortar and pestle from AMIS (Modderfontein, South Africa) were employed for reference use. This allowed us to check the reliability of the method.

Inductively coupled plasma mass spectrometry (ICP-MS) and inductively coupled optical emission spectrometry (ICP-OES)

Powdered samples of nucleus and cortex were prepared for ICP-MS and ICP-OES analyses through wet digestion. The procedure of sample preparation was developed by modifying the procedure of Segal et al. (2005) and it is explained in the Annex 1 that include also analytical parameters, limit of detection (LOD) and the R^2 of the calibration curve for each analyzed element.

ICP-MS and ICP-OES were used due to their capability of providing highly reliable data also for elements at very low concentrations which could not be detected through pXRF for most of the samples due to the lower sensitivity of this instrument. In particular, the concentration of thirty-three minor and trace elements were measured through ICP-MS (Ba, Bi, Cd, Cr, Co, Cu, Pb, Li, Mn, Mo,

Ni, Sr, Tl, V, Zn, U, Th, Sc, Y and REE, i.e.: La, Ce, Pr, Nd, Sm, Eu, Gd, Tb, Dy, Ho, Er, Tm, Yb, Lu) while ICP-OES was used for three major elements (Na, Mg and Al). Furthermore, to enhance the quality control track, reference materials was employed by the authors during the run of the analysis in their own laboratories. The method reliability was tested by using the same materials employed for pXRF analysis.

Statistical data processing

Principal component analysis (PCA) was used on the samples to explore large geochemical dataset by reducing the variables number which point out the variance structure of the dataset. Data were previously autoscaled and the model was validated through the leave one out method. Cluster analysis (CA) was used to observe the presence of a different group of samples in Serrat and Serreta cherts on the basis of seven variables ($\sum$REE, La_n/La^*, Ce_n/Ce^*, Eu_n/Eu^*, Gd_n/Gd^*, La_n/Yb_n, Y/Ho). Raw data of these samples were autoscaled prior to processing and the furthest neighbor agglomerative clustering method was employed to build the hierarchical model according to the Euclidean distance among objects.

Multivariate statistics was performed through PLS Toolbox 6.5 by Eigenvector Research Inc. (Wenatchee, WA, USA) running in MATLAB R2014b from MathWorks Inc. (Natick, MA, USA).

Rare earth elements (REE) parameters

To evaluate REE anomalies, cortex and nucleus data were normalized by using Post Archaean Australian Shale (PAAS) REE data, according to the values reported by McLennan (1989). Normalized values are indicated by "n" as subscript (e.g.: La_n: normalized lanthanum). Anomalies are calculated as suggested by Lawrence, Greig, Collerson, and Kamber (2006):

- La_n/La^* where $La^* = Pr_n \cdot (Pr_n/Nd_n)^2$
- Ce_n/Ce^* where $Ce^* = Pr_n \cdot (Pr_n/Nd_n)$
- Eu_n/Eu^* where $Eu^* = (Tb_n^2 \cdot Sm_n)^{1/3}$
- Gd_n/Gd^* where $Gd^* = Tb_n \cdot (Tb_n^2/Dy_n)$

In fact, the above-cited proposed formulas avoid under- or overestimations that can be caused by the calculation of REE anomalies using elements which show anomalous values themselves (e.g.: the oxygenation conditions of a particular depositional environment can cause Ce anomalies in sediments, thus, calculating La anomalies through Ce can be misleading). The used anomalies are considered positive when the result of the equation is higher than 1 and negative when

Table 2. REE total amount and REE parameters.

Chert type	Sample	$\sum$REE	La_n/La^*	Ce_n/Ce^*	Eu_n/Eu^*	Gd_n/Gd^*	La_n/Yb_n	Y/Ho
Serrat	N1	8.0	1.72	0.67	1.23	1.12	1.63	40
	N2	8.0	1.63	0.62	1.22	1.15	1.52	41
	N3	6.6	1.48	0.68	1.23	1.13	1.48	39
	N4	7.2	1.51	0.80	1.17	1.13	1.70	48
	N7	9.2	1.43	0.67	1.27	1.12	1.80	45
	N9	7.4	1.75	0.58	1.26	1.14	1.60	47
	N10	6.6	1.75	1.21	0.57	1.16	1.67	48
	$\mu \pm \sigma$	7.6 ± 0.9	1.6 ± 0.1	0.65 ± 0.08	1.23 ± 0.03	1.14 ± 0.01	1.6 ± 0.1	44 ± 4
	C1	6.9	1.49	0.67	1.37	1.24	1.51	58
	C2	9.2	1.37	0.70	1.37	1.23	1.61	48
	C3	4.3	1.29	0.86	1.40	1.12	1.48	41
	C4	10.0	1.60	0.68	1.42	1.24	1.33	34
	C7	12.0	1.42	0.54	1.37	1.25	1.92	36
	C9	3.3	1.25	0.75	1.44	1.17	1.19	35
	C10	3.4	1.27	0.69	1.43	1.23	1.40	37
	$\mu \pm \sigma$	7 ± 3	1.4 ± 0.1	0.70 ± 0.09	1.40 ± 0.03	1.21 ± 0.05	1.5 ± 0.2	41 ± 9
Mariola	N11	2.4	1.40	0.94	1.27	1.16	1.55	42
	N12	2.1	1.45	1.01	1.23	1.18	2.17	46
	N13	1.9	1.33	0.97	1.23	1.05	1.60	44
	N14	1.9	1.34	0.96	1.26	1.09	1.71	42
	N15	2.5	1.25	0.95	1.20	1.14	1.70	33
	N16	2.3	1.44	0.98	1.22	1.09	1.46	35
	N17	2.5	1.39	0.98	1.17	1.13	1.78	37
	N18	2.1	1.39	0.98	1.25	1.10	1.62	39
	$\mu \pm \sigma$	2.2 ± 0.2	1.37 ± 0.07	0.97 ± 0.02	1.23 ± 0.03	1.12 ± 0.04	1.7 ± 0.2	40 ± 4
	C11	3.1	1.11	0.89	1.45	1.26	1.49	39
	C12	3.6	1.19	0.92	1.52	1.24	1.71	40
	C13	4.0	1.30	0.86	1.46	1.33	1.39	37
	C14	6.3	1.29	0.85	1.45	1.26	1.26	39
	C15	3.1	1.21	0.92	1.43	1.26	1.47	39
	C16	2.7	1.10	0.86	1.46	1.20	1.55	39
	C17	2.6	1.08	0.96	1.43	1.21	1.47	35
	C18	2.9	1.12	0.90	1.43	1.27	1.22	32
	$\mu \pm \sigma$	3 ± 1	1.18 ± 0.09	0.90 ± 0.04	1.45 ± 0.03	1.26 ± 0.04	1.4 ± 0.2	37 ± 3
Serreta	N19	0.3	1.36	1.11	2.37	1.04	1.93	34
	N22	10.4	1.73	0.63	1.19	1.09	1.50	32
	N24	11.2	1.68	0.64	1.20	1.09	1.39	31
	N25	1.7	1.49	0.83	1.24	1.12	1.54	43
	N26	4.5	1.63	0.86	1.29	1.20	1.32	41
	N30	4.4	1.79	0.59	1.21	1.05	1.74	44
	N31	2.9	1.42	0.90	1.26	1.06	1.47	44
	N32	2.2	1.40	0.87	1.24	1.02	1.39	40
	N33	3.7	1.49	0.90	1.33	1.08	1.57	46
	N34	4.4	1.43	0.88	1.27	1.06	1.58	40
	N36	4.8	1.30	0.82	1.35	1.03	1.31	39
	N37	16.8	1.50	0.62	1.19	1.04	1.38	30
Serreta	N38	2.5	1.42	0.85	1.24	1.04	1.23	38
	N39	8.5	1.69	0.66	1.16	1.06	1.69	37
	N40	9.0	1.76	0.60	1.23	1.05	1.46	34
	N41	5.8	1.62	0.64	1.22	1.05	1.42	35
	N42	3.3	1.59	0.87	1.20	1.07	1.56	39
	N43	3.9	1.32	0.87	1.23	1.02	1.42	34
	N44	3.6	1.30	0.85	1.26	1.02	1.28	33
	$\mu \pm \sigma$	5 ± 4	1.5 ± 0.2	0.8 ± 0.1	1.3 ± 0.3	1.06 ± 0.04	1.5 ± 0.2	38 ± 5
	C19	2.0	1.07	0.84	1.40	1.34	1.21	33
	C22	6.7	1.17	0.59	1.32	1.16	1.34	33
	C24	6.6	1.16	0.70	1.37	1.11	1.46	33
	C25	1.3	1.12	0.87	1.36	1.11	1.22	31
	C26	2.8	1.03	0.79	1.37	1.18	1.12	33
	C30	4.3	1.18	0.65	1.41	1.17	1.79	38
	C31	2.0	0.97	0.84	1.41	1.14	1.18	32
	C32	1.7	1.09	0.77	1.43	1.20	1.11	32
	C33	5.0	0.96	0.77	1.38	1.17	1.27	33
	C34	2.6	0.96	0.76	1.40	1.17	1.14	31
	C36	3.5	1.20	1.00	1.41	1.19	1.01	28
	C37	10.8	1.37	0.72	1.47	1.15	1.43	52
	C38	1.4	0.95	0.84	1.46	1.07	1.00	30
	C39	3.1	0.99	0.87	1.43	1.03	1.23	29
	C40	4.8	1.00	0.78	1.32	1.13	1.13	28
	C41	7.5	1.42	0.66	1.41	1.19	1.18	48
	C42	3.5	1.21	0.67	1.41	1.13	1.26	34

Table 2. Continued.

Chert type	Sample	$\sum$REE	La$_n$/La*	Ce$_n$/Ce*	Eu$_n$/Eu*	Gd$_n$/Gd*	La$_n$/Yb$_n$	Y/Ho
	C43	3.8	0.93	0.77	1.40	1.12	1.20	33
	C44	2.5	0.90	0.80	1.45	1.18	1.14	30
	$\mu \pm \sigma$	4 ± 2	1.1 ± 0.1	0.8 ± 0.1	1.40 ± 0.04	1.15 ± 0.06	1.2 ± 0.2	34 ± 6
All N samples		5 ± 4	1.5 ± 0.2	0.8 ± 0.2	1.3 ± 0.2	1.09 ± 0.05	1.6 ± 0.2	39 ± 5
All C samples		5 ± 3	1.2 ± 0.2	0.8 ± 0.1	1.41 ± 0.04	1.19 ± 0.07	1.3 ± 0.2	36 ± 7

Notes: $\sum$REE = REE total amount expressed as µg/g. REE anomalies were calculated according to Lawrence et al. (2006): La* = Pr$_n$ (Pr$_n$/Nd$_n$)^2, Ce* = Pr$_n$ (Pr$_n$/Nd$_n$), Eu* = (Tb$_n \cdot$ Sm$_n^2$)$^{1/3}$, Gd* = (Tb$_n^2$/Dy$_n$). For anomalies calculation, REE were normalized by using Post Archaean Australian Shale (PAAS) (McLennan, 1989) except for Y and Ho which were not normalized.

lower. Y anomalies are evidenced by the ratio Y/Ho, commonly calculated without any normalization, while the enrichment or depletion in light REE (LREE: La, Ce, Pr and Nd) compared with heavy REE (HREE: Ho, Er, Tm, Yb and Lu) is calculated by the ratio La$_n$/Yb$_n$. These parameters are employed in the study of chert and other sedimentary rocks (Sugahara, Sugitani, Mimura, Yamashita, & Yamamoto, 2010) but their use as provenance markers in archaeometric studies is scarce (Lecuit et al., 2018; Orozco-Köhler & Gallello, 2017).

Results and discussion

Major, minor and trace elements

The concentrations of major, minor and trace elements are shown in online supplementary materials (Annex 2 and Annex 3) respectively.

Concerning major elements (Annex 2), as visible in Figure 2, nucleus and cortex samples are predominantly composed by Si and the most relevant impurities are Ca, Fe and Al. The other major elements (Ti, K, P, Mg, Na) do not exceed 0.10 wt% in almost all the samples both for cortex and nucleus. It can be noticed that all the chert samples are characterized by a lower amount of Si in cortex than in nucleus, and cortex samples are enriched in almost all major elements than nucleus ones. This can be caused by different substitution rate of the original sediment by silica in the marginal areas of the chert or either by weathering of less stable silica minerals in the external part and external contamination, and elements leaching from the inner core of the chert to the peripheral one, in which porosities they could reprecipitate and recrystallize (Pawlikowki & Wasilewski, 2002). It should be noted that nucleus has in most of the cases the higher concentration of Na than cortex, possibly
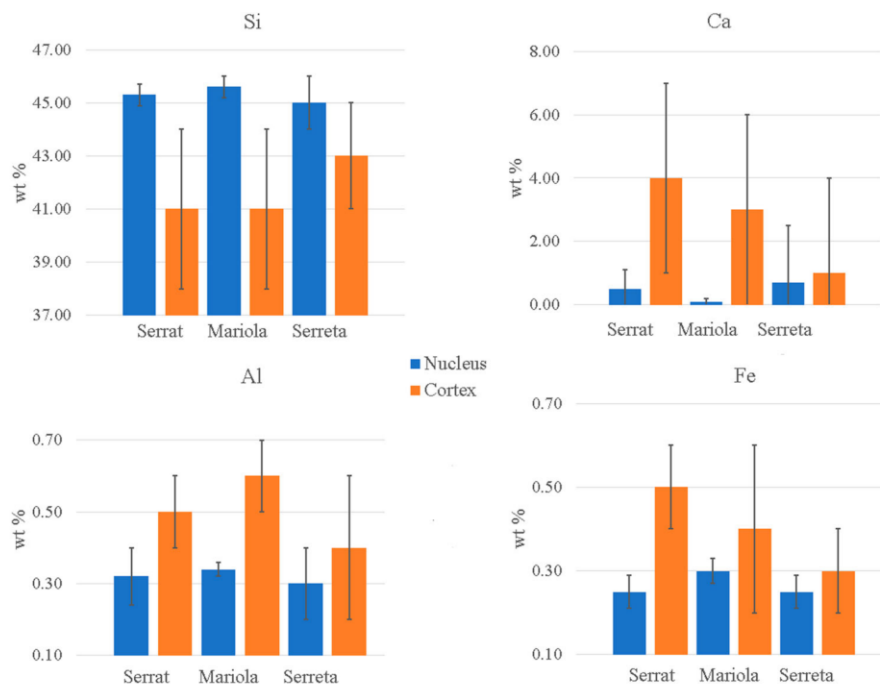
Figure 2. Mean and standard deviation of the concentration of Si and of chert major impurities (Ca, Al and Fe) in nucleus and cortex expressed as wt%.

due to weathering or to a moderate increase of sodium in the chert core during diagenesis (Murray, 1994), while P shows similar concentrations in both parts.

Most of minor and trace elements (Annex 2 for Zr and Annex 3 for the others) in nucleus samples show average values below 10 µg/g for the three chert types, except for Li, Ba and Sr. Though many elemental concentration distributions of cortex and nucleus samples show overlapping, most of cortex samples are enriched in trace elements compared to nucleus ones, although Li and Zn do not follow this trend. Ba and Sr were found in particular higher concentrations in cortex, which is probably related with the high presence of Ca-bearing minerals.

Rare earth elements (REE)

REE total amount ($\sum$REE) (Table 2) in the nucleus is 7.6 ± 0.9 µg/g for Serrat cherts, 2.2 ± 0.2 µg/g for Mariola cherts and 5 ± 4 µg/g for Serreta cherts, this last shows also a higher variance and contains the samples with the lowest and the highest $\sum$REE values (N19: 0.26 µg/g, N37: 16.80 µg/g). In cortex samples, $\sum$REE is 7 ± 3 µg/g for Serrat chert, 3 ± 1 µg/g for Mariola and 4 ± 2 µg/g for Serreta.

The cortex is enriched in REE compared to the nucleus in Font del Barxell (Mariola) samples and in three out of seven samples from Barranc de les Coves (Serrat). On the other hand, most of the cortex samples of Serreta chert are depleted in REE compared to the nucleus ones. It must be underlined that Yttrium behavior is similar to $\sum$REE one.

Looking at the other REE parameters, nucleus samples of Serrat and Serreta cherts have negative Ce anomalies ($Ce_n/Ce^* = 0.65 \pm 0.08$ and 0.8 ± 0.1 respectively). On the contrary, Mariola chert samples do not have significant Ce anomaly ($Ce_n/Ce^* = 0.97 \pm 0.02$). The three chert types show slight positive anomalies or no anomalies of Gd (Gd_n/Gd^* for all nucleus samples is 1.09 ± 0.05), low positive anomalies of Eu (Eu_n/Eu^* is 1.3 ± 0.2) and positive La anomalies (La_n/La^* for all nucleus samples is 1.6 ± 0.2). Moreover, they show light rare earth elements (LREE) enrichment on heavy rare earth elements (HREE) (La_n/Yb_n for all nucleus samples is 1.6 ± 0.2). Concerning yttrium fractionation, the three chert types show overlapping intervals of Y/Ho ratio, ranging between 39 and 48 in Serrat chert and averagely lower in both Mariola and Serreta cherts, going from 33 to 46 and from 30 to 44 respectively.

In the case of cortex samples, Ce anomalies are similar to the nucleus samples ($Ce_n/Ce^* = 0.8 \pm 0.1$) as long as Y/Ho ratio (Y/Ho = 34 ± 6). In addition, these samples show lower positive anomalies or no anomalies of La ($La_n/La^* = 1.2 \pm 0.2$), and higher positive anomalies of Gd ($Gd_n/$

Gd^* is 1.19 ± 0.07) and Eu ($Eu_n/Eu^* = 1.41 \pm 0.04$) than nucleus ones. A lower enrichment in LREE over HREE was also observed for Mariola ($La_n/Yb_n = 1.4 \pm 0.2$) and Serreta chert ($La_n/Yb_n = 1.2 \pm 0.2$) cortex samples.

The dissimilarities between cortex and nucleus that were pointed out can be explained in different ways. Differences in REE patterns between chert and host rock have been observed before and attributed to diagenetic factors (Murray, Buchholtz ten Brink, Gerlach, Russ, & Jones, 1992). Cortex is often located in the outer part of chert nodules; thus, it is possible that it conserves a different REE pattern than the internal one. Furthermore, REE fractionation could be influenced by weathering and contamination. However, less intense enrichment in LREE over HREE, lower positive La anomalies and higher Eu positive anomalies are consistent with the lower silicon levels detected in cortex; in fact, REE patterns of sediments rich in silica minerals tends to have negative Eu anomalies and LREE enrichment over HREE (Götze & Lewis, 1994); also, the high content of alkaline earth metals observed in most of the cortex samples can contribute to explain La depletion and HREE enrichment since heavy lanthanides are more easily complexed by carbonates than light rare earths (Laveuf & Cornu, 2009). The higher concentration of carbonates could also explicate the increase in Gd positive anomalies (Kim, Byrne, & Lee, 1991).

Principal component analysis (PCA) study

PCA was used to observe chemical features of cortex and nucleus samples for each chert type and to identify differences between the two parts of this rock. All the analyzed elements were employed in order to carry out the study. Figure 3 shows PCA plots on the left and the variables contributions on the right for Serrat (Figure 3a,b), Mariola (Figure 3c,d) and Serreta (Figure 3e,f) cherts. The first two principal components explain more than 60% of the total variance.

It is worth noting that for the three group of samples (Figure 3b,d,f) PC1 is correlated in a positive direction with REE, together with Ca and some trace elements (Y, Sr, Ni, Co, Mn and Sc), while it is negatively correlated with Si. Most of the major, minor and trace elements play a more important role in the positive values of the second component, especially for Serrat and Serreta cherts.

In Figure 3(a,c) can be observed that the nucleus and cortex of Serrat and Mariola cherts are clearly different. In particular, the cortex samples of Serrat chert have positive values on the PC2 axis, due to their higher contents in most of major, minor and trace elements (Figure 3b).
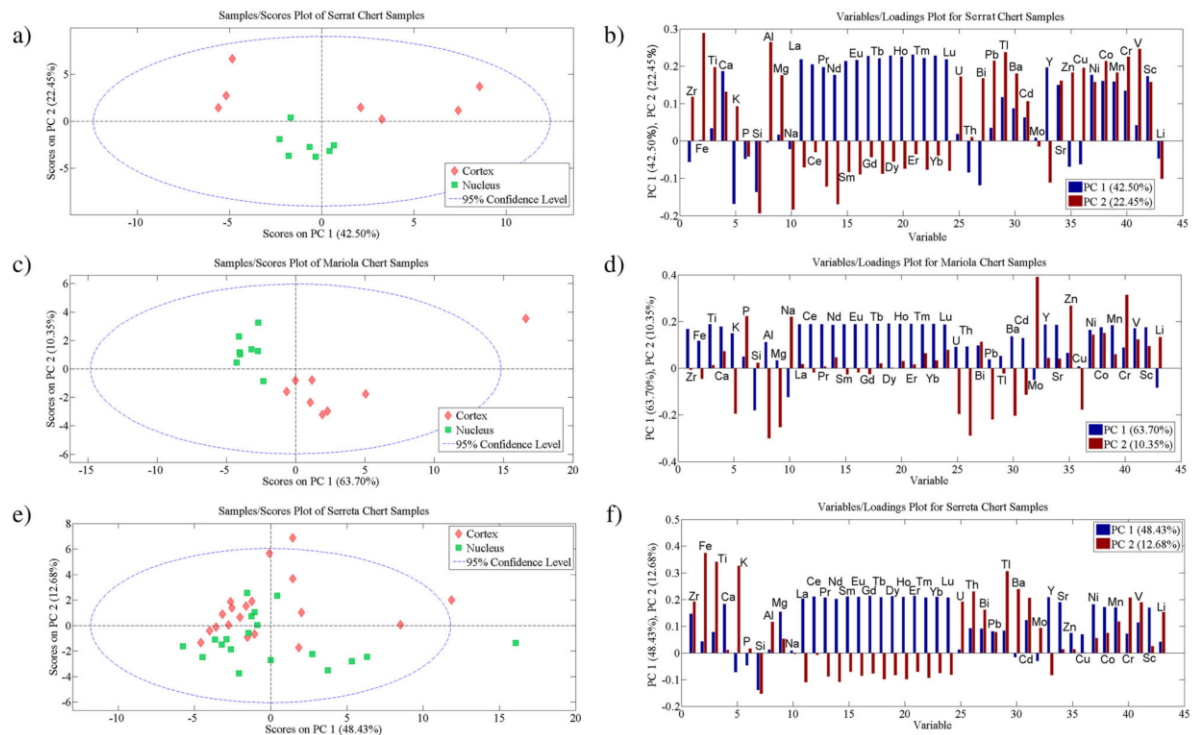
Figure 3. Diagrams of PCA study of cortex and nucleus samples. Samples/scores plots and variables/loadings plot of Serrat (a, b), Mariola (c, d) and Serreta (e, f) cherts.

The difference between the two parts is particularly evident for Mariola chert samples, since cortex and nucleus groups are perfectly separated also on PC1 thanks to the contribution of almost all elements (Figure 3d). Concerning Serreta chert, the difference between nucleus and cortex is less clear (Figure 3e). However, a tendence can be seen on PC2 axis since cortex has higher values than nucleus samples, which fall in most of the cases in the negative axis. It must be noticed that Fe, Ti and K are the variables with the highest positive and Si with the lowest negative contributions on PC2 (Figure 3f). In conclusion, cortex and nucleus groups show differences in the three analyzed chert types. For Serrat and Mariola, cortex values are also more scattered than the nucleus one.

The results of the comparison of nucleus and cortex through multivariate statistics together with the analytical data exposed in the previous section can be of great importance in the evaluation of data from chert chemical analysis applied to provenance studies. Cortex seems to have recurring elements and REE parameters that distinguish it from the inner core and this fact suggests that these features should be used with caution for discriminating different groups of samples, since difference could be caused by the mixture of the two parts. Furthermore, although it is not the main purpose of this study,

the chemical differentiation using the above-mentioned markers could result useful to recognize the cortex presence and its amount.

The results of PCA by using just nucleus samples and all the analyzed elements as variables (Annex 4) and by using only REE, Y, Al, Fe and Ti concentrations as variables (Figure 4), according to Murray (1994) suggestion, are almost identical. PC1 and PC2 explain 82.46% and 12.72% of the variance respectively, and PC1 values are influenced mainly by REE and Y while the three major elements have high relevance on PC2 (Figure 4b). As can be seen in the PCA diagram (Figure 4a), Mariola samples group together very tightly and quite isolated in the second quadrant of the diagram due to their homogenous composition and are easily distinguishable from the other cherts. Serrat samples are plotted in the positive axis of PC1 but show a certain dispersion on PC2 because of the different levels of major elements. On the other hand, Serreta samples are highly dispersed. PC1 is negative for most of the samples from the three outcrops, which fall both in positive and negative PC2 axis. Some samples (N22, N24, N37, N39-41) fall instead in the positive PC1 axis, mixed with Serrat chert samples. Among them, N37 is plotted out of the confidence interval, which is not surprising due to its high REE concentration.
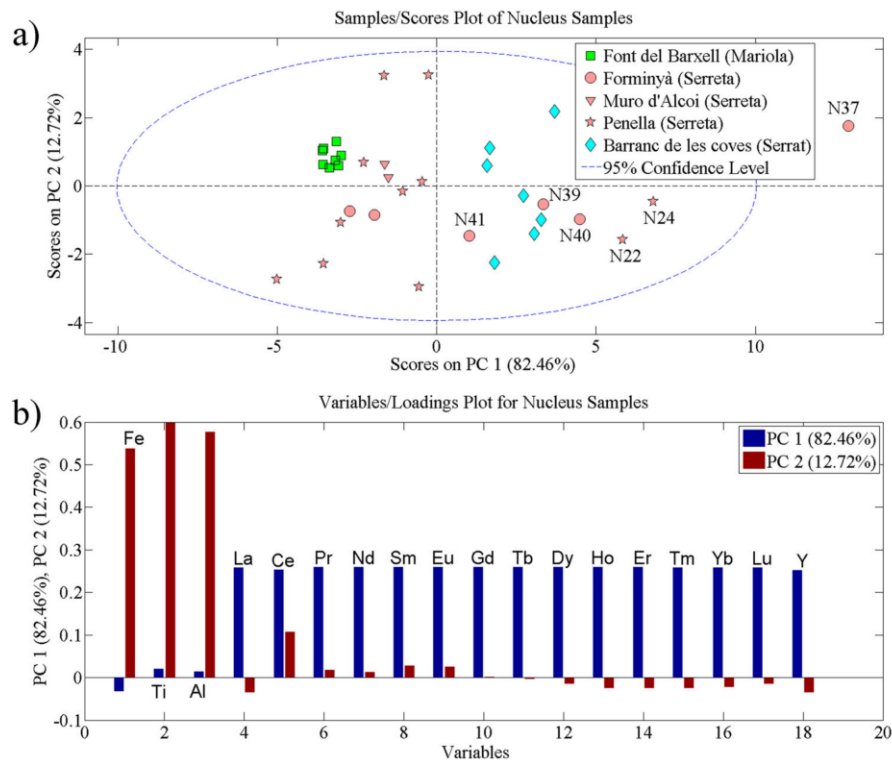
Figure 4. Diagrams of PCA study of nucleus samples by using Fe, Ti, Al, REE and Y as variables: (a) samples/scores plot, (b) variables/loadings plot.

PCA with nucleus and cortex samples (Annex 6) employing REE, Y, Al, Ti and Fe shows more overlapping among the groups; in fact, both Serreta and Serrat samples fall among Mariola ones. Finally, nucleus samples show a chemical homogeneity (Figure 4) which better than the cortex (Annex 5) helps in discriminating among different cherts.

In Mariola and Serrat cherts, the higher dispersion of cortex samples in the plot could be explained by the different degree of weathering and contamination (Annex 5), since the nucleus samples show homogeneous values especially on the PC1 axis (Figure 4a). Serreta chert sample show instead highly dispersed samples both for cortex and nucleus; for this reason, the variability can probably be explained by different silicification events, as suggested by Molina Hernández (2015), occurred in different sedimentary environmental conditions (Annex 5 and Figure 4a).

Provenance discrimination of outcrops

Nucleus REE data permit to distinguish easily Mariola and Serrat cherts. In particular, the samples show different $\sum$REE, since Mariola chert has very low levels of rare earth elements compared to the Serrat one, which is

also reflected by the results of PCA (Figure 4a). It is interesting to notice also that the two chert types can be distinguished by their Ce anomalies. In fact, Ce_n/Ce^* ranges between 0.57 and 0.80 in Serrat chert, while it goes from 0.94 up to 1.01 in Mariola one. Both Serrat and Mariola cherts REE patterns are influenced by exchange with seawater, as testified by their Y/Ho ratio (Y/Ho is 44 ± 4 and 40 ± 4 respectively), but sedimentary environments could have been characterized by different oxygenation conditions as marked by Ce anomaly (Tostevin et al., 2016).

Nucleus samples of Serreta chert show a high variability and the distinction with the other cherts and in particular with Serrat is not clearly observed. Such a variability could be explained by the presence of different silicification events, as previously said. Though Mariola and Serreta cherts can be easily distinguished in PCA diagram (Figure 4a), we can see that Serreta samples are also characterized in almost all the cases by stronger Ce negative anomalies than Mariola ones (0.8 ± 0.1 and 0.97 ± 0.02 respectively).

Cluster analysis (CA) was employed to distinguish between Serreta and Serrat nucleus samples on the basis of the REE parameters ($\sum$REE, La_n/La^*, Ce_n/Ce^*, Eu_n/Eu^*, Gd_n/Gd^*, La_n/Yb_n, Y/Ho). As visible in the dendrogram (Figure 5), CA allowed the separation between
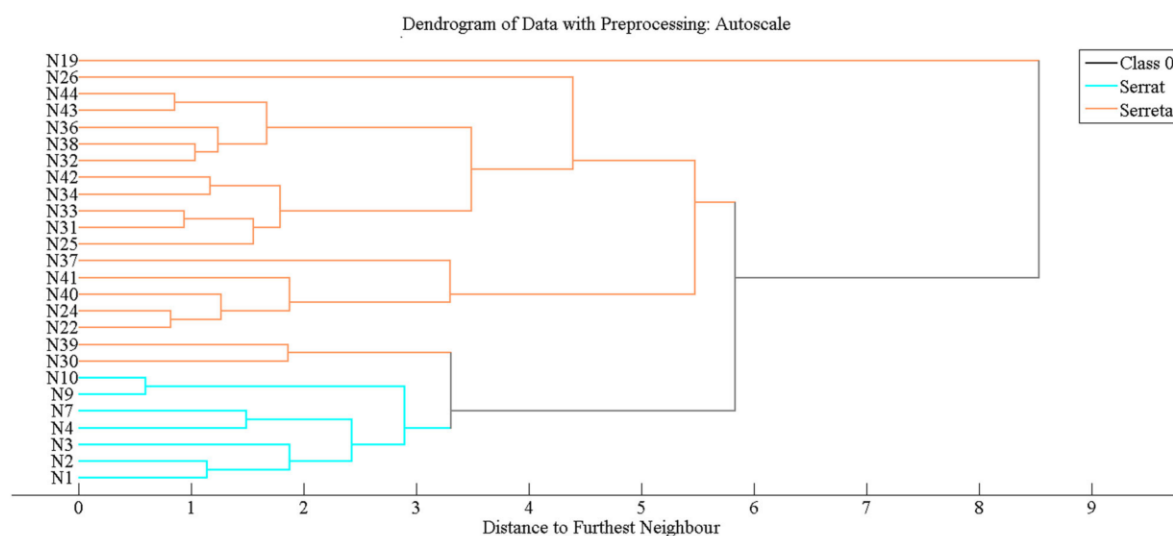
Figure 5. Cluster analysis of Serrat and Serreta nucleus samples by using REE parameters as variables.

the samples of the two chert types. Furthermore, CA points out the different groups of Serreta chert on the basis of the selected variables. N19 shows the higher distance from the other samples, due to its peculiar REE data. The other samples clustering roughly reflects their distribution on PC1 axis (Figure 4a): in particular, N22, N24, N37 and N40-41 fall in the PC1 positive axis and are characterized by higher $\sum$REE (range: 5.8–16.8 µg/g) and more intense Ce negative anomalies (Ce_n/Ce^* range: 0.60–0.64) than the samples grouped above in the dendrogram (N25-26, N31-34, N36, N38, N42-44; $\sum$REE range: 1.7–4.8 µg/g, Ce_n/Ce^* range: 0.83–0.90). While the last samples have $\sum$REE lower than Serrat chert ($\sum$REE range: 6.6–9.2 µg/g), N22, N24, N37 and N40-41 show lower values of Y/Ho ratio (Y/Ho ranges between 30 and 35, while it ranges between 39 and 48 for Serrat chert) and lower Gd positive anomalies (Gd_n/Gd^* ranges between 1.04 and 1.09, while it ranges between 1.12 and 1.16 for Serrat). Among the Serreta samples, N30 and N39 show the highest affinity with the Serrat chert; however, the two groups are still distinguishable and, in particular, it is evident that N30 and N39 have less intense Gd positive anomalies than Serrat cherts (Gd_n/Gd^* is 1.05 and 1.06 vs 1.12 up to 1.16).

Conclusion

The developed analytical approach separating cortex and internal nucleus of each sample showed very interesting results. PCA study employing major, minor and trace elements evidenced relevant difference between the two parts of the rock. Most of the measured elements show higher concentrations in the cortex than in nucleus

samples. However, the inner core is in most of the cases richer in Si, Na, Li and Zn. REE general trend is less clear but the employed parameters showed a fractionation which is marking differences between cortex and nucleus.

In the set of measured elements, REE, Y, Al, Ti and Fe show to be the pivotal ones for discriminating among different cherts, probably due to their role in fingerprinting different sedimentary environments. The concentrations of these elements showed a higher homogeneity for nucleus samples. PCA allowed a first separation which was improved through a deeper insight in REE by using parameters such as REE total amount, elemental anomalies and LREE vs HREE relationship. The identification of distinctive chemical characteristics for three chert types widely employed in the area during the Prehistory will certainly be a useful tool in order to understand the economic role of these rocks and mobility pattern strategies in both diachronic and synchronic perspective with the goal to explore socioecological dynamics of prehistoric populations in Eastern Iberia.

The study revealed the potentiality of the employed approach through the selection of the appropriate rock part and the correct elemental markers to discriminate the provenance of different cherts, although further studies need to be carried out in both archaeological artifacts and geologic samples from ancient exploited quarries.

Acknowledgements

Disclosure statement

No potential conflict of interest was reported by the authors.

Funding

Notes on contributors

Mirco Ramacciotti graduated in Archaeology at the University of Pisa (Italy) and is currently a PhD student at the Department of Prehistory, Archaeology and Ancient History of the University of Valencia, where he works with the ArchaeChemis research unit (https://www.uv.es/archaechemis) on archaeological lithic and lithoid materials through spectroscopy and spectrometry techniques. His thesis is focused on the study of archaeological lithic artifacts employing archaeometric methods.

Gianni Gallello has completed his PhD at the University of Valencia (Spain) where he founded ArchaeChemis (2014) and he is head of the group. He was granted by the European Commission with a Marie Curie individual fellowship (MATRIX project), hosted by the University of York (Department of Archaeology and Department of Environment and Geography). In the last few years, his research activity has been focused on the chemical analysis of a wide range of archaeological materials such as sediments, human remains, stones, mortars, ceramics, etc. He has developed new methodological proposals through the employment of novel sampling strategies, Rare Earth Elements, major and trace element analysis and multivariate statistics.

Agustín Pastor has been Full Professor at the Department of Analytical Chemistry of the University of Valencia since 2007. During his career, he has dealt with the development of analytical methods such as chromatography and spectrometry and he has managed several projects in the field of analytical chemistry. He has been also the head of ArchaeChemis research unit since 2014.

Agustín Diez Castillo got a PhD in History at the University of Cantabria in 1996 with a dissertation about the prehistoric peopling in the western valleys of Cantabria. He moved to Berkley (California) for four years, thanks to a scholarship of the Fundación Marcelino Botín, where he worked at the Department of Anthropology and at the Archaeological Research Facility with prof. Margaret Conkey. He came to the Department of Prehistory, Archaeology and Ancient History of the University of Valencia in 2000, thanks to the Reincorporation Program for Doctors and Technologists Abroad. His main research lines are landscape archaeology, cultural contacts between last hunters-gatherers communities and first farmers in the Cantabrian area as well as in the Mediterranean one and the employment of new technologies in cultural heritage study, such as the development of the Archaeological Information System SIDGEIPA.

Oreto García Puchol got her PhD in History from the University of Valencia in 2002. From 2010 to 2015 she was a "Ramon y Cajal" researcher at the Department of Prehistory, Archaeology and Ancient History (University of Valencia), where she is currently a PhD researcher integrated in the PREMEDOC Research Group. She specializes in socioecological dynamics during the recent Prehistory in the Western Mediterranean. Her research interests include the Mesolithic, Neolithic transition, cultural transmission, lithic technology, the emergence of social hierarchies, Mesolithic and Neolithic funerary practices and 3D Archaeology. She has directed archaeological fieldworks in the Mediterranean basin of Iberia, including sites like Falguera Rock Shelter, Pastora Cave and Cocina Cave. Currently, she heads the EVOLPAST Research Project funded by the Government of Spain.

ORCID

Mirco Ramacciotti http://orcid.org/0000-0001-8937-3134
Gianni Gallello http://orcid.org/0000-0003-3641-8815
Agustín Pastor http://orcid.org/0000-0001-9454-1999
Agustín Diez Castillo http://orcid.org/0000-0001-9122-2941
Oreto García Puchol http://orcid.org/0000-0001-9716-6039

References

Arena, L., Ortega, L., García-Martínez, M. J., Querol, E., & Llamas, J. F. (2011). Geochemical characterization of the mining district of Linares (Jaen, Spain) by means of XRF and ICP-AES. *Journal of Geochemical Exploration*, *108*(1), 21–26. doi:10.1016/j.gexplo.2010.09.002

Aura, J. E. (2014). Coves de Santa Maira (Castell de Castells, Alacant). In R. Sala Ramos (Ed.), *Pleistocene and Holocene hunter-gatherers in Iberia and the Gibraltar strait: The current archaeological record* (pp. 353–356). Burgos: Universidad de Burgos and Fundación Atapuerca.

Aura, J. E., & Villaverde, V. (2014). La cova del Parpalló (Gandía, Valencia) [The cave of Parpalló (Gandía, Valencia). In R. Sala Ramos (Ed.), *Pleistocene and Holocene hunter-gatherers in Iberia and the Gibraltar strait: The current archaeological record* (pp. 402–410). Burgos: Universidad de Burgos and Fundación Atapuerca.

Bernabeu, J., & Molina, L. (2009). *La Cova de les Cendres (Moraira-Teulada, Alicante)* [The cave of Cendres (Moraira-Teulada, Alicante)]. Alicante: Museo Arqueológico de Alicante - MARQ.

Bernabeu, J., Orozco, T., Diez Castillo, A., Gómez, M., & Molina, L. (2003). Mas d'is (Penàguila, Alicante). Aldeas y recintos monumentales del Neolítico inicial en el valle del Serpis [Mas d'Is (Penàguila, Alicante). Villages and monumental enclosures of the early Neolithic in the Valley of Serpis]. *Trabajos de Prehistoria*, *60*(2), 39–59. doi:10.3989/tp.2003.v60.i2.80

Bernabeu Aubán, J., García Puchol, O., & Orozco-Köhler, T. (2018). New insights relating to the beginning of the Neolithic in the eastern Spain: Evaluating empirical data and modelled predictions. *Quaternary International*, *470*(B), 439–450. doi:10.1016/j.quaint.2017.03.071

Bustillo, M. A. (2010). Chapter 3 silicification of continental carbonates. In A. M. Alonso-Zarza & L. H. Tanner (Eds.), *Developments in Sedimentology*, *62*, 153–178. doi:10.1016/S0070-4571(09)06203-7

Bustillo, M. A., Castañeda, N., Capote, M., Consuegra, S., Criado, C., Díaz-Del-Río, P., … Terradas, X. (2009). Is the macroscopic classification of flint useful? A petroarchaeological analysis and characterization of flint raw materials from the Iberian Neolithic mine of Casa Montero. *Archaeometry*, *51*(2), 175–196. doi:10.1111/j.1475-4754.2008.00403.x

Cacho, C., Fumanal, M. P., López, P., López, J. A., Pérez, M., Martínez, R., … García-Carrillo, M. (1995). El Tossal de la Roca (Vall d'Alcalà, Alicante). Reconstrucción paleoambiental y cultural de la transición del tardiglaciar al Holoceno inicial. *Recerques del Museu d'Alcoi*, *4*, 11–101.

DeMaster, D. J. (2003). The diagenesis of biogenic silica: Chemical transformations occurring in the water column, seabed, and crust. In H. D. Holland & K. K. Turekian (Eds.), *Treatise on geochemistry* (Vol. 7, pp. 87–98). Elsevier. doi:10.1016/B0-08-043751-6/07095-X

Dibble, H. L., Schurmans, U. A., Iovita, R. P., & McLaughlin, M. V. (2005). The measurement and interpretation of cortex in lithic assemblages. *American Antiquity*, *70*(3), 545–560. doi:10.2307/40035313

Domènech, E., Bergadà, M. M., Riquelme, J. A., Vera, J. L., Lozano, M. C., Roca de Togores, C., & Wood, R. (2014). El Paleolítico superior de la Cova Beneito (Muro, Alacant, España) [The Upper Palaeolithic of Beneito Cave (Muro, Alicante, Spain)]. In R. Sala Ramos (Ed.), *Pleistocene and Holocene hunter-gatherers in Iberia and the Gibraltar strait: The current archaeological record* (pp. 345–353). Burgos: Universidad de Burgos and Fundación Atapuerca.

Eixea, A., Roldán, C., Villaverde, V., & Zilhão, J. (2014). Middle Palaeolithic flint procurement in Central Mediterranean Iberia: Implications for human mobility. *Journal of Lithic Studies*, *1*(1), 103–115. doi:10.2218/jls.v1i1.783

Eixea, A., Roldán, C., Villaverde, V., & Zilhão, J. (2016). Caracterización del sílex del Abrigo de la Quebrada (Chelva, Valencia). Resultados y valoración en el contexto Paleolítico Medio de la región central del Mediterráneo ibérico [Characterization of the chert of the Abrigo de la Quebrada (Chelva, Valencia). Results and valuation in the Middle Palaeolithic context of the central region of the Iberian Mediterranean]. *Cuadernos de Prehistoria y Arqueología de la Universidad de Granada*, *26*, 313–326. doi:10.30827/cpag.v26i0.7404

Evans, A. A., Wolframm, Y. B., Donahue, R. E., & Lovis, W. A. (2007). A pilot study of "black chert" sourcing and implications for assessing hunter-gatherer mobility strategies in northern England. *Journal of Archaeological Science*, *34*, 2161–2169. doi:10.1016/j.jas.2007.03.007

Gallello, G., Orozco, T., Pastor, A., de la Guardia, M., & Bernabeu, J. (2016). Regional provenance of dolerite prehistoric objects through mineral analysis. *Microchemical Journal*, *124*, 167–174. doi:10.1016/j.microc.2015.08.018

Gallello, G., Pastor, A., Diez Castillo, A., & Bernabeu, J. (2014). Lanthanides Revealing Anthropogenic Impact within a stratigraphic sequence. *Journal of Archaeology*, 2014, Article ID 767065, 8. doi:10.1155/2014/767085

Gallello, G., Pastor, A., Diez Castillo, A., La Roca, N., & Bernabeu, J. (2013). Anthropogenic units fingerprinted by REE in archaeological stratigraphy: Mas D'Is (Spain) case. *Journal of Archaeological Science*, *40*(2), 799–809. doi:10.1016/j.jas.2012.10.005

Gallello, G., Ramacciotti, M., Lezzerini, M., Hernandez, E., Calvo, M., Morales, A., … de la Guardia, M. (2017). Indirect chronology method employing rare earth elements to identify Sagunto Castle mortar construction periods. *Microchemical Journal*, *132*, 251–261. doi:10.1016/j.microc.2017.02.009

Galván, B., Mallol, C., Hernández, C. M., Machado, J., Sistiaga, A., Molina, F. J., … Afonso, R. (2014). El Salt. Últimos neandertales de la montaña alicantina (Alcoy, España) [El Salt. Last Neanderthals of the Alicante mountain (Alcoy, Spain)]. In R. Sala Ramos (Ed.), *Pleistocene and Holocene hunter-gatherers in Iberia and the Gibraltar strait: The current archaeological record* (pp. 380–388). Burgos: Universidad de Burgos and Fundación Atapuerca.

García Puchol, O., & Aura Tortosa, J. E. (2006). *El Abric de la Falguera (Alcoi, Alacant). 8.000 años de ocupación humana en la cabecera del río Alcoi* [The Abric de la Falguera (Alcoi, Alacant). 8000 years of human occupation in the headwaters of the Alcoi River]. Alcoy: Museu Arqueologic Municipal d'Alcoi.

García Puchol, O., Diez Castillo, A., & Pardo-Gordó, S. (2018). New insights into the neolithization process in southwest Europe according to spatial density analysis from calibrated radiocarbon dates. *Archaeological and Anthropological Sciences*, *10*(7), 1807–1820. doi:10.1007/s12520-017-0498-1

García Puchol, O., & Salazar García, D. C. (2017). *Times of neolithic transition along the Western Mediterranean. Fundamental issues in archaeology*. Cham: Springer. doi:10.1007/978-3-319-52939-4

Götze, J., & Lewis, R. (1994). Distribution of REE and trace elements in size and mineral fractions of high-purity quartz sands. *Chemical Geology*, *114*, 43–57. doi:10.1016/0009-2541(94)90040-X

Graetsch, H. A., & Grünberg, J. M. (2012). Microstructure of flint and other chert raw materials. *Archaeometry*, *54*(1), 18–36. doi:10.1111/j.1475-4754.2011.00610.x

Herrero-Alonso, D., Tarriño-Vinagre, A., Neira-Campos, A., & Fuertes-Prieto, N. (2016). Chert from the Vegamián formation: A new raw-material supply source in the Cantabrian Mountains (NW Spain) during prehistory. *Journal of Lithic Studies*, *3*(2), 1–21. doi:10.2218/jls.v3i2.1449

Hesse, R. (1989a). Diagenesis #13. Origin of chert: Diagenesis of biogenic siliceous sediments. *Geoscience Canada*, *15*(3), 171–192.

Hesse, R. (1989b). Silica diagenesis: Origin of inorganic and replacement cherts. *Earth-Science Reviews*, *26*, 253–284. doi:10.1016/0012-8252(89)90024-X

Iturbe, G., Fumanal, M. P., Sarrión, J.S., Cortell, E., Martínez, R., Guillem, P. M., … Vandermeersch, B. (1993). Cova Beneito (Muro, Alicante): una perspectiva interdisciplinar [Beneito Cave (Muro, Alicante): An interdisciplinary perspective]. *Recerques del Museu d'Alcoi*, 2, 23–88.

Kim, K., Byrne, R., & Lee, J. H. (1991). Gadolinium behaviour in seawater: A molecular basis for gadolinium anomalies. *Marine Chemistry*, 36, 107–120. doi:10.1016/S0304-4203 (09)90057-3

Landry, D. B., Milne, B., & ten Bruggencate, R. E. (2018). Combining remote sensing, geophysics, and lithic provenance and reduction to understand long-term continuity in Paleo-Inuit chert quarrying and seasonal inland travels on southern Baffin Island, NU. *Quaternary International*, in Press. doi:10.1016/j.quaint.2018.04.021

Laveuf, C., & Cornu, S. (2009). A review on the potentiality of rare earth elements to trace pedogenetic processes. *Geoderma*, 154(1–2), 1–12. doi:10.1016/j.geoderma.2009.10.002

Lawrence, M. G., Greig, A., Collerson, K. D., & Kamber, B. S. (2006). Rare earth element and yttrium variability in South East Queensland waterways. *Aquatic Geochemistry*, 12(1), 39–72. doi:10.1007/s10498-005-4471-8

Lecuit, M., Fronteau, G., Boulvain, F., Dechamps, S., Eyssautier-Chuine, S., Piavaux, M., & Yans, J. (2018). Geochemical characterization of "Lorraine limestones" from the Saint-Paul Cathedral of Liège (Belgium): Assumptions for the true provenance of the building stones. *Environmental Earth Sciences*, 77, 361. doi:10.1007/s12665-018-7554-8

Lendínez Gonzalez, A., Muñoz del Real, J. L., & Pascual Muñoz, H. (2008). *Memoria de la hoja no. 822 (Benissa), Mapa geológico de España E. 1:50.000. Segunda serie - Primera edición*. Madrid: Instituto Geológico y Minero de España (IGME).

Luedtke, B. E. (1992). *An archaeologist's guide to chert and flint*. Los Angeles: Cotsen Institute of Archaeology Press.

Martínez del Olmo, W., & Benzaquen, M. (1975). *Memoria de la hoja no. 820 (Ontinyent), Mapa geológico de España E. 1:50.000. Segunda serie - Primera edición*. Madrid: Instituto Geológico y Minero de España (IGME).

McLennan, S. M. (1989). Rare earth elements in sedimentary rocks: Influence of provenance and sedimentary processes. *Reviews in Mineralogy and Geochemistry*, 21(1), 169–200.

Molina Hernández, F. J. (2015). *El sílex del Prebético y cuencas neógenas en Alicante y Sur de Valencia: su caracterización y estudio aplicado al Paleolítico Medio* [The chert of the Prebético and neógenes basins in Alicante and South of Valencia: Its characterization and study applied to the Middle Paleolithic] (Doctoral dissertation). University of Alicante, Alicante, Spain. Retrieved from http://hdl.handle. net/10045/56446

Molina Hernández, F. J., Tarriño Vinagre, A., Galván Santos, B., & Hernández Gómez, C. M. (2011). Estudio macroscópico y áreas de aprovisionamiento de la industria silícea del yacimiento mesolítico y neolítico de Benámer [Macroscopic study and supply areas of the siliceous industry of the Mesolithic and Neolithic site of Benámer]. In P. Torregrosa, F. J. Jover & E. López (Eds.), *Benámer (Muro d'Alcoi, Alicante). Mesolíticos y neolíticos en las tierras meridionales valencianas* [Benámer (Muro d'Alcoi, Alicante). Mesolithic and Neolithic in the Valencian southern lands] (pp. 121–131). Valencia: Diputació de València.

Moreau, L., Brandl, M., Filzmoser, P., Hauzenberger, C., Goemaere, É, Jadin, I., … Schmitz, R. W. (2016). Geochemical sourcing of flint artifacts from Western Belgium and the German Rhineland: Testing hypotheses on Gravettian period mobility and raw material economy. *Geoarchaeology. An International Journal*, 31(3), 229–243. doi:10.1002/gea.21564

Munksgaard, C. N., Lim, K., & Livingstone, D. (2003). Rare earth elements as provenance indicators in North Australian estuarine and coastal marine sediments. *Estuarine, Coastal and Shelf Science*, 57(3), 399–409. doi:10.1016/S0272-7714 (02)00368-2

Murray, R. W. (1994). Chemical criteria to identify the depositional environment of chert: General principles and applications. *Sedimentary Geology*, 90(3–4), 213–232. doi:10. 1016/0037-0738(94)90039-6

Murray, R. W., Buchholtz ten Brink, M. R., Gerlach, D. C., Russ IIIG. P., & Jones, D. L. (1992). Rare earth, major, and trace element composition of Monterey and DSDP chert and associated host sediment: Assessing the influence of chemical fractionation during diagenesis. *Geochimica et Cosmochimica Acta*, 56, 2657–2671. doi:10.1016/0016-7037(92)90351-I

Nazaroff, A. J., Baysal, A., & Çiftçi, Y. (2013). The importance of chert in Central Anatolia: Lessons from the neolithic assemblage at Çatalhöyük, Turkey. *Geoarchaeology: An International Journal*, 28, 340–362. doi:10.1002/gea.21446

Newlander, K., & Linb, Y. (2017). Integrating visual and chemical data to source chert artifacts in the North American Great Basin. *Journal of Archaeological Sciences: Reports*, 11, 578–591. doi:10.1016/j.jasrep.2016.12.037

Orozco-Köhler, T., & Gallello, G. (2017). Testing a new methodological approach to define the use of dolerite outcrops for prehistoric tool production in Mediterranean Iberia. In T. Pereira, X. Terradas, & N. Bicho (Eds.), *Raw materials exploitation in Prehistory: Sourcing, processing and distribution* (pp. 193–205). Newcastle upon Tyne: Cambridge Scholars Publishing.

Ortega, D., Roqué, C., Ibáñez, J., Beamud, E., Larrasoaña, J. C., Sáez, A., & Terradas, X. (2017). The chert from the castelltallat formation (south-central Pyrenees): Archaeometric characterisation and archaeological implications. *Archaeological and Anthropological Science*, 10, 1329–1346. doi:10.1007/s12520-016-0458-1

Pawlikowki, M., & Wasilewski, M. (2002). Mineralogical investigation of desert patina on flint artifacts: A case study. *Mediterranean Archaeology and Archaeometry*, 2(2), 23–34.

Prudêncio, M. I., Roldán, C., Dias, M. I., Marques, R., Eixea, A., & Villaverde, V. (2016). A micro-invasive approach using INAA for new insights into Palaeolithic flint archaeological artefacts. *Journal of Radioanalytical and Nuclear Chemistry*, 308 (1), 195–203. doi:10.1007/s10967-015-4294-z

Ramacciotti, M., Rubio, S., Gallello, G., Lezzerini, M., Columbu, S., Hernandez, E., … de la Guardia, M. (2018). Chronological classification of ancient mortars employing spectroscopy and spectrometry techniques: Sagunto (Valencia, Spain) case. *Journal of Spectroscopy*, 2018, Article ID 9736547, 10. doi:10.1155/2018/9736547

Sánchez de la Torre, M., Le Bourdonnec, F. X., Gratuze, B., Domingo, R., García-Simón, L. M., Montes, L., … Utrilla, P. (2017). Applying ED-XRF and LA-ICP-MS to geochemically characterize chert. The case of the Central-Eastern pre-pyrenean lacustrine cherts and their presence in the

Magdalenian of NE Iberia. *Journal of Archaeological Science: Reports*, *13*, 88–98. doi:10.1016/j.jasrep.2017.03.037

Schmich, S., & Wilkens, B. (2006). Non-destructive identification and characterization of lithics from the Polop Alto: A preliminary assessment using proton induced X-ray emission (PIXE). In O. García Puchol & J. E. Aura Tortosa (Eds.), *El Abric de la Falguera (Alcoi, Alacant). 8000 años de ocupación humana en la cabecera del río de Alcoi* [Abric de la Falguera (Alcoi, Alacant). 8000 years of human occupation at the head of the Alcoi River] (pp. 164–170). Alcoy: Artes Gráficas Alcoy.

Segal, I., Nathan, Y., Zbenovich, V., & Barzilay, E. (2005). Geochemical characterization of cherts and flint artifacts from the Modi'in area. *Israel Journal of Earth Sciences*, *54*(4), 229–236.

Skarpelis, N., Carter, T., Contreras, D. A., & Mihailović, D. D. (2017). Characterization of the siliceous rocks at Stélida, an early prehistoric lithic quarry (Northwest Naxos, Greece), by petrography and geochemistry: A first step towards chert sourcing. *Journal of Archaeological Science: Reports*, *12*, 819–833. doi:10.1016/j.jasrep.2016.11.015

Sugahara, H., Sugitani, K., Mimura, K., Yamashita, F., & Yamamoto, K. (2010). A systematic rare-earth elements and yttrium study of Archean cherts at the Mount Goldsworthy greenstone belt in the Pilbara Craton: Implications for the origin of microfossil-bearing black cherts. *Precambrian Research*, *177*, 73–87. doi:10.1016/j.precamres.2009.10.005

Ten Bruggencate, R. E., Milne, S. B., Fayek, M., Park, R. W., Stenton, D. R., & Hamilton, A. C. (2018). Characterizing southern Baffin Island chert: A cautionary tale for provenance research. *Journal of Archaeological Science: Reports*, *22*, 324–329. doi:10.1016/j.jasrep.2016.03.016

Ten Bruggencate, R. E., Milne, S. B., Park, R. W., Fayek, M., & Stenton, D. R. (2017). Combining chert provenance and least-cost pathway analyses to reconstruct pre-Dorset and Dorset mobility on southern Baffin Island. *Journal of Archaeological Science: Reports*, *14*, 651–661. doi:10.1016/j.jasrep.2017.06.030b1

Thacker, P. T., & Ellwood, B. B. (2002). The magnetic susceptibility of cherts: Archaeological and geochemical implications of source variation. *Geoarchaeology: An International Journal*, *17*(5), 465–482. doi:10.1002/gea.10023

Thiry, M., Fernandes, P., Milnes, A., & Raynal, J.-P. (2014). Driving forces for the weathering and alteration of silica in the regolith: Implications for studies of prehistoric flint tools. *Earth-Science Reviews*, *136*, 141–154. doi:10.1016/j.earscirev.2014.05.008.

Tostevin, R., Shields, G. A., Tarbuck, G. M., He, T., Clarkson, M. O., & Wood, R. A. (2016). Effective use of cerium anomalies as redox proxy in carbonate-dominated marine settings. *Chemical Geology*, *438*, 146–162. doi:10.1016/j.chemgeo.2016.06.027.

Vera, J. A. (2004). *Geología de España* [Geology of Spain]. Madrid: Instituto Geológico y Minero de España (IGME).

Villaverde, V., Roman, D., Martínez, R., Badal, E., Guillem, P. M., Pérez, M., … Borao, M. (2014). Cova de les Cendres [Cendres Cave]. In R. Sala Ramos (Ed.), *Pleistocene and Holocene hunter-gatherers in Iberia and the Gibraltar strait: The current archaeological record* (pp. 388–389). Burgos: Universidad de Burgos and Fundación Atapuerca.

Zhangdog, J., Fuchun, L., Junji, C., Sumin, W., & Jimin, Y. (2006). Geochemistry of Daihai lake sediments, inner Mongolia, North China: Implications for provenance, sedimentary sorting, and catchment weathering. *Geomorphology*, *80*(3–4), 147–163. doi:10.1016/j.geomorph.2006.02.006.

Zilhao, J. (2001). Radiocarbon evidence for maritime pioneer colonization at the origins of farming in west Mediterranean Europe. *Proceedings of the National Academy of Sciences of the United States of America*, *98*(24), 14180–14185. doi:10.1073/pnas.241522898

Annex 1. Sample preparation, analytical procedures and instrumental settings for ICP-MS and ICP-OES analyses

Sample preparation and analytical procedures for ICP-MS and ICP-OES

About 0.25 g of each sample was put in a polytetrafluoroethylene (PTFE) vessel and 2.25 mL of HCl (37%) and 0.75 mL of HNO_3 (69%) were added. Samples were heated on a sand bath and removed from the sand bath when they were almost dry, then, 1.5 mL of HF (48%) and 4.5 mL of HNO_3 were added. The vessels were covered and leaved at room temperature for one night. The day after the vessel were heated to almost dryness on a sand bath and 3 mL of HNO_3 were added to evaporate HF residue. When close to complete evaporation, 3 mL of HNO_3 1 M were added, the vessels were covered and heated to the boiling point of the solution and then removed from the sand bath. The solutions were carefully poured in plastic tubes and the volume was brought up to 10 mL. 5 mL of these solutions were used for carrying out the analyses and measuring the concentrations of thirty-three elements: Ba, Bi, Cd, Cr, Co, Cu, Pb, Li, Mn, Mo, Ni, Sr, Tl, V, Zn, U, Th, Sc, Y and REE (La, Ce, Pr, Nd, Sm, Eu, Gd, Tb, Dy, Ho, Er, Tm, Yb, Lu). Multi-element solutions for ICP analysis in HNO_3 5%, containing the mentioned elements at a concentration of 1000 mg/L, were used to prepare the calibration standards. 5 ml volumetric flasks were used adding 1.50 mL of a 1M HNO_3 and the corresponding volumes of standard solutions and filling up to 5mL volume with H_2O. Rh was used as internal standard. The analyses were performed on the prepared dilutions through a Perkin Elmer Elan DRCII ICP-MS (Concord, Ontario, Canada). 0.2 mL of each 10 mL sample solution was used for ICP-OES analysis after being brought up to 5 mL with 0.25 ml of HNO_3, 0.25 mL of HCl and 4.3 mL of H_2O. These solutions were used to measure Al, Mg and Na. Multi-element solution for ICP analysis in HNO_3 5% was used to prepare the calibration standards. For ICP-OES, 5

ml volumetric flasks were used adding 0.25 mL of HNO_3 and 0.25 mL of HCl and the corresponding volumes of standard solutions and filling up to 5mL with H_2O. Re was used as internal standard. The analyses were performed with a Perkin Elmer 5300 DV ICP-OES (Concord, Ontario, Canada). The elements concentration in the standards goes from 0.1 μg/g up to 30 μg/g.

ICP-MS parameters employed for the analysis

Nebulizer Gas Flow	0.92 L/min
RF power	1100 W
Nebulizer pump	20 rpm
Tubes internal diameter	0,76 mm
Lens voltage	6.5-8.5 V
Analog stage	-1950 V
Pulse stage	1050 V
Read Delay	15 s
Sample flush	60 s
Reading parameters	• Dwell Time UMA: 50 ms • Sweeps: 20 • Readings: 1 • Replicates: 3

Mass, detection limit and coefficient of determination of the element analyzed by ICP-MS

Element	Mass (Da)	LOD [μg/g]	R^2	Element	Mass (Da)	LOD [μg/g]	R^2
U	238	0.00016	0.9999	Ce	140	0.0007	0.9994
Th	232	0.0005	0.9988	La	139	0.0007	0.9995
Bi	209	0.0003	0.9981	Ba	138	0.0012	0.9992
Pb	207	0.0013	0.9989	Cd	111	0.004	0.9999
Tl	205	0.0017	0.9985	Mo	95	0.004	0.9999
Lu	175	0.0002	0.9982	Y	89	0.0003	0.9999
Yb	172	7E-05	0.9980	Sr	88	0.007	0.9998
Tm	169	0.00019	0.9976	Zn	64	0.05	0.9999
Er	166	9E-05	0.9981	Cu	63	0.05	0.9991
Ho	165	0.00010	0.9976	Ni	60	0.8	0.9993
Dy	162	0.00017	0.9984	Co	59	0.015	0.9998
Tb	159	4E-05	0.9989	Mn	55	0.14	0.9997
Gd	158	0.0004	0.9991	Cr	52	0.98	0.9996
Sm	152	0.0003	0.9981	V	51	0.03	0.9996
Eu	151	0.0003	0.9995	Sc	45	0.019	0.9992
Nd	142	0.0007	0.9993	Li	7	0.0017	0.9997
Pr	141	0.0003	0.9990	Rh*	103		

Note: LOD = Limit of detection. The star (*) marks the internal standard.

ICP-OES parameters employed for the analysis of the chert samples

Type of detector	Solid state
Type of nebulizer	Cross-flow
Type of spray chamber	Scott
Argon flow rate	• Plasma 15 L/min
	• Auxiliar 0.2 L/min
	• Nebulizer 0.8 L/min
RF generator power	1300 W
Sample aspiration rate	1.10 mL/min
Internal tube diameter	0.76 mm
Plasma stabilization time	15 s
Start Nebulizer	Gradual
Wash time between samples	60 s
Plasma visualization	• Radial (Na, Mg)
	• Axial (Al)
Reading parameters	• Reading time: 60 s
	• Delay time: 50 s
	• Replicates: 3

Wavelength, detection limit and coefficient of determination of the element analyzed by ICP-OES

Element	Wavelength [nm]	LOD [wt%]	R^2
Al	396.153	0.00012	0.9999
Mg	285.213	0.00004	0.9998
Na	589.592	0.00001	0.9999
Re*	197.248		

Note: LOD = Limit of detection. The star (*) marks the internal standard.

Annex 2. Results of pXRF and ICP-OES analyses.

Chert type	Sample	Zr	Fe	Ti	Ca	K	P	Si	Al*	Mg*	Na*	Sample	Zr	Fe	Ti	Ca	K	P	Si	Al*	Mg*	Na*
Serrat	N1	7	0.21	0.01	0.62	0.02	0.04	45.51	0.26	0.01	0.07	C1	10	0.37	0.01	7.44	<LOD	<LOD	39.38	0.36	0.03	0.04
	N2	<LOD	0.25	0.01	0.45	0.04	0.03	44.88	0.29	0.01	0.08	C2	10	0.56	0.02	3.91	0.02	0.03	41.69	0.48	0.03	0.05
	N3	9	0.27	0.02	0.09	0.05	0.03	45.86	0.34	0.01	0.08	C3	11	0.80	0.02	0.33	0.08	0.03	43.03	0.56	0.02	0.05
	N4	10	0.27	0.02	0.43	0.07	0.04	44.90	0.41	0.01	0.09	C4	11	0.50	0.01	8.94	<LOD	0.04	34.78	0.54	0.06	0.05
	N7	10	0.31	0.02	1.73	0.04	0.03	45.24	0.44	0.02	0.10	C7	<LOD	0.49	0.02	5.35	0.04	<LOD	43.58	0.53	0.04	0.05
	N9	11	0.26	0.01	0.19	0.04	0.03	44.85	0.29	0.01	0.07	C9	12	0.47	0.02	1.09	0.06	0.04	43.97	0.54	0.02	0.05
	N10	7	0.20	0.01	0.09	0.03	0.03	45.61	0.21	0.004	0.06	C10	7	0.48	0.01	1.09	0.05	0.02	43.13	0.68	0.12	0.05
	μ ± σ	9 ± 2	0.25 ± 0.04	0.012 ± 0.04	0.5 ± 0.6	0.04 ± 0.01	0.034 ± 0.02	45.3 ± 0.4	0.32 ± 0.08	0.009 ± 0.005	0.08 ± 0.01	μ ± σ	10 ± 1	0.5 ± 0.1	0.016 ± 0.003	4 ± 3	0.05 ± 0.02	0.03 ± 0.01	41 ± 3	0.5 ± 0.1	0.05 ± 0.04	0.05 ± 0.01
Mariola	N11	8	0.30	0.01	0.06	0.05	0.04	45.63	0.35	0.02	0.06	C11	14	0.80	0.02	0.52	0.09	0.02	41.06	0.69	0.21	0.04
	N12	11	0.28	0.01	0.17	0.05	0.03	45.98	0.37	0.04	0.06	C12	10	0.33	0.02	3.41	0.06	0.03	41.18	0.90	0.58	0.05
	N13	9	0.35	0.01	0.34	0.03	0.02	44.70	0.31	0.04	0.06	C13	17	0.38	0.03	2.85	0.12	0.02	42.01	0.63	0.06	0.04
	N14	11	0.30	0.02	0.18	0.04	0.03	45.64	0.37	0.01	0.06	C14	23	0.65	0.05	10.53	0.11	0.05	33.93	0.62	0.04	0.05
	N15	9	0.28	0.01	0.11	0.04	0.04	45.68	0.34	0.04	0.06	C15	16	0.30	0.02	1.89	0.10	0.03	42.91	0.35	0.03	0.05
	N16	9	0.29	0.01	0.04	0.04	0.03	45.78	0.36	0.02	0.05	C16	8	0.29	0.02	1.56	0.08	0.03	43.60	0.62	0.14	0.05
	N17	9	0.31	0.02	0.07	0.04	0.03	46.07	0.33	0.01	0.06	C17	11	0.37	0.02	3.64	0.05	<LOD	41.24	0.52	0.03	0.05
	N18	9	0.26	0.02	0.08	0.05	0.03	45.51	0.32	0.04	0.06	C18	15	0.24	0.02	0.84	0.10	0.03	43.94	0.61	0.02	0.04
	μ ± σ	9 ± 1	0.30 ± 0.03	0.014 ± 0.001	0.1 ± 0.1	0.04 ± 0.01	0.03 ± 0.01	45.6 ± 0.4	0.34 ± 0.02	0.03 ± 0.02	0.057 ± 0.003	μ ± σ	14 ± 5	0.4 ± 0.2	0.03 ± 0.01	3 ± 3	0.09 ± 0.02	0.03 ± 0.01	41 ± 3	0.6 ± 0.1	0.1 ± 0.2	0.047 ± 0.003
Serreta	N19	<LOD	0.25	0.01	0.07	0.015	0.04	45.77	0.05	0.03	0.02	C19	9	0.39	0.01	1.55	0.01	0.03	44.21	0.25	0.05	0.01
	N22	10	0.21	0.01	1.71	<LOD	0.03	44.26	0.22	0.01	0.06	C22	10	0.23	0.01	0.76	0.01	0.03	42.87	0.24	0.005	0.04
	N24	8	0.22	0.01	1.87	0.014	0.03	43.30	0.30	0.02	0.07	C24	11	0.36	0.02	0.86	0.03	0.03	42.27	0.31	0.01	0.05
	N25	<LOD	0.18	0.01	0.01	0.031	0.04	45.02	0.18	0.002	0.04	C25	<LOD	0.21	0.01	0.12	0.03	0.04	44.01	0.28	0.004	0.04
	N26	7	0.24	0.01	0.05	0.043	0.04	45.36	0.34	0.004	0.08	C26	8	0.31	0.01	0.87	0.04	0.03	43.59	0.34	0.01	0.07
	N30	<LOD	0.18	0.01	0.05	0.017	0.03	46.40	0.13	0.003	0.04	C30	<LOD	0.39	0.01	1.51	0.02	<LOD	45.72	0.31	0.01	0.06
	N31	<LOD	0.22	0.01	0.05	0.038	0.03	44.95	0.59	0.01	0.15	C31	<LOD	0.38	0.01	0.55	0.04	0.04	42.80	0.68	0.03	0.05
	N32	<LOD	0.21	0.01	0.02	0.038	0.03	46.44	0.27	0.004	0.07	C32	<LOD	0.30	0.01	0.46	0.03	0.03	44.00	0.37	0.01	0.05
	N33	10	0.34	0.02	0.11	0.083	0.03	44.42	0.51	0.01	0.05	C33	12	0.65	0.03	0.23	0.09	0.03	42.73	0.27	0.01	0.05
	N34	<LOD	0.27	0.01	0.01	0.035	0.03	44.71	0.38	0.01	0.07	C34	<LOD	0.24	0.01	0.06	0.03	0.03	43.70	1.06	0.02	0.04
	N36	8	0.29	0.02	0.06	0.060	0.03	43.80	0.50	0.01	0.11	C36	10	0.54	0.03	0.07	0.09	0.03	42.36	0.31	0.01	0.05
	N37	12	0.31	0.02	7.80	<LOD	0.01	41.29	0.41	0.08	0.08	C37	13	0.43	0.02	10.98	<LOD	0.05	37.53	0.48	0.11	0.04
	N38	9	0.28	0.01	0.02	0.036	0.04	45.28	0.22	0.003	0.05	C38	<LOD	0.24	0.01	0.05	0.03	0.04	43.16	0.41	0.01	0.06
	N39	<LOD	0.25	0.01	0.46	0.025	0.03	46.44	0.27	0.01	0.06	C39	9	0.28	0.02	0.33	0.05	0.03	43.70	0.05	0.02	0.03
	N40	8	0.24	0.01	1.17	0.013	0.02	45.40	0.24	0.01	0.06	C40	9	0.42	0.02	1.07	0.06	0.02	42.71	0.48	0.03	0.05
	N41	<LOD	0.21	0.01	0.08	0.033	0.03	45.28	0.24	0.01	0.06	C41	9	0.31	0.01	7.88	<LOD	0.04	35.93	0.37	0.07	0.04
	N42	<LOD	0.25	0.01	0.29	0.031	0.04	46.22	0.24	0.004	0.06	C42	<LOD	0.27	0.01	0.58	0.02	0.04	45.78	0.27	0.01	0.04
	N43	7	0.28	0.01	0.16	0.036	0.04	45.73	0.32	0.01	0.09	C43	8	0.35	0.02	0.13	0.05	0.03	44.16	0.38	0.01	0.08
	N44	9	0.28	0.01	0.16	0.035	0.03	45.87	0.35	0.01	0.10	C44	9	0.32	0.02	0.05	0.05	0.03	44.83	0.36	0.01	0.10
	μ ± σ	9 ± 2	0.25 ± 0.04	0.012 ± 0.004	0.7 ± 1.8	0.03 ± 0.02	0.03 ± 0.01	45 ± 1	0.3 ± 0.1	0.01 ± 0.02	0.07 ± 0.03	μ ± σ	10 ± 2	0.3 ± 0.1	0.015 ± 0.006	1 ± 3	0.03 ± 0.01	0.03 ± 0.01	43 ± 2	0.4 ± 0.2	0.02 ± 0.03	0.05 ± 0.02
	All N samples	9 ± 1	0.26 ± 0.04	0.013 ± 0.004	0.6 ± 1.4	0.04 ± 0.01	0.03 ± 0.01	45 ± 1	0.3 ± 0.1	0.02 ± 0.02	0.07 ± 0.02	All C samples	11 ± 3	0.4 ± 0.1	0.02 ± 0.01	2 ± 3	0.05 ± 0.03	0.03 ± 0.01	42 ± 3	0.5 ± 0.2	0.1 ± 0.1	0.05 ± 0.01

Note: Concentrations are expressed as weight percentage (wt%) except for Zr ones which are expressed in µg/g. All the concentrations were measured through pXRF except for the elements marked with star (*) which were measured through ICP-OES. <LOD = Under the limit of detection, which correspond 6 µg/g for Zr and 0.01wt% for K and P.

Annex 3. Results of ICP-MS analysis.

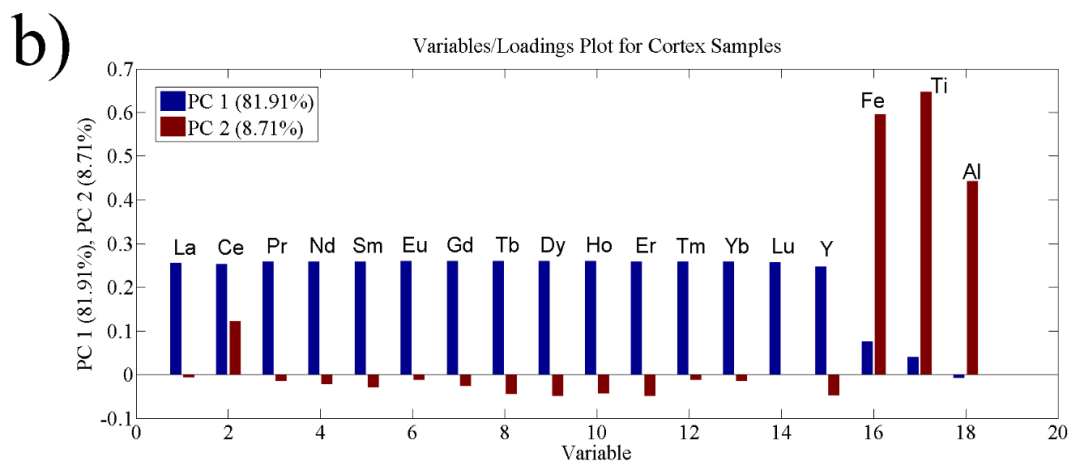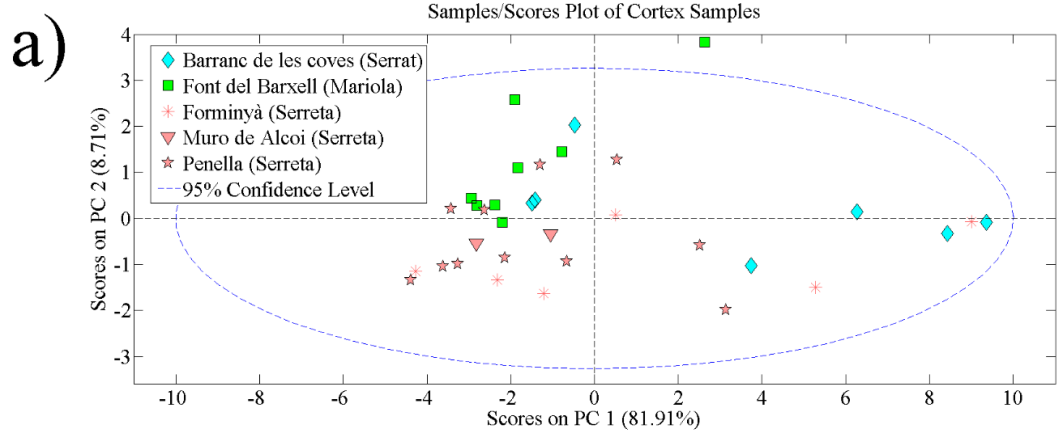| Chert type	Sample	La	Ce	Pr	Nd	Sm	Eu	Gd	Tb	Dy	Ho	Er	Tm	Yb	Lu	U	Th	Bi	Pb	Tl	Ba	Cd	Mo	Y	Sr	Zn	Cu	Ni	Co	Mn	Cr	V	Sc	Li
Serrat	N1	2	2	0.4	2	0.3	0.08	0.3	0.05	0.3	0.05	0.13	0.017	0.10	0.014	0.5	0.3	0.010	0.4	0.008	6	0.05	0.11	1.9	13	2	2	1.1	0.16	1.6	3	3	0.3	23
	N2	2	2	0.4	2	0.4	0.08	0.3	0.05	0.3	0.05	0.14	0.017	0.10	0.015	0.6	0.3	0.011	0.6	0.008	10	0.06	0.3	2	13	5	3	1.9	0.4	1.8	3	3	0.7	22
	N3	1.6	1.8	0.4	1.7	0.3	0.07	0.3	0.04	0.2	0.04	0.11	0.013	0.08	0.012	0.5	0.4	0.015	0.6	0.012	14	0.04	0.09	1.5	8	4	1.8	1.1	0.3	3	2	2	0.4	23
	N4	1.7	2	0.4	1.7	0.3	0.07	0.3	0.04	0.2	0.04	0.10	0.013	0.08	0.011	0.9	0.5	0.009	0.6	0.02	20	0.07	0.09	1.7	21	8	5	1.4	0.3	8	7	6	0.4	17
	N7	2	3	0.5	2	0.4	0.10	0.4	0.05	0.3	0.05	0.13	0.015	0.09	0.013	0.3	0.3	0.009	0.6	0.012	21	0.04	0.08	2	38	5	3	1.2	0.3	4	1.7	3	0.6	30
	N9	2	1.7	0.4	1.9	0.3	0.08	0.3	0.04	0.3	0.05	0.13	0.016	0.09	0.014	0.5	0.3	0.011	0.4	0.008	17	0.03	0.12	2	11	3	2	1.6	0.3	1.2	1.8	3	0.7	23
	N10	1.9	1.5	0.4	1.7	0.3	0.07	0.3	0.04	0.2	0.04	0.11	0.014	0.08	0.012	0.4	0.2	0.009	0.3	0.005	5	0.03	0.07	2	9	4	1.4	1.9	0.14	0.9	2	1.7	0.5	17
	μ±σ	2.0±0.2	2.0±0.4	0.4±0.1	1.9±0.2	0.33±0.04	0.08±0.01	0.31±0.04	0.04±0.01	0.24±0.03	0.04±0.01	0.12±0.01	0.015±0.002	0.09±0.01	0.013±0.02	0.5±0.2	0.33±0.08	0.011±0.002	0.5±0.1	0.010±0.005	13±6	0.05±0.02	0.12±0.07	1.9±0.2	16±10	4±2	3±1	1.5±0.4	0.3±0.1	2±1	3±2	3±1	0.5±0.2	22±4
Mariola	N11	0.5	0.9	0.12	0.5	0.10	0.02	0.08	0.011	0.06	0.012	0.03	0.004	0.03	0.004	0.9	0.3	0.007	0.9	0.08	13	0.02	0.08	0.5	7	3	6	0.8	0.14	2	2	3	0.5	15
	N12	0.5	0.8	0.10	0.4	0.08	0.02	0.06	0.008	0.04	0.007	0.02	0.003	0.016	0.002	0.6	0.18	0.004	0.2	0.010	14	0.02	0.17	0.3	12	4	0.7	1.1	0.13	1.9	2	3	0.3	17
	N13	0.4	0.7	0.09	0.4	0.08	0.02	0.06	0.009	0.05	0.008	0.02	0.003	0.019	0.003	0.6	0.16	0.006	0.3	0.012	12	0.02	0.3	0.4	11	4	1.0	1.7	0.2	2	8	3	0.5	21
	N14	0.4	0.7	0.10	0.4	0.07	0.02	0.06	0.008	0.04	0.008	0.02	0.003	0.018	0.003	0.6	0.18	0.006	0.3	0.022	10	0.02	0.15	0.3	7	4	1.1	1.3	0.14	2	4	3	0.4	18
	N15	0.5	0.9	0.13	0.6	0.10	0.02	0.08	0.011	0.06	0.010	0.03	0.004	0.02	0.004	0.8	0.2	0.007	0.4	0.014	15	0.01	0.15	0.3	11	3	1.7	0.8	0.12	2	10	2	1.1	23
	N16	0.5	0.8	0.11	0.5	0.09	0.02	0.07	0.010	0.06	0.010	0.03	0.004	0.03	0.004	0.6	0.2	0.007	0.5	0.03	13	0.02	0.3	0.4	10	11	1.7	2	0.16	3	12	3	0.9	27
	N17	0.6	0.9	0.12	0.5	0.10	0.02	0.08	0.010	0.06	0.010	0.03	0.004	0.02	0.004	0.6	0.2	0.007	0.6	0.018	8	0.01	0.16	0.4	6	3	1.5	1.1	0.3	1.7	7	3	0.3	29
	N18	0.5	0.8	0.10	0.5	0.08	0.02	0.07	0.009	0.05	0.008	0.02	0.003	0.02	0.003	0.6	0.17	0.005	0.3	0.011	13	0.02	0.18	0.3	10	2	0.8	0.8	0.3	1.7	3	3	0.3	21
	μ±σ	0.5±0.1	0.8±0.1	0.11±0.01	0.5±0.1	0.09±0.03	0.019±0.002	0.07±0.01	0.010±0.001	0.05±0.01	0.009±0.001	0.026±0.004	0.003±0.001	0.021±0.01	0.003±0.001	0.7±0.1	0.21±0.04	0.006±0.001	0.4±0.2	0.02±0.02	12±2	0.019±0.004	0.2±0.1	0.4±0.1	9±2	4±3	1.8±0.8	1.2±0.4	0.2±0.1	2±0.3	6±4	2.6±0.2	0.5±0.3	21±5
Serreta	N19	0.05	0.10	0.011	0.05	0.03	0.01	0.008	0.001	0.01	0.001	0.002	0.0003	0.002	0.0003	4	0.01	0.004	0.03	0.002	32	0.02	0.05	0.03	7	0.5	0.4	0.9	0.04	0.7	3	1.0	0.03	10
	N22	3	3	0.6	3	0.5	0.11	0.5	0.06	0.4	0.07	0.19	0.02	0.14	0.02	0.8	0.3	0.014	0.5	0.007	11	0.04	0.12	2	23	2	1.2	1.2	0.19	4	5	6	0.4	16
	N24	3	3	0.6	3	0.5	0.12	0.5	0.07	0.4	0.07	0.20	0.03	0.16	0.02	0.5	0.4	0.014	0.5	0.012	13	0.04	0.06	2	26	2	0.8	2	0.17	6	7	3	0.6	23
	N25	0.4	0.5	0.08	0.4	0.07	0.02	0.06	0.009	0.05	0.009	0.02	0.003	0.019	0.003	0.8	0.12	0.006	0.3	0.004	4	0.01	0.06	0.4	4	1.3	0.6	0.9	0.07	0.6	<LOD	1.8	1.4	7
	N26	1.1	1.4	0.2	1.0	0.2	0.05	0.19	0.03	0.16	0.03	0.08	0.009	0.06	0.007	0.8	0.2	0.003	0.6	0.008	31	0.03	0.17	1.2	9	1.5	1.0	0.5	0.16	0.7	5	8	0.8	25
	N30	1.3	1.1	0.2	1.1	0.19	0.04	0.18	0.03	0.15	0.03	0.07	0.009	0.05	0.008	0.6	0.13	0.006	0.3	0.006	7	0.02	0.06	1.2	5	3	3	0.3	0.08	0.4	<LOD	3	0.19	8
	N31	0.7	1.0	0.15	0.7	0.12	0.03	0.11	0.02	0.09	0.016	0.04	0.006	0.03	0.005	0.8	0.15	0.007	0.4	0.007	9	0.02	0.2	0.7	6	2	1.3	0.3	0.13	0.5	<LOD	3	0.4	16
	N32	0.5	0.7	0.11	0.5	0.09	0.02	0.08	0.012	0.06	0.012	0.03	0.004	0.03	0.004	0.99	0.19	0.008	0.5	0.013	11	0.01	0.2	0.5	5	2	2	0.8	0.2	0.6	<LOD	3	0.7	16
	N33	0.8	1.2	0.18	0.8	0.16	0.04	0.14	0.02	0.10	0.019	0.05	0.007	0.04	0.006	4	0.3	0.008	0.3	0.015	35	0.03	0.19	0.9	24	3	0.7	0.4	0.14	2	<LOD	7	0.3	24
	N34	1.0	1.5	0.2	1.0	0.18	0.04	0.16	0.02	0.12	0.02	0.06	0.008	0.05	0.007	0.7	0.3	0.010	0.5	0.012	18	0.02	0.06	0.9	8	5	0.7	1.1	0.09	2	2	4	0.3	30
	N36	1.0	1.5	0.3	1.2	0.2	0.06	0.19	0.03	0.15	0.03	0.08	0.009	0.06	0.009	0.3	0.3	0.015	1.0	0.012	40	0.05	0.14	1.1	8	6	2	1.8	0.5	2	2	6	1.6	41
	N37	4	4	0.9	4	0.8	0.18	0.8	0.11	0.6	0.11	0.3	0.04	0.22	0.03	1.3	0.3	0.017	1.2	0.02	16	0.09	0.3	3	149	3	5	1.0	18	4	7	4	25	
	N38	0.6	0.8	0.13	0.6	0.10	0.02	0.09	0.014	0.08	0.015	0.04	0.005	0.03	0.005	0.9	0.16	0.008	0.5	0.005	5	0.01	0.4	0.6	9	5	1.3	1.8	0.3	1.3	1.1	3	1.2	14
	N39	2	2	0.5	2	0.4	0.08	0.4	0.05	0.3	0.05	0.14	0.017	0.10	0.014	0.3	0.3	0.013	0.6	0.008	13	0.03	0.2	1.9	9	5	1.5	1.7	0.3	1.9	<LOD	4	1.2	23
	N40	2	2	0.5	2	0.4	0.10	0.4	0.06	0.3	0.06	0.16	0.02	0.12	0.018	0.8	0.2	0.009	0.5	0.006	6	0.04	0.11	2	23	5	0.8	1.1	0.4	3	<LOD	4	1.0	15
	N41	1.5	1.5	0.3	1.5	0.3	0.06	0.3	0.04	0.2	0.04	0.10	0.013	0.08	0.012	0.6	0.2	0.011	0.5	0.007	4	0.04	0.19	1.3	12	3	1.7	1.1	0.3	1.6	<LOD	3	0.3	14
	N42	0.8	1.1	0.17	0.8	0.14	0.03	0.13	0.018	0.10	0.019	0.05	0.007	0.04	0.006	0.5	0.18	0.008	0.7	0.005	6	0.02	0.19	0.7	7	4	2	1.7	0.3	1.5	<LOD	3	0.2	17
	N43	0.8	1.4	0.2	0.9	0.17	0.04	0.14	0.020	0.11	0.020	0.05	0.007	0.04	0.007	1.4	0.3	0.013	0.6	0.012	22	0.08	0.5	0.7	9	4	1.3	1.5	0.19	2	1.3	5	1.0	24
	N44	0.8	1.2	0.19	0.8	0.16	0.04	0.14	0.020	0.11	0.020	0.05	0.007	0.04	0.007	1.2	0.3	0.015	1.7	0.013	20	0.06	0.5	0.7	10	3	3	1.9	0.2	1.6	2	5	0.9	24
	μ±σ	1±1	1±1	0.3±0.2	1±1	0.2±0.2	0.05±0.04	0.2±0.2	0.03±0.03	0.2±0.2	0.03±0.03	0.09±0.08	0.011±0.009	0.07±0.06	0.010±0.008	1±1	0.23±0.09	0.010±0.004	0.6±0.4	0.009±0.005	16±11	0.03±0.02	0.2±0.1	1.2±0.8	18±32	3±2	1.5±0.8	1±1	0.2±0.2	3±4	3±2	4±2	0.7±0.7	20±8
All N samples		1±1	1.5±0.8	0.3±0.2	1.2±0.9	0.2±0.2	0.05±0.04	0.2±0.2	0.03±0.02	0.2±0.1	0.03±0.02	0.08±0.07	0.010±0.008	0.06±0.05	0.009±0.007	0.9±0.8	0.24±0.09	0.009±0.004	0.6±0.3	0.01±0.01	14±9	0.03±0.02	0.2±0.1	1.1±0.8	16±24	4±2	1.3±0.8	0.2±0.2	3±4	3±2	4±2	0.7±0.7	20±7	

Chert type	Sample	La	Ce	Pr	Nd	Sm	Eu	Gd	Tb	Dy	Ho	Er	Tm	Yb	Lu	U	Th	Bi	Pb	Tl	Ba	Cd	Mo	Y	Sr	Zn	Cu	Ni	Co	Mn	Cr	V	Sc	Li
Serrat	C1	1.9	1.9	0.3	1.4	0.3	0.07	0.3	0.04	0.3	0.05	0.14	0.015	0.09	0.012	0.4	0.16	0.012	1.3	0.014	12	0.4	0.13	2.7	26	5	2	2	0.5	20	5	3	1.8	10
	C2	2	3	0.5	1.9	0.4	0.10	0.4	0.05	0.3	0.06	0.16	0.018	0.11	0.014	0.4	0.4	0.012	0.9	0.015	17	0.11	0.21	2.7	58	2	1.1	2	0.4	18	5	3	0.6	18
	C3	1.1	1.5	0.2	0.8	0.18	0.04	0.17	0.02	0.12	0.02	0.06	0.008	0.05	0.007	0.7	0.4	0.03	3	0.019	15	0.12	0.13	0.8	17	25	32	2	0.6	12	6	6	0.8	22
	C4	3	3	0.5	2.0	0.4	0.11	0.5	0.06	0.4	0.07	0.22	0.02	0.16	0.02	0.9	0.16	0.006	0.7	0.02	32	0.09	0.08	3	123	2.0	1.0	3	0.8	18	11	6	3	15
	C7	4	3	0.6	3	0.6	0.13	0.6	0.07	0.4	0.07	0.20	0.02	0.14	0.018	0.5	0.3	0.010	3	0.02	25	0.09	0.13	2	68	5	7	3	0.6	23	8	4	1.8	22
	C9	0.8	1.0	0.16	0.7	0.14	0.03	0.15	0.017	0.11	0.019	0.06	0.007	0.05	0.007	0.6	0.3	0.008	0.3	0.012	15	0.04	0.13	0.7	32	1.7	1.2	1.6	0.3	5	3	3	0.4	18
	C10	0.9	1.0	0.17	0.7	0.16	0.04	0.15	0.018	0.11	0.019	0.06	0.007	0.05	0.006	0.7	0.05	0.006	0.3	0.07	0.9	64	3	3	0.4	0.3	9	5	2	0.9	21			
	μ±σ	2±1	2.0±0.8	0.4±0.2	1.4±0.7	0.3±0.2	0.07±0.04	0.3±0.2	0.04±0.02	0.3±0.1	0.04±0.02	0.13±0.07	0.014±0.007	0.09±0.03	0.012±0.006	0.6±0.2	0.3±0.1	0.013±0.007	1±1	0.016±0.005	21±8	0.1±0.1	0.13±0.04	2±1	55±36	6±8	7±11	2.3±0.8	0.5±0.2	14±7	6±2	4±2	1.3±0.9	18±4
Mariola	C11	0.7	1.2	0.15	0.6	0.13	0.03	0.13	0.015	0.09	0.015	0.05	0.005	0.04	0.005	0.9	0.3	0.007	1.5	0.03	26	0.03	0.12	0.6	18	4	11	1.8	0.4	4	5	4	0.5	19
	C12	0.8	1.4	0.17	0.7	0.15	0.03	0.15	0.016	0.10	0.015	0.05	0.005	0.04	0.005	0.8	0.3	0.006	0.4	0.017	35	0.04	0.06	0.6	39	2	0.8	1.5	0.3	9	4	3	2	22
	C13	0.9	1.4	0.19	0.8	0.19	0.04	0.18	0.02	0.12	0.02	0.07	0.007	0.05	0.007	0.7	0.3	0.004	0.4	0.02	58	0.04	0.07	0.8	58	4	0.6	2	0.5	13	5	3	2	14
	C14	1.5	2	0.3	1.2	0.3	0.06	0.3	0.03	0.2	0.04	0.12	0.014	0.09	0.013	0.8	0.3	0.010	0.7	0.04	36	0.06	0.17	1.4	105	8	1.5	7	2	33	14	8	6	14
	C15	0.7	1.16	0.15	0.6	0.14	0.03	0.12	0.014	0.09	0.014	0.04	0.005	0.03	0.005	0.9	0.3	0.006	0.4	0.018	32	0.018	0.08	0.6	28	3	1.0	1.8	0.4	8	7	3	3	22
	C16	0.6	1.0	0.13	0.5	0.12	0.02	0.10	0.012	0.07	0.012	0.04	0.004	0.03	0.004	0.8	0.3	0.006	0.7	0.02	24	0.02	0.08	0.5	24	3	1.5	2	0.5	5	5	2	1.6	23
	C17	0.5	1.0	0.12	0.5	0.11	0.02	0.10	0.011	0.07	0.011	0.03	0.004	0.03	0.004	0.5	0.2	0.008	1.6	0.02	23	0.06	0.11	0.4	26	5	1.2	4	0.6	12	5	3	1.1	12
	C18	0.6	1.1	0.14	0.6	0.13	0.03	0.12	0.014	0.08	0.014	0.05	0.005	0.03	0.005	0.8	0.3	0.005	0.8	0.3	29	0.04	0.09	0.5	18	4	0.8	1.2	0.2	9	5	2	0.9	15
	μ±σ	0.8±0.3	1.3±0.4	0.17±0.06	0.7±0.2	0.15±0.05	0.03±0.01	0.15±0.06	0.017±0.007	0.10±0.04	0.017±0.008	0.05±0.03	0.006±0.003	0.04±0.02	0.006±0.003	0.8±0.1	0.28±0.04	0.007±0.002	0.9±0.7	0.024±0.008	32±12	0.04±0.02	0.10±0.03	0.7±0.3	39±29	4±2	3±4	3±2	0.6±0.7	12±9	6±3	4±2	2±2	17±4
Serreta	C19	0.5	0.7	0.10	0.4	0.11	0.02	0.08	0.010	0.06	0.011	0.03	0.004	0.03	0.004	6	0.17	0.004	0.2	0.009	67	0.09	0.10	0.3	15	0.6	0.6	1.2	0.14	2	3	2	1.1	8
	C22	1.6	1.8	0.4	1.5	0.3	0.07	0.3	0.04	0.3	0.04	0.13	0.014	0.09	0.012	0.9	0.4	0.006	0.2	0.009	9	0.06	0.12	1.4	7	0.3	0.7	0.5	0.16	1.0	3	5	2	16
	C24	1.6	2	0.3	1.4	0.3	0.06	0.3	0.04	0.2	0.04	0.13	0.014	0.08	0.011	0.5	0.5	0.012	0.5	0.015	18	0.04	0.14	0.9	13	1.1	1.1	1.2	0.3	9	5	3	0.3	21
	C25	0.3	0.5	0.07	0.3	0.06	0.011	0.05	0.006	0.04	0.006	0.019	0.002	0.017	0.002	1.2	0.16	0.007	0.3	0.005	8	0.04	0.05	0.19	7	0.9	1.3	0.19	0.07	1.0	1.7	1.5	0.7	7
	C26	0.6	1.0	0.15	0.6	0.13	0.03	0.12	0.015	0.09	0.017	0.05	0.006	0.04	0.006	0.8	0.2	0.006	0.3	0.02	18	0.08	0.16	0.5	10	1.6	1.2	0.8	0.17	2	5	5	0.9	19
	C30	1.2	1.4	0.2	0.8	0.19	0.04	0.18	0.02	0.13	0.02	0.07	0.007	0.05	0.007	0.6	0.2	0.007	0.6	0.013	23	0.06	0.09	0.8	10	3	2	1.4	0.18	2	3	3	1.4	9
	C31	0.4	0.8	0.10	0.4	0.09	0.018	0.08	0.009	0.06	0.010	0.03	0.004	0.03	0.004	0.7	0.18	0.009	0.4	0.012	10	0.04	0.3	0.3	5	1.8	0.8	0.8	0.2	1.9	3	3	1.2	17
	C32	0.4	0.6	0.09	0.4	0.08	0.018	0.08	0.009	0.06	0.010	0.03	0.004	0.02	0.004	1.1	0.2	0.007	0.3	0.014	15	0.02	0.2	0.3	6	1.1	1.1	1.0	0.17	1.0	4	3	0.4	15
	C33	1.1	1.8	0.3	1.0	0.2	0.05	0.2	0.02	0.15	0.03	0.09	0.010	0.07	0.009	7	0.5	0.015	1.3	0.03	44	0.05	0.2	0.9	24	5	1.5	1.7	0.3	8	6	8	1.1	23
	C34	0.6	0.9	0.14	0.5	0.12	0.03	0.11	0.013	0.08	0.014	0.05	0.005	0.04	0.005	0.7	0.3	0.006	0.4	0.011	11	0.05	0.5	0.4	5	3	0.3	0.4	0.09	3	5	5	0.6	21
	C36	0.7	1.4	0.17	0.7	0.15	0.03	0.13	0.017	0.11	0.018	0.06	0.007	0.05	0.007	0.4	0.4	0.015	1.3	0.019	28	0.09	0.13	0.5	8	4	1.7	1.5	0.4	9	6	5	0.6	27
	C37	3	3	0.5	2.3	0.5	0.11	0.6	0.07	0.4	0.07	0.2	0.02	0.14	0.018	5	0.3	0.007	0.7	0.016	11	0.09	0.12	3.6	101	3	5	5.9	1.6	31	6	7	5	10
	C38	0.3	0.5	0.07	0.3	0.06	0.011	0.05	0.006	0.04	0.006	0.02	0.003	0.02	0.003	3	0.17	0.007	1.3	0.006	6	0.017	0.5	0.2	18	3	2	1.0	0.4	1.1	4	3	0.4	8
	C39	0.7	1.2	0.15	0.6	0.13	0.03	0.12	0.013	0.08	0.014	0.05	0.04	0.006	0.3	0.3	0.011	1.5	0.013	10	0.03	0.06	0.4	7	6	1.9	1.6	1.2	4	10	5	0.3	19	
	C40	1.0	1.7	0.2	0.9	0.2	0.05	0.2	0.03	0.15	0.03	0.09	0.011	0.07	0.010	1.4	0.5	0.012	2	0.03	13	0.10	0.10	0.8	14	4	0.9	1.4	0.3	10	5	3	0.4	12
	C41	1.8	2	0.4	1.6	0.4	0.09	0.4	0.05	0.3	0.06	0.18	0.018	0.12	0.015	1.0	0.2	0.007	7	0.009	8	0.11	0.08	3	55	78	121	5	1.0	30	3	3	4	12
	C42	0.8	1.0	0.19	0.8	0.17	0.04	0.17	0.02	0.13	0.02	0.07	0.007	0.05	0.006	0.6	0.3	0.007	0.2	0.008	12	0.04	0.7	10	8	3	1.9	0.3	4	5	3	0.3	18	
	C43	0.8	1.4	0.2	0.8	0.19	0.04	0.17	0.02	0.13	0.020	0.07	0.007	0.05	0.006	1.1	0.4	0.010	0.4	0.016	16	0.03	1.1	0.6	10	3	1.0	1.1	0.11	4	5	4	0.5	22
	C44	0.5	0.9	0.13	0.5	0.10	0.02	0.12	0.012	0.08	0.012	0.04	0.004	0.04	0.004	0.8	0.2	0.007	0.5	0.012	20	0.06	0.9	2	9	2	1.1	1.2	0.2	9	5	2	0.2	20
	μ±σ	0.9±0.6	1.3±0.7	0.2±0.1	0.8±0.5	0.2±0.1	0.04±0.03	0.2±0.1	0.02±0.02	0.1±0.1	0.02±0.02	0.08±0.05	0.008±0.005	0.05±0.03	0.007±0.004	2±2	0.3±0.1	0.009±0.004	1±1	0.014±0.007	18±14	0.06±0.03	0.3±0.3	0.9±0.9	18±23	7±17	8±27	2±1	0.3±0.4	7±8	4±1	4±2	1±1	16±6
All C samples		1.1±0.8	1.5±0.7	0.2±0.1	0.9±0.6	0.2±0.1	0.05±0.03	0.2±0.1	0.02±0.02	0.2±0.1	0.03±0.02	0.08±0.06	0.009±0.006	0.06±0.04	0.008±0.005	1±2	0.3±0.1	0.010±0.005	1±1	0.017±0.008	22±14	0.07±0.07	0.2±0.3	1.0±0.9	30±31	6±13	6±21	2±1	0.4±0.5	9±9	5±2	4±2	1±1	17±5	

Note: The concentrations are expressed in μg/g. <LOD = under the limit of detection which for Cr is 0.98 μg/g.

Annex 4. Diagrams of PCA study of nucleus samples by using all elements as variables: a) sample/scores plot, b) variables/loadings plot.

Annex 5. Diagrams of PCA study of cortex samples by using REE, Y, Fe, Ti and Al as variables: a) sample/scores plot, b) variables/loadings plot.
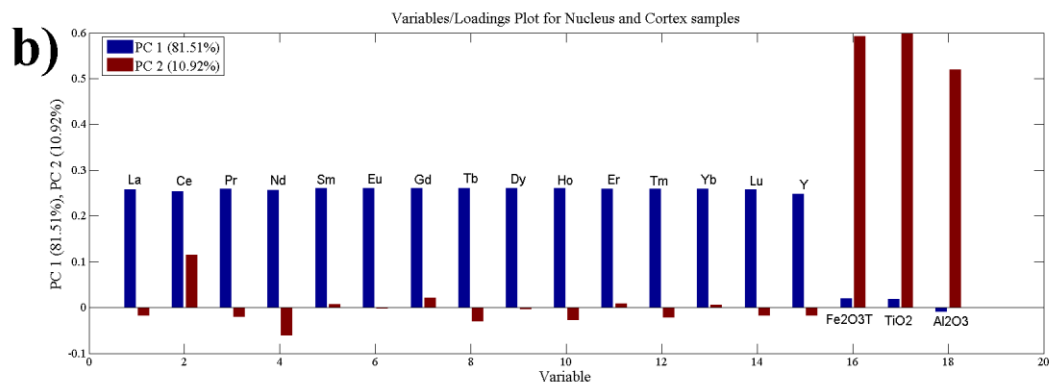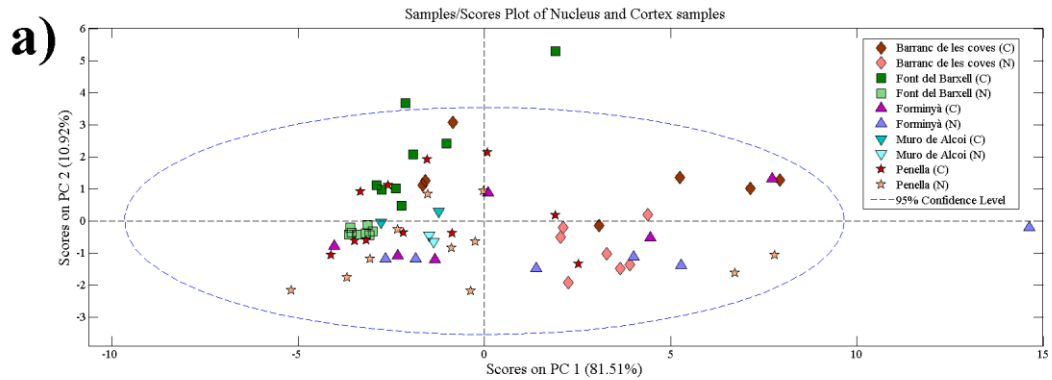
Annex 6. Diagrams of PCA study of cortex and nucleus samples by using REE, Y, Fe, Ti and Al as variables: a) sample/scores plot, b) variables/loadings plot.

Anexo B

Ramacciotti et al. (2022). Moving to the land: First archaeometric study of chert procurement at Cueva de la Cocina (Eastern Iberia)

Moving to the land: First archaeometric study of chert procurement at Cueva de la Cocina (Eastern Iberia)

Mirco Ramacciotti[1,2], Oreto García Puchol[3,*], Alfredo Cortell-Nicolau[3], Gianni Gallello[3,4], Angel Morales-Rubio[2], Agustín Pastor[2]

[1] Department of Prehistory, Archaeology and Ancient History, University of Valencia, Avenida de Blasco Ibáñez 28., 46010 Valencia, Spain.

[2] Analytical Chemistry Department, University of Valencia, Edifici Jeroni Muñoz, Dr. Moliner 50, 46100 Burjassot, Spain.

[3] PREMEDOC Department of Prehistory, Archaeology and Ancient History,University of Valencia, Avenida de Blasco Ibáñez 28. 46010 Valencia, Spain.

[4] Department of Archaeology, University of York, King's Manor, York, YO17EP, UK.

* Corresponding author

The present work is the first attempt using an archaeometric approach to characterize the potential chert outcrops and retrace the provenance of the chert raw materials in the Mesolithic and Neolithic contexts of the Eastern Iberia central site of Cueva de la Cocina (Dos Aguas, Valencia). Therefore, a research project aimed to identify and characterize potential sources in the surroundings of the site was carried out, as a first step, to test some hypothesis related to raw materials provenance hypotheses. Elemental profiles of several archaeological artifacts and of geological samples collected in different local and non-local outcrops were obtained using X-ray fluorescence spectroscopy and inductively coupled plasma mass spectrometry. Then, chemical data were processed using multivariate statistics in order to investigate the possible links between the outcrops and archaeological artifacts. Preliminary results point to the use of local raw materials and also the presence of rocks outcropping in a perimeter of more than fifty kilometres around Cueva de la Cocina, opening a new window to investigate the socioecological dynamics of the last hunter-gatherer and the first farmers inhabitants from a diachronic point of view in this region.

Keywords: Mesolithic, Neolithic, raw materials, provenance, chert, REE.

1. Introduction

For the first time, archaeological chert artefacts related to Mesolithic and Neolithic sequences at Cueva de la Cocina and its potential raw material sources were characterized to observe similarities in their chemical features.

The site, located nearby Dos Aguas (Valencian Community, Spain), is a large cavity opened in La Ventana ravine, a tributary stream flowing from the valley of La Canal through the Falón ravine, ending in the Xúquer river (Figure 1). This area, which is ~40 km distant from the Mediterranean Sea, represents the south-eastern end of the Iberian System. Well-known in the archaeological literature (Fortea, 1973; Fortea et al., 1987; García Puchol, 2005; Martí Oliver et al., 2009; García Puchol et al., 2018; Pericot, 1945), Cueva de la Cocina has been considered a pivotal site for explaining the sequence of the last Mesolithic hunter-gatherer groups in Eastern Iberia relating with blades and trapezes techno-complexes (Binder et al., 2012; Martí Oliver et al., 2009). The rich Mesolithic deposit includes numerous biological and cultural remains that comprise a remarkable concentration of lithic tools. Nevertheless, the top levels have been interpreted as an acculturation process with the arrival of the Neolithic groups in the neighboring areas (Fortea, 1973), although for some authors these finds are just a product of taphonomic and post-depositional processes (Cortell-Nicolau et al., 2020; García Puchol, 2005; 2018; Juan Cabanilles & García Puchol, 2013; Pardo-Gordó et al., 2018). Recent archaeological surveys have identified chert outcrops that might have been used as a raw material source in La Canal valley and in the nearby locality of La Paridera (Pardo-Gordó et al., 2016; 2017).

This work aims to identify the potential sources of chert found in Cueva de la Cocina, providing new data of the chert distribution in the region. First, potential outcrops have been identified and sampled, then, geochemical characterization was carried out and the obtained results were compared with some archaeological artifacts in a first attempt to test potential cherts use. Considering the Holocene sequence in the site, some archaeological questions emerge. On the one hand, Cocina presents a succession of occupation episodes that encompasses the development of the last Mesolithic technocomplex with blades and trapezes (named Geometric Mesolithic in the Spanish literature) from the middle of the 9th to the middle of the 8th millennium cal BP. Thus, the first hypotheses suggested by the observation of macroscopic characteristics (grain, color, cortex description) regarding variability in a diachronic view (García Puchol,

2005) could be tested. The identification of potential local raw materials will permit us to imply direct strategies of procurement considering continuities and/or different degrees of variability. On the other hand, the expansion of the sequence into the Neolithic provides an opportunity to compare chert procurement from the Mesolithic components and broader patterns observed in other regions from the beginning of the Neolithic (García Puchol, 2005; 2009).
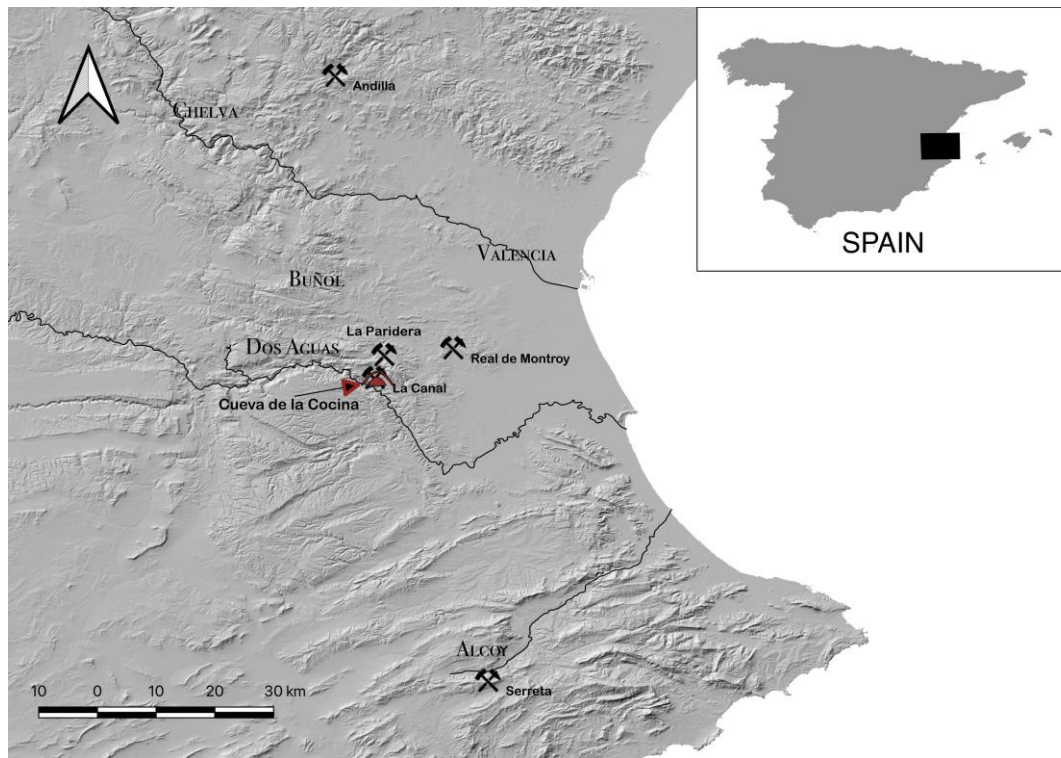
Figure 1. Map of Cueva de la Cocina and the sampled outcrops.

In order to compare natural and archaeological samples, we have selected a lithic tool collection from the archaeological assemblage of Cueva de la Cocina. Due to the destructive nature of the analysis carried out, the initial test was developed upon artifacts coming from disturbed levels, considering the variability observed through macroscopic analysis in archaeological context. Forty-two fragments were selected for the analysis. Chert nodules were collected from three outcrops at proximal to sub-regional scale, from few hundreds of meters up to 16 km from Cueva de la Cocina. However, several artifacts have macroscopic features different from the local rocks (García-Puchol, 2005). This is why geologic samples of Domeño chert outcropping in the northern area of the Valencia province (Eixea et al., 2011) were collected from the outcrop of Andilla and analysed. All these samples were analysed by a portable X-ray fluorescence spectrometer (pXRF) and an inductively coupled plasma mass

spectrometer (ICP-MS) to obtain major, minor and trace elements concentrations. Elemental data from Serreta chert type outcropping in the southern Valencian Community and analysed in a previous work (Ramacciotti et al., 2019a) were included in the study due to the presence of Cueva de la Cocina artifacts showing similar macroscopic features. Principal component analysis (PCA) was employed for exploratory data analysis, and in order to evaluate the possible link between the potential outcrops and the archaeological materials a quadratic discriminant analysis (QDA) model was built.

1.1 Assessing lithic raw material procurement

Chert was one of the most employed lithotypes for the manufacturing of stone tools due to its properties that allow the production of durable and sharp objects of different sizes (Luedtke, 1992). A radius within 10 km from a settlement is often considered the maximum distance for local lithic raw materials sources for hunter-gatherer groups (Ditchfield & Ward, 2019; Frahm & Hauck, 2017; Gómez de Soler et al., 2020). However, while supply from local chert deposits provides information about the relationship between human groups and their immediate surroundings, the presence of chert types potentially from tens to hundreds of kilometres from an investigated site (Boulanger et al., 2015; Chatzimpaloglou et al., 2020; O'Leary et al., 2017) raises interesting questions about possible long distance procurement, exchange networks, large settlement movements and colonization from different territories (Borrell, 2019; Forenbaher & Perhoc, 2015; Hess & Riede, 2020; Landry et al., 2018; Olofsonn & Rodushkin 2011; Parow-Souchon & Purschwitz, 2020; Speer, 2014; Robb & Farr, 2008; Tykot, 2003).

Sourcing chert artifacts to potential raw material outcrops is a challenging task. Archaeologists have often relied on macroscopic features like colour or translucency (Luedtke, 1992) but the variability of these characteristics within a single outcrop, along with the indiscernibility of chert samples from others by naked-eye examination alone led to the introduction of several characterization techniques from the natural sciences (Delluniversità et al., 2019 and references therein). Other studies evidenced the limitations of an approach based only on macroscopic characterization (Calogero, 1992; Hess, 1996; Sánchez de la Torre, 2019). Methods based on multielement analysis have been often employed in chert provenance studies. Several analytical techniques have been used. X-ray fluorescence spectroscopy (XRF) is employed for

determining major and minor elements concentrations, due to the possibility of performing fast non-destructive analysis with minimal sample preparation (Mehta et al., 2017). However, more sensitive techniques such as neutron activation analysis (NAA; Stewart et al., 2020; Boulanger et al., 2015) and Inductively Coupled Plasma Mass Spectrometry (ICP-MS; Brandl et al., 2018; Ten Bruggencate et al., 2015) are also used to determine trace elements concentration. The goal of this approach is to identify elemental features which discriminate geologic samples from one deposit from others in order to source the geological origin of the raw materials used to manufacture artifacts, often employing multivariate statistics techniques of classification like discriminant analysis (DA; Moreau et al., 2019; O'Leary et al., 2017). For example, among the possible markers, rare earth elements (REE: La, Ce, Pr, Nd, Sm, Eu, Gd, Tb, Dy, Ho, Er, Tm, Yb, Lu, and Sc and Y) have shown to be particularly effective in discriminating different types of cherts and solving provenance issues (Finkel et al., 2018; Olofsonn & Rodushkin, 2011; Ramacciotti et al., 2019a; Elefanti et al., 2021). Indeed, robust geochemical studies proved that different sedimentary environments distinguish chert through characteristic REE levels and fractionation (Murray, 1994) and they were employed as provenance markers in studies carried out on a wide range of geoarchaeological materials (Aura Tortosa et al., 2020; Gallello et al., 2016; Lecuit et al., 2018; Ramacciotti et al., 2019b; 2020). However, discriminating between chert deposits is often a challenging task since chert is composed almost entirely of silicon dioxide (SiO_2) and most metals are found at trace concentrations with frequently overlapping distributions, especially working at a local scale and with outcrops within the same geological levels (Speer, 2016), although these analytical approaches have also been successfully used (Parish & Werra, 2018).

1.2 Geological setting and description of local chert outcrops

Cueva de la Cocina is in the south-east end of the Iberian System, a mountain range within the Iberian plateau, together with the Catalan Coastal Range, and extending for ~400 km through the part of the peninsula in the NW-SE direction, with a wideness of ~250 km, between the Meseta Central (W) and the Ebro basin (E), and it is limited to the north by the Cantabrian Mountains and to the south by the Prebaetic System and the coastal plain of Valencia (Vera, 2004). The range is an intraplate Alpine orogenic system resulting from the tectonic inversion of Mesozoic basins during the Paleogene,

characterized by horsts and grabens, filled up with alluvial and lacustrine sediments in the Cenozoic, originated by Neogene stretching tectonic processes (Gutiérrez et al., 2014). The landscape is characterized by large planation surfaces extending on Jurassic and Cretaceous levels, often 1000 m or more above sea level, spaced out by "neotectonic grabens and uplifted blocks, fluvial valleys, poljes and areas of residual relief" (Gutiérrez et al., 2008).

The surroundings of La Canal plateau, where Cueva de la Cocina is located, are characterized by moderate elevations, with a maximum of 946 m at Pico del Ave. The above-quoted tableland is limited to the north by the depression of Dos Aguas and by the Sierra del Caballon, and by the Macizo del Caroig to the south. Xúquer river flow (NW-SE) excavated a deep and narrow valley which represents La Canal's west margin. The altitude of the land decreases to the east, where the Magro River Valley extends and the Valencian plain starts. The area is dominated by Cretaceous levels, characterized by a sequence of sedimentary carbonate rocks (limestone-dolomite series and marlstone), although Jurassic outcrops appear along with sporadic Triassic ones. Tertiary conglomerates, and Tertiary and Quaternary sedimentary deposits prevail in contrast to the east (García Velez et al., 1981).

Until recently, the area had not been surveyed in order to identify possible siliceous raw materials sources. However, the geological map indicates the presence of chert nodules in a micritic limestone belonging to the Upper Cretaceous levels (Santonian – Lower Campanian). This part of the sequence is characterized by a succession of neritic and lacustrine facies, which indicate a basin instability and a marine regression (García Velez et al., 1981). Three outcrops for Upper Cretaceous chert, were identified during the last surveys (Pardo-Gordó et al., 2016; 2017). One of the identified outcrops is located in La Canal, just a few hundred meters distant from Cueva de la Cocina. Here the chert appears as nodules and lenses both contained within the limestone pertaining to the Sierra de Utiel Formation (Fm, Vilas et al., 1982), and nearby. A second and more distant outcrop was identified at La Paridera, 6 km north-east from Cueva de la Cocina as the crow flies. The deposit is well-known by local people and was exploited until the past century to make agricultural tools. Furthermore, some archaeological artefacts have been collected during the field surveys (Pardo-Gordó et al., 2017), suggesting the use of the area during prehistoric times. The parent rock was found in the Paleogene conglomerates outcropping in the area, but the above-quoted

Upper Cretaceous limestone, probable a primary source, outcrops in the vicinity, as well. Finally, a more distant outcrop was found at Real de Montroy, 15 km north-east from Cueva de la Cocina. This area is characterized by an alluvial fan linked to Early Jurassic sedimentary levels at El Cerro but Upper Cretaceous levels (Sierra de Utiel Fm) outcrops all around, and chert nodules were found in association with the parent limestone, although no evidence of prehistoric human activity was found during the field survey.

2. Materials and Methods

2.1 Sampling

Macroscopic features of each sample are reported in the Table 1 while their origin is indicated by sample name (LC: La Canal, LP: La Paridera, RM: Real de Montroy, AN: Andilla, AR: archaeological sample). The sampled deposits can be seen in Figure 1.
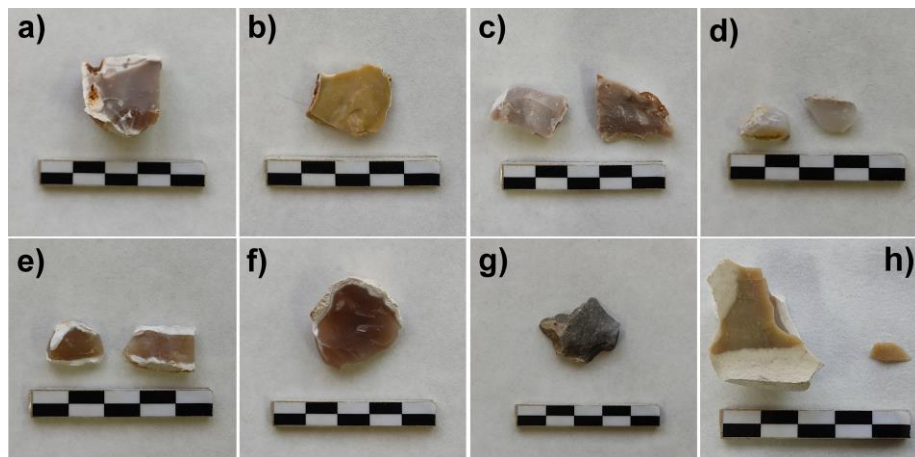
Figure 2. Natural cherts from the different outcrops according to their macroscopic features: a) LC03, b) LC11 and c) LC17 from La Canal (LC); d) LP07 and e) LP11 from La Paridera (LP); f) RM04 from Real de Montroy (RM); g) AN04 (Domeño chert) from Andilla (AN); h) M43 from Serpis Valley (Serreta chert; Ramacciotti et al., 2019a).

Forty-three samples from three different chert outcrops, classified as proximal (adjacent to the site) and local (up to 15 km, less than one day of travel), pertaining to the same geologic unit (Sierra de Utiel Fm), were sampled and analyzed. Eighteen samples were collected from the proximal outcrop of La Canal (LC). Most nodules have whiteish to grey cortex and a reddish patina on the outer surface, while inner color varies (yellow, brown, and more frequently reddish) and is opaque to translucent, depending on the sample (Figure 2a-c). Eleven samples were collected from the local

secondary outcrop of La Paridera (LP). The samples have developed a white cortex of different thickness and have suffered certain degrees of weathering, and are characterized by semi- to translucent inner nucleus of various colours (Figure 2d-e). Fourteen samples were collected from the local outcrop of Real de Montroy (RM). Chert fragments developed whiteish cortex while most of them show translucent and weak red inner portions, similar to some samples of LP and LC (Figure 2f).

Table 1. Samples names and macroscopic features. Sample acronyms indicate the origin: LC = La Canal, RM = Real de Montroy, AN = Andilla, AR = archaeological sample.

Sample	Color	Code	TL	Sample	Color	Code	TL	Type	Sample	Color	Code	TL	Type
LC01	Very P. brown	10 YR 7/3	1	RM04	W. red	2.5 YR 4/2	2	-	AR13	P. brown	2.5 Y 7/4	1	F*
LC02	P. red	2.5 YR 7/2	1	RM05	W. red	2.5 YR 4/2	2	-	AR15	White	8/N	2	B*
LC03	Reddish gray	5 YR 5/2	2	RM06	W. red	2.5 YR 4/2	2	-	AR16	Olive yellow	2.5 Y 6/6	2	B*
LC04	Pinkish white	5 YR 8/2	0	RM07	W. red	2.5 YR 4/2	2	-	AR17	L. reddish brown	5 YR 6/3	2	F*
LC06	Reddish brown	2.5 YR 5/3	1	RM08	P. brown	10 YR 6/3	1	-	AR18	Pinkish gray	7.5 YR 7/2	2	F*
LC07	Pinkish gray	7.5 YR 6/2	1	RM09	P. red	2.5 YR 6/2	1	-	AR19	P. red	2.5 YR 7/2	1	F*
LC08	Brown	10 YR 5/3	1	RM10	W. red	2.5 YR 4/2	2	-	AR21	L. red	10 R 6/6	0	F*
LC09	Brownish yellow	10 YR 6/6	1	RM12	W. red	2.5 YR 4/2	2	-	AR22	Reddish brown	2.5 YR 5/4	2	B*
LC10	P. red	10 R 6/2	1	RM13	White	8/N	1	-	AR23	Strong brown	7.5 YR 5/6	2	B*
LC11	Olive yellow	2.5 Y 6/6	1	RM14	W. red	2.5 YR 4/2	2	-	AR24	P. red	10 R 6/4	1	F*
LC13	P. brown	2.5 Y 7/4	1	RM15	Brown	7.5 YR 5/2	0	-	AR25	P. brown	10 YR 6/3	1	F*
LC14	Pinkish gray	7.5 YR 6/2	1	AN01	Gray	5/N	0	-	AR27	P. brown	2.5 Y 7/4	0	F*
LC15	L. brownish gray	10 YR 6/2	1	AN02	Gray	5/N	0	-	AR28	W. red	10 R 5/4	1	F*
LC16	P. brown	2.5 Y 7/4	1	AN03	Gray	5/N	0	-	AR29	Reddish gray	2.5 YR 5/1	0	F*
LC17	P. red	2.5 YR 6/2	1	AN04	Gray	5/N	0	-	AR30	Gray	5 YR 6/1	0	F*
LC18	W. red	2.5 YR 4/2	2	AN05	Gray	5/N	0	-	AR31	Pinkish gray	5 YR 6/2	0	F
LC19	P. red	2.5 YR 6/2	1	AN06	L. gray	7/N	0	-	AR32	Yellowish brown	10 YR 5/8	1	F*
LC20	P. brown	10 YR 6/3	1	AN07	L. gray	7/N	0	-	AR33	P. brown	2.5 Y 8/4	0	F*
LP01	L. reddish brown	2.5 YR 6/3	1	AN08	L. gray	7/N	0	-	AR34	White	8/N	2	F*
LP02	L. reddish brown	2.5 YR 6/3	1	AN09	Gray	5/N	0	-	AR35	W. red	2.5 YR 4/2	1	F*
LP03	Reddish gray	5 YR 5/2	1	AR01	L. gray	2.5 Y 7/2	0	F	AR36	L. olive brown	2.5 Y 5/3	2	F*
LP04	Brownish yellow	10 YR 5/6	2	AR02	Brownish yellow	10 YR 6/6	1	F	AR39	Grayish brown	2.5 YR 5/2	0	F
LP05	L. reddish brown	2.5 YR 6/3	1	AR03	Pinkish gray	5 YR 7/2	2	F*	AR40	D. reddish brown	5 YR 3/3	1	F*
LP06	L. reddish brown	2.5 YR 6/3	1	AR04	Yellowish brown	10 YR 6/6	2	B*	AR41	Grey	5/N	0	F*
LP07	White	8/N	1	AR05	L. yellowish brown	2.5 Y 6/4	1	C	AR42	W. red	2.5 YR 5/2	2	B*
LP08	Yellowish brown	10 YR 5/4	2	AR06	Brownish yellow	10 YR 6/6	2	B*	AR43	White	8/N	0	F*
LP09	White	8/N	1	AR07	D. reddish gray	10 R 4/1	1	B*	AR44	Pinkish gray	7.5 YR 6/2	0	F*
LP10	Pinkish gray	5 YR 6/2	2	AR08	L. grey	10 YR 7/1	0	F*	AR45	L. brown	7.5 YR 6/3	2	F*
LP11	Grayish brown	10 YR 5/2	2	AR09	L. yellowish brown	2.5 Y 6/4	2	F*	AR46	Yellowish brown	10 YR 5/8	2	F*
RM01	W. red	2.5 YR 4/2	2	AR10	Weak red	10 R 5/4	2	F*	AR47	P. brown	2.5 Y 7/4	2	B*
RM02	W. red	2.5 YR 4/2	2	AR11	L. yellowish brown	2.5 Y 6/4	2	F*					
RM03	W. red	2.5 YR 4/2	2	AR12	White	8/N	2	B*					

Notes: samples colour and codes were given according to Munsell Color System (L: light; W: weak, P: pale, D: dark); translucency (TL) was estimated by naked-eye and samples were classified by an arbitrary discrete scale going from 0 (opaque) to 2 (translucent). C: chunk, F: flake; B: blade; (*): fragment.

Nine geologic chert fragments were collected in a non-local (beyond a day of travel) colluvial secondary outcrop in the immediate proximity of the Mesolithic open-air settlement of Mangranera (García-Puchol, 2005), close to the village of Andilla (AN; Valencian Community, Spain) and about 65 km north of Cueva de la Cocina. From a macroscopic point of view, the collected samples are visually similar to the Domeño type chert, and are opaque and light grey to grey, in some cases showheing a whiteish patinated surface (Figure 2g). The primary source for this chert type has been visually identified as the Middle Jurassic carbonate levels surrounding the town of Chelva,

which is about 70 km north of Cocina, although it is common also in secondary contexts in colluvial deposits and in the Turia river alluvia (Eixea et al., 2016). Geological studies indicate that this period, taking place after the Early Jurassic marine transgression, was characterized by deepening-shallowing cycles and deposition of sediment happened on an open-marine environment (Assens Caparrós et al., 1980; Gómez & Fernández-López, 2006). However, the Middle Jurassic limestone with chert outcrops occurs also in the mountains north-west of Buñol, which are about 23 km distant from the Cueva de la Cocina (García Velez et al., 1980). Finally, forty-two archaeological samples (AR) were selected from the artifacts found during the recent archaeological excavations, mostly fragments of blades and flakes, and one chunk (AR05). These first samples were selected due to them being out of their primary archaeological context and the destructive nature of the analysis; thus, they cannot be attributed to the different phases of occupation of Cueva de la Cocina. The artifacts have variable macroscopic features, showing different colours and levels of translucency (Figure 3). However, while most of them have characteristics which are compatible with local chert (Figure 3a-c), some artifacts show features that are not common in local natural samples. Not many grayish nodules have been found among the local samples but, as previously stated, Domeño chert is very common north of Cueva de la Cocina and can be the source for some of the grayish archaeological artifacts (AR08, 29, 30, 31, 39 and 41, Figure 3d). Furthermore, some samples of yellowish-brownish cherts (called *sílex melado* in the Spanish archaeological literature; AR02, 04, 06, 09, 11, 13, Figure 3e, 16, 23, 25, 32-33, 36, 46-47) may also be non-local types. Finally, two samples exhibit red hues (AR21, 28, Figure 3f) and, although reddish nodules were observed in both LC and LP outcrops, thermal alteration can turn chert colour to red (Mathur et al., 2020).

In order to document the possible presence of non-local samples, especially among the *sílex melado* ones that occur also in the Prebaetic System, previously published data from seventeen samples of Serreta chert were used (N19 and N37 were excluded due to their anomalous concentrations for several elements). These samples were collected about 60 km south of Cueva de la Cocina in the surrounding of Alcoy (Alicante, Spain) and analyzed employing the same laboratory procedures and equipment of the present paper (Ramacciotti et al., 2019a). This chert, characterized by high flaking quality, outcrops in situ within the Eocene limestone levels of La Serreta but occurs also in the local Oligocene conglomerates, due to the strong erosive action of marine

transgressions and regressions (Martínez del Olmo & Benzaquen, 1975). as Additionally, La Serreta chert is found in the foothill colluvial deposits and alluvial deposits of the Serpis river (Molina Hernandéz et al., 2016). The variability in this chert's macroscopic features suggests a complex petrogenesis, probably linked to slightly different depositional environments and multiple silicification events (Molina Hernández, 2016), tied to the geologic evolution of the area (Geel, 2000) which led to complex marine facies (Vera, 2004).
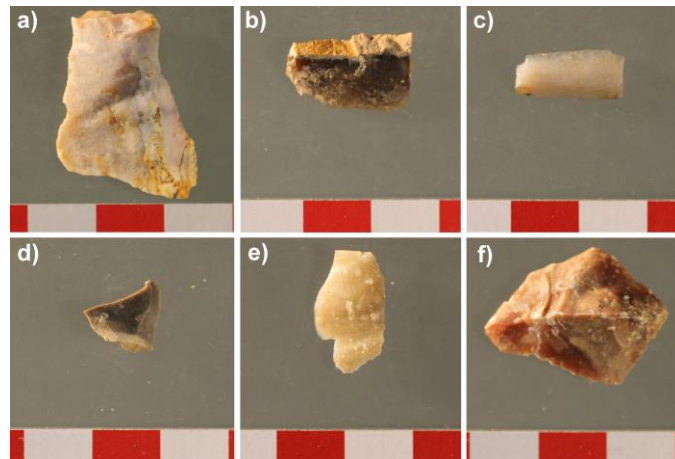
Figure 3. Main chert types among the archaeological artefacts: a) AR01, b) AR07, c) AR12, d) AR41, e) AR13 and f) AR28.

2.2. Multielement analysis

The samples were analysed by X-ray fluorescence spectroscopy employing a pXRF, to determine their content in major elements, and inductively coupled plasma mass spectrometry (ICP-MS) to obtain trace elements including rare earth elements (REE, Annex 1a).

Prior to analysis, geologic samples were fragmented with a tungsten carbide (WC) jaw crusher (Retsch, BB 50) and only fresh rock chips were selected. Exterior incrustations were removed from Cocina chert artifacts employing diluted acetic acid (10%), then, clean samples were fragmented with the WC jaw crusher and small chips were selected, trying to avoid cortical and weathered parts when feasible. The selected chips of the natural and archaeologic samples were subsequently powdered and homogenised with an agate mortar and pestle.

Each powdered sample was analysed by an S1 Titan pXRF by Bruker (Kennewick, Washington DC, USA) equipped with a Rhodium X-ray tube (50 keV) and X-Flash®SDD detector (resolution: 147 eV; Full Width at Half Maximum, FWHM: 5.9

keV). K, Ca, Ti and Fe concentrations were determined employing GeoChem Trace internal calibration.

Trace elements (Ba, Bi, Cd, Cr, Co, Cu, Pb, Li, Mn, Mo, Ni, Sr, Tl, V, Zn, U, Th) and REE (La, Ce, Pr, Nd, Sm, Eu, Gd, Tb, Dy, Ho, Er, Tm, Yb, Lu, including Sc and Y) concentrations were measured employing an Elan DRCII ICP-MS (Concord, Ontario, Canada). Powdered samples were processed via wet digestion through multiple acid attack (HCl, HNO_3 and HF) for ICP-MS analysis was carried out as explained in Ramacciotti et al. (2019a).

Since certified reference materials made of chert are not developed, blank silica powder (AMIS0484) and quartzite chips (AMIS0439), previously powdered through an agate mortar, from AMIS (Modderfontein, South Africa) were employed for reference to check the accuracy of the method.

The limits of detection (LD) for ICP-MS analysis are reported in Annex 1b.

2.3. Analysis of data

Data analysis was run in R (version: 4.0.2; R Core Team, 2020). Principal component analysis (PCA) was employed to carry out exploratory statistics of the dataset. A first PCA was performed on the samples from the local outcrops (LC, LP, RM), from AN and including the archaeological ones, and all the measured elemental concentrations, previously standardised (i.e.: transformed to Z-scores), were employed as variables. A second PCA model was built by using the artifacts and samples from LC, LP, RM, AN, as well as data of Serreta chert from the Serpis Valley (Ramacciotti et al., 2019a), except for the outliers of each outcrop (LC04, as well as N19 and N37 from Serreta samples). This last model was built employing rare earth elements, including Sc and Y, concentrations as variables. In order to investigate the relationship between the geological natural and archaeological samples in the PCA space, we used quadratic discriminant analysis (QDA), given that, for our data, it offers a better fit with less components compared to linear discriminant analysis (LDA). Models were built through "MASS" package (version: 7.3-53; Venables & Ripley, 2002) employing the geologic samples as a training set subdivided into three classes according to their geologic setting and the exploratory statistics of the chemical data ("Proximal": LC, 17 samples; "Local": RM and LP, 25 samples; "Non-Local": AN and Serreta, 26 samples). Discriminant analysis aims to find boundaries which divide the variable space in different regions according to the distributions of the classes of known observations and consequently, allowing to compute the posterior probability that an

unclassified observation pertains to one of the classes; while LDA obtains linear boundaries, QDA computes quadratic ones (Siqueira et al., 2017). Quadratic discriminant analysis is considered a "safe choice" dealing with non-normal multivariate distributions, especially in case of classes characterized by different covariance matrices (Finch & Schneider, 2006). The models were built employing the scores of the REE-based PCA as variables to reduce predictor numbers and avoid collinearity among variables. The number of PCs to be employed and the accuracy of the different models were evaluated employing leave-one-out cross-validation (LOOCV) through "caret" package (version: 6.0-86; Kuhn, 2020). The package "ggplot2" (version: 3.3.2; Wickham, 2016) was employed for data visualisation.

3. Results and Discussion

3.1 Multielement analysis results

The results of the multielement analysis were reported in the supplementary online materials (Annex 2 for major and trace elements concentrations, and Annex 3 for REE concentrations and fractionation parameters calculated after normalization with Post Archean Australian Shale (PAAS) values, McLennan, 1989, and as suggested by Lawrence et al., 2006, for Ce and Eu).
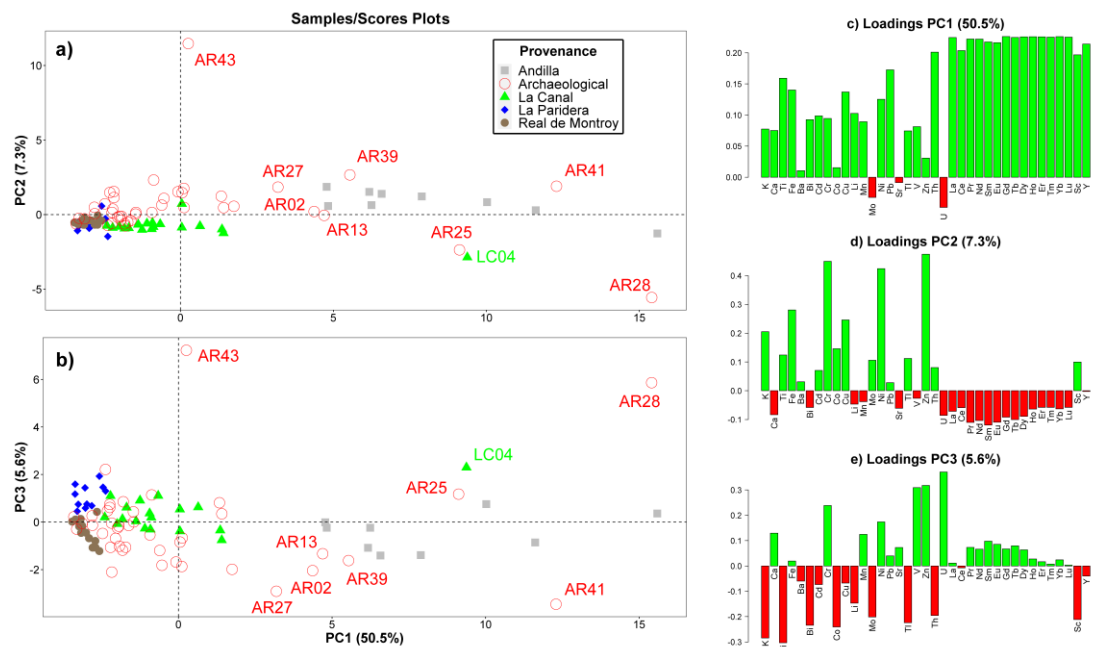
Figure 4. Results from PCA analysis on natural (AN, LC, LP, RM) and archaeologic (AR) samples employing all the analysed elements as variables. PC1 vs PC2 and PC1 vs PC3 samples/scores plots (a, b) and variables/loadings plots for PC1 (c), PC2 (d) and PC3 (e).

Principal component analysis was employed for the exploratory analysis of the dataset. PC1 accounts for 50.5% of the overall variance while PC2 and PC3 for 7.3% and 5.6%, respectively. Samples/scores plot in Figure 4a points out that the four analysed outcrops are characterized by different chemical features. Samples from La Paridera (LP), Real de Montroy (RM) and La Canal (LC) fall together, mostly in the negative PC1-axis, which is not surprising since these cherts come from the Upper Cretaceous levels of a defined area. However, the samples from LP and RM group are characterized by lowest scores for the first PC and by negative PC2 scores. On the other hand, most samples from LC have higher PC1 scores than LP and RM ones. Finally, Andilla (AN) samples have the highest PC1 scores and are plotted on the positive PC1-axis. This PCA plot allowed the identification of an outlier LC04, which has a very high PC1 score. Concerning PC3 (Figure 4b), most of the samples fall within 2 standard deviations of the mean, however, samples from LP show higher scores than RM ones.

The variables/loadings plots (Figure 4c-e) permit to evaluate the main features of the different outcrops and the chemical differences of the rocks.

As visible in Figure 4c, most of the variables have positive coefficients for PC1. This means PC1 scores are positively correlated with these elements. Indeed, AN samples, having the highest scores, show higher levels of most of the major (Fe, K, Ti) and the trace elements (Cd, Cr, Co, Cu, Ni, Pb, Th, Tl, Zn), while samples from LP and RM, having the lowest scores, show the lowest concentrations of most of metals such as Fe, Ti, Mn, Ni, Th, Tl. On the other hand, LC outcrop has intermediate levels between AN, and LP and RM for most of the elements, although it shows the highest concentrations for Ca, and Li and V. The entire REE group is characterized by very high loadings for PC1, indicating the strong contribution of these elements to the present model and a major role in the discrimination of the cherts, probably due to their capability to characterize different sedimentary environments, as suggested by several studies (Ramacciotti et al., 2019a and references therein). In particular, it can be observed that AN outcrop has the highest REE, Y and Sc concentrations, followed by LC and, finally, by RM and LP, which instead show the lowest ones. AN REE concentrations are similar to the ones obtained by Prudêncio et al. (2016) by NAA, although the three Domeño type chert samples analysed in this work show relevantly higher levels of Ce compared to the other REE than AN01-09, which suggests possible

variability within the outcrops. The REE pattern of AN samples also shows also unique features compared to the local geologic samples due to their stronger negative Ce anomalies, averagely lower La_n/Yb_n ratio and higher enrichment of Y over Ho. These parameters are usually considered a proxy for marine sedimentary environments (Tostevin et al., 2016), which is consistent with optical microscopy analysis (Eixea et al., 2011) and the geologic history of the area during the Middle Jurassic (Gómez & Fernández-López, 2006). Conversely, most samples from LC and RM show no anomalies for Ce and higher degrees of enrichment of light REE (LREE) over heavy REE (HREE), as suggested by La_n/Yb_n values. La Paridera outcrop shows higher variance for REE parameters (except for Eu_n/Eu^*). REE patterns prevalent for LC and RM cherts are consistent with a coastal environment although variance of chemical features found in the chert from the three Cretaceous outcrops could be explained by the occurrence of different silicification events in an evolving scenario (García Vélez et al., 1981).

The samples from Andilla have the highest PC2 scores, showing concentrations of major (K, Ti and Fe) and trace elements (in particular: Cr, Ni and Zn) which are positively correlated with PC2 (Figure 4d). Finally, PC3 loadings (Figure 4e) illustrate that chert from La Paridera have higher concentrations of V and U, more positively correlated with PC3 than Real de Montroy ones which have higher levels of Mo, negatively correlated with the same PC.

Concerning the archaeological samples, most of them show PC1 scores similar to the local cherts, although many have slightly higher PC2 and slightly lower PC3 ones. Eight artifacts plot farther from the group of local cherts, three yellowish-brownish chert artifacts (AR02, 13, 25), two greyish samples (AR39, 41), AR28 (reddish chert), AR27 and AR43, the last one probably due to its anomalous high levels of Co, Zn and Ni. AR39 and AR41 match AN cherts from the macroscopic point of views, however, origin of the other above-quoted samples is hard to explain with the current data of the studied outcrops.

3.2 Raw materials and artifacts origin

A second PCA was carried out including Serreta chert data (Ramacciotti et al., 2019a). LC04 was excluded, as well as N19 and N37 from Serreta samples, due to its anomalous chemical features compared to the other samples from their classes. REE,

Sc and Y were employed as variables to build the model. Indeed, as previously evidenced, local (LP and RM), proximal (LC), and non-local (AN) samples showed different amounts of REE and distinctive fractionation parameters.
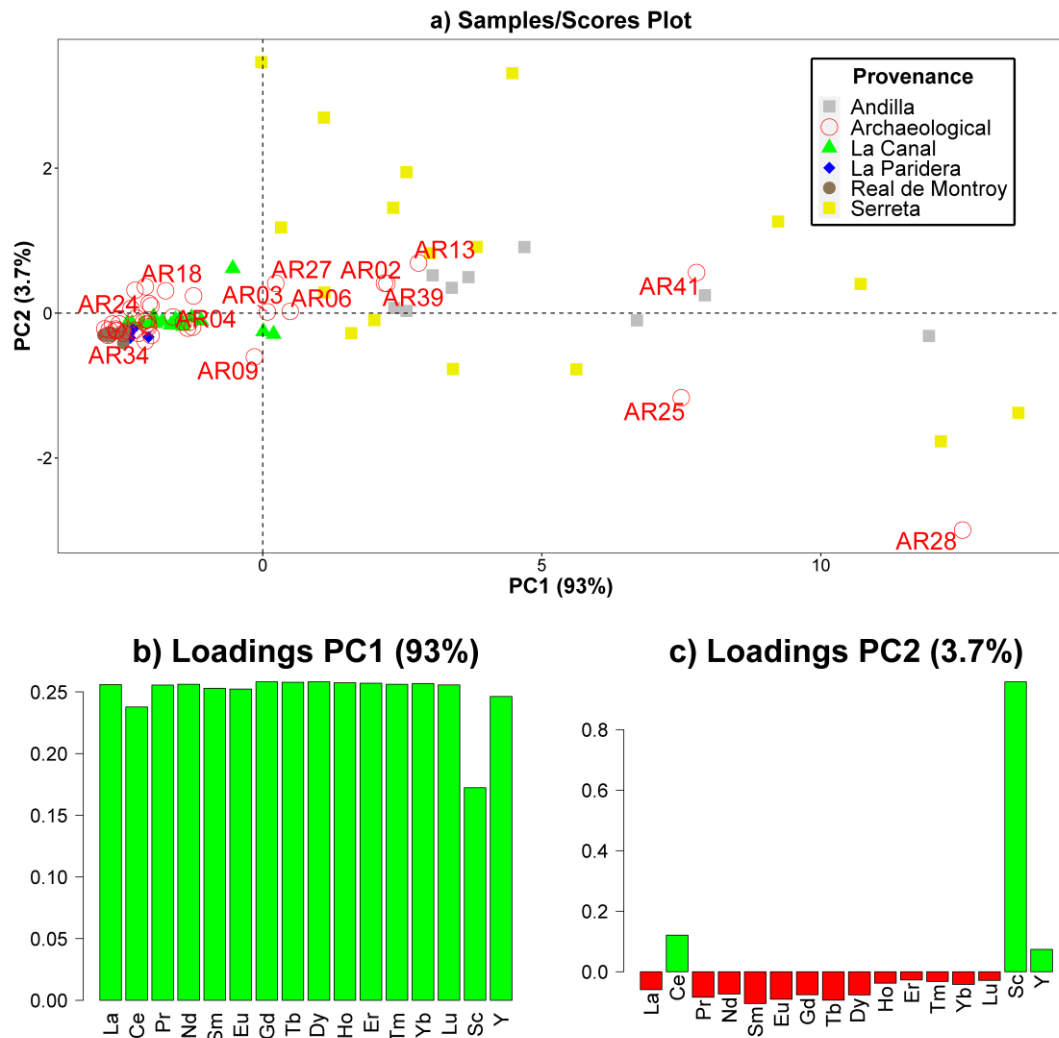
Figure 5. Results from PCA analysis including Serreta samples employing REE, Sc and Y as variables. PC1 vs PC2 samples/scores plots (a) and variables/loadings plots for PC1 (b), PC2 (c).

The PCA study suggests that Serreta samples have different chemical features, compared to local rocks (Figure 5), being scattered in the first and fourth quadrants of the samples/scores plot (Figure 5a) with AN chert. Variables/loadings plot for PC1 and PC2 (Figure 5b-c), explaining 93% and 3.7% of the overall variance respectively, suggests that the distribution of the first axis is mainly driven by total REE amount, while on PC2 Sc is the most influential variable. PC3 represents only 1.6% of the overall variance, reveals a slight separation between Serreta and AN samples due to the higher scores of the first ones. PC3 loadings suggest that the variance on this axis

is driven by REE fractionation. In particular by fractionation of LREE (positive loadings) and HREE (negative loadings), as well as by Ce and Y. AN samples show more intense negative Ce anomalies (Ce_n/Ce^* is 0.52 ± 0.13 for AN and 0.78 ± 0.12 for Serreta), higher levels of Y compared to Ho (Y/Ho is 44 ± 4 for AN and 38 ± 5 for Serreta) and lower levels of LREE over HREE (La_n/Yb_n is 1.17 ± 0.33 for AN and 1.46 ± 0.14 for Serreta). Proximal and local outcrops show a certain degree of discrimination on this axis, although it is less evident from the data. The archaeological samples mostly fall within or close to the cherts from the proximal and the local outcrops, including some grayish and yellowish-brownish chert artifacts. However, some samples fall within the non-local cherts (AR02, 13, 25, 39, 41) or between the two groups (AR03, 06, 09, 27).

In order to furtherly explore the PCA results and the possible origin of the analyzed artifacts, quadratic discriminant analysis (QDA) was used on the geologic samples as a training set and the REE-based PCA scores of the above-quoted model as variables. The different classes were evaluated on the basis of the geologic setting and of the grouping observed in the PCA. Samples from LC (Proximal), and from LP and RM (Local) belong to the same geologic formation, but they can be chemically distinguished. Serreta and AN (Non-Local) belong to two different formations, the PCA model is scarcely effective in discriminating between them but they have characteristic macroscopic features. Leave-one-out cross-validation was employed to test different models and choose the appropriate number of PC to be used as variables (Annex 5). Models using from two up to ten PCs were tested. The accuracy of the QDA for the first three models is above 0.90. It slightly increases from the first (PC1 and PC2, ~0.93) up to the second model (PC1 to PC3, ~0.94), then it decreases steadily (Annex 5a). Thus, a QDA model with PC1-3 was employed to perform classification. As a measure of confidence, we also used LDA analysis, which needed more complexity for similar accuracy, but whose results were only slightly different (Annex 5b). The confusion matrix table in Annex 5c shows the classification performance for each class after cross-validation. In particular, we can observe that each non-local sample was correctly classified. On the other hand, two out of seventeen proximal samples were classified as non-local. Finally, two out of twenty-five local samples were classified as proximal.
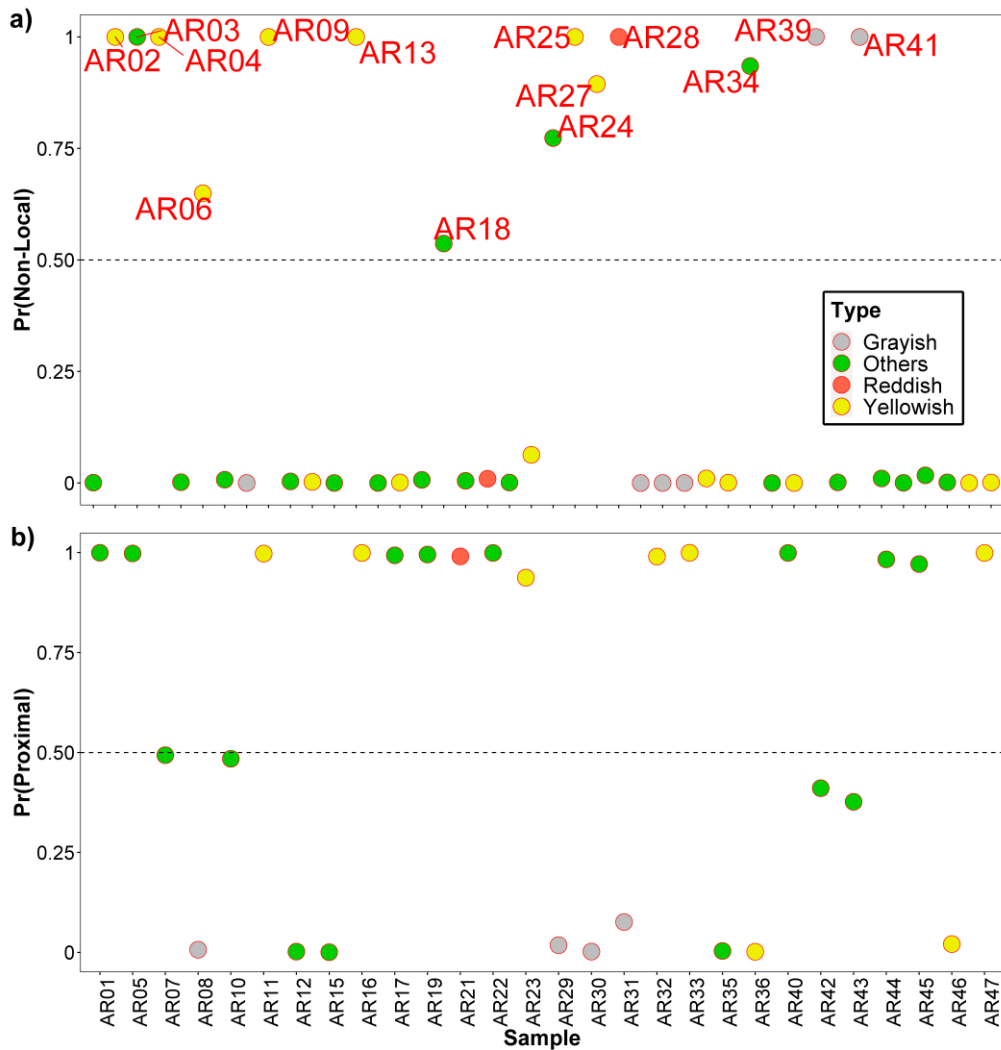
Figure 6. Posterior probabilities for QDA model classification of the archaeological samples (AR): probability for non-local classification of all the artefacts (a) and for proximal classification for samples for which Pr(Non-Local) is lower than 0.50 (b).

Figure 6a shows the probability of each archaeological sample, colored according to their macroscopic features, pertaining to the allochthonous chert outcrops. As shown, fourteen out of forty-two analysed samples show REE levels and patterns which deviate from the studied local chert. Furthermore, QDA suggests that at least a part of the yellowish-brownish artifacts could be made with not-identified raw materials and possibly with Serreta chert from the Serpis valley. Eight yellowish-brownish artifacts, visually similar to Serreta chert, fall within local and proximal outcrops and AR06 posterior probabilities for proximal and non-local origin are close. Gray samples AR39 and AR41 chemical features, together with their macroscopic characteristics, suggest that they were made with Domeño chert. The four grayish samples which fall within proximal and local deposits (AR08, AR29-31) show not only lower REE total

amounts, but also completely different REE fractionation parameters such as positive Eu anomalies and higher enrichment of LREE over HREE, while they have neither Ce negative anomalies nor high Y/Ho ratio. One reddish chert (AR28) falls with non-local samples, although its REE parameters are quite peculiar. Finally, among the other type of samples, only four are assigned to non-local deposits (AR03, AR18, AR24 and AR34). They have macroscopic features similar to some samples from proximal and local outcrops and are grouped closer to the nearby geological samples, but show slightly different REE levels and fractionation parameters compared to the collected natural samples, evidenced by their PC2 and PC3 scores. Among them, AR18 posterior probability for non-local grouping is just ~54%. They possibly pertain to a yet unidentified outcrop. Figure 6b shows the posterior probability for proximal classification of the samples for which QDA gave a posterior probability of being non-local below 0.5. Focusing on the samples classified as "Others", most of them seem to group with the proximal outcrop of La Canal (eight out of fifteen), while the other ones group with the local outcrops. However, posterior probabilities of AR07, AR10, AR42-43 are very close for the two provenances. Grayish cherts group with local samples. While an origin from La Canal would have been plausible due to the macroscopic variability of nodules from this outcrop, they are not comparable to the cherts from LP and RM which are very different from a geochemical point of view. Furthermore, their positive Eu anomalies are uncommon in the collected samples from these two outcrops. These data suggest that they could have been procured from a still unknown and unsampled outcrop.

4. Archaeological conclusions

The eastern of the Iberian Peninsula reflects a long-term prehistoric population that shows some degree of continuity from the Middle Palaeolithic (Cova de Bolomor, Cova Negra, Abrics del Salt) and a more intensive occupation since the Upper Palaeolithic (Cova del Parpalló, Mallaetes, Cova de les Cendres among others). These population dynamics have been deeply investigated considering the entire area in a wide chronological frame (Barton et al., 2018). From recent times some general palaeodemographic approaches contributed to explore the fluctuations in the density of occupations from the end of the Pleistocene to the development of the Holocene

(Barton et al. 2018; Fyfe et al. 2019; García Puchol et al. 2015). Previous research studies have also underlined the boom episode produced by the arrival of the first farmers around 7600 cal BP showing several sites encompassing recent prehistoric times followed by increasing and decreasing episodes in a non-lineal pattern (Bernabeu et al. 2016). Contrary to other areas like Cantabrian Mountains, Basque-Cantabrian Basin and north-western Pyrenees (e.g.: Olivares et al., 2009; 2013; Tarriño-Vinagre et al., 2015; 2016) or the Ebro Basin (e.g.: Ortega et al., 2018; Sánchez de la Torre et al., 2019; 2020), systematic analytical studies of lithic procurement are not common in the studied region, despite some remarkable exceptions like the works conducted in the Prebaetic mountains of the Alicante province (Villaverde et al., 1999). In particular, the extensive survey project conducted by Molina Hernández and colleagues (Molina Hernández, 2016; Molina Hernández et al., 2011; 2016) has produced a valuable recognition of the entire area identifying several chert outcrops from numerous locations in primary and secondary positions, linking the natural sources with its use by the prehistoric inhabitants. Nevertheless, specific geochemical characterization has been carried out on a very limited number of geologic samples collected from the Upper Serpis valley located in the Prebaetic system (Eixea et al., 2016; Prudêncio et al., 2016; Schmich & Wilkens, 2006). Recently, Ramacciotti et al. (2019a) used multielement analysis to characterize chert from five outcrops in the above-quoted area, including three outcrops of Serreta chert, evidencing the inner chemical variability of this source. Research on Domeño chert, especially related to the lithic materials from Abrigo de la Quebrada (Chelva, Valencia), includes the geochemical characterization of it, which is widely present in the prehistoric sites of the north of Valencia and the south of Castellón provinces (Eixea et al., 2016; Prudêncio et al., 2016). Given the state of the area's chert source research, the present work fills a void by identifying potential chert quarries from an under investigated area, characterizing chert deposits and artifacts, and discusses the results in a wider regional and chronological context.

The QDA model for Cueva de la Cocina archaeological chert artifacts indicates that most of the analyzed artifacts have been made with chert from the outcrops closer to the site, especially from the proximal outcrop of La Canal, which is only a few hundred meters from the site. However, the current results open up to the possible presence of allochthonous chert from greater distance as well. Macroscopic characteristics suggest

that the artifacts AR39 and AR41 were probably made with Domeño chert which would indicate a circulation of this rock which reached at least the centre of the Valencian region. Moreover, cross-checking macroscopic features and with elemental data highlights the possible presence of another unknown source for grayish chert. Finally, at least a part of the *sílex melado* artifacts has chemical levels which deviate from the analyzed local and proximal rocks, being potentially made with Serreta chert, outcropping in the Serpis valley (Alicante) about 60 km south of the site.

Answering the question of the chert supply strategies of Cueva de la Cocina inhabitants between Meso- and Neolithic peoples on the basis of the results obtained in this preliminary study will constitute the next research objective. So far, only forty-two samples were geochemically analyzed, which limits possible inferences. Despite this, the preliminary macroscopic analysis conducted, point out to the prevalence of proximal chert at the beginning of the Mesolithic sequence, and an increasing variability at the last stage of the Mesolithic period (García Puchol et al. 2005). First of all, the use of local and especially proximal chert quarries is consistent with raw materials sourcing patterns observed in other Mesolithic settlements of the Valencian Community (Martí Oliver et al., 2009; Molina Hernández et al., 2011). A minor presence of allochthonous cherts is not uncommon in the above listed sites. In this case, the presence of cherts coming from tens of kilometres to the south (Serreta chert) and to the north (Domeño chert) of Cueva de la Cocina could mark a mobility complementary to the interior-coast scheme which is supported by the presence of seafood remains (Martí Oliver et al., 2009). The yellowish-brownish chert has a prominent role in both Western and Eastern Mediterranean from the Early Neolithic, in connection to the Cardial contexts (Binder, 1998; García Puchol, 2005). The increasing occurrence of yellowish-brownish chert marks the stratigraphic levels of several Neolithic settlements in the southern Valencian Community as well (García Puchol, 2009), and is probably tied to the exploitation of La Serreta outcrops by the first Neolithic groups who settled in this area (Molina Hernández et al., 2011). Thus, Serreta chert may also be seen as a proxy for the Neolithic wave spreading from the Southern Valencian Community, marking the inclusion of Cueva de la Cocina in the sphere of influence of these settlements, which could either be contacts made between these groups or just the inclusion of the cave into the network of Neolithic sites.

Conclusion

The archaeometric study of chert artifacts from Cueva de la Cocina provided initial data to advance the dynamic study of raw materials procurement at the site.

Local (RM and LP), proximal (LC) and non-local (AN) cherts were studied by multielement analysis. PCA was employed for an exploratory analysis of the data and REE, Sc and Y were used to build a model using QDA in discriminating the chert deposits. The model also included the geochemical data from Serreta chert from the Valley of Serpis due to the macroscopic similarity of the material type to of the analyzed artifacts.

According to the multielement analysis and the statistics, local outcrops, especially the proximal one of La Canal, confirmed their importance as a source of raw materials, consistent with previous research carried out on other sites occupied during the Mesolithic in the Valencian Community, indicating the reliance on a local chert source. The possible presence in Mesolithic components of cherts of Domeño and Serreta types, outcropping tens of kilometres north and south of Cocina, could suggest large movements on the N-S axis, complementary to well-established interior-coast ones, and possible complex social dynamics among the last hunter-gatherer groups in the area. However, the presence of Serpis chert in younger deposits of Cocina could also be a sign of the integration of the site inhabitants within the network of sites connected with the Neolithic settlements of the Serpis Valley.

Further studies must be done widening the collection of geological samples from the potential source areas and analyzing artifacts from different known archaeological levels to investigate any potential diachronic sourcing variability. Non-destructive or micro-destructive techniques should be used in order to analyze a large number of archaeological artifacts and obtain more robust statistical results.

In conclusion, though the first archaeometric study of chert from Cueva de la Cocina allowed a preliminary understanding of the raw material procurement patterns linked to the chert artifacts at the site, it leaves open several critical issues, such as patterns of mobility on north-south axes in the different phases, and continuities and discontinuities in chert supply along the different occupation periods between the Mesolithic levels described and the Neolithic, exploring behavioral explanations. These questions deserve to be answered, since they give interesting insights to the

social dynamics of the last hunter-gatherer groups and the neolithization of Eastern Iberia.

Acknowledgments

References

Assens Caparrós, J., Gómez Fernández, J.J., & Ramírez del Pozo, J. (1980). *Memoria de la hoja no. 721 (Cheste), Mapa geológico de España E. 1:50.000. Segunda serie* (1st ed.). Madrid: Instituto Geológico y Minero de España (IGME).

Aura Tortosa, J.E., Gallello, G., Roldán, C., Cavallo, G., Pastor, A., & Murcia-Mascarós, S. (2020). Characterization and sources of Paleolithic-Mesolithic ochre from Coves de Santa Maira (Valencian Region, Spain). Geoarchaeology, 36, 72-91. doi:10.1002/gea.21821

Barton, C. M., Tortosa, J. E. A., Garcia-Puchol, O., Riel-Salvatore, J. G., Gauthier, N., Conesa, M. V., & Bouchard, G. P. (2018). Risk and resilience in the late glacial: a case study from the western Mediterranean. *Quaternary Science Reviews*, 184, 68-84. doi:10.1016/j.quascirev.2017.09.015

Bernabeu, J., García-Puchol, O., Barton, M., McClure, S., Pardo Gordó, S. (2016). Radiocarbon dates, climatic events, and social dynamics during the Early Neolithic in

Mediterranean Iberia. *Quaternary International*, 403, 201-210. doi:10.1016/j.quaint.2015.09.020

Binder, D. (1998). Silex "blond" et complexité des assemblages lithiques dans le Néolithique liguro-provençal. In d'Anna, A., & Binder, D. (Ed.), *Production et identité culturelle, actualité de la recherche: actes de la deuxième session, Arles (Bouches-du-Rhône), 8 et 9 novembre 1996* (pp. 111-128). Antibes: APDCA.

Binder, D., Collina, C., Guilbert, R., Perrin, T., García-Puchol, O. (2012). Pressure-knapping blade production in the North-Western Mediterranean Region during the seventh millennium cal BC. En Desrosiers, P.M. (Ed.), *The emergence of pressure blade making: from origin to modern experimentation*. Springer Science & Business Media.

Borrell F., Bosch J., Gibaja J.F., Schmidt P., & Terradas X. (2019). The status of imported Barremian-Bedoulian flint in north-eastern Iberia during the Middle Neolithic. Insights from the variscite mines of Gavà (Barcelona). *PLOS ONE*, 14, e0224238. doi:10.1371/journal.pone.0224238

Boulanger, M. T., Buchanan, B., O'Brien, M. J., Redmond, B. G., Glascock, M. D., & Eren, M. I. (2015). Neutron activation analysis of 12,900-year-old stone artifacts confirms 450–510+ km Clovis tool-stone acquisition at Paleo Crossing (33ME274), northeast Ohio, USA. *Journal of Archaeological Science*, 53, 550-558. doi:10.1016/j.jas.2014.11.005

Brandl, M., Martinez, M. M., Hauzenberger, C., Filzmoser, P., Nymoen, P., & Mehler, N. (2018). A multi-technique analytical approach to sourcing Scandinavian flint: Provenance of ballast flint from the shipwreck "Leirvigen 1", Norway. *PLOS ONE*, 13,.e0200647 doi:10.1371/journal.pone.0200647

Calogero, B. L. (1992). Lithic misidentification. Man in the Northeast, 43, 87-90.

Chatzimpaloglou, P., French, C., Pedley, M., & Stoddart, S. (2020). Connecting chert sources of Sicily with Neolithic chert artefacts of Malta. *Journal of Archaeological Science: Reports*, 29, 102111. doi:10.1016/j.jasrep.2019.102111

Cortell-Nicolau, A., García-Puchol, O., & Shennan, S. (2020). Cultural continuities and discontinuities at the Neolithic transition in Eastern Iberia: an analysis of the

morphometry of geometric microliths. *Archaeological and Anthropological Sciences*, 12, 1-18. doi:10.1007/s12520-020-01204-0

Delluniversità, E., Muntoni, I. M., Allegretta, I., Tarantini, M., Monno, A., Maiorano, P., Girone, A., Morsili, M., Terzano, R., & Eramo, G. (2019). Development of a multiparametric characterisation protocol for chert investigation and application on the Gargano Promontory mines. *Archaeological and Anthropological Sciences*, 11, 6037-6063. doi:10.1007/s12520-019-00875-8

Ditchfield, K., & Ward, I. (2019). Local lithic landscapes and local source complexity: Developing a new database for geological sourcing of archaeological stone artefacts in North-Western Australia. *Journal of Archaeological Science: Reports*, 24, 539-555. doi:10.1016/j.jasrep.2019.02.012

Eixea, A., Villaverde, V., & Zilhão, J. (2011). Aproximación al aprovisionamiento de materias primas líticas en el yacimiento del Paleolítico medio del Abrigo de la Quebrada (Chelva, Valencia). *Trabajos de Prehistoria*, 68, 65-78. doi:10.3989/tp.2011.11059

Eixea, A., Roldán, C., Villaverde, V., & Zilhão, J. (2016). Caracterización del sílex del Abrigo de la Quebrada (Chelva, Valencia). Resultados y valoración en el contexto del Paleolítico Medio de la región central del Mediterráneo ibérico. *Cuadernos de Prehistoria y Arqueología de la Universidad de Granada*, 26, 313-326.

Elefanti, P., Marshall, G., Stergiou, C.L., Kotjabopoulou, E. (2021). Raw material procurement at Boila Rockshelter, Epirus, as an indicator of hunter-gatherer mobility in Greece during the Late Upper Palaeolithic and Early Mesolithic. Journal of Archaeological Science: Reports, 35, 102719. doi:10.1016/j.jasrep.2020.102719

Fife, R.M., Woodbridge, J., Palmisano, A., Bevan, A., Shennan, S., Burjachs, F., Legarra Herrero, B., García Puchol, O., Sebastián Carrión, J., Revelles, J., & Roberts, N. (2019). Prehistoric palaeodemographics and regional land cover change in Eastern Iberia. *The Holocene*, 29, 799-815. doi:10.1177/0959683619826643

Finch, W. H., & Schneider, M. K. (2006). Misclassification rates for four methods of group classification: Impact of predictor distribution, covariance inequality, effect

size, sample size, and group size ratio. *Educational and Psychological Measurement*, 66, 240-257. https://doi.org/10.1177/0013164405278579

Finkel, M., Barkai, R., Gopher, A., Tirosh, O., & Ben-Yosef, E. (2019). The "Flint Depot" of prehistoric northern Israel: Comprehensive geochemical analyses of flint extraction and reduction complexes and implications for provenance studies. *Geoarchaeology*, 34, 661-683. doi:10.1002/gea.21727

Forenbaher, S., & Perhoc, Z. (2015). Lithics artifacts from Q24 Nakovana (Peljesac): Continuity and change from early Neolithic until the End of Prehistory. Prilozi Instituta za arheologiju u Zagrebu, 32, Zagreb 5–74.

Fortea, J. (1973). *Los complejos microlaminares y geométricos del Epipaleolítico mediterráneo español*. Salamanca: Universidad de Salamanca.

Fortea, J., Martí, B., Fumanal, P., Dupré, M., & Pérez Ripoll, M. (1987). Epipaleolítico y neolitización en la zona oriental de la Península Ibérica. In J. Guilaine, J. Courtin, J-L. Roudil, & J.-L Vernet (Eds.), *Premieres communautés paysannes en Méditerranée Occidentale* (pp. 581-592). Paris: CNRS Éditions. doi:10.4000/books.editionscnrs.945

Frahm, E., & Hauck, T. C. (2017). Origin of an obsidian scraper at Yabroud Rockshelter II (Syria): Implications for Near Eastern social networks in the early Upper Palaeolithic. *Journal of Archaeological Science: Reports*, 13, 415-427. doi:10.1016/j.jasrep.2017.04.021

Gallello, G., Orozco, T., Pastor, A., de la Guardia, M., & Bernabeu, J. (2016). Regional provenance of dolerite prehistoric objects through mineral análisis. Microchemical Journal, 124, 167-174. doi:10.1016/j.microc.2015.08.018

García-Puchol, O. (2005). *El proceso de neolitización en fachada mediterránea de la península Ibérica: tecnología y tipología de la piedra tallada*. Oxford: British Archaeological Reports Limited.

García Puchol, O. G., Balaguer, L. M., Tortosa, J. E. A., & Aubán, J. B. (2009). From the Mesolithic to the Neolithic on the Mediterranean Coast of the Iberian Peninsula. *Journal of Anthropological Research*, 65(2), 237-251. doi:10.3998/jar.0521004.0065.205

García Puchol, O., McClure, S. B., Juan-Cabanilles, J., Diez-Castillo, A., Bernabeu, J., Martí-Oliver, B., Pardo-Gordó, S., Pascual-Benito, J.L., Pérez-Ripoll, M., Molina-

Balaguer, Ll., & Kennet, D.J. (2018). Cocina Cave revisited: Bayesian radiocarbon chronology for the last hunter-gatherers and first farmers in Eastern Iberia. *Quaternary International*, 472, 259–271. doi: 10.1016/j.quaint.2016.10.037

García Vélez, A., García Ruz, L., Muelas Peña, A., Soubrier González, J., & Forcat, C. (1981). *Memoria de la hoja no. 746 (Llombay), Mapa geológico de España E. 1:50.000. Segunda seri*e (1st ed.). Madrid: Instituto Geológico y Minero de España (IGME).

García Velez, A., Soubrier González, J., Muelas Peña, A., Goy Goy, J.L., Zazo Cardeña, C., García Ruz, L. (1980). *Memoria de la hoja no. 721 (Cheste), Mapa geológico de España E. 1:50.000. Segunda serie* (1st ed.). Madrid: Instituto Geológico y Minero de España (IGME).

Geel, T. (2000). Recognition of stratigraphic sequences in carbonate platform and slope deposits: empirical models based on microfacies analysis of Palaeogene deposits in southeastern Spain. *Palaeogeography, Palaeoclimatology, Palaeoecology*, 155, 211-238. doi:10.1016/S0031-0182(99)00117-0

Gómez, J. J., & Fernández-López, S. R. (2006). The Iberian Middle Jurassic carbonate-platform system: Synthesis of the palaeogeographic elements of its eastern margin (Spain). Palaeogeography, *Palaeoclimatology, Palaeoecology*, 236, 190-205. doi:10.1016/j.palaeo.2005.11.008

Gómez de Soler, B.G., Soto, M., Vallverdú, J., Vaquero, M., Bargalló, A., Chacón, M.G., Romagnoli, F., & Carbonell, E. (2020). Neanderthal lithic procurement and mobility patterns through a multi-level study in the Abric Romaní site (Capellades, Spain). *Quaternary Science Reviews*, 237, 106315. doi:10.1016/j.quascirev.2020.106315

Gutiérrez, F., Gutiérrez, M., Gracia, F. J., McCalpin, J. P., Lucha, P., & Guerrero, J. (2008). Plio-Quaternary extensional seismotectonics and drainage network development in the central sector of the Iberian Chain (NE Spain). *Geomorphology*, 102, 21-42. doi:10.1016/j.geomorph.2007.07.020

Gutiérrez F., Gutiérrez M., & Martín-Serrano Á. (2014). The Geology and Geomorphology of Spain: A Concise Introduction. In F. Gutiérrez, & M. Gutiérrez M. (Eds.), *Landscapes and Landforms of Spain. World Geomorphological Landscapes* (pp. 1-23). Dordrecht: Springer. doi:10.1007/978-94-017-8628-7_1

Hess, T., & Riede, F. (2020). The use of lithic raw materials at the Early Mesolithic open-air site Feuersteinacker (Vogelsbergkreis, Germany). *Geoarchaeology*, 36, 252-265. doi:10.1002/gea.21828

Hess, S.C. (1996). Chert provenance analysis at the Mack Canyon Site, Sherman County, Oregon: An evaluative study. *Geoarchaeology*, 11, 51-81. doi:10.1002/(SICI)1520-6548(199601)11:1<51::AID-GEA3>3.0.CO;2-9

Juan-Cabanilles, J., & García Puchol, O. (2013). Rupture et continuité dans la néolithisation du versant méditerranéen de la péninsule Ibérique: mise à l'épreuve du modèle de dualité culturelle. In J. Jaubert, N. Fourment, & P. Depaepe (Eds.), *Transitions, Ruptures et Continuité durant la Préhistoire* (pp. 405-417). Paris: Société préhistorique française.

Kuhn, M. (2020). caret: Classification and Regression Training. R package version 6.0-86. https://CRAN.R-project.org/package=caret

Landry, D. B., Milne, B., & Rachel, E. (2018). Combining remote sensing, geophysics, and lithic provenance and reduction to understand long-term continuity in Paleo-Inuit chert quarrying and seasonal inland travels on southern Baffin Island, NU. *Quaternary International*, 549, 155-162. doi:10.1016/j.quaint.2018.04.021

Lawrence, M. G., Greig, A., Collerson, K. D., & Kamber, B. S. (2006). Rare earth element and yttrium variability in South East Queensland waterways. *Aquatic Geochemistry*, 12, 39-72. doi:10.1007/s10498-005-4471-8

Lecuit, M., Fronteau, G., Boulvain, F., Dechamps, S., Eyssautier-Chuine, S., Piavaux, M., & Yans, J. (2018). Geochemical characterization of "Lorraine limestones" from the Saint-Paul Cathedral of Liège (Belgium): Assumptions for the true provenance of the building stones. *Environmental Earth Sciences*, 77, 361. doi:10.1007/s12665- 018-7554-8

Luedtke, B. E. (1992). *An archaeologist's guide to chert and flint*. Los Angeles: University of California.

Martí Oliver, B., Aura, J. E., Juan, J., García, O., & Fernández, J. (2009). El mesolítico geométrico de tipo "cocina" en el País Valenciano. El Mesolítico Geométrico en la Península Ibérica. *Monografías Arqueológicas*, 44, 205-258.

Martínez del Olmo, W., & Benzaquen, M. (1975). *Memoria de la hoja no. 820 (Ontinyent), Mapa geológico de España E. 1:50.000. Segunda serie* (1st ed.). Madrid: Instituto Geográfico Minero de España (IGME).

Mathur, R., Burns, J., Powell, W., Boryk, R., Sheetz, B., D'Amico, P., & Harney, P. (2020). Evaluation of Fe isotope values as a provenance tool for chert artefacts from the north-eastern United States. *Archaeometry*, 62, 156-168. doi:10.1111/arcm.12572

McLennan, S. M. (1989). Rare earth elements in sedimentary rocks: Influence of provenance and sedimentary processes. *Reviews in Mineralogy and Geochemistry*, 21, 169-200.

Mehta, J. M., McCall, G., Marks, T., & Enloe, J. (2017). Geochemical source evaluation of archaeological chert from the Carson mounds site in northwestern Mississippi using portable X-ray fluorescence (pXRF). *Journal of Archaeological Science: Reports*, 11, 381-389. doi:10.1016/j.jasrep.2016.12.014

Molina Hernández, F. J., Tarriño Vinagre, A., Galván Santos, B., & Hernández Gómez, C. M. (2011). Estudio macroscópico y áreas de aprovisionamiento de la industria silícea del yacimiento Mesolítico y Neolítico de Benàmer. In P. Torregrosa Gimenez, F. Jover Maestre, & E. López Seguí (Eds.), *Benàmer (Muro d'Alcoi, Alicante): mesolíticos y neolíticos en las tierras meridionales valencianas* (pp. 121-131). Valencia: Museu de Prehistòria de València.

Molina Hernández, F. J. (2016). *El sílex del Prebético y cuencas neógenas en Alicante y Sur de Valencia: su caracterización y estudio aplicado al Paleolítico Medio* (Doctoral dissertation). Alicante: University of Alicante.

Molina Hernández, F. J., Tarriño Vinagre, A., Galván Santos, B., & Hernández Gómez, C. M. (2016). El sílex del Prebético de Alicante: tipos, variabilidad y áreas de captación y talla del Pleistoceno. *Cuadernos de Prehistoria y arqueología de la Universidad de Granada*, 26, 283-311. doi:10.30827/cpag.v26i0.7403

Moreau, L., Ciornei, A., Gjesfjeld, E., Filzmoser, P., Gibson, S. A., Day, J., Nigst, P.R., Macleod, R.A., Niţă, L., & Anghelinu, M. (2019). First Geochemical 'Fingerprinting' of Balkan and Prut Flint from Palaeolithic Romania: Potentials, Limitations and Future Directions. *Archaeometry*, 61, 521-538. doi:10.1111/arcm.12433

Murray, R. W. (1994). Chemical criteria to identify the depositional environment of chert: general principles and applications. *Sedimentary Geology*, 90, 213-232. doi:10.1016/0037-0738(94)90039-6

O'Leary, M. J., Ward, I., Key Jr, M. M., Burkhart, M. S., Rawson, C., & Evans, N. (2017). Challenging the 'offshore hypothesis' for fossiliferous chert artefacts in southwestern Australia and consideration of inland trade routes. *Quaternary Science Reviews*, 156, 36-46. doi:10.1016/j.quascirev.2016.11.016

Olivares, M., Tarriño, A., Murelaga, X., Baceta, J. I., Castro, K., & Etxebarria, N. (2009). Non-destructive spectrometry methods to study the distribution of archaeological and geological chert samples. *Spectrochimica Acta Part A: Molecular and Biomolecular Spectroscopy*, 73, 492-497. doi:10.1016/j.saa.2008.12.036

Olivares, M., Irazola, M., Murelaga, X., Baceta, J. I., Tarriño, A., Castro, K., & Etxebarria, N. (2013). Sourcing sedimentary cherts with archaeological use through the combination of chromatographic and spectroscopic techniques. *Applied geochemistry*, 33, 252-259. doi:10.1016/j.apgeochem.2013.02.020

Olofsson, A., & Rodushkin, I. (2011). Provenancing flint artefacts with ICP–MS using REE signatures and Pb isotopes as discriminants: preliminary results of a case study from northern Sweden. *Archaeometry*, 53, 1142-1170. doi:10.1111/j.1475-4754.2011.00605.x

Ortega, D., Roqué, C., Ibáñez, J., Beamud, E., Larrasoaña, J. C., Sáez, A., & Terradas, X. (2018). The chert from the Castelltallat Formation (south-central Pyrenees): archaeometric characterisation and archaeological implications. *Archaeological and Anthropological Sciences*, 10, 1329-1346. doi:10.1007/s12520-016-0458-1

Pardo-Gordó, S., García Puchol, O., Diez Castillo, A., Cortell, A., & Molina, L. (2016). Prospección arqueológica en la Canal de Dos Aguas (València). El territorio inmediato a Cueva de la Cocina. *SAGVNTVM. Papeles del Laboratorio de Arqueología de Valencia*, 48, 197-200. doi:10.7203/SAGVNTVM.48.90

Pardo-Gordó, S., García Puchol, O., Castillo, A. A. D., McClure, S. B., Cabanilles, J. J., Ripoll, M. P., Molina Balaguer, Ll., Bernabeu Aubán, J., Pascual Benito, J.Ll., Kennet, D.J., Nicolau Cortell, A., Tsante, N., & Basile, M. (2018). Taphonomic processes inconsistent with indigenous Mesolithic acculturation during the transition

to the Neolithic in the Western Mediterranean. *Quaternary International*, 483, 136-147. doi:10.1016/j.quaint.2018.05.008

Pardo-Gordó, S., Puchol, O. G., Nicolau, A. C., & Balaguer, L. M. (2017). Segunda campaña de prospección en el territorio inmediato a Cueva de la Cocina: el Valle del Magre. *SAGVNTVM. Papeles del Laboratorio de Arqueología de Valencia*, 49, 187-190. doi:10.7203/SAGVNTVM.49.10976

Parish, R. M., & Werra, D. H. (2018). Characterizing "Chocolate" Flint Using Reflectance Spectroscopy. Archaeologia Polona, 56, 89-101. https://doi.org/10.23858/APa56.2018.007

Parow-Souchon, H., & Purschwitz, C. (2020). Variability in chert raw material procurement and use during the Upper Paleolithic and Early Neolithic of the southern Levant: A regional perspective from the Greater Petra area. *Journal of Archaeological Science: Reports*, 29, 102087. doi:10.1016/j.jasrep.2019.102087

Pericot, L. (1945). La Cueva de la Cocina (Dos Aguas). Nota preliminar. *Archivo de Prehistoria Levantina*, 2, 39-71.

Prudêncio, M. I., Roldán, C., Dias, M. I., Marques, R., Eixea, A., & Villaverde, V. (2016). A micro-invasive approach using INAA for new insights into Palaeolithic flint archaeological artefacts. *Journal of Radioanalytical and Nuclear Chemistry*, 308, 195-203. doi:10.1007/s10967-015-4294-z

R Core Team (2020). R: A language and environment for statistical computing. R Foundation for Statistical Computing, Vienna, Austria. https://www.R-project.org/.

Ramacciotti, M., Gallello, G., Pastor, A., Diez Castillo, A., & García Puchol, O. (2019a). Chert Nucleus and Cortex Characterization for Archaeological Provenance Study Tested in the Prebaetic System Region (Valencian Community, Spain). *Lithic Technology*, 44, 166-180. doi:10.1080/1977261.2019.1618043

Ramacciotti, M., Rubio, S., Gallello, G., Lezzerini, M., Raneri, S., Hernandez, E., Calvo, M., Columbu, S., Morales, A., Pastor, A., & de la Guardia, M. (2019b). Chemical and mineralogical analyses on stones from Sagunto Castle (Spain). Journal of Archaeological Science: Reports, 24, 931-938. doi:10.1016/j.jasrep.2019.03.017

Ramacciotti, M., Gallello, G., Aranegui Gascó, C., Hernández, E., & Pastor, A. (2020(. Análisis químicos de los sillares de arenisca del Castillo de Sagunto. *Archivo de Prehistoria Levantina*, 33, 231-242.

Robb, J.E., & Farr, R.H. (2008). Substances in Motion: Neolithic Mediterranean "Trade". In E. Blake, & A.B. Knapp (Eds.), *The Archaeology of Mediterranean Prehistory* (pp. 24-45). Padstow, UK: Blackwell Publishing. doi:10.1002/9780470773536.ch2Sánchez De La Torre, M., García-Simón, L.M., Le Bourdonnec, F.-X, Domingo, R. (2019). Geochemical fingerprinting of Monegros cherts: Redefining the origin of a prehistoric tracer. *Archaeometry*, 61, 1233-1245. doi:10.1111/arcm.12494Sánchez de la Torre, M., Utrilla, P., Domingo, R., Jiménez, L., Le Bourdonnec, F. X., & Gratuze, B. (2020). Lithic raw material procurement at the Chaves cave (Huesca, Spain): A geochemical approach to defining Palaeolithic human mobility. *Geoarchaeology*, 35, 856-870. doi:10.1002/gea.21808

Schmich, S., & Wilkens, B. (2006). Non-destructive identification and characterization of lithics from the Polop Alto: A preliminary assessment using proton induced X-ray emission (PIXE). In O. García Puchol, & J.E. Aura Tortosa (Eds.), *El abric de la Falguera (Alcoi, Alacant): 8.000 años de ocupación humana en la cabecera del río de Alcoi* (pp. 164-170). Alicante: Museo Arqueológico de Alicante-MARQ.

Siqueira, L. F., Júnior, R. F. A., de Araújo, A. A., Morais, C. L., & Lima, K. M. (2017). LDA vs. QDA for FT-MIR prostate cancer tissue classification. *Chemometrics and Intelligent Laboratory System*s, 162, 123-129. doi: 10.1016/j.chemolab.2017.01.021

Speer, C. A. (2014). LA-ICP-MS analysis of Clovis period projectile points from the Gault Site. *Journal of Archaeological Science*, 52, 1-11. doi:10.1016/j.jas.2014.08.014

Speer, C. A. (2016). A comparison of instrumental techniques at differentiating outcrops of Edwards Plateau chert at the local scale. *Journal of Archaeological Science: Reports*, 7, 389-393. doi:10.1016/j.jasrep.2016.05.026

Stewart, S. T., Murphy, S., Bikoulis, P., McCartney, C., Manning, S. W., & Hancock, R. G. (2020). Early Neolithic chert variability in central Cyprus: Geo-chemical and spatial analyses. *Journal of Archaeological Science: Reports*, 29, 102088. doi:10.1016/j.jasrep.2019.102088

Tarriño-Vinagre, A., Elorrieta, I., & García-Rojas, M. (2015). Flint as raw material in prehistoric times: Cantabrian Mountain and Western Pyrenees data. *Quaternary International*, 364, 94-108. doi:10.1016/j.quaint.2014.10.061

Tarriño-Vinagre, A., Muñoz-Fernández, E., Baigorri, I. E., Normand, C., del Río, P. R., García-Rojas, M., & Pérez-Bartolomé, M. (2016). El sílex en la cuenca vasco-cantábrica y el Pirineo occidental: materia prima lítica en la Prehistoria. *Cuadernos de Prehistoria y Arqueología de la Universidad de Granada*, 26, 191-228. doi:10.30827/cpag.v26i0.7400

Ten Bruggencate, R. E., Milne, S. B., Fayek, M., Park, R. W., & Stenton, D. R. (2015). Characterization of chert artifacts and two newly identified chert quarries on southern Baffin Island. *Lithic Technology*, 40, 189-198. doi:10.1179/2051618515Y.0000000006

Tostevin, R., Shields, G. A., Tarbuck, G. M., He, T., Clarkson, M. O., & Wood, R. A. (2016). Effective use of cerium anomalies as a redox proxy in carbonate-dominated marine settings. *Chemical Geology*, 438, 146-162. doi:10.1016/j.chemgeo.2016.06.027

Tykot, R. H. (2003). Determining the source of lithic artifacts and reconstructing trade in the ancient world. In N. Kardulias, & R.W. Yerkes (Eds.) *Written in stone: the multiple dimensions of lithic analysis* (pp. 59-85). Lanham, MD: Lexington Books.

Venables, W. N., & Ripley, B. D. (2002). Modern Applied Statistics with S (4th edition). New York, Springer. doi:10.1007/978-0-387-21706-2

Vera, J.A. (2004). Geología de España. Instituto Geológico y Minero de España.

Vilas, L., Mas, R., García, A., Arias, C., Alonso, A., Meléndez, N., & Rincón, R. (1982) Ibérica Suroccidental. In Univ. Complutense Madrid (Ed.) *El Cretácico de España* (pp. 457-514). Madrid: Editorial de la Universidad Complutense de Madrid.

Villaverde, V., Martínez Valle, R., Badal, E., Guillem, P. M., García, R., & Menargues, J. (1999). El Paleolítico superior de la Cova de les Cendres (Teulada-Moraira, Alicante). Datos proporcionados por el sondeo efectuado en los cuadros A/B-17. *Archivo de Prehistoria Levantina*, 23, 9-65.

Wickham, H. (2016). *ggplot2: Elegant Graphics for Data Analysis*. New York: Springer-Verlag. doi:10.1007/978-0-387-98141-3

Annex 1

Limit of detection (LD) for ICP-MS analysis expressed as mg/kg.

Element	Mass (DA)	LD	Element	Mass (DA)	LD
La	139	0.00016	Bi	209	0.0010
Ce	140	0.0003	Cd	111	0.0014
Pr	141	0.0004	Cr	52	0.0014
Nd	142	0.0005	Co	59	0.0011
Sm	152	0.00011	Cu	63	0.0009
Eu	151	0.00012	Li	7	0.0009
Gd	158	0.00019	Mn	55	0.00016
Tb	159	0.00011	Mo	95	0.0009
Dy	162	0.00012	Ni	60	0.0014
Ho	165	7E-05	Pb	207	0.0015
Er	166	9E-05	Sr	88	0.0016
Tm	169	7E-05	Tl	205	0.0015
Yb	172	4E-05	V	51	0.0012
Lu	175	5E-05	Zn	64	0.009
Sc	45	8E-05	Th	232	0.0009
Y	89	3E-05	U	238	0.0008
Ba	138	0.0019	Rh	103	Internal standard

Annex 2

Major and trace elements concentrations.

Sample	K	Ca	Ti	Fe	Ba	Bi	Cd	Co	Cr	Cu	Li	Mn	Mo	Ni	Pb	Sr	Tl	V	Zn	Th	U
LC01	N/D	3.02	0.006	0.07	4.80	0.010	0.021	0.191	0.729	0.321	21.5	7.92	0.118	1.21	0.056	16.6	0.009	11.7	0.272	0.120	1.76
LC02	0.01	1.54	0.007	0.06	3.27	0.006	0.013	0.163	0.304	0.164	14.5	3.63	0.031	0.520	<LD	9.22	0.004	8.03	<LD	0.083	1.33
LC03	0.03	0.58	N/D	0.06	6.14	0.006	0.005	0.104	0.294	0.177	12.3	5.52	0.037	0.406	0.046	3.54	0.005	21.6	0.253	0.065	3.17
LC04	0.02	2.88	0.010	0.12	17.0	0.018	0.060	0.420	2.09	0.706	14.2	106	0.101	2.07	0.564	7.66	0.024	7.53	2.04	0.444	5.91
LC06	0.03	0.90	0.008	0.08	5.60	0.009	0.011	0.191	0.938	0.447	17.8	10.2	0.134	0.122	0.182	10.4	0.007	8.56	0.314	0.136	4.34
LC07	0.03	0.39	0.007	0.08	5.10	0.011	0.020	0.289	2.59	0.679	30.7	12.7	0.038	0.611	0.356	4.59	0.007	4.18	0.262	0.217	2.61
LC08	N/D	14.66	0.010	0.07	14.1	0.007	0.039	0.378	0.758	0.292	10.1	9.54	0.018	2.67	0.284	132	0.016	4.09	1.79	0.055	1.20
LC09	0.02	2.38	0.011	0.09	95.2	0.015	0.012	0.172	<LD	0.218	3.55	4.76	0.650	0.495	0.204	38.5	0.008	13.7	1.08	0.119	1.96
LC10	N/D	2.60	0.007	0.06	9.32	0.006	0.012	0.167	0.514	0.168	12.9	4.10	0.041	0.260	0.102	46.6	0.004	8.44	0.659	0.063	0.768
LC11	0.01	4.09	0.010	0.09	3.44	0.009	0.012	0.258	0.280	0.201	20.5	4.02	0.230	0.983	0.123	24.0	0.009	9.59	0.982	0.080	0.787
LC13	N/D	10.95	N/D	0.08	3.43	0.008	0.018	0.272	0.808	0.233	14.4	8.79	0.236	2.78	0.212	44.4	0.007	9.28	0.859	0.096	1.33
LC14	N/D	5.78	0.008	0.07	5.81	0.006	0.019	0.187	0.620	0.198	11.7	4.78	0.052	0.808	0.174	38.4	0.006	7.24	0.772	0.090	1.33
LC15	0.02	3.79	0.009	0.09	5.62	0.034	0.053	0.219	0.224	0.409	16.4	7.10	0.286	0.948	0.303	17.0	0.032	12.5	1.30	0.162	2.43
LC16	0.06	0.36	0.015	0.15	3.44	0.007	0.036	0.293	0.916	0.385	18.8	7.76	0.042	2.95	0.153	47.3	0.007	12.4	1.07	0.108	1.22
LC17	N/D	5.02	N/D	0.06	4.25	0.006	0.016	0.320	0.397	0.274	13.3	5.02	0.030	1.14	0.125	33.4	0.004	7.35	0.372	0.066	1.48
LC18	0.03	0.27	0.007	0.05	4.83	0.006	0.010	0.093	0.155	0.268	8.84	3.18	0.051	0.054	0.044	2.56	0.006	12.2	0.024	0.060	2.47
LC19	N/D	6.08	0.010	0.07	5.03	0.009	0.016	0.285	0.616	0.386	26.5	12.3	0.036	1.81	0.139	25.3	0.008	16.6	0.491	0.125	1.81
LC20	N/D	5.17	N/D	0.07	3.47	0.007	0.023	0.165	0.723	0.253	10.4	6.51	0.075	0.753	0.227	26.7	0.006	12.1	0.192	0.092	1.55
Mean	*0.02*	*3.91*	*0.008*	*0.08*	*11.1*	*0.010*	*0.022*	*0.232*	*0.720*	*0.321*	*15.5*	*12.4*	*0.123*	*1.14*	*0.183*	*29.3*	*0.009*	*10.4*	*0.708*	*0.121*	*2.08*
SD	*0.01*	*3.81*	*0.003*	*0.02*	*21.3*	*0.007*	*0.015*	*0.089*	*0.654*	*0.160*	*6.5*	*23.5*	*0.154*	*0.93*	*0.134*	*29.9*	*0.008*	*4.3*	*0.585*	*0.090*	*1.31*
LP01	0.03	0.18	0.006	0.05	27.7	0.004	0.011	0.159	0.162	0.193	1.59	13.2	0.344	0.063	0.147	2351*	0.003	2.47	2.78	0.050	5.07
LP02	0.04	0.22	0.006	0.07	0.595	0.002	0.008	0.087	<LD	0.153	0.646	0.138	0.086	<LD	0.143	5.68	0.002	1.52	1.16	0.024	6.58
LP03	0.03	0.18	N/D	0.05	0.392	<LD	0.013	0.138	<LD	0.207	0.233	0.394	0.118	<LD	0.147	1.35	<LD	0.221	0.458	0.016	3.62
LP04	0.01	0.68	0.006	0.05	1.96	<LD	0.008	0.073	1.32	0.534	0.692	0.292	<LD	<LD	0.072	9.62	0.002	5.59	0.417	0.044	3.37

LP05	0.01	0.54	N/D	0.05	1.74	<LD	0.022	0.096	1.87	0.315	0.268	0.116	<LD	<LD	0.121	10.2	0.002	9.47	3.16	0.011	4.52
LP06	0.02	0.70	N/D	0.06	3.72	0.003	0.014	0.169	4.83	0.768	1.38	0.657	0.009	<LD	0.159	31.2	0.008	9.88	0.981	0.050	5.19
LP07	0.01	1.16	N/D	0.04	10.1	<LD	0.011	0.158	<LD	0.234	1.12	1.41	0.022	0.034	0.048	54.4	0.002	4.77	1.44	0.034	8.11
LP08	N/D	1.23	N/D	0.05	4.06	0.002	0.010	0.161	12.7	0.754	0.391	0.262	0.011	0.421	0.066	30.0	0.003	2.12	0.380	0.025	5.89
LP09	0.01	0.43	N/D	0.04	5.24	0.002	0.017	0.068	0.061	0.869	0.499	0.432	0.015	<LD	0.107	51.3	<LD	2.15	2.87	0.033	3.01
LP10	N/D	1.31	N/D	0.04	4.75	<LD	0.007	0.038	1.49	0.976	0.140	0.590	0.051	0.262	0.032	19.0	0.003	4.19	0.330	0.003	4.98
LP11	0.01	0.53	0.006	0.05	1.24	<LD	0.019	0.088	<LD	0.313	0.318	0.416	<LD	<LD	0.055	17.2	<LD	2.10	0.464	0.052	5.06
Mean	*0.02*	*0.65*	*0.004*	*0.049*	*5.59*	*0.001*	*0.013*	*0.112*	*2.04*	*0.483*	*0.662*	*1.63*	*0.060*	*0.071*	*0.100*	*23.0*	*0.002*	*4.04*	*1.31*	*0.031*	*5.04*
SD	*0.01*	*0.42*	*0.002*	*0.007*	*7.84*	*0.001*	*0.005*	*0.046*	*3.84*	*0.306*	*0.492*	*3.85*	*0.102*	*0.140*	*0.046*	*18.5*	*0.002*	*3.18*	*1.11*	*0.017*	*1.48*
RM01	0.03	0.18	0.006	0.05	19.1	0.004	0.007	0.104	1.17	0.163	0.432	2.04	0.696	0.657	0.055	55.6	<LD	0.434	1.85	0.019	1.54
RM02	0.03	0.22	N/D	0.05	8.99	0.013	0.020	0.279	1.34	0.243	5.55	8.45	2.68	0.697	0.122	5.62	0.004	0.660	1.54	0.047	1.59
RM03	0.03	0.18	N/D	0.04	3.35	0.006	0.024	0.098	0.705	0.067	0.647	1.78	1.04	0.468	0.210	1.35	0.002	0.312	0.846	0.023	2.08
RM04	0.03	0.24	N/D	0.04	0.789	0.004	0.012	0.043	0.268	0.174	0.224	0.777	0.529	0.227	0.123	2.09	<LD	0.300	0.359	0.015	2.50
RM05	0.03	0.23	N/D	0.05	2.25	0.005	0.008	0.318	0.900	0.216	0.410	2.39	0.178	0.394	0.078	1.11	<LD	0.359	0.690	0.026	1.85
RM06	0.02	0.75	0.006	0.05	3.18	0.009	0.023	0.112	0.285	0.203	5.01	0.676	1.25	0.438	0.274	4.90	0.003	0.379	0.908	0.020	1.49
RM07	0.02	0.20	N/D	0.04	10.5	0.031	0.010	0.059	0.152	1.26	0.318	1.70	0.177	0.088	0.215	14.4	<LD	0.383	1.07	0.029	2.72
RM08	0.03	0.22	N/D	0.04	8.80	0.015	0.031	0.151	0.404	0.272	10.0	0.719	1.81	0.483	0.266	4.19	0.003	0.743	0.539	0.055	1.04
RM09	0.02	0.25	0.006	0.04	1.35	0.014	0.018	0.150	0.077	0.139	13.4	0.623	0.640	0.116	0.101	3.24	0.003	0.547	0.984	0.036	0.813
RM10	0.03	0.60	N/D	0.05	4.49	0.012	0.013	0.182	0.146	0.162	1.36	3.22	2.66	0.495	0.164	23.1	0.003	0.815	0.776	0.042	5.13
RM12	0.03	N/D	N/D	0.04	0.266	0.002	0.011	0.152	0.518	0.158	0.243	0.225	0.199	0.343	0.040	0.864	<LD	0.218	1.14	0.012	0.867
RM13	0.04	0.19	N/D	0.03	1.20	0.007	0.017	0.083	0.690	0.118	8.81	0.483	0.123	0.205	0.152	2.75	0.002	0.210	0.832	0.011	0.139
RM14	0.02	0.43	N/D	0.04	1.71	0.011	0.007	0.133	0.318	0.100	0.774	2.00	0.983	0.256	0.095	3.45	0.002	0.460	0.294	0.036	2.14
RM15	0.03	0.19	0.007	0.05	85.6	0.006	0.012	0.245	0.712	1.09	6.33	0.853	0.388	0.421	0.163	18.2	0.005	0.974	0.929	0.018	7.43
Mean	*0.03*	*0.28*	*0.004*	*0.044*	*10.8*	*0.010*	*0.015*	*0.151*	*0.549*	*0.312*	*3.82*	*1.85*	*0.954*	*0.378*	*0.147*	*10.1*	*0.002*	*0.485*	*0.911*	*0.028*	*2.24*
SD	*0.01*	*0.19*	*0.002*	*0.005*	*22.2*	*0.007*	*0.007*	*0.081*	*0.389*	*0.372*	*4.40*	*2.09*	*0.870*	*0.184*	*0.073*	*14.8*	*0.001*	*0.232*	*0.417*	*0.013*	*1.90*
AN01	0.05	4.36	0.012	0.17	12.6	0.018	0.107	1.28	7.54	2.15	19.5	17.8	0.104	4.69	0.594	43.5	0.063	7.02	4.90	0.442	0.482
AN02	0.03	4.02	0.015	0.14	8.57	0.009	0.238	0.590	5.27	1.71	6.89	12.3	0.135	2.34	0.637	27.3	0.018	3.49	16.4	0.401	0.375
AN03	0.05	1.65	0.017	0.15	8.88	0.010	1.23	0.690	5.29	2.26	10.1	6.76	0.152	2.43	0.988	25.0	0.023	4.84	13.4	0.298	0.466

AN04	0.07	2.11	0.017	0.18	13.7	0.013	0.159	1.62	7.76	1.88	10.8	10.2	0.561	3.74	0.864	22.5	0.035	5.34	3.73	0.630	0.567
AN05	0.06	1.23	0.021	0.11	12.6	0.011	0.463	0.502	6.62	2.12	8.34	4.97	0.338	3.23	0.682	21.0	0.033	5.34	12.3	0.510	0.493
AN06	0.06	2.19	0.013	0.15	9.57	0.006	0.469	0.540	13.7	0.98	3.87	3.87	0.324	2.76	0.572	24.2	0.034	4.15	4.29	0.409	0.929
AN07	0.02	2.97	0.013	0.15	9.07	0.010	0.311	0.481	4.63	2.40	5.04	4.49	0.226	1.86	0.859	22.8	0.011	4.01	5.90	0.251	0.491
AN08	0.01	6.97	0.015	0.17	8.34	0.010	0.223	0.679	5.31	2.23	6.91	11.5	0.526	6.76	0.886	34.6	0.034	3.85	10.7	0.375	0.773
AN09	0.08	0.58	0.019	0.12	10.6	0.011	1.16	0.472	6.18	1.95	8.34	4.73	0.143	1.62	0.872	20.0	0.021	4.48	18.3	0.475	0.350
Mean	*0.049*	*2.90*	*0.016*	*0.147*	*10.4*	*0.011*	*0.484*	*0.761*	*6.92*	*1.96*	*8.87*	*8.53*	*0.279*	*3.27*	*0.773*	*26.8*	*0.030*	*4.72*	*9.99*	*0.421*	*0.547*
SD	*0.023*	*1.96*	*0.003*	*0.021*	*2.0*	*0.003*	*0.421*	*0.406*	*2.75*	*0.42*	*4.56*	*4.76*	*0.171*	*1.62*	*0.152*	*7.6*	*0.015*	*1.07*	*5.51*	*0.113*	*0.188*
AR01	0.05	0.48	0.012	0.09	20.4	0.011	0.017	1.27	2.80	0.747	11.0	4.46	0.340	1.56	0.233	16.3	0.065	7.37	2.84	0.126	3.42
AR02	0.10	1.61	0.022	0.10	85.2	0.015	0.080	4.78	1.69	0.726	20.6	3.97	0.081	1.14	0.354	17.0	0.024	4.30	4.42	0.276	2.43
AR03	N/D	1.95	0.008	0.06	7.43	0.007	0.012	6.60	1.05	0.713	24.5	3.32	0.158	3.36	0.503	41.3	0.009	6.10	8.09	0.193	0.850
AR04	0.06	0.37	N/D	0.08	330	0.011	0.015	2.06	2.18	0.155	6.67	10.2	0.392	0.966	0.108	51.5	0.023	6.45	6.42	0.106	2.35
AR05	N/D	6.41	0.007	0.08	16.9	0.002	0.025	3.37	1.60	5.25	1.80	13.3	1.81	3.91	0.192	31.4	0.014	3.95	6.00	0.039	8.28
AR06	0.05	0.57	0.012	0.05	5.29	0.022	0.010	4.71	7.68	0.434	11.1	1.02	0.189	1.51	0.306	5.33	0.014	2.60	10.3	0.213	1.09
AR07	0.03	0.22	0.006	0.04	13.8	0.002	0.012	3.96	1.78	0.266	1.11	0.963	0.173	1.94	0.163	5.41	0.001	2.52	1.28	0.016	1.99
AR08	0.03	0.19	0.007	0.05	24.1	0.007	0.006	1.18	3.27	0.150	18.3	0.463	0.265	0.546	0.962	7.53	0.002	1.16	1.47	0.037	0.737
AR09	0.05	1.08	0.007	0.31	24.2	0.008	0.011	2.56	1.78	1.02	2.66	13.1	0.127	1.77	0.587	4.20	0.011	8.01	1.86	0.069	3.31
AR10	0.02	0.67	N/D	0.08	2.01	0.003	0.119	1.69	1.33	0.126	1.85	0.651	0.162	0.687	0.133	61.8	0.007	3.68	1.82	0.067	13.7
AR11	0.04	0.26	0.007	0.06	3.98	0.010	0.069	0.972	0.077	0.124	3.52	1.71	0.073	0.467	0.319	7.88	0.004	9.43	1.50	0.115	1.14
AR12	0.03	N/D	0.006	0.03	4.11	0.002	0.005	1.09	1.75	0.097	0.072	0.504	0.086	0.629	0.045	6.58	0.0004	0.277	1.47	0.007	0.769
AR13	0.07	0.54	0.016	0.07	17.8	0.008	0.035	4.67	1.19	1.40	17.3	1.31	0.297	1.36	0.549	5.18	0.010	3.84	5.31	0.295	0.436
AR15	0.02	0.18	N/D	0.03	15.7	0.001	0.219	0.117	0.116	<LD	0.128	0.259	0.033	0.214	0.030	13.4	0.0004	0.248	5.99	0.006	0.791
AR16	0.05	0.19	N/D	0.08	18.9	0.009	0.008	1.89	1.58	0.060	6.39	3.09	0.258	0.899	0.093	20.1	0.012	6.09	0.887	0.079	1.55
AR17	0.05	0.25	0.008	0.06	12.7	0.005	0.026	1.90	0.63	0.251	7.34	5.93	0.125	1.37	0.183	12.9	0.007	18.1	2.17	0.136	2.21
AR18	0.04	0.25	0.008	0.06	3.53	0.011	0.016	2.07	1.79	0.367	3.99	5.04	0.258	0.951	0.590	5.81	0.023	7.62	2.72	0.112	5.85
AR19	0.01	2.70	0.010	0.06	4.82	0.008	0.027	1.24	0.83	0.083	6.03	3.09	0.082	0.957	0.250	23.0	0.010	4.28	1.89	0.099	2.43
AR21	0.09	0.29	0.009	0.16	18.5	0.019	0.043	2.44	2.08	1.09	6.76	6.51	0.564	1.58	0.917	39.9	0.026	15.8	5.67	0.117	1.58
AR22	0.05	0.22	0.009	0.03	10.9	0.015	0.091	0.883	0.036	<LD	7.32	0.65	0.087	0.144	0.228	5.64	0.009	0.480	2.39	0.114	0.578

Sample																					
AR23	0.06	0.19	0.006	0.04	3.85	0.007	0.023	0.925	0.266	0.186	4.56	1.02	2.07	1.01	0.432	8.07	0.020	4.66	5.62	0.066	1.20
AR24	0.03	0.40	N/D	0.09	0.841	0.005	0.012	2.10	1.43	<LD	1.03	2.96	0.377	1.17	0.222	4.76	0.003	6.14	3.69	0.099	4.72
AR25	0.02	1.51	N/D	0.11	4.10	0.007	1.63	4.57	0.20	<LD	13.7	4.05	0.269	1.61	0.442	15.3	0.005	3.67	5.15	0.184	0.616
AR27	0.04	2.67	0.010	0.12	7.71	0.017	1.17	3.27	0.50	1.34	13.3	9.67	0.950	2.20	0.587	18.0	0.273	11.3	5.05	0.267	0.700
AR28	N/D	4.51	0.008	0.08	22.3	0.019	0.034	3.04	0.33	1.15	10.7	2.79	0.063	1.83	1.88	60.1	0.009	43.1	4.67	0.217	7.25
AR29	0.02	0.28	N/D	0.04	20.7	0.003	0.006	7.94	1.21	0.677	8.25	1.43	0.278	3.61	0.343	5.22	0.005	1.04	3.92	0.025	0.378
AR30	0.06	0.26	N/D	0.18	2.33	0.002	0.006	1.85	1.34	0.464	2.81	7.35	0.968	1.46	0.470	7.54	0.005	1.81	13.0	0.013	0.421
AR31	0.02	0.43	0.009	0.08	28.3	0.004	0.050	0.942	10.183	0.586	5.17	0.804	2.34	0.759	0.108	43.9	0.028	2.86	3.39	0.035	3.33
AR32	0.05	1.82	0.008	0.11	11.2	0.009	0.010	2.42	1.04	0.447	9.67	4.06	0.466	1.54	0.584	34.5	0.019	9.62	1.86	0.308	0.978
AR33	0.07	0.46	0.010	0.09	35.1	0.009	0.122	2.22	0.89	1.03	10.7	7.03	1.13	3.00	0.210	15.4	0.076	2.42	6.35	0.176	0.865
AR34	0.04	0.22	N/D	0.03	4.67	0.006	0.439	1.57	0.05	<LD	0.442	1.28	0.041	0.734	0.282	5.02	0.001	6.82	3.06	0.015	2.98
AR35	0.05	0.18	N/D	0.04	22.5	0.008	0.008	1.90	2.55	0.221	0.799	1.35	0.331	0.931	0.169	2.51	0.001	2.85	3.29	0.067	2.86
AR36	0.03	N/D	0.007	0.05	0.766	0.004	0.001	0.84	1.720	<LD	0.781	0.373	0.084	0.560	0.063	2.58	0.001	0.286	1.85	0.022	3.51
AR39	0.05	0.69	0.020	0.19	36.1	0.012	0.026	7.57	2.91	3.27	13.8	7.22	0.279	4.02	0.540	21.5	0.020	6.36	6.00	0.493	0.454
AR40	0.05	0.53	0.009	0.12	34.8	0.018	0.039	2.7	11.26	1.11	8.67	11.1	0.524	2.35	0.459	44.0	0.023	11.2	3.53	0.189	1.92
AR41	0.33	1.65	0.024	0.13	12.9	0.018	0.024	6.92	1.93	3.38	18.9	9.73	0.264	3.60	0.595	30.2	0.028	7.96	9.22	0.634	0.390
AR42	0.04	0.12	0.007	0.04	2.17	0.004	0.014	2.26	1.50	0.241	2.46	1.05	1.82	1.85	0.546	5.19	0.012	2.18	4.53	0.043	2.66
AR43	0.07	0.29	N/D	0.20	15.2	0.004	0.169	30.1	0.424	1.45	4.28	13.3	0.299	11.2	0.366	3.36	0.002	20.1	149	0.035	4.48
AR44	0.24	0.57	0.007	0.06	3.79	0.008	0.006	1.44	1.64	0.992	5.75	1.61	0.739	1.44	0.202	36.2	0.007	3.22	3.86	0.091	2.12
AR45	0.02	0.22	0.007	0.05	11.8	0.013	0.009	1.16	0.18	0.090	2.28	9.45	0.103	0.663	0.579	4.58	0.008	3.65	2.38	0.087	7.94
AR46	0.04	0.20	0.006	0.05	3.99	0.023	0.011	1.93	1.37	<LD	1.40	4.35	0.685	1.09	0.323	3.06	0.002	2.05	3.80	0.080	2.87
AR47	0.03	0.29	0.006	0.06	5.31	0.024	0.008	0.777	2.22	0.024	8.08	1.25	0.187	0.519	0.196	15.4	0.006	6.19	2.12	0.134	1.29
Mean	*0.05*	*0.86*	*0.008*	*0.08*	*22.2*	*0.009*	*0.111*	*3.28*	*1.91*	*0.708*	*7.28*	*4.35*	*0.472*	*1.74*	*0.389*	*18.3*	*0.020*	*6.47*	*7.62*	*0.131*	*2.60*
SD	*0.06*	*1.26*	*0.005*	*0.06*	*50.9*	*0.006*	*0.305*	*4.65*	*2.37*	*1.047*	*6.16*	*3.97*	*0.571*	*1.80*	*0.322*	*16.8*	*0.043*	*7.36*	*22.50*	*0.128*	*2.67*

Note: elemental concentrations for K, Ca, Ti and Fe are expressed as weight percent (wt%) while for the other elements are expressed as mg/kg. N/D: not detected; <LD: below the limit of detection. *Sr concentration of LP01 was measured by pXRF due to ICP-MS signal saturation caused by very high concentrations.

Annex 3

Rare earth elements (REE) concentrations and fractionation parameters.

Sample	La	Ce	Pr	Nd	Sm	Eu	Gd	Tb	Dy	Ho	Er	Tm	Yb	Lu	Sc	Y	TREE	Ce_n/Ce^*	Eu_n/Eu^*	La_n/Yb_n	Y/Ho
LC01	0.294	0.518	0.063	0.244	0.046	0.009	0.040	0.005	0.025	0.004	0.012	0.002	0.012	0.002	0.113	0.108	1.28	0.93	1.10	1.79	26
LC02	0.153	0.365	0.037	0.138	0.027	0.005	0.021	0.002	0.013	0.002	0.006	0.001	0.006	0.001	0.080	0.050	0.778	1.06	1.04	1.82	25
LC03	0.115	0.265	0.026	0.105	0.020	0.004	0.016	0.002	0.010	0.002	0.005	0.001	0.005	0.001	0.076	0.043	0.576	1.15	1.09	1.73	28
LC04	1.48	2.13	0.350	1.40	0.325	0.071	0.310	0.041	0.234	0.040	0.112	0.014	0.092	0.012	0.281	1.14	6.61	0.70	1.15	1.19	28
LC06	0.182	0.466	0.043	0.164	0.032	0.006	0.027	0.003	0.016	0.003	0.008	0.001	0.007	0.001	0.119	0.071	0.960	1.17	1.13	1.80	27
LC07	0.434	0.768	0.110	0.463	0.101	0.022	0.091	0.013	0.074	0.013	0.036	0.005	0.033	0.005	0.167	0.343	2.17	0.85	1.14	0.96	27
LC08	0.387	0.755	0.088	0.355	0.076	0.017	0.068	0.009	0.047	0.008	0.023	0.003	0.021	0.003	0.426	0.183	1.86	0.99	1.25	1.38	23
LC09	0.240	0.499	0.054	0.211	0.073	0.019	0.034	0.004	0.020	0.003	0.010	0.001	0.009	0.001	0.144	0.081	1.18	1.03	1.87	1.88	26
LC10	0.172	0.409	0.043	0.169	0.035	0.007	0.027	0.003	0.016	0.002	0.007	0.001	0.007	0.001	0.093	0.080	0.898	1.08	1.23	1.93	33
LC11	0.217	0.531	0.052	0.204	0.039	0.008	0.035	0.004	0.020	0.003	0.009	0.001	0.008	0.001	0.107	0.078	1.13	1.15	1.13	2.06	26
LC13	0.271	0.564	0.060	0.232	0.046	0.009	0.042	0.005	0.028	0.005	0.014	0.002	0.013	0.002	0.134	0.120	1.29	1.05	1.11	1.59	26
LC14	0.293	0.637	0.071	0.280	0.055	0.011	0.046	0.005	0.028	0.004	0.013	0.002	0.011	0.001	0.105	0.121	1.46	1.01	1.12	1.95	28
LC15	0.400	0.750	0.112	0.351	0.069	0.019	0.064	0.013	0.043	0.012	0.023	0.008	0.022	0.008	0.162	0.153	1.89	0.60	1.28	1.34	12
LC16	0.326	0.673	0.075	0.294	0.056	0.011	0.049	0.006	0.031	0.005	0.014	0.002	0.013	0.002	0.150	0.140	1.56	1.01	1.14	1.88	28
LC17	0.182	0.433	0.042	0.163	0.033	0.007	0.029	0.004	0.020	0.003	0.009	0.001	0.008	0.001	0.094	0.078	0.935	1.16	1.15	1.61	26
LC18	0.092	0.241	0.022	0.088	0.017	0.003	0.013	0.002	0.009	0.001	0.004	0.001	0.004	0.001	0.071	0.042	0.497	1.23	0.89	1.60	30
LC19	0.340	0.661	0.076	0.297	0.063	0.013	0.055	0.007	0.037	0.006	0.017	0.002	0.016	0.002	0.149	0.166	1.59	0.98	1.16	1.60	28
LC20	0.248	0.553	0.061	0.245	0.045	0.008	0.039	0.004	0.023	0.004	0.011	0.001	0.009	0.001	0.099	0.114	1.25	1.05	1.05	1.93	32
Mean	*0.324*	*0.623*	*0.077*	*0.300*	*0.064*	*0.014*	*0.056*	*0.007*	*0.039*	*0.007*	*0.019*	*0.003*	*0.016*	*0.003*	*0.143*	*0.173*	*1.55*	*1.01*	*1.17*	*1.67*	*27*
SD	*0.305*	*0.408*	*0.073*	*0.289*	*0.069*	*0.015*	*0.066*	*0.009*	*0.051*	*0.009*	*0.025*	*0.003*	*0.020*	*0.003*	*0.086*	*0.251*	*1.34*	*0.16*	*0.19*	*0.29*	*4*
LP01	0.149	0.258	0.029	0.113	0.031	0.008	0.023	0.003	0.017	0.003	0.009	0.001	0.009	0.001	0.033	0.122	0.656	1.00	1.53	1.26	37
LP02	0.016	0.029	0.004	0.014	0.003	0.001	0.003	0.0005	0.002	0.001	0.001	0.0003	0.002	0.0004	0.015	0.018	0.076	0.77	1.13	0.62	35
LP03	0.025	0.041	0.007	0.027	0.006	0.001	0.006	0.001	0.005	0.001	0.002	0.0004	0.003	0.001	0.012	0.034	0.126	0.70	1.13	0.58	43
LP04	0.094	0.195	0.021	0.085	0.016	0.002	0.013	0.002	0.008	0.001	0.003	0.0004	0.003	0.0004	0.039	0.036	0.445	1.05	0.82	2.39	32
LP05	0.036	0.071	0.008	0.035	0.008	0.002	0.008	0.001	0.007	0.001	0.004	0.001	0.005	0.001	0.024	0.059	0.189	1.10	1.22	0.51	41

Sample	La	Ce	Pr	Nd	Sm	Eu	Gd	Tb	Dy	Ho	Er	Tm	Yb	Lu	Sc	Y	TREE	Ce_n/Ce^*	Eu_n/Eu^*	La_n/Yb_n	Y/Ho
LP06	0.118	0.231	0.026	0.099	0.021	0.004	0.017	0.002	0.011	0.002	0.006	0.001	0.005	0.001	0.054	0.049	0.545	0.96	1.12	1.60	27
LP07	0.034	0.061	0.007	0.028	0.009	0.002	0.006	0.001	0.004	0.001	0.002	0.0003	0.003	0.0004	0.016	0.028	0.159	1.09	1.64	0.87	42
LP08	0.053	0.140	0.015	0.071	0.019	0.005	0.018	0.002	0.014	0.002	0.007	0.001	0.007	0.001	0.016	0.053	0.356	1.24	1.25	0.59	22
LP09	0.062	0.105	0.015	0.063	0.014	0.003	0.010	0.001	0.007	0.001	0.003	0.0005	0.004	0.001	0.025	0.033	0.289	0.85	1.17	1.23	28
LP10	0.011	0.016	0.002	0.010	0.004	0.001	0.002	0.0003	0.002	0.0003	0.001	0.0001	0.001	0.0001	0.006	0.016	0.051	0.94	1.72	0.81	46
LP11	0.030	0.099	0.007	0.038	0.011	0.003	0.012	0.002	0.011	0.002	0.006	0.001	0.008	0.001	0.013	0.056	0.231	1.99	1.16	0.27	28
Mean	*0.057*	*0.113*	*0.013*	*0.053*	*0.013*	*0.003*	*0.011*	*0.001*	*0.008*	*0.001*	*0.004*	*0.0006*	*0.005*	*0.0007*	*0.023*	*0.046*	*0.284*	*1.06*	*1.26*	*0.98*	*35*
SD	*0.045*	*0.083*	*0.009*	*0.035*	*0.008*	*0.002*	*0.007*	*0.001*	*0.005*	*0.001*	*0.003*	*0.0004*	*0.003*	*0.0004*	*0.014*	*0.029*	*0.197*	*0.34*	*0.27*	*0.61*	*8*
RM01	0.032	0.063	0.007	0.028	0.012	0.003	0.004	0.0005	0.007	0.0004	0.001	0.0002	0.001	0.0002	0.011	0.018	0.160	1.06	2.19	1.77	41
RM02	0.081	0.189	0.021	0.087	0.019	0.004	0.011	0.001	0.008	0.001	0.004	0.001	0.004	0.001	0.042	0.040	0.432	1.09	1.30	1.55	31
RM03	0.030	0.062	0.007	0.029	0.007	0.001	0.004	0.001	0.003	0.0005	0.002	0.0002	0.002	0.0003	<LD	0.016	0.148	1.12	1.22	1.37	32
RM04	0.031	0.055	0.006	0.025	0.005	0.001	0.004	0.0005	0.003	0.0005	0.002	0.0002	0.002	0.0003	0.002	0.012	0.135	1.11	1.13	1.44	25
RM05	0.041	0.090	0.010	0.040	0.008	0.002	0.006	0.001	0.004	0.001	0.002	0.0003	0.002	0.0003	0.004	0.017	0.206	1.11	1.18	1.26	24
RM06	0.041	0.079	0.009	0.037	0.008	0.002	0.006	0.001	0.004	0.001	0.002	0.0003	0.002	0.0003	0.019	0.015	0.192	1.13	1.36	1.43	22
RM07	0.023	0.048	0.005	0.022	0.009	0.002	0.004	0.0005	0.003	0.0004	0.001	0.0002	0.001	0.0002	0.013	0.017	0.121	1.11	1.95	1.31	39
RM08	0.068	0.129	0.016	0.068	0.018	0.004	0.012	0.002	0.009	0.001	0.004	0.001	0.004	0.001	0.026	0.036	0.338	0.95	1.37	1.13	25
RM09	0.045	0.088	0.010	0.041	0.008	0.001	0.006	0.001	0.004	0.001	0.002	0.0003	0.003	0.0004	0.007	0.019	0.209	1.12	0.99	1.31	31
RM10	0.068	0.140	0.015	0.066	0.015	0.003	0.010	0.001	0.007	0.001	0.004	0.0005	0.004	0.001	0.024	0.027	0.335	1.14	1.25	1.33	24
RM12	0.018	0.031	0.003	0.014	0.003	0.0004	0.002	0.0003	0.002	0.0003	0.001	0.0001	0.001	0.0002	0.003	0.010	0.075	1.21	0.89	1.48	33
RM13	0.023	0.044	0.005	0.021	0.005	0.001	0.004	0.0004	0.002	0.0003	0.001	0.0002	0.001	0.0002	0.003	0.011	0.107	1.14	1.09	1.72	32
RM14	0.046	0.098	0.010	0.042	0.009	0.002	0.007	0.001	0.005	0.001	0.002	0.0003	0.002	0.0004	0.017	0.021	0.226	1.16	1.09	1.41	29
RM15	0.041	0.084	0.009	0.038	0.047	0.016	0.007	0.001	0.005	0.001	0.003	0.0004	0.002	0.0003	<LD	0.023	0.254	1.18	3.29	1.35	27
Mean	*0.042*	*0.09*	*0.009*	*0.04*	*0.012*	*0.003*	*0.006*	*0.0008*	*0.005*	*0.0007*	*0.002*	*0.0003*	*0.002*	*0.0004*	*0.012*	*0.020*	*0.210*	*1.12*	*1.45*	*1.42*	*30*
SD	*0.019*	*0.04*	*0.005*	*0.02*	*0.011*	*0.004*	*0.003*	*0.0004*	*0.002*	*0.0003*	*0.001*	*0.0001*	*0.001*	*0.0002*	*0.012*	*0.009*	*0.101*	*0.06*	*0.64*	*0.17*	*6*
Sample	**La**	**Ce**	**Pr**	**Nd**	**Sm**	**Eu**	**Gd**	**Tb**	**Dy**	**Ho**	**Er**	**Tm**	**Yb**	**Lu**	**Sc**	**Y**	**TREE**	**Ce_n/Ce^***	**Eu_n/Eu^***	**La_n/Yb_n**	**Y/Ho**
AN01	2.24	2.49	0.506	2.16	0.378	0.091	0.400	0.0605	0.347	0.071	0.192	0.025	0.147	0.021	0.734	3.24	9.13	0.61	1.18	1.13	46
AN02	1.18	0.948	0.237	0.968	0.172	0.039	0.185	0.0252	0.141	0.029	0.079	0.011	0.069	0.010	0.623	1.25	4.09	0.47	1.13	1.26	44
AN03	0.819	0.749	0.166	0.706	0.133	0.030	0.143	0.0212	0.125	0.027	0.080	0.012	0.077	0.012	0.575	1.23	3.10	0.56	1.09	0.79	45
AN04	2.11	1.81	0.463	1.92	0.347	0.073	0.339	0.0453	0.236	0.044	0.114	0.014	0.085	0.013	0.798	1.92	7.61	0.47	1.11	1.83	44

AN05	1.09	1.17	0.260	1.12	0.216	0.047	0.211	0.0297	0.162	0.032	0.089	0.012	0.078	0.012	0.818	1.32	4.53	0.56	1.12	1.03	41
AN06	0.585	0.953	0.166	0.801	0.157	0.038	0.169	0.0227	0.123	0.024	0.063	0.008	0.051	0.007	0.405	0.937	3.17	0.80	1.22	0.84	40
AN07	0.802	0.598	0.168	0.674	0.139	0.033	0.149	0.0222	0.127	0.027	0.074	0.010	0.059	0.009	0.403	1.25	2.89	0.41	1.15	1.01	47
AN08	1.82	1.19	0.355	1.41	0.260	0.057	0.278	0.0390	0.219	0.044	0.119	0.015	0.087	0.013	0.582	2.26	5.91	0.38	1.10	1.54	51
AN09	0.934	0.774	0.222	0.874	0.188	0.042	0.188	0.0266	0.143	0.028	0.076	0.010	0.062	0.009	0.581	1.15	3.58	0.40	1.14	1.12	41
Mean	*1.29*	*1.19*	*0.282*	*1.18*	*0.221*	*0.050*	*0.229*	*0.032*	*0.180*	*0.036*	*0.099*	*0.013*	*0.079*	*0.012*	*0.613*	*1.62*	*4.89*	*0.52*	*1.14*	*1.17*	*44*
SD	*0.61*	*0.60*	*0.130*	*0.54*	*0.089*	*0.020*	*0.090*	*0.013*	*0.075*	*0.015*	*0.040*	*0.005*	*0.028*	*0.004*	*0.151*	*0.74*	*2.21*	*0.13*	*0.04*	*0.33*	*4*
AR01	0.291	0.536	0.059	0.247	0.046	0.011	0.034	0.004	0.022	0.004	0.011	0.001	0.009	0.002	0.141	0.103	1.28	1.08	1.36	2.48	28
AR02	0.816	1.16	0.170	0.768	0.175	0.046	0.138	0.019	0.104	0.020	0.057	0.007	0.041	0.007	0.507	0.766	3.52	0.89	1.49	1.47	38
AR03	0.568	2.40	0.124	0.470	0.082	0.017	0.080	0.009	0.044	0.007	0.020	0.003	0.020	0.003	0.130	0.146	3.85	2.12	1.15	2.12	21
AR04	0.218	0.439	0.040	0.169	0.144	0.049	0.023	0.003	0.013	0.002	0.007	0.001	0.007	0.001	0.147	0.067	1.12	1.32	3.50	2.19	30
AR05	0.157	0.306	0.030	0.127	0.030	0.008	0.023	0.003	0.016	0.003	0.009	0.001	0.008	0.001	0.090	0.094	0.72	1.21	1.46	1.49	32
AR06	0.543	0.774	0.116	0.518	0.097	0.023	0.093	0.013	0.074	0.014	0.041	0.005	0.032	0.005	0.276	0.562	2.35	0.87	1.24	1.26	39
AR07	0.031	0.056	0.007	0.032	0.012	0.004	0.006	0.001	0.005	0.001	0.002	0.0002	0.001	0.0002	0.065	0.021	0.16	1.00	1.88	1.60	31
AR08	0.090	0.148	0.018	0.071	0.021	0.006	0.010	0.001	0.007	0.001	0.004	0.001	0.004	0.001	0.032	0.032	0.38	0.94	1.91	1.88	27
AR09	0.128	0.234	0.038	0.187	0.070	0.021	0.086	0.015	0.091	0.017	0.044	0.005	0.033	0.005	0.049	0.675	0.97	0.89	1.30	0.29	40
AR10	0.106	0.233	0.029	0.135	0.030	0.007	0.024	0.004	0.019	0.003	0.010	0.001	0.012	0.002	0.045	0.080	0.62	1.05	1.20	0.63	25
AR11	0.143	0.295	0.029	0.115	0.019	0.004	0.016	0.002	0.010	0.002	0.005	0.001	0.005	0.001	0.103	0.050	0.65	1.19	1.12	1.94	28
AR12	0.014	0.026	0.003	0.012	0.004	0.001	0.002	0.000	0.002	0.0003	0.001	0.0001	0.001	0.0002	0.034	0.007	0.07	1.21	1.88	0.79	28
AR13	1.04	1.68	0.240	1.07	0.187	0.040	0.157	0.020	0.111	0.019	0.056	0.007	0.042	0.007	0.612	0.712	4.67	0.90	1.20	1.81	37
AR15	0.027	0.035	0.004	0.019	0.010	0.003	0.004	0.0006	0.003	0.001	0.001	0.0002	0.001	0.0002	0.009	0.020	0.11	1.26	2.22	1.45	36
AR16	0.170	0.327	0.037	0.151	0.031	0.007	0.021	0.002	0.013	0.002	0.007	0.001	0.007	0.001	0.086	0.087	0.78	1.05	1.29	1.91	35
AR17	0.168	0.341	0.035	0.144	0.029	0.006	0.022	0.003	0.015	0.003	0.008	0.001	0.006	0.001	0.184	0.078	0.78	1.17	1.30	1.98	31
AR18	0.134	0.288	0.030	0.127	0.023	0.004	0.019	0.002	0.012	0.002	0.007	0.001	0.007	0.001	0.259	0.063	0.66	1.18	1.09	1.48	29
AR19	0.181	0.339	0.039	0.160	0.030	0.006	0.024	0.003	0.015	0.003	0.008	0.001	0.007	0.001	0.176	0.079	0.82	1.03	1.15	1.93	30
AR21	0.213	0.475	0.050	0.214	0.045	0.010	0.037	0.004	0.020	0.003	0.008	0.001	0.006	0.001	0.259	0.099	1.09	1.16	1.36	2.69	32
AR22	0.161	0.301	0.039	0.163	0.033	0.007	0.024	0.003	0.016	0.003	0.007	0.001	0.006	0.001	0.113	0.064	0.76	0.93	1.28	2.08	25
AR23	0.094	0.172	0.020	0.082	0.016	0.003	0.012	0.002	0.010	0.002	0.006	0.001	0.005	0.001	0.149	0.047	0.43	0.99	1.16	1.30	28
AR24	0.078	0.241	0.018	0.081	0.016	0.002	0.017	0.002	0.012	0.002	0.006	0.001	0.005	0.001	0.232	0.065	0.48	1.70	0.62	1.17	32

AR25	1.96	1.62	0.370	1.68	0.302	0.069	0.299	0.044	0.254	0.048	0.134	0.017	0.097	0.014	0.283	1.87	6.91	0.57	1.16	1.50	39
AR27	0.629	1.20	0.134	0.558	0.099	0.020	0.086	0.011	0.060	0.010	0.028	0.004	0.024	0.004	0.374	0.295	2.86	1.07	1.13	1.97	31
AR28	2.67	2.04	0.777	3.31	0.693	0.151	0.505	0.077	0.370	0.056	0.145	0.019	0.126	0.019	0.210	1.11	11.0	0.32	1.21	1.56	20
AR29	0.057	0.088	0.011	0.047	0.017	0.005	0.008	0.001	0.005	0.001	0.002	0.0003	0.002	0.0003	0.046	0.023	0.24	1.00	1.92	2.28	29
AR30	0.071	0.117	0.012	0.053	0.010	0.002	0.009	0.001	0.006	0.001	0.003	0.0004	0.003	0.0004	0.035	0.033	0.29	1.16	1.37	1.86	28
AR31	0.104	0.191	0.026	0.114	0.034	0.009	0.019	0.003	0.014	0.002	0.006	0.001	0.005	0.001	0.048	0.066	0.53	0.91	1.61	1.47	28
AR32	0.293	0.877	0.070	0.289	0.058	0.010	0.046	0.005	0.027	0.004	0.013	0.002	0.012	0.002	0.236	0.106	1.71	1.50	1.05	1.78	25
AR33	0.294	0.604	0.063	0.267	0.058	0.014	0.038	0.005	0.027	0.005	0.015	0.002	0.015	0.002	0.130	0.132	1.41	1.18	1.44	1.46	27
AR34	0.076	0.062	0.017	0.074	0.018	0.005	0.017	0.003	0.020	0.004	0.012	0.002	0.015	0.003	0.016	0.133	0.33	0.46	1.28	0.37	34
AR35	0.037	0.086	0.010	0.044	0.017	0.005	0.007	0.001	0.005	0.001	0.002	0.0004	0.003	0.0004	0.037	0.022	0.22	1.11	2.05	1.07	28
AR36	0.037	0.069	0.008	0.036	0.006	0.001	0.005	0.0006	0.003	0.000	0.001	0.0002	0.002	0.0003	0.031	0.014	0.17	1.04	1.04	1.74	29
AR39	0.833	0.827	0.170	0.810	0.159	0.041	0.143	0.020	0.109	0.021	0.059	0.008	0.048	0.008	0.528	0.816	3.25	0.67	1.39	1.29	39
AR40	0.285	0.605	0.065	0.270	0.060	0.014	0.039	0.005	0.025	0.004	0.012	0.002	0.011	0.002	0.126	0.109	1.40	1.12	1.43	1.85	25
AR41	2.44	1.46	0.412	1.89	0.300	0.068	0.285	0.040	0.225	0.044	0.123	0.016	0.096	0.015	0.899	1.860	7.43	0.47	1.18	1.89	42
AR42	0.054	0.114	0.012	0.051	0.010	0.002	0.008	0.001	0.006	0.001	0.003	0.0005	0.004	0.001	0.068	0.030	0.27	1.19	1.14	0.98	26
AR43	0.091	0.261	0.021	0.090	0.023	0.005	0.014	0.002	0.008	0.001	0.003	0.0004	0.003	0.0004	0.038	0.029	0.52	1.56	1.47	2.60	22
AR44	0.290	0.490	0.054	0.226	0.040	0.009	0.035	0.005	0.028	0.005	0.017	0.003	0.025	0.005	0.109	0.132	1.23	1.11	1.16	0.87	25
AR45	0.145	0.320	0.033	0.134	0.029	0.007	0.021	0.003	0.017	0.003	0.009	0.001	0.009	0.001	0.076	0.077	0.73	1.16	1.33	1.24	26
AR46	0.089	0.193	0.022	0.094	0.020	0.005	0.016	0.002	0.013	0.002	0.007	0.001	0.008	0.001	0.053	0.051	0.47	1.08	1.27	0.86	22
AR47	0.172	0.316	0.038	0.161	0.028	0.005	0.021	0.003	0.013	0.002	0.006	0.001	0.006	0.001	0.097	0.051	0.77	0.99	1.01	2.06	24
Mean	*0.381*	*0.532*	*0.083*	*0.363*	*0.075*	*0.017*	*0.059*	*0.008*	*0.044*	*0.008*	*0.022*	*0.003*	*0.018*	*0.003*	*0.170*	*0.259*	*1.6*	*1.07*	*1.40*	*1.59*	*30*
SD	*0.608*	*0.573*	*0.141*	*0.619*	*0.121*	*0.027*	*0.097*	*0.014*	*0.075*	*0.013*	*0.035*	*0.004*	*0.028*	*0.004*	*0.182*	*0.447*	*2.2*	*0.32*	*0.45*	*0.56*	*6*

Note: elemental concentrations are expressed as mg/kg. <LD: under the limit of detection. TREE: total lanthanides concentration. Population mean and standard deviation (SD) are estimated on the collected samples substituting <LD with lowest measured value divided by two. REE anomalies were calculated according to Lawrence et al. (2006): $Ce^* = Pr_n \cdot (Pr_n/Nd_n)$, $Eu^* = (Sm_n^2 \cdot Tb_n)^{1/3}$. For anomalies and fractionation parameters calculation, REE were normalized by using Post Archaean Australian Shale (PAAS) (McLennan, 1989) except for Y and Ho which were not normalized.
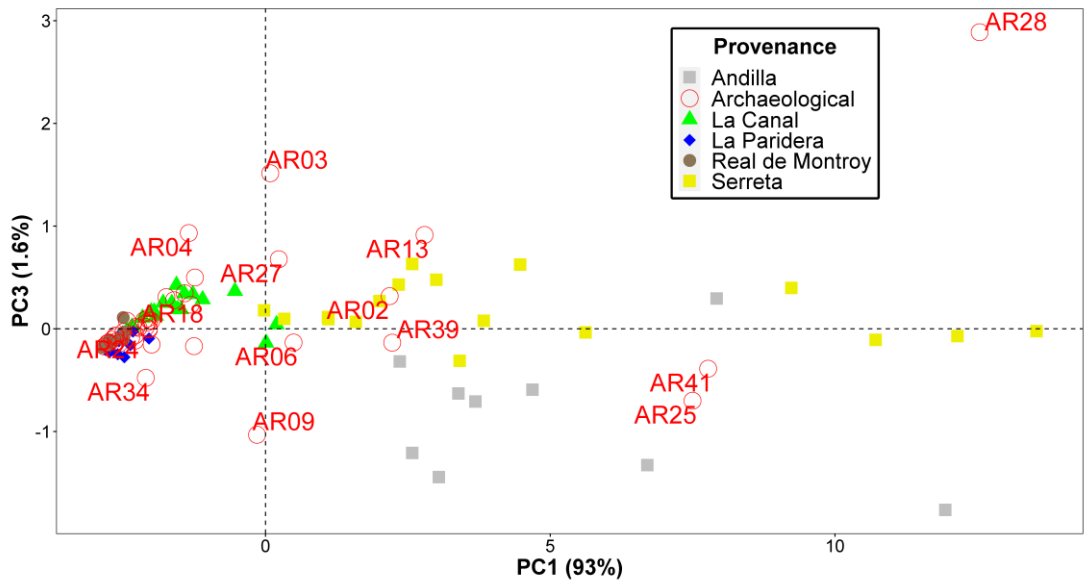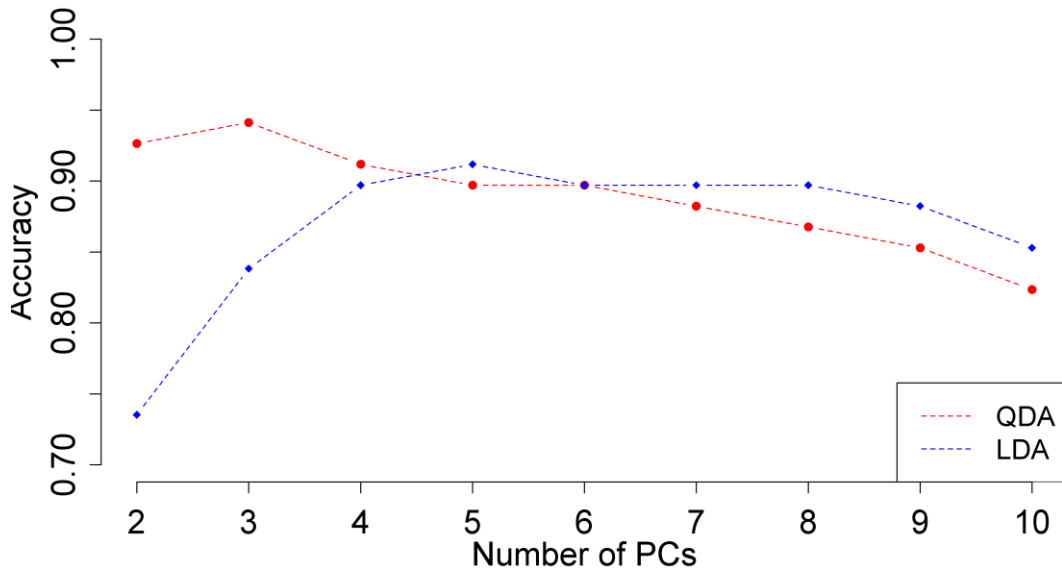
a) Samples/scores plot of PC1 vs PC3 employing also Serreta chert samples and REE, Sc and Y as variables
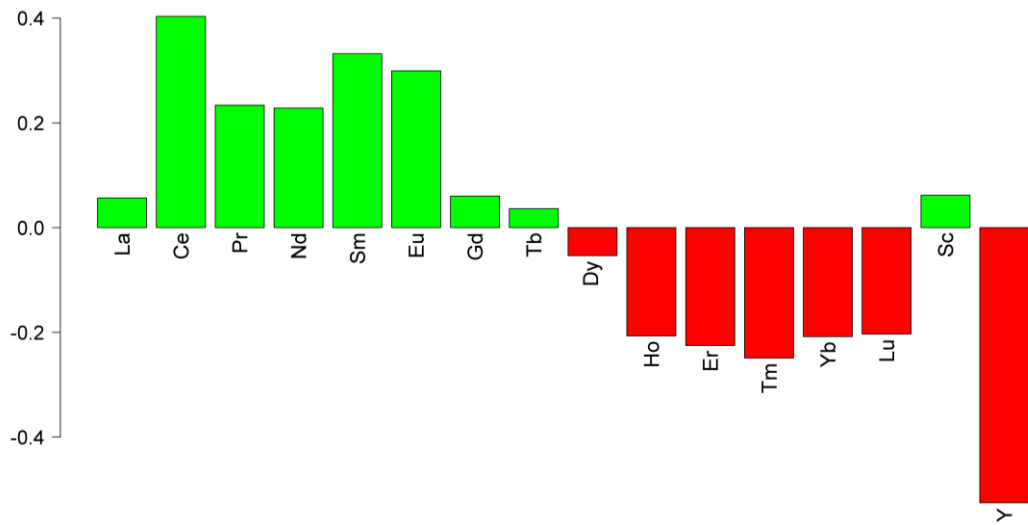
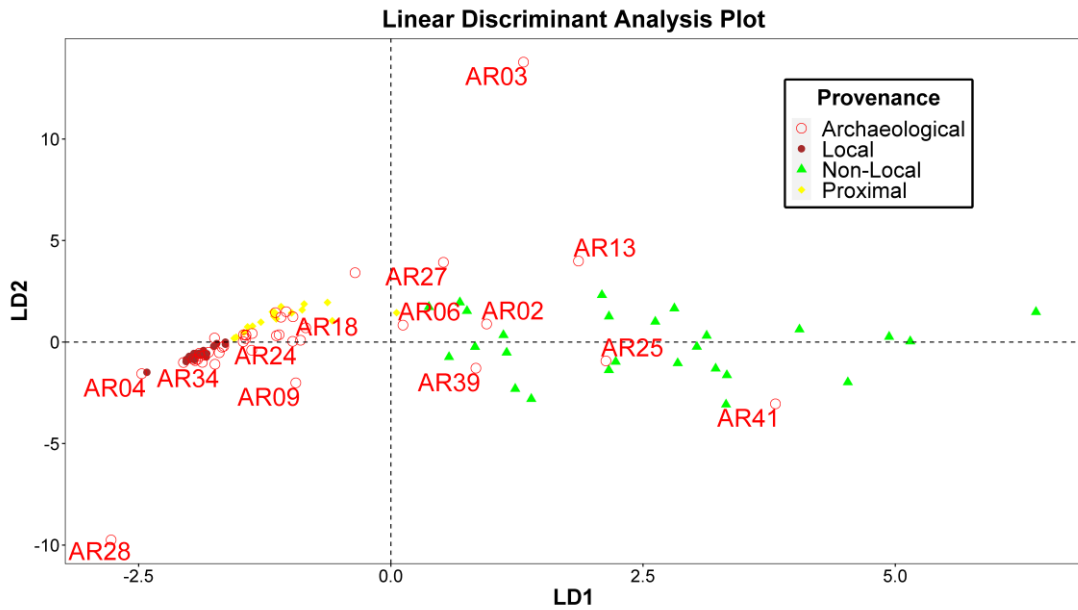b) Variables/loadings plot for PC3 (1.6%) of the PCA models with Serreta chert samples and REE as variables.

Leave-One-Out Cross-Validation

a) Accuracy for QDA and LDA models employing from two up to ten PCs tested by LOOCV.

b) Linear Discriminant Analysis scatter plot employing PC1-5 as variables.

As can be observed in the scatter plot, the results for LDA do not deviate consistently from the ones obtained by QDA. Indeed, most of the archaeological samples fall within the cherts from the local and the proximal outcrops, while only few samples have scores close to not-local ones.

c) Confusion matrix of LOOCV for proximal (LC), local (LP and RM) and non-local (Serreta and AN) classifications in QDA model employing PC1 to PC3 as variables.

Predicted	Actual			
	Proximal	**Local**	**Non-Local**	
Proximal	22	3	0	25
Local	0	34	0	34
Non-Local	3	0	38	41
	25	37	38	100

Anexo C

Ramacciotti et al. (2018). Chronological classification of ancient mortars employing spectroscopy and spectrometry techniques: Sagunto (Valencia, Spain) Case

Research Article

Chronological Classification of Ancient Mortars Employing Spectroscopy and Spectrometry Techniques: Sagunto (Valencia, Spain) Case

M. Ramacciotti,[1,2] S. Rubio,[2] G. Gallello [1,2,3] M. Lezzerini [4,5] S. Columbu,[6] E. Hernandez,[7] A. Morales-Rubio,[2] A. Pastor,[2] and M. de la Guardia[2]

[1]Department of Prehistory, Archaeology and Ancient History, Faculty of Geography and History, University of Valencia, Av. Blasco Ibáñez 28, 46010 Valencia, Spain
[2]Department of Analytical Chemistry, Faculty of Chemistry, University of Valencia, C/ Dr. Moliner 50, 46100 Burjassot, Valencia, Spain
[3]Department of Archaeology, University of York, King's Manor, York YO1 7EP, UK
[4]Department of Earth Sciences, University of Pisa, Via S. Maria 53, 56126 Pisa, Italy
[5]Applied and Laser Spectroscopy Laboratory, ICCOM-CNR, Via G. Moruzzi 1, 56124 Pisa, Italy
[6]Department of Chemical and Geological Sciences, University of Cagliari, Via Trentino 51, 09127 Cagliari, Italy
[7]Sagunto Archaeological Museum, C/ del Castillo 23, 46500 Sagunto, Valencia, Spain

Correspondence should be addressed to G. Gallello; gianni.gallello@york.ac.uk

Forty-two mortar samples, from two archaeological excavations located in Sagunto (Valencian Community, Spain), were analysed by both portable energy dispersive X-ray fluorescence spectroscopy (pED-XRF) and inductively coupled plasma mass spectrometry (ICP-MS) to determine major and minor elements and traces including rare earth elements (REEs). Collected data were crossed with those previously obtained from Sagunto Castle mortars, and principal component analysis (PCA) was applied to discriminate the construction phases of the unearthed buildings. REE permitted to ascribe most of the masonries to the Roman Imperial period. Moreover, a statistical model was built by employing partial least squares discriminant analysis (PLS-DA) in order to classify the mortars from Roman Imperial period and from Islamic period due to the problematic overlapping between these two phases. Results confirmed the effectiveness of the developed indirect chronology method, based on REE data, to discriminate among historic mortars from different construction periods on a wide scale including different Sagunto archaeological sites.

1. Introduction

Mortar is a building material composed essentially of binder and aggregate fractions and, in some cases, of additives of different types [1–3]. In particular, lime mortar had a key function in Roman architecture: Roman people made their walls and structures with this material adding reactive materials, like pozzolan materials (i.e., *pulvis puteolanus* and *cocciopesto*), to give a hydraulic character to the mortars [4–8]. The use of mortar in architecture is documented during the Middle Ages and in the following historical periods [6–13].

The chemical analysis by statistical approach, together with mineralogical and petrographic characterization of ancient mortars and polished stones, has shown to be a useful tool in the interpretation of the construction phases of several archaeological sites and historical complexes [14–20]. Moreover, ancient mortars are subjected to decay phenomena which also must be detected and evaluated for conservation issues [21–24].

TABLE 1: Sample description including area and building of sampling sites and mortar type.

Sample	Archaeological excavation	Building	Mortar type
C05	Los Huertos Street	Circus MSU1005	Lime mortar
C06	Los Huertos Street	Circus MSU1006	Lime mortar
C07	Los Huertos Street	Circus MSU1007	Lime mortar
C08	Los Huertos Street	Circus MSU1008	Lime mortar
C09	Los Huertos Street	Circus MSU1009	Lime mortar
C10a	Los Huertos Street	Circus MSU1010a	Lime mortar
C10b	Los Huertos Street	Circus MSU1010b	Lime mortar
C20	Los Huertos Street	Circus MSU1020	Lime mortar
C26	Los Huertos Street	Circus MSU1026	Lime mortar
CLC	Los Huertos Street	Cloaca	Lime mortar
EW	Los Huertos Street	Eastern Wall	Lime mortar
JMN	Los Huertos Street	Northern Jamb	Lime mortar
NR	Los Huertos Street	Noria	Lime mortar
NW	Los Huertos Street	Northern Wall	Lime mortar
P15	Los Huertos Street	Pilaster MSU3015	Lime mortar
P16	Los Huertos Street	Pilaster MSU3016	Lime mortar
P17	Los Huertos Street	Pilaster MSU3017	Lime mortar
P18	Los Huertos Street	Pilaster MSU3018	Lime mortar
R3a	Los Huertos Street	Room 3 MSU1032	Lime mortar
R3b	Los Huertos Street	Room 3 MSU1050	Lime mortar
UN1	Los Huertos Street	Unknown MSU3038	Lime mortar
UN2	Los Huertos Street	Unknown MSU6006	Lime mortar
WLL	Los Huertos Street	Well	Lime mortar
RS10A	Railroad Station	MSU1010a	Lime mortar
RS10B	Railroad Station	MSU1010b	Lime mortar
RS10C	Railroad Station	MSU1010c	Lime mortar
RS11A	Railroad Station	MSU1011a	Lime mortar
RS11B	Railroad Station	MSU1011b	Lime mortar
RS11C	Railroad Station	MSU1011c	Lime mortar

TABLE 1: Continued.

Sample	Archaeological excavation	Building	Mortar type
RS24A	Railroad Station	MSU1024a	Lime mortar
RS24B	Railroad Station	MSU1024b	Lime mortar
RS24C	Railroad Station	MSU1024c	Lime mortar
RS25A	Railroad Station	MSU1025a	Lime mortar
RS25B	Railroad Station	MSU1025b	Lime mortar
RS25C	Railroad Station	MSU1025c	Lime mortar
RSLW	Railroad Station	Long Wall	Lime mortar
R1a	Los Huertos Street	Room 1 MSU3029	Earth mortar
R1b	Los Huertos Street	Room 1 MSU3030	Earth mortar
R1c	Los Huertos Street	Room 1 MSU3039	Earth mortar
R2a	Los Huertos Street	Room 2 MSU3062	Earth mortar
R2b	Los Huertos Street	Room 2 MSU3063	Earth mortar
R2d	Los Huertos Street	Room 2 MSU3064	Earth mortar

Note. MSU: masonry stratigraphic unit.

This paper shows the results of the analyses carried out on ancient mortars collected from buildings discovered during two recent archaeological excavations at Sagunto, a town located in the Eastern Spain, ca. 30 km north of Valencia, close to the Costa del Azahar on the Mediterranean Sea. Sagunto is well known in the world for its complex history, and its area has been occupied since the Iberian Age. During the Roman period, Sagunto was interested in constructing important buildings such as the Circus and the Theatre. Thereafter, Sagunto was occupied by Islamic people, and during the Modern Ages, the city was involved in the Napoleonic Wars [25].

The collected mortar samples were analysed by both portable energy dispersive X-ray fluorescence spectroscopy (pED-XRF) and by an inductively coupled plasma mass spectrometer (ICP-MS) to determine their major elements, minor elements, and trace elements. The mineral element concentration and, in particular, the measured contents of rare earth elements (REE) of these samples were compared with those previously obtained from Sagunto Castle [26] by applying principal component analysis (PCA) and partial least squares discriminant analysis (PLS-DA) to determine the construction periods.

2. Materials and Methods

2.1. Sampling. The studied mortars (Table 1) were sampled during two archaeological excavations located in the city of
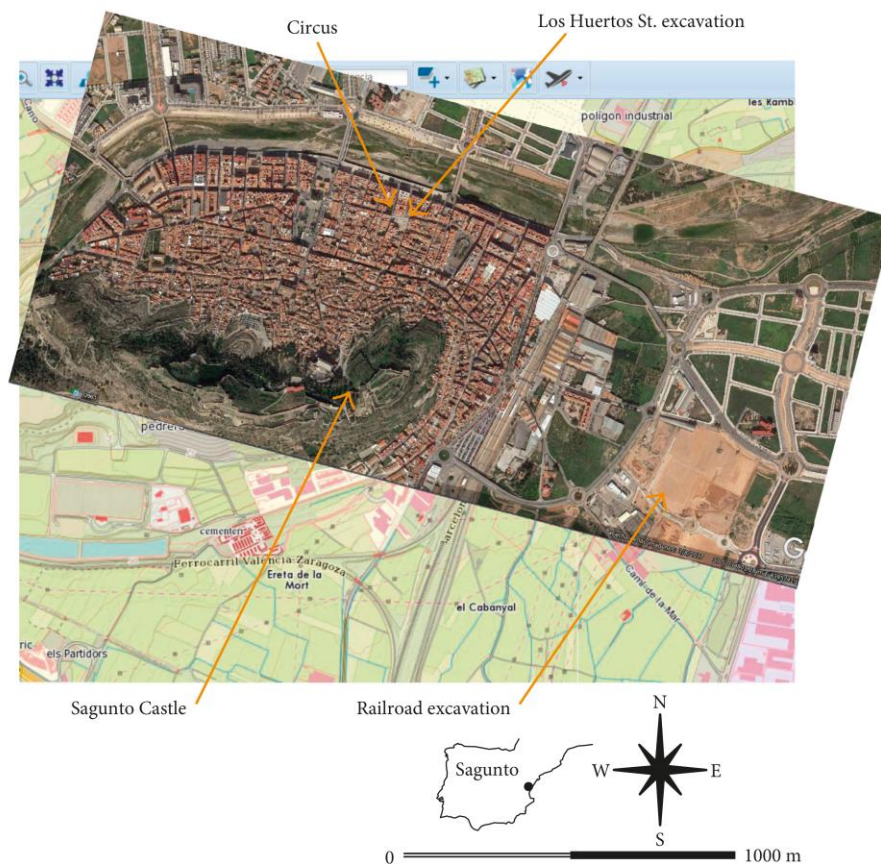
FIGURE 1: Map of the city of Sagunto with the area of sampling (the satellite picture was obtained from Google Earth while the map of Sagunto from the Institut Cartogràfic Valencià, http://www.icv.gva.es).

Sagunto (Figure 1). Twenty-nine samples were collected during the archaeological excavation of Los Huertos St., an area characterized by the presence of buildings and materials from the Roman Imperial phase and from the Islamic occupation in the Middle Ages. Twenty-three samples of lime mortars were collected from these buildings: nine samples come from the Circus (C), a building dating back to the Roman Imperial period, one from the cloaca (CLC), one from a jamb (JMN), two from two different walls (Eastern Wall, EW, and Northern Wall, NW), one from a noria (NR), and four from a pilaster (P). Six samples of earth mortar come from two rooms that the archaeologists interpreted as may belong to the Islamic occupation (Room 1, samples R1 and Room 2, samples R2), and in this study, they were analysed as control samples. Two samples of lime mortar were collected from Room 3 (R3), two from an unidentified building (UN), and one from a well (WLL). Thirteen samples of lime mortars were collected from different masonries during the emergency archaeological excavation of an area close to Sagunto's Railroad Station (RS named samples). Data of twenty-three lime mortar samples from different buildings of the Castle of Sagunto, studied by Gallello et al. [26], were taken into account as the calibration set to perform data analysis and to date the structures of the above-quoted excavations. Part of the calibration samples come from masonries dating back to the Roman Imperial Period: five samples from the Theatre (TR) and one from the Curia (CUR); the other samples come from masonries dated back to the Islamic occupation phase: four samples from the first part of the Islamic Wall (MI), one of the wall which was considered modern before the study (MM), one from a Hermitage (ERM), two from two Islamic reworks of the Torre Central Estudiantes (TCE), and two from the *tabernae* of the Imperial Forum. Moreover, two samples from the Curia (CUR) and five samples from the Basilica of the Imperial Forum (FBI), whose dating was uncertain between the above-quoted two phases, were added to the dataset.

2.2. Major and Minor Elements Determination.

All the analyses were carried out on each entire mortar sample previously pulverized ($D_{max} < 63 \mu m$) and homogenized through Agatha mortar and pestle. Major and minor element concentrations were obtained by using a S1 Titan energy dispersive portable X-ray fluorescence spectrometer (pED-XRF) from Bruker (Kennewick, Washington DC, USA) equipped with an Rh X-ray tube and X-Flash® SDD. Geochem-trace calibration was used to perform the quantitative analyses, and

Table 2: Accuracy of pED-XRF analysis evaluated through the use of CRM (soil NIM GBW07408 and limestone NCS DC60108a) reference samples. As regards NCS DC60108a, not detected Ti concentration and uncertainty of Al_2O_3 determination in the limestone sample are related to the sensitivity of the spectrometer.

Element	NIM GBW07408		NCS DC60108a	
	Certified	Measured	Certified	Measured
Al_2O_3	11.92 ± 0.15	12.06 ± 0.81	0.33 ± 0.03	0.61 ± 0.19
SiO_2	58.61 ± 0.13	52.87 ± 3.71	2.09 ± 0.06	2.76 ± 0.05
CaO	8.27 ± 0.12	8.60 ± 0.28	51.61 ± 0.15	50.31 ± 3.15
Ti	0.38 ± 0.01	0.37 ± 0.01	0.009 ± 0.001	N/D
Fe	3.13 ± 0.03	3.27 ± 0.09	0.12 ± 0.02	0.15 ± 0.01

Note. Certified and measured values of the analyzed elements. The values are expressed as weight percentages (wt.%). N/D: not detected.

Table 3: ICP-MS parameters employed for the mineral analysis.

Instrumental conditions	
Vacuum pressure (Pa)	5.8×10^{-6}
Flow of plasma gas Ar (L/min)	1.0
RF power (W)	1550
RF coupling (V)	1.80
Sampling depth (mm)	8.0
Nebulizer pump (rps)	0.3
Lens	
Extraction lens 1 (V)	0
Extraction lens 2 (V)	−200
Omega lens (V)	9.2
Omega lens deviation (V)	−120
Sample parameters	
Carrier flow (L/min)	0.35
Work mode	HMI-8
Integration parameters	
Acquisition mode	Spectrum
Per peak points	1
Replicates	3
Per replicas' readings	100
Dwell time UMA (s)	0.5–1

Table 4: Analytical features of mineral elements determination in mortar samples by ICP-MS.

Element	Mass	LOD	LOQ	R^2
La	139	0.0009	0.003	0.9994
Ce	140	0.0009	0.003	0.9993
Pr	141	0.0003	0.0010	0.9991
Nd	142	0.002	0.007	0.9994
Sm	152	0.0002	0.0007	0.9992
Eu	151	0.0005	0.0017	0.9998
Gd	158	0.004	0.015	0.9993
Tb	159	0.00011	0.0004	0.9989
Dy	162	0.0007	0.002	0.9991
Ho	165	7.4E-05	0.0002	0.9991
Er	166	0.0003	0.0011	0.9989
Tm	169	0.00017	0.0006	0.9986
Yb	172	0.0006	0.002	0.9989
Lu	175	0.00015	0.0005	0.9990
Sc	45	0.02	0.08	0.9999
Y	89	0.0013	0.004	0.9999
Ba	138	0.002	0.008	0.9992
Bi	209	0.006	0.018	0.9991
Cd	111	0.003	0.011	0.9998
Cr	52	0.4	1.3	0.9999
Co	59	0.008	0.03	0.9998
Cu	63	0.009	0.03	0.9998
Pb	207	0.12	0.4	0.9993
Li	7	0.0016	0.005	0.9996
Mn	55	0.17	0.58	0.9998
Mo	95	0.012	0.04	0.9998
Ni	60	0.009	0.03	0.9990
Sr	88	0.011	0.04	0.9996
Tl	205	0.0018	0.006	0.9988
V	51	1.2	4	0.9998
Zn	64	0.2	0.8	0.9994
Rh*	103			

Note. Mass, detection limit (LOD), quantification limit (LOQ), and R^2 of 31 elements detected in the studied samples being LOD and LOQ expressed as μg/g for all elements. *Internal standard.

S1 Sync software from Bruker was employed to measure Al_2O_3, SiO_2, CaO, Ti, and Fe. The accuracy of the measurements was verified by using the following certified reference materials: soil NIM GBW07408 and limestone NCS DC60108a (Table 2). All the reading's standard errors range between 1 and 5 wt.%, except for Al_2O_3 measured on NCS DC60108a, whose standard deviation increases up to 22 wt.% for concentration less than 0.5 wt.% probably due to the low sensitivity of the instrument for the determination of this element.

2.3. Trace Elements and REE Determination. Previously pulverized and homogenized samples of each entire mortar were prepared for the inductively coupled plasma mass spectrometry (ICP-MS) analysis. The mortars digestion method was developed by Gallello et al. [26] in order to provide reproducible and comparable results compatible with the sensitivity of the analytical method employed. The wet digestion consisted in the addition of 1.35 mL of HCl (37%) and 0.45 mL of HNO_3 (69%) to ca. 0.15 g of each

sample in glass tubes, which were heated in a boiling water bath for about 40 min. Then, the solutions were poured into plastic tubes and brought up to 25 mL with purified water. The concentration of the following elements: Ba, Bi, Cd, Cr, Co, Cu, Pb, Li, Mn, Mo, Ni, Sr, Tl, V, and Zn, REE (La, Ce, Pr, Nd, Sm, Eu, Gd, Tb, Dy, Ho, Er, Tm, Yb, and Lu), Sc, and Y were determined. Two multielement stock solutions for the ICP analysis in 5% HNO_3, containing the abovequoted elements at a concentration of 1000 mg/L, were used as stock standards for calibration. 5 mL volumetric flasks were used in adding the corresponding volume of standard solutions 0.15 mL of HNO_3, 0.45 mL of HCl, and the water necessary to reach the final volume. The concentration of trace elements ranges from 1 μg/L to 600 μg/L except for REE, Y, and Sc that ranges from 1 μg/L to 100 μg/L. The measurement accuracy was verified by using the certified reference materials soil NIM GBW07408 and limestone NCS DC60108a. As the internal standard, 50 μL of a 1000 mg/L Rh solution was added to each sample and to each calibration standard. The analyses were performed through an Agilent 7900 inductively coupled plasma mass spectrometer. The measurement conditions that are shown in Table 3 shows the

ICP-MS parameters employed for the analyses, and Table 4 shows the main analytical features obtained for the measured mass of each considered isotope, including the instrumental detection and quantification limits (LOD and LOQ), and the coefficient of determination (R^2) of the corresponding calibration lines.

2.4. Statistical Data Processing. The PCA models were built by using data obtained from a total of forty-two analysed samples, and the set of data obtained from samples dated to the Roman Imperial period and the Islamic occupation phase obtained previously by Gallello et al. [26]. Major and minor elements and trace elements including REE were employed as variables. This technique was used to explore large geochemical datasets by reducing the number of variables and providing a deep insight into the structure of the variance of the dataset. Data were processed through mean center and autoscale prior to modelling, and the obtained model was cross validated through leave-one-out method.

The PLS-DA model was built employing twenty-two samples as a calibration set: nine samples from the Circus (Los Huertos Street excavation) and samples studied by Gallello et al. [26] including five from the Roman Theatre, TR, built during the Roman Imperial Period and eight samples from Islamic masonries (two samples from the Imperial Forum tabernae, TFI, four samples from the first part of the Islamic Wall, MI, and two from the Torre Central Estudiantes, TCE). Five of these samples (C07, C08, C10b, and two TR samples) were randomly selected as an internal validation set to test the model (data not shown). Sixteen variables were employed (REE, Y, and Sc). Finally, thirty-seven mortar samples dated back to Roman Imperial period, Islamic occupation phase, and also some uncertain samples were included as the test set to predict their class. Data were preprocessed employing mean centering and autoscale, and "leave one out" cross validation method was employed for the evaluation of results. Data analysis was carried out using the PLS Toolbox 6.5 for Eigenvector Research Inc., (Wenatchee, WA, USA) running in Matlab R2014b from MathWorks Inc., (Natick, MA, USA).

3. Results and Discussion

3.1. Geochemical Results. The analytical results of major and minor elements as well as trace elements and REE data are reported in the Supplementary Materials (Annexes 1 and 2).

Lime mortar samples from the Railroad Station and from the Circus area buildings have comparable amounts of Al_2O_3 and SiO_2 which range from 0.44 to 1.05 wt.% and from 11.30 to 26.97 wt.%, respectively, except for samples RS25A (Al_2O_3: 3.02 wt.%; SiO_2: 34.86 wt.%) and RS11C (Al_2O_3: 5.17 wt.%; SiO_2: 36.72 wt.%), which are both from the Railroad Station and show particularly high values of these two chemical components. On the contrary, Railroad Station's samples have lower concentration of CaO (30 ± 4 wt.%) and higher one of Fe (1.3 ± 0.1 wt.%) and Ti (0.12 ± 0.01 wt.%) than Los Huertos Street mortars (CaO: 40 ± 3 wt.%; Fe: 0.99 ± 0.14 wt.%;

TABLE 5: Pearson correlation coefficient (ρ) between $\sum$REE and each measured element for the three groups of mortar.

Element	Railroad Station Lime mortars	Los Huertos Street Lime mortars	Earth mortars
Al_2O_3	−0.21	**0.57**	0.61
SiO_2	−0.45	0.21	−0.23
CaO	−0.08	**−0.43**	−0.7
Fe	0.18	0.3	**0.76**
Ti	−0.1	0.28	**0.81**
^{209}Bi	−0.21	0.23	**0.95**
^{207}Pb	0.41	0.03	−0.09
^{205}Tl	−0.42	**0.5**	**0.97**
^{138}Ba	0.15	0.06	**0.85**
^{111}Cd	0.01	0.02	0.58
^{95}Mo	−0.04	−0.29	**0.95**
^{89}Y	**0.59**	0.25	0.6
^{88}Sr	0	**−0.41**	**0.76**
^{64}Zn	0.37	−0.24	**0.93**
^{63}Cu	−0.19	−0.22	**0.9**
^{60}Ni	0.32	0.15	**0.89**
^{59}Co	**0.51**	**0.51**	**0.96**
^{55}Mn	0.23	−0.06	**0.94**
^{52}Cr	0.48	**0.55**	**0.94**
^{51}V	**0.56**	0.24	**0.88**
^{45}Sc	0.49	**0.75**	**0.71**
^{7}Li	0.19	0.35	**0.82**

Note. Statistically significant values of ρ are given in bold ($p = 0.05$).

Ti: 0.08 ± 0.02 wt.%). The samples of earth mortars from Room 1 (R1a, R1b, and R1c) and Room 2 (R2a, R2b, and R2d) show the lowest values of CaO (15.3 ± 1.1 wt.%) and the highest ones of Al_2O_3 (10.9 ± 1.1 wt.%), SiO_2 (37.8 ± 1.7 wt.%), Fe (2.4 ± 0.3 wt.%), and Ti (0.25 ± 0.02 wt.%).

The lime mortar samples from Los Huertos Street and from the Railroad Station have comparable concentrations in almost all the measured trace elements. In particular, it is worth noticing that the two groups of samples show similar REE total amounts ($\sum$REE) (Los Huertos Street: 20 ± 4 μg/g; Railroad Station: 20 ± 2 μg/g) and Sc concentrations (Los Huertos Street: 1.1 ± 0.3 μg/g; Railroad Station: 1.1 ± 0.1 μg/g), while samples from Los Huertos Street have a slightly higher concentration of Y than the ones from the Railroad Station excavation (4.1 ± 0.8 μg/g and 3.5 ± 0.4 μg/g resp.). Concerning the earth mortars from Room 1 and Room 2, they have comparable contents of REE, Y, and Sc. REE total amounts go from 37 μg/g to 53 μg/g, and Y and Sc range from 5 μg/g to 10 μg/g and from 2 μg/g to 3 μg/g, respectively.

To give a deep insight into the mechanisms that influence the amount of REE in the mortar samples, it is interesting to look at the correlation among the REE and analysed elements for each group of mortars. Table 5 shows the Pearson correlation coefficient (ρ) considering as variables REE total amounts and the indicated elements for each group of mortars considered separately (see Supplementary Materials Annex 2). Only statistically significant data were taken into account given $p = 0.05$. REE concentration of Los Huertos Street lime mortar samples show positive correlations, as well as for Sc ($\rho = 0.75$), which has a chemical behaviour similar to lanthanides, with Al_2O_3 ($\rho = 0.57$), Tl ($\rho = 0.50$),
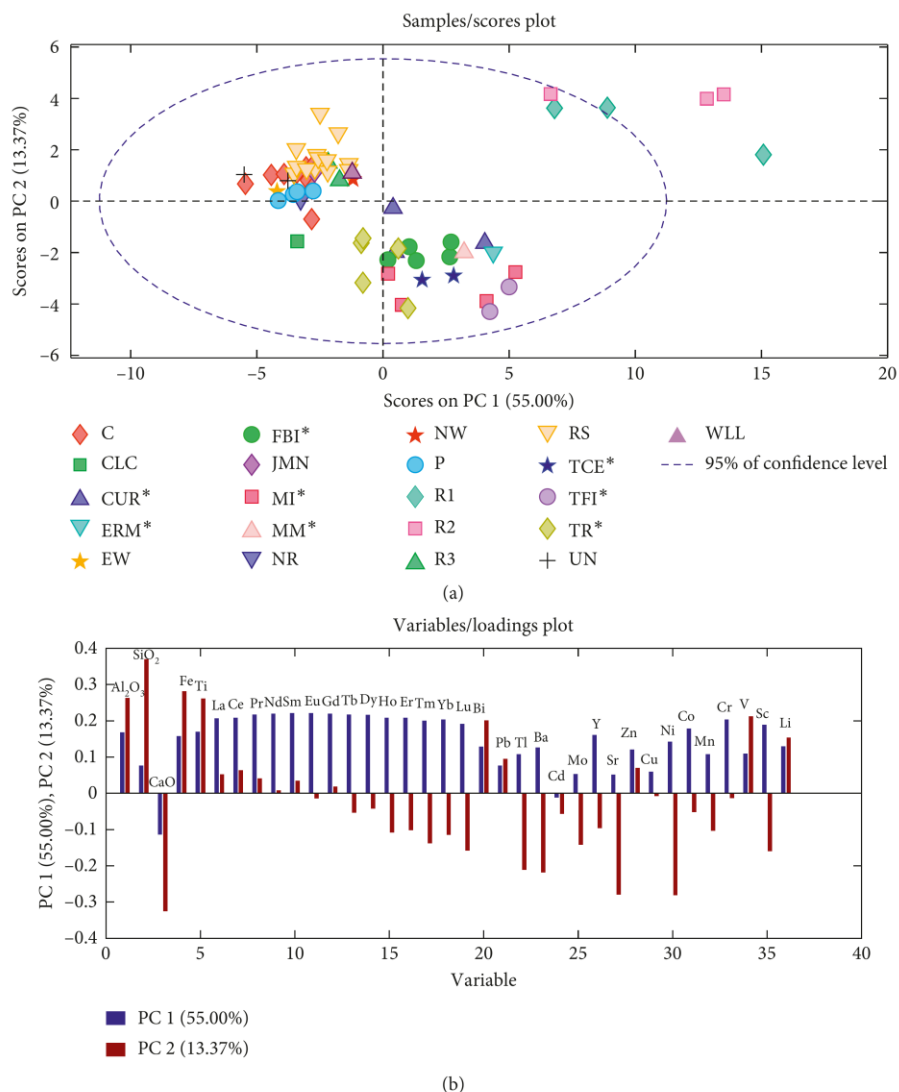
(a)

(b)

FIGURE 2: PCA study employing all the measured element concentrations. Scores (a) and loadings (b) plot of PC1 and PC2. The samples marked with a star (*) are related to Sagunto Castle buildings [17]. ERM = Hermitage; FBI = Imperial Basilica; FRW = Wester Republican Forum; MI = Islamic Wall (1st section); MII = Islamic Wall (2nd section); MM = Modern Wall; SMR = Republican Wall; TCE = Torre Central Estudiantes; TFI = Imperial Forum tabernae; TMP = Republican Diana's Temple; TR = Roman Theatre.

Co ($\rho = 0.51$), and Cr ($\rho = 0.55$) and negative correlations with Ca ($\rho = -0.43$) and Sr ($\rho = -0.41$), which suggests that the major contribution to the amount of REE comes from limestone clay impurities or from aluminosilicates and silicate rock clasts present in the aggregate fraction [27]. Concerning the lime mortar samples from the Railroad Station excavation, significant correlations were not detected among major elements and REE. However, significant positive correlations were found with Y ($\rho = 0.59$), Co ($\rho = 0.51$) and V ($\rho = 0.56$). As regards earth mortars (R1 and R2) from Los Huertos Street, in this case, the REE total amount has high positive correlations with most of the trace elements (for Bi, Tl, Ba, Mo, Sr, Zn, Cu, Ni, Co, Mn, Cr, V, Sc, and Li, ρ goes from 0.71 to 0.97) and, among the major

elements, with Fe ($\rho = 0.76$) and Ti ($\rho = 0.81$), suggesting that the major contribution in lanthanides comes probably from clay fraction, other silicate minerals, and silicate rock clasts.

3.2. Chemometrics for Construction Phase Discrimination. The identification of the construction phases of the buildings was conducted by comparing the mortars from the Railroad Station and Los Huertos Street to the ones from Sagunto Castle published by Gallello et al. [26], and whose construction periods were retraced in the same work. In particular, this previous study was focused on REE concentrations due to their proved effectiveness in
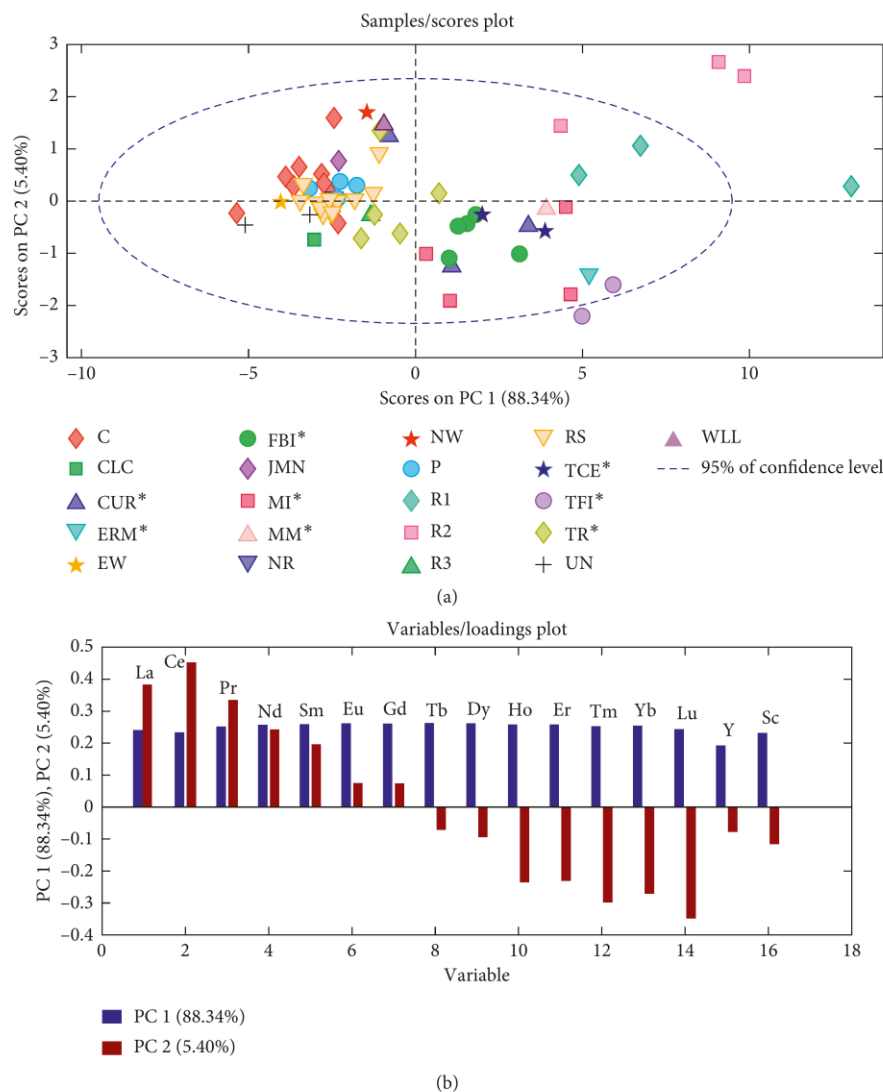
Figure 3: PCA study employing only REE, Y, and Sc concentrations. Scores (a) and loadings (b) plot of PC1 and PC2. The legend for Sagunto Castle samples' classes (*) is indicated in Figure 2.

archaeometric studies about provenance and raw materials of lithic and lithoid archaeological artifacts [28–30].

To compare the samples from the excavations to the Imperial and Islamic mortars from Sagunto Castle [26], the principal component analysis (PCA) was carried using all variables (i.e., elements) (Figure 2). Figure 2(b) shows the contribution of the variables in PC1 (55.00% of samples' variance) and PC2 (13.37% of samples' variance). Figure 2(a) shows the position of each sample in a diagram where the x-axis corresponds to PC1 coordinates and y-axis to PC2. Most of the samples of Los Huertos Street and all Railroad Station are grouped together in the left side of the plot, while the samples dated back both to Imperial Roman period and Islamic period from de Castle are grouped in the right part of the graph. The samples of earth mortars from Room 1 (R1a, R1b, and R1c) and Room 2 (R2a, R2b, and R2d) of Los Huertos Street are plotted in

the upper right side of the diagram, at the limit of the confidence interval or out of it.

In Figure 3(b), the contribution of the REE employed as variables is shown. PC1 explains 88.34% of the data variance and PC2 explains 5.40%. Lime mortar samples from Los Huertos Street and all Railroad Station excavations are grouped with the mortars from the Roman Theatre (TR) (Figure 3(a)), suggesting that the dating to the Roman Imperial period was also confirmed by the archaeological data while the earth mortar samples are plotted in PC1 and PC2 positive directions. Finally, a separation between mortars from Imperial Period (PC1 negative direction), and mortars from the Islamic Period, located in the left lower area of PC can be appreciated.

Since the discrimination of lime mortars from Roman Imperial and Islamic buildings seems to be the most
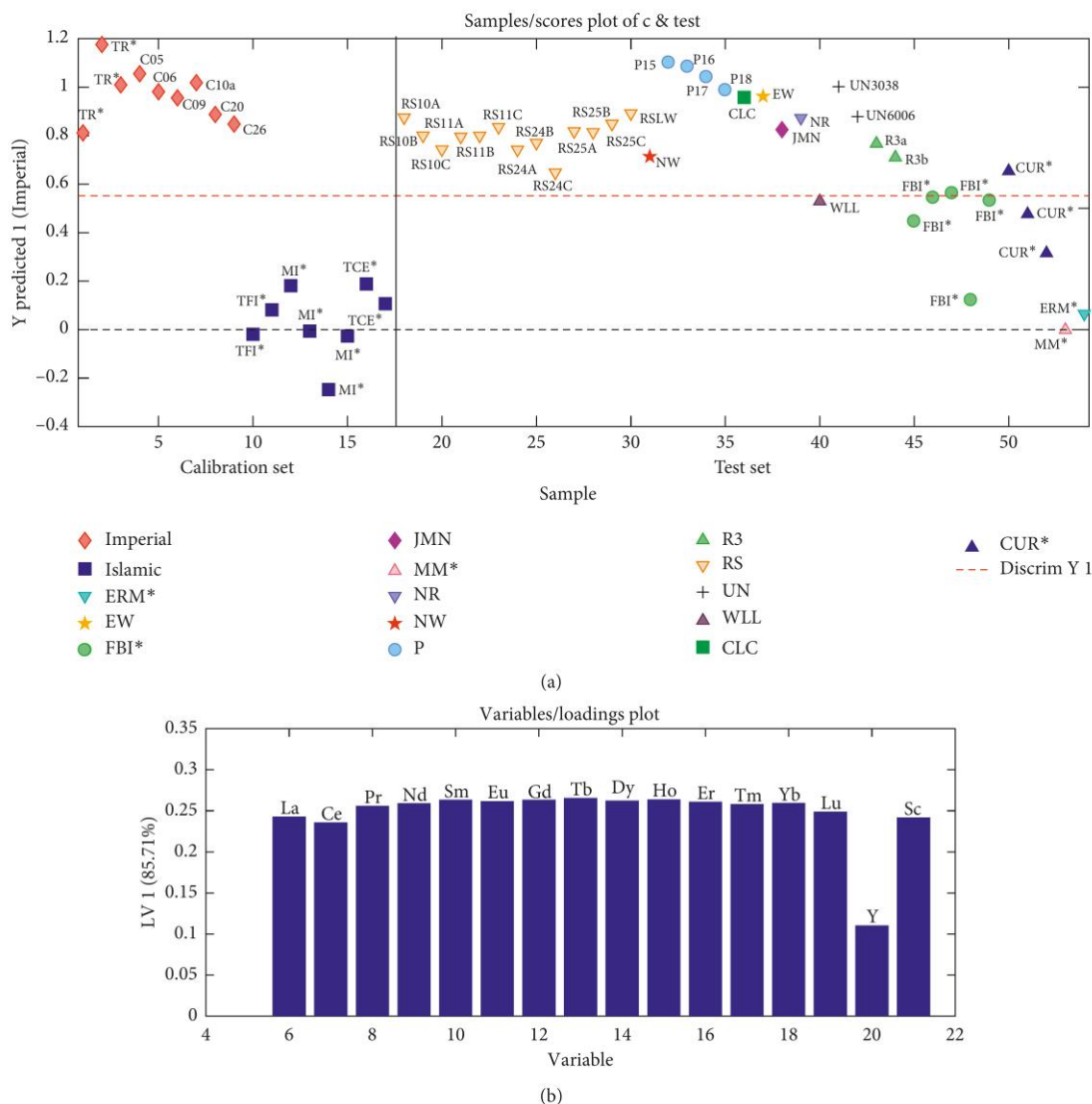
FIGURE 4: PLS-DA results. (a) Calibration set and predicted class membership of the other samples. (b) VIP scores of the PLS-DA model. The legend for Sagunto Castle classes (*) is indicated in Figure 2.

problematic issue, the principal least squares discriminant analysis (PLS-DA) was employed to build a statistical model to classify uncertain samples. The calibration set and validation set were established by using samples from buildings and masonries that were previously classified by Gallello et al. [26] and by archaeological data as Roman Imperial (C and TR) or as Islamic (MII, TFI, and TCE) (Figure 4(a)). Figure 4(b) shows the contribution of each variable to the model. As it can be seen, the model clearly separates between mortars of the two different construction phases. Subsequently, the model was applied to a test set composed of uncertain Roman Imperial period or Islamic mortars (Figure 4(a)). The PLS-DA results confirmed that all the mortars from Los Huertos Street and Railroad Station are

classified as Roman Imperial period materials except for sample WLL that has been classified as Islamic, which is coherent with the archaeological data that confirm the occupation of the area during the Islamic phase. As observed, on the contrary of Los Huertos Street, in Railroad Station samples, major elements are not correlated with REE (Table 5), and this could suggest that the mortars were made in a different way or this is an indicator of recycling building materials, and, according to the archaeological wall stratigraphy interpretation, the Railroad Station structures could be dated after the Imperial period. Thus, maybe they were built during the Late Roman Age. On the contrary, one mortar sample from the Basilica of the Imperial Forum (FBI SC) and one mortar from the Curia testify the presence of

both Roman Imperial masonries and Islamic reworks in Roman buildings due to the heavy reemployment of the Imperial Forum area during the Islamic occupation [26].

The use of REE, Y, and Sc as variables has shown their high effectiveness in the discrimination of different kinds of mortars to retrace the construction history of archaeological sites and monuments. The comparison among mortars coming from different archaeological excavations and monuments of the same geographical area seems to be a very viable method to solve chronological issues related to the construction phases of both structures unearthed during archaeological excavations and historical complexes.

4. Conclusion

The study of the historic mortars from two archaeological excavations (i.e., Los Huertos Street and Railroad Station) located in the city of Sagunto permitted us to solve issues that had remained unanswered in the previous studies on these building materials.

The use of multivariate statistics employing REE as variables allowed us to classify the lime mortars belonging to the Imperial Roman period, in line with the archaeological data; however, the case of the Railroad Station structure needs deeper studies to confirm the chronology as Imperial Roman or Late Roman Ages. Also, it was possible to establish the chronological phase of some masonries of Sagunto Castle whose period of construction was uncertain and that can be attributed to the phase of the Islamic occupation or to the Roman Imperial period. The PLS-DA model was helpful to discriminate among mortars of uncertain attribution and that can be useful for possible future studies in Sagunto area.

The correlation among REE and major/minor and trace elements shows that the mechanisms that allowed REE to be discriminating parameters between Sagunto mortars belonging to different periods are related to chemical weathering processes involving limestone clay impurities, aluminosilicates, and silicate rock clasts present in the aggregate fraction. Therefore, further works need to be developed focusing the understanding of the chemical processes that are influencing the REE distributions.

Summarizing, the present study has confirmed the effectiveness of REE data in building materials as markers of different construction phases and has proved the usefulness of the application of the ancient mortar analysis on a geographical scale wider than a single archaeological excavation or monuments.

Data Availability

The data used to support the findings of this study are included within the article and supplementary materials.

Conflicts of Interest

The authors declare that there are no conflicts of interest with any institution or funding body.

Supplementary Materials

Annex 1: concentrations of the measured major and minor elements obtained by pED-XRF. Annex 2: trace elements and REE results obtained by ICP-MS. (*Supplementary Materials*)

References

[1] A. Moropoulou, A. Bakolas, and K. Bisbikou, "Investigation of the technology of historic mortars," *Journal of Cultural Heritage*, vol. 1, no. 1, pp. 45–58, 2000.

[2] M. Theodoridou, I. Ioannou, and M. Philokyprou, "New evidence of early use of artificial pozzolanic material in mortars," *Journal of Archaeological Science*, vol. 40, no. 8, pp. 3263–3269, 2013.

[3] M. Franzini, L. Leoni, M. Lezzerini, and F. Sartori, "The mortar of the "Leaning Tower" of Pisa: the product of a medieval technique for preparing high-strength mortars," *European Journal of Mineralogy*, vol. 12, no. 6, pp. 1151–1163, 2000.

[4] F. Marra, A. Danti, and M. Gaeta, "The volcanic aggregate of ancient Roman mortars from the Capitoline Hill: petrographic criteria for identification of Rome's "pozzolans" and historical implications," *Journal of Volcanology and Geothermal Research*, vol. 308, pp. 113–126, 2015.

[5] M. Lezzerini, M. Ramacciotti, F. Cantini et al., "Archaeometric study of natural hydraulic mortars: the case of the Late Roman Villa dell'Oratorio (Florence, Italy)," *Archaeological and Anthropological Science*, vol. 9, no. 4, pp. 603–615, 2017.

[6] M. Lezzerini, S. Pagnotta, S. Raneri et al., "Examining the reactivity of volcanic ash in ancient mortars by using a micro-chemical approach," *Mediterranean Archaeology and Archaeometry*, In press.

[7] S. Columbu and A. M. Garau, "Mineralogical, petrographic and chemical analysis of geomaterials used in the mortars of Roman Nora theatre (south Sardinia, Italy)," *Italian Journal of Geosciences*, vol. 136, no. 2, pp. 238–262, 2017.

[8] S. Columbu, "Petrographic and geochemical investigations on the volcanic rocks used in the Punic-Roman archaeological site of Nora (Sardinia, Italy)," *Earth Environmental Sciences*, In press.

[9] J. Elsen, A. Brutsaert, M. Deckers, and R. Brulet, "Microscopical study of ancient mortars from Tournai (Belgium),"

Materials Characterization, vol. 53, no. 2–4, pp. 289–294, 2004.

[10] C. Borges, A. Santos Silva, and R. Veiga, "Durability of ancient lime mortars in humid environment," *Construction and Building Materials*, vol. 66, pp. 606–620, 2014.

[11] M. Lezzerini, S. Legnaioli, G. Lorenzetti, V. Palleschi, and M. Tamponi, "Characterization of historical mortars from the bell tower of St. Nicholas church (Pisa, Italy)," *Construction and Building Materials*, vol. 69, pp. 203–214, 2014.

[12] D. Miriello, F. Antonelli, C. Apollaro et al., "New data about the ancient mortars from the archaeological site of Kyme (Turkey): compositional characterization," *Minerals Engineering*, vol. 84, pp. 497–517, 2015.

[13] S. Columbu, F. Sitzia, and G. Ennas, "The ancient pozzolanic mortars and concretes of Heliocaminus baths in Hadrian's Villa (Tivoli, Italy)," *Archaeological and Anthropological Sciences*, vol. 9, no. 4, pp. 523–553, 2017.

[14] F. Carò, M. P. Riccardi, and M. T. Mazzilli Savini, "Characterization of plasters and mortars as a tool in archaeological studies: the case of Lardirago Castle in Pavia, Northern Italy," *Archaeometry*, vol. 50, no. 1, pp. 85–100, 2008.

[15] E. Arizio, R. Piazza, W. R. L. Cairns, L. Apollonia, and A. Botteon, "Statistical analysis on ancient mortars: a case study of the Balivi Tower in Aosta (Italy)," *Construction and Building Materials*, vol. 47, pp. 1309–1316, 2013.

[16] C. Corti, L. Ramazzi, R. Bugini et al., "Thermal analysis and archaeological chronology: the ancient mortars of the site of Baradello (Como, Italy)," *Thermochimica Acta*, vol. 572, pp. 71–84, 2013.

[17] F. Marra, E. D'Ambrosio, M. Gaeta, and M. Mattei, "Petrochemical identification and insights on chronological employment of the volcanic aggregates used in ancient Roman mortars," *Archaeometry*, vol. 58, no. 2, pp. 177–200, 2016.

[18] A. M. Conte, L. Corda, D. Esposito, and E. Giorgi, "Characterization of mortars from the medieval Abbey of Cerrate (southern Italy)," *Journal of Archaeological Science: Reports*, vol. 12, pp. 463–479, 2017.

[19] S. Columbu, "Provenance and alteration of pyroclastic rocks from the Romanesque Churches of Logudoro (north Sardinia, Italy) using a petrographic and geochemical statistical approach," *Applied Physics A*, vol. 123, p. 165, 2017.

[20] S. Columbu, F. Sitzia, and G. Verdiani, "Contribution of petrophysical analysis and 3D digital survey in the archaeometric investigations of the Emperor Hadrian's Baths (Tivoli, Italy)," *Rendiconti Lincei*, vol. 26, no. 4, pp. 455–474, 2015.

[21] I. Papayianni and M. Stefanidou, "Durability aspects of ancient mortars of the archaeological site of Olynthos," *Journal of Cultural Heritage*, vol. 8, no. 2, pp. 193–196, 2007.

[22] I. Papayianni, V. Pachta, and M. Stefanidou, "Analysis of ancient mortars and design of compatible repair mortars: the case study of Odeion of the archaeological site of Dion," *Construction and Building Materials*, vol. 40, pp. 84–92, 2013.

[23] M. Lezzerini, F. Antonelli, S. Columbu et al., "The documentation and conservation of the cultural heritage: 3D laser scanning and GIS techniques for thematic mapping of the stonework of the façade of St. Nicholas Church (Pisa, Italy)," *International Journal of Architectural Heritage: Conservation, Analysis, and Restoration*, vol. 10, no. 1, pp. 9–19, 2016.

[24] S. Columbu, M. Palomba, F. Sitzia, and M. R. Murgia, "Geochemical and mineral-petrographic studies of stones and mortars from the Romanesque Saccargia Basilica (Sardinia, Italy) to define their origin and alteration," *Italian Journal of Geosciences*, vol. 137, no. 3, pp. 1–27, 2018.

[25] P. P. Ripollés, *Opulentissima Saguntum*, Bancaja, Sagunto, Spain, 2004.

[26] G. Gallello, M. Ramacciotti, M. Lezzerini et al., "Indirect chronology method employing rare earth elements to identify Sagunto Castle mortar construction periods," *Microchemical Journal*, vol. 132, pp. 251–261, 2017.

[27] H. R. Rollins, *Using Geochemical Data: Evaluation, Presentation, Interpretation*, Pearson Education Limited, London, UK, 1993.

[28] G. Gallello, T. Orozco, A. Pastor, M. de la Guardia, and J. Bernabeu, "Regional provenance of dolerite prehistoric objects through mineral analysis," *Microchemical Journal*, vol. 124, pp. 167–174, 2016.

[29] A. Hein, P. M. Day, P. S. Quinn, and V. Kilikoglou, "The geochemical diversity of Neogene clay deposits in Crete and its implications for provenance studies of Minoan pottery," *Archaeometry*, vol. 46, no. 3, pp. 357–384, 2004.

[30] S. Cagno, M. Mendera, T. Jeffries, and K. Janssens, "Raw materials for post-medieval Tuscan glassmaking: new insight from LA-ICP-MS analyses," *Journal of Archaeological Science*, vol. 37, no. 12, pp. 3030–3036, 2010.

Annex 1

Sample	Al$_2$O$_3$	SiO$_2$	CaO	Fe	Ti
C05	0.66	18.74	40.73	0.90	0.07
C06	0.75	21.95	38.49	1.02	0.08
C07	0.85	25.95	38.46	1.11	0.08
C08	0.74	25.41	37.77	1.24	0.10
C09	0.67	23.56	34.43	1.07	0.10
C10a	0.67	26.97	37.44	1.03	0.09
C10b	0.73	14.68	42.41	0.89	0.07
C20	0.83	25.06	38.59	1.02	0.09
C26	0.73	14.81	42.84	0.96	0.07
CLC	0.76	11.30	46.29	0.85	0.06
R1a	10.07	36.99	16.48	2.21	0.23
R1b	11.24	41.01	14.85	2.45	0.24
R1c	10.26	36.27	15.90	2.35	0.25
R2a	12.53	38.63	13.98	2.86	0.29
R2b	11.29	36.47	14.30	2.73	0.27
R2d	9.71	37.59	16.58	2.22	0.23
R3a	0.95	21.31	40.84	1.25	0.11
R3b	0.77	19.27	34.73	1.12	0.08
JMN	0.92	22.42	37.22	1.04	0.08
EM	0.83	18.31	42.13	1.01	0.08
NW	1.01	22.82	37.43	1.11	0.09
NR	0.61	14.58	40.95	0.85	0.06
P15	0.65	17.19	45.35	0.81	0.05
P16	0.58	19.19	42.25	0.78	0.05
P17	0.73	18.64	42.83	0.87	0.06
P18	0.56	18.70	42.71	0.79	0.06
UN1	0.72	22.31	41.76	0.94	0.08
UN2	0.82	23.73	39.12	1.06	0.09
WLL	1.05	21.56	34.87	1.12	0.09
RS10A	0.58	24.37	32.81	1.12	0.11
RS10B	0.65	23.11	33.23	1.41	0.12
RS10C	0.77	24.57	31.75	1.44	0.13
RS11A	0.58	22.47	33.90	1.28	0.11
RS11B	0.62	25.42	34.42	1.27	0.11
RS11C	5.07	36.72	18.97	1.44	0.13
RS24A	0.64	22.88	34.14	1.30	0.11
RS24B	0.70	21.65	32.39	1.37	0.11
RS24C	0.44	17.55	27.34	1.30	0.11
RS25A	3.02	34.86	26.75	1.50	0.14
RS25B	0.62	23.38	31.42	1.51	0.12
RS25C	0.72	20.25	33.79	1.28	0.11
RSLW	0.57	25.88	28.79	1.19	0.10

Note: Concentration of elements expressed as wt%.

Annex 2

Sample	La	Ce	Pr	Nd	Sm	Eu	Gd	Tb	Dy	Ho	Er	Tm	Yb	Lu	∑REE	Bi	Pb	Tl	Ba	Cd	Mo	Y	Sr	Zn	Cu	Ni	Co	Mn	Cr	V	Sc	Li
C05	3	5	0.7	3	0.6	0.14	0.6	0.08	0.4	0.08	0.2	0.03	0.2	0.02	14	0.06	19	0.03	57	0.2	0.3	3	302	18	9	6	3	198	5	8	0.8	3
C06	4	6	0.9	4	0.8	0.2	0.7	0.10	0.5	0.09	0.2	0.03	0.2	0.03	19	0.03	3	0.02	50	0.06	0.2	3	204	5	6	6	3	215	5	7	0.9	3
C07	5	7	1.0	5	0.9	0.2	0.8	0.12	0.6	0.11	0.3	0.04	0.2	0.03	21	0.04	7	0.02	37	0.2	0.2	4	192	5	5	6	4	205	5	6	1.0	4
C08	5	7	1.0	4	0.9	0.2	0.7	0.10	0.5	0.09	0.3	0.03	0.2	0.03	20	0.04	6	0.03	77	0.11	0.4	4	200	19	8	6	5	571	5	7	1.0	4
C09	5	6	1.0	5	0.9	0.2	0.8	0.12	0.6	0.11	0.3	0.04	0.2	0.03	20	0.04	7	0.02	43	0.11	0.3	4	204	11	14	7	4	181	6	12	1.1	4
C10a	4	6	0.9	4	0.8	0.2	0.7	0.11	0.5	0.10	0.3	0.03	0.2	0.03	18	0.03	11	0.02	43	0.6	0.4	4	229	16	11	7	4	222	5	9	1.0	4
C10b	5	6	1.0	4	0.9	0.2	0.8	0.12	0.6	0.11	0.3	0.04	0.2	0.03	20	0.03	5	0.010	76	0.13	0.4	5	258	4	6	11	4	533	5	11	1.1	3
C20	6	9	1.2	5	1.0	0.2	0.9	0.11	0.6	0.10	0.3	0.03	0.2	0.03	25	0.05	25	0.02	71	0.06	0.2	4	177	9	8	7	3	217	5	10	1.1	5
C26	5	6	1.0	4	0.9	0.2	0.9	0.13	0.7	0.13	0.3	0.04	0.3	0.04	19	0.04	32	0.007	45	0.02	0.2	4	205	2	6	15	3	166	6	29	0.9	3
CLC	4	5	0.8	4	0.8	0.2	0.8	0.11	0.6	0.12	0.3	0.04	0.2	0.04	17	0.02	30	0.02	80	0.10	0.3	4	577	20	19	10	3	374	4	1	1.0	6
EW	4	5	0.8	4	0.8	0.2	0.7	0.10	0.5	0.10	0.3	0.03	0.2	0.03	17	0.04	46	0.02	63	0.11	0.3	3	317	14	15	10	3	209	5	2	1.0	7
JMN	5	8	1.1	5	1.0	0.2	0.9	0.12	0.6	0.11	0.3	0.04	0.2	0.03	23	0.10	11	0.02	50	0.10	0.13	4	195	13	13	10	3	176	5	2	1.2	8
NR	5	7	1.0	4	0.9	0.2	0.8	0.12	0.6	0.12	0.3	0.04	0.2	0.03	21	0.03	42	0.02	43	0.07	0.2	4	221	12	7	10	3	181	5	4	1.1	6
NW	6	11	1.3	5	1.1	0.2	0.9	0.12	0.6	0.10	0.3	0.04	0.2	0.03	28	0.07	9	0.05	70	0.4	0.2	4	172	11	8	9	7	231	9	13	1.8	6
P15	5	6	0.9	4	0.8	0.2	0.7	0.10	0.6	0.10	0.3	0.04	0.2	0.03	19	0.03	8	0.015	42	0.2	0.2	5	223	7	5	7	3	288	4	9	0.9	3
P16	6	7	1.0	5	0.9	0.2	0.9	0.12	0.6	0.12	0.3	0.04	0.2	0.03	21	0.03	5	0.015	29	0.3	0.10	6	200	3	4	7	3	173	4	9	1.0	4
P17	6	7	1.1	5	1.0	0.2	0.9	0.13	0.7	0.12	0.3	0.04	0.2	0.03	22	0.03	20	0.012	33	0.11	0.2	6	195	5	5	8	4	217	4	14	1.1	4
P18	5	6	1.0	4	0.9	0.2	0.8	0.12	0.6	0.12	0.3	0.04	0.2	0.04	21	0.03	15	0.010	33	0.08	0.2	5	248	9	4	8	3	175	4	13	1.1	3
R1a	7	13	1.8	8	1.8	0.4	1.7	0.23	1.2	0.20	0.5	0.07	0.4	0.06	37	0.11	74	0.06	65	0.08	0.4	6	232	26	25	16	6	296	12	18	2	12
R1b	9	16	2	9	2	0.4	1.8	0.25	1.3	0.23	0.6	0.08	0.5	0.07	43	0.14	8	0.08	79	0.06	0.5	6	230	27	28	17	6	375	14	21	3	14
R1c	11	18	3	12	3	0.6	2	0.34	1.8	0.31	0.9	0.11	0.6	0.09	53	0.2	5	0.10	89	0.13	0.7	10	343	36	33	23	8	439	17	31	3	15
R2a	11	20	3	11	2	0.5	2	0.29	1.5	0.25	0.7	0.08	0.5	0.07	53	0.2	103	0.11	110	0.07	0.6	7	273	43	40	19	9	454	18	25	3	20
R2b	11	21	2	11	2	0.5	2	0.28	1.4	0.24	0.6	0.08	0.5	0.07	53	0.2	67	0.11	126	0.08	0.6	6	257	43	34	20	9	398	20	28	2	21
R2d	8	14	1.8	8	1.8	0.4	1.6	0.22	1.1	0.19	0.5	0.06	0.4	0.05	39	0.15	78	0.07	71	0.05	0.4	5	221	21	23	15	6	323	13	22	2	13
R3a	5	7	1.1	5	1.0	0.2	1.0	0.14	0.7	0.14	0.4	0.05	0.3	0.04	22	0.04	27	0.010	42	0.05	0.3	4	192	7	5	12	4	172	7	12	1.5	8
R3b	4	8	1.0	4	0.9	0.2	0.8	0.12	0.6	0.11	0.3	0.04	0.2	0.04	21	0.08	152	0.03	48	0.003	0.4	3	181	8	10	10	4	167	7	14	1.6	6
UN1	3	4	0.7	3	0.7	0.2	0.6	0.09	0.5	0.09	0.2	0.03	0.2	0.03	13	0.06	6	0.012	41	0.02	0.2	3	197	6	5	9	3	149	5	5	1.0	5
UN2	4	6	0.9	4	0.8	0.2	0.8	0.11	0.6	0.11	0.3	0.04	0.2	0.03	18	0.02	8	0.011	42	0.07	0.1	4	201	4	6	10	3	210	5	5	1.1	5
WL	6	11	1.3	6	1.1	0.3	0.9	0.13	0.6	0.11	0.3	0.04	0.3	0.04	29	0.05	26	0.04	51	0.03	0.2	3	194	6	5	10	4	175	8	9	1.7	8
RS10A	4	6	0.9	4	0.9	0.2	0.8	0.11	0.6	0.10	0.3	0.03	0.2	0.03	18	0.08	8	0.09	63	0.03	0.4	3	259	12	7	6	3	180	5	4	1.1	4
RS10B	4	6	0.9	4	1.0	0.2	0.9	0.13	0.7	0.12	0.3	0.04	0.2	0.03	19	0.11	10	0.08	57	0.11	0.4	3	202	12	16	6	3	175	5	3	1.0	3
RS10C	4	7	1.0	5	1.0	0.2	1.0	0.13	0.7	0.12	0.3	0.04	0.2	0.04	20	0.13	13	0.07	50	0.08	0.4	3	167	10	6	6	2	158	4	2	0.9	3
RS11A	4	6	0.9	4	1.0	0.2	0.9	0.12	0.6	0.11	0.3	0.04	0.2	0.03	19	0.09	10	0.06	49	0.04	0.4	3	253	8	5	5	2	167	4	3	0.8	3
RS11B	4	6	0.9	4	1.0	0.2	0.9	0.12	0.7	0.12	0.3	0.04	0.2	0.04	19	0.10	11	0.05	63	0.04	0.4	3	221	11	8	6	3	191	4	3	0.9	3
RS11C	4	6	0.9	4	0.9	0.2	0.9	0.12	0.6	0.11	0.3	0.04	0.2	0.03	19	0.12	10	0.04	47	0.05	0.3	3	143	7	4	6	3	184	4	4	1.0	3
RS24A	5	8	1.1	5	1.0	0.2	1.0	0.13	0.7	0.13	0.3	0.04	0.3	0.04	22	0.08	13	0.03	57	0.05	0.4	4	207	10	5	6	3	238	5	6	1.0	4
RS24B	5	7	1.1	5	1.1	0.2	1.0	0.14	0.7	0.13	0.3	0.04	0.3	0.04	23	0.09	78	0.04	47	0.05	0.5	4	225	15	6	7	3	238	6	7	1.1	4
RS24C	6	9	1.3	6	1.1	0.2	1.0	0.13	0.7	0.12	0.3	0.04	0.3	0.04	26	0.08	13	0.03	62	0.05	0.4	4	203	13	6	8	3	197	6	8	1.3	4
RS25A	4	7	1.0	4	1.0	0.2	0.9	0.13	0.7	0.12	0.3	0.04	0.2	0.03	20	0.09	16	0.03	48	0.06	0.5	4	255	18	7	8	3	231	7	7	1.2	5
RS25B	4	7	1.0	4	0.9	0.2	0.9	0.12	0.6	0.11	0.3	0.04	0.2	0.03	20	0.07	11	0.02	42	0.06	0.4	4	199	10	6	7	3	284	7	8	1.2	5
RS25C	4	6	1.0	4	0.9	0.2	0.9	0.12	0.7	0.12	0.3	0.04	0.2	0.04	20	0.2	10	0.04	54	0.06	0.4	4	224	12	6	9	3	226	6	7	1.2	5
RSLW	4	7	0.9	4	0.9	0.2	0.8	0.11	0.6	0.10	0.3	0.03	0.2	0.03	19	0.07	13	0.03	42	0.04	0.3	3	138	10	5	6	3	227	6	7	1.2	6

Note: Concentrations of elements in µg/g. ∑ REEs: Total sum of rare earth elements (REEs).

Anexo D

Ramacciotti et al. (2019b). Chemical and mineralogical analyses on stones from Sagunto Castle (Spain)

Chemical and mineralogical analyses on stones from Sagunto Castle (Spain)

Mirco Ramacciotti[a,b], Sonia Rubio[b], Gianni Gallello[b,c,*], Marco Lezzerini[d,e], Simona Raneri[d], Emilia Hernandez[f], Matias Calvo[f], Stefano Columbu[g], Angel Morales[b], Agustin Pastor[b], Miguel de la Guardia[b]

[a] Department of Prehistory, Archaeology and Ancient History, Faculty of Geography and History University of Valencia, Av. Blasco Ibáñez, 28, 46010, Valencia, Spain
[b] Department of Analytical Chemistry, University of Valencia, C/ Dr. Moliner 50, 46100 Burjassot, Valencia, Spain
[c] Department of Archaeology, University of York, King's Manor, YO17EP York, UK
[d] Department of Earth Sciences, University of Pisa, Via S. Maria 53, 56126 Pisa, Italy
[e] Applied and Laser Spectroscopy Lab., ICCOM-CNR, Via G. Moruzzi 1, 56124 Pisa, Italy
[f] Sagunto Archaeological Museum, C/ del Castillo 23, 46500 Sagunto, Valencia, Spain
[g] Department of Chemical and Geological Sciences, University of Cagliari, Via Trentino 51, 09127 Cagliari, Italy

ABSTRACT

For the first time, an archaeometric study was carried out on the carbonate rock ashlars of the Sagunto Castle. The studied site is one of the most important and best preserved Spanish archaeological and architectural monuments, characterized by different construction phases from the Roman period to Modern Ages. Forty samples collected from thirteen different structures of Sagunto Castle and two quarries, located in the Sagunto's hill were used for comparative purposes. The samples were analyzed by X-ray diffraction, X-ray fluorescence and inductively coupled plasma mass spectrometry to determine their mineralogical and elemental composition. The obtained data show similar chemical and mineralogical features between the rocks outcropping in the city quarries and some of those employed to build the structures, suggesting that rocks could have been used to build the structures from different periods along the centuries.

1. Introduction

Chemical and mineralogical analyses of ancient stones have been used to identify raw material provenance and to better understand the constructive phases of both, archaeological sites (Ferrini et al., 2012; Columbu et al., 2014) and architectural monuments (Sammarco et al., 2015; Lezzerini et al., 2017), as well as to understand the exploitation and circulation of raw materials in the past (Dreesen and Dusar, 2004; Storemyr et al., 2007; Antonelli et al., 2014; Gallello et al., 2016). The analysis of the stones used for building ancient monuments could be also useful for conservation purposes, like getting specimens for laboratory tests, identifying replacement stone sources, and better understanding decay processes (Cardell et al., 2003; Brilli et al., 2010; Török and Přikryl, 2010; De Kock et al., 2015; Hopkinson et al., 2015; Aalil et al., 2016; Berthonneau et al., 2016; Lezzerini et al., 2016).

The present research aims to obtain the first chemical and mineralogical data of the stones used in the buildings of the Sagunto Castle, and to estimate their relationship with the stone material identified in the ancient quarries. Taking into account the difficult access to the amount of samples to be collected, allowed by the authorities, a

chemical and mineralogical approach was developed on a set of forty building stone samples collected from thirteen different structures of the Castle (Fig. 1) and from two local quarries. Sagunto was inhabited by Iberian people before the V century BCE, but the expansion of the city and the construction of the most important structures started following the Roman conquest. The Sagunto Castle was characterized by several occupation phases since the Republican Roman period (Aranegui et al., 1987) to the Napoleonic Wars. During the past century, the site was also interested by restoration works and was designated as heritage of cultural interest by the public authorities (Ripollés Alegre and Llorens Forcada, 2004; Monserrat, 2007). Nowadays, this monument is preparing its candidature to be nominated UNESCO world heritage. The structures of the Sagunto Castle were built widely employing stones. The main used lithotypes are from the sedimentary sequences outcropping in the surrounding area of the site, and the Sagunto Castle itself is located on a hill where dolostone, marlstone and dolomitic limestone outcrop (Goy et al., 1972). Furthermore, the archaeologists identified two ancient quarries on the northern side of the hill. In this study, X-ray diffraction (XRD) was used to determine the main mineralogical phases of the samples, while X-ray fluorescence
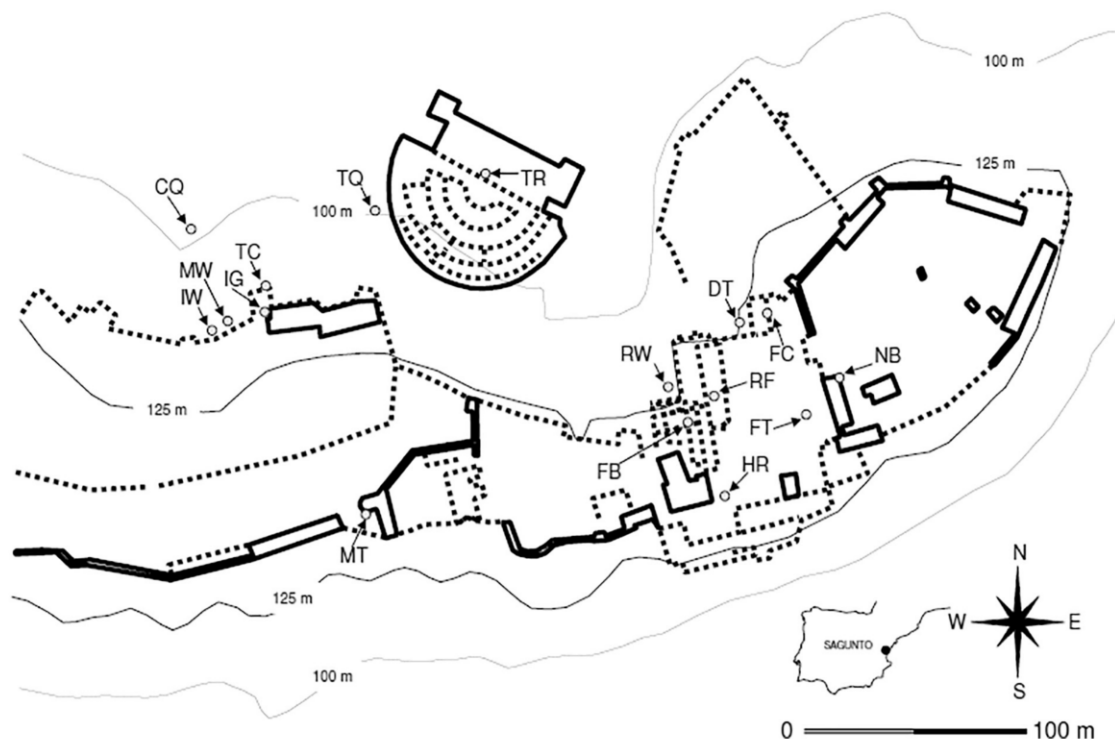
Fig. 1. Map of Sagunto Castle with sampling points (modified from Gallello et al., 2017).

(XRF) and inductively coupled plasma mass spectrometry (ICP-MS) were employed to determine major and minor chemical elements and trace chemical elements, respectively. The obtained data were processed by multivariate statistics.

The importance behind this research is related to the high cultural significance of the Sagunto Castle archaeological site and the unique possibility to produce significant data, which was quite difficult due to the high protective policy that restricts the access to building stone and outcrop sampling.

2. Materials and methods

2.1. Sampling

Forty stone samples were collected from different structures of the Sagunto Castle. They are representative of the different chronological phases identified during the archaeological studies (Table 1). Due to conservation issues, we were allowed by the authorities to collect just around 1 g of each sample in order to perform the analysis, limiting the range of analytical methods to be performed. A small surface portion of each ashlar was scraped to remove the external surface, in order to avoid weathered material, and small chips of rock were then collected by using a chisel.

Twenty-two samples were collected from buildings whose foundation was dated to the Roman Republican period (Roman Republican wall, RW; Diana Temple, DT; Republican Forum, RF; Central Estudiantes Tower, TC). However, concerning TC, the archaeological evidence and mortars analysis (Gallello et al., 2017) suggest important reworks in the subsequent phases.

The Roman Imperial phase led to the building of important monumental structure such as the Theatre (TR), from which two samples were collected. Moreover, five samples were collected from the Imperial Forum (Curia, FC; Basilica, FB; *Tabernae*, FT), an area affected by reworks during the Islamic phase.

As indicative of the Islamic period, begun in the VIII century and endured with reversal of fate until the reconquest of the XIII century, four samples were collected from different buildings (Islamic Gate, IG; Islamic Wall, IW; Moneda Tower, MT). Three samples were also collected from Modern Age buildings (Hermitage, HR; Modern Wall, MW; Napoleonic Barracks, NB).

In order to evaluate the possible relationship between construction building stones and local outcropping sedimentary rocks, four representative samples of the two ancient quarries on the hill of the Sagunto Castle located at Calvario (CQ – Calvario Quarry) and at the Theatre (TQ – Theatre Quarry) areas, were taken. These quarries are formed by dolostone and dolomitic limestone of Triassic "Muschelkalk" outcrop (Goy et al., 1972).

2.2. Methods

We have designed an analytical method approach in order to provide reproducible and comparable results compatible with the small amount of available sample. Qualitative mineralogical analyses were carried out on powders through X-ray diffraction (XRD) by using an automatic diffractometer Philips PW 1830/1710 under the following experimental conditions: Bragg-Brentano geometry, Ni-filtered CuK$_\alpha$ radiation obtained at 40 kV and 20 mA, 5–60°2θ investigated range in step of 0.02° with a counting time per step of 2 s. To identify the mineralogical phases in the X-ray spectra, a search/match approach (DIFFRACPlus EVA) was used by comparing experimental peaks with PDF2 reference patterns.

Major and minor chemical elements were determined by X-ray fluorescence (XRF) on fused glass disks utilizing an ARL 9400 XP+ sequential X-ray spectrometer under the instrumental conditions reported by Lezzerini et al. (2013). Within the range of the measured concentrations, the analytical uncertainties determined on international standards vary from 20% (Na$_2$O) to 1% relative (CaO), with a mean value of 5% relative for the major elements (Lezzerini et al.,

Table 1
List and identification of collected samples.

Sample	Building	Period	Sample	Building/quarry	Period
RW1	Republican wall	Roman Republican	RF2	Republican forum	Roman Republican
RW2	Republican wall		RF3	Republican forum	
RW3	Republican wall		FC1	Imperial forum Curia	Roman imperial
RW4	Republican wall		FC2	Imperial forum Curia	
RW5	Republican wall		FB1	Imperial forum basilica	
RW6	Republican wall		FT1	Imperial forum tabernae	
RW7	Republican wall		FT2	Imperial forum tabernae	
RW8	Republican wall		TR2	Theatre	
TC1	Torre central estudiantes		TR3	Theatre	
TC2	Torre central estudiantes		IG1	Islamic gate	Islamic period
TC3	Torre central estudiantes		IG2	Islamic gate	
TC4	Torre central estudiantes		IW1	Islamic wall	
TC5	Torre central estudiantes		MT1	Moneda tower	
TC6	Torre central estudiantes		HR1	Hermitage	Modern ages
TC7	Torre central estudiantes		MW1	Modern wall	
TC8	Torre central estudiantes		NB1	Napoleonic barrack	
TC9	Torre central estudiantes		CQ1	Calvario quarry	–
DT1	Republican Diana temple		CQ2	Calvario quarry	–
DT2	Republican Diana temple		TQ1	Theatre quarry	–
RF1	Republican forum		TQ2	Theatre quarry	–

2013; Lezzerini et al., 2014). The total amount of volatile components was determined as loss on ignition (LOI) in 105–950 °C temperature range.

Trace elements (Ba, Bi, Cd, Cr, Co, Cu, Pb, Li, Mn, Mo, Ni, Sr, Tl, V, Zn), REE (La, Ce, Pr, Nd, Sm, Eu, Gd, Tb, Dy, Ho, Er, Tm, Yb, Lu), Sc and Y were determined by ICP-MS. The dissolution of homogenized samples was carried out by adding 1.35 ml of hydrochloric acid and 0.45 ml of nitric acid (using high purity 37% HCl and 69% HNO_3) to 0.15 g of sample in glass tubes, while placing them in a water bath at 100 °C for 40 min. The obtained solutions were cautiously transferred into plastic tubes of 50 ml and diluted up to 15 ml with purified water. The calibration standards were prepared from a stock solution for ICP analysis in HNO_3 5% (w/v), containing the mentioned elements at a concentration of 100 µg/ml. Solutions were analyzed with a Perkin Elmer Elan DRCII ICP-MS (Concord, Ontario, Canada). Digested Samples were filtered employing filter paper (Whatman™N.1, 70 mm) to eliminate the insoluble residue and to avoid the obstruction of the nebulization system. Concentrations between 1 and 600 µg/l were used for calibration purpose of most of the elements (Ba, Bi, Cd, Cr, Co, Cu, Pb, Li, Mn, Mo, Ni, Sr, Tl, V, Zn, La, Ce, Pr, Nd), and concentrations between 1 and 100 µg/l for Sm, Eu, Gd, Tb, Dy, Ho, Er, Tm, Yb, Lu. All standards were purchased from Sharlab S.L. (Barcelona). Soil JDo-1 and limestone NCS DC73375 certified materials were used to control the quality of measurements. Rhodium was used as internal standard.

Selected major and trace elements data obtained on studied stone samples were processed through multivariate statistics. Specifically, Principal Component Analysis (PCA) was carried out employing 40 samples and 21 variables (Na_2O, MgO, CaO, MnO, Fe_2O_3T, REE, Y and Sc). This statistic method was used to explore large geochemical datasets reducing the number of variables and providing a deep insight into the structure of their variance. Data were pre-processed through mean centering and autoscaling. Venetian blind cross validation was carried out as the way to test the prediction capability of the built model. The PLS Toolbox 8.2 for Eigenvector Research Inc. (Wenatchee, WA, USA) running in the software MatlabR2016b from Mathworks Inc. (Natick, MA, USA) was used for statistical treatments.

3. Results and discussion

3.1. Mineralogical composition

The collected XRD spectra (Table 2) revealed that calcite and dolomite are the main mineralogical phases in the studied samples. So,

looking at calcite and dolomite relative amounts, the presence of almost three different lithotypes could be estimated:

Group 1: limestones characterized by the presence of calcite and traces of dolomite (19 samples: RW1-6, RW8, TC1, DT1, RF1, FC1-2, FB1, FT1, TR2-3, IG1-2, MW1);

Group 2: calcitic dolostones characterized by high contents of dolomite and traces or small amounts of calcite (10 samples: TC4, TC6, TC8-9, RF2, IW1, HR1, NB1, TQ1-2);

Group 3: stones characterized by high amount of calcite and dolomite, even with different relative proportion (11 samples: RW7, TC2-3, TC5, TC7, DT2, RF3, FT2, MT1, CQ1-2).

Additionally, minor contents of quartz were detected in each sample and a small amount of feldspars was found in samples of the second and third group. Furthermore, traces of phyllosilicates in sample RF2 and small amount of gypsum in the samples from the Islamic Gate (IG1-2) were found. In limestone gypsum is a typical secondary mineral in limestone that can be produced by the reaction of calcite and sulfuric acid due to environmental chemical alterations as air pollution (Charola et al., 2007). However it is difficult to understand if the presence of this mineral is due to the conservation state of the masonries, since it was detected only in the Islamic Gate samples.

3.2. Major and minor elements

Chemical XRF data reported in Table 2 indicates that MgO and CaO are the most representative components of the analyzed samples showing a strong negative correlation (Fig. 2a). These results confirm those obtained by mineralogical analyses, in fact according to Frolova classification of calcite-dolomite series (Frolova, 1959), CaO/MgO ratio can be used to discriminate between calcite- and dolomite-rich carbonate rocks. Based on the aforementioned classification criterion, the CaO/MgO ratio was calculated in order to verify discriminations inferred by mineralogical composition, and better define the geological nature of rock samples in which both calcite and dolomite were identified.

Samples of Group 1 exhibit a CaO/MgO ratio > 50.1, confirming the previous classification as limestones; samples of Group 2, identified as calcitic dolostones by XRD data, can be precisely defined as slightly calcitic dolostones, being characterized by a CaO/MgO ratios ranging from 1.8 to 2.0. For all the other samples, the calculated CaO/MgO ratios allow us to discriminate calcitic dolostones (CaO/MgO ratios from 2.3 to 3.3: TC5, DT2, RF3, FT2 and CQ1), dolomitic limestones (CaO/MgO ratios of 4.2, RW7, and 8.3, CQ2), and slightly dolomitic

Table 2

Main mineralogical phases of Sagunto Castle samples and estimated amounts of oxides determined by XRF, XRD, and their volatile components (LOI).

Sample	Cal	Dol	Qtz	Fsp	Other	L.O.I.	Na₂O	MgO	Al₂O₃	SiO₂	P₂O₅	K₂O	CaO	TiO₂	MnO	Fe₂O₃ T	CaO/MgO	Classification
RW1	XXX	tr	X	–	–	42.8	0.02	0.95	0.43	1.69	0.08	0.28	53.2	0.03	0.01	0.47	56.0	Ls.
RW2	XXX	–	X	–	–	38.4	0.03	0.57	0.71	11.6	0.09	0.27	48.1	0.02	0.01	0.31	84.4	Ls.
RW3	XXX	–	X	–	–	41.5	0.03	0.86	1.26	3.25	0.13	0.69	51.7	0.06	0.01	0.56	60.1	Ls.
RW4	XXX	–	X	–	–	42.1	0.05	0.54	0.89	2.37	0.08	0.49	52.9	0.05	0.01	0.46	98.0	Ls.
RW5	XXX	–	X	–	–	43.1	0.02	0.57	0.31	1.14	0.07	0.20	54.2	0.02	0.01	0.37	95.0	Ls.
RW6	XXX	–	X	–	–	42.8	0.02	0.55	0.47	1.45	0.14	0.26	53.7	0.02	0.02	0.52	97.7	Ls.
RW7	XX	XXX	X	X	–	43.4	0.01	5.73	0.49	1.71	0.09	0.27	47.4	0.04	0.05	0.82	8.3	Dolomitic ls.
RW8	XXX	–	X	–	–	43.1	0.02	0.63	0.36	1.03	0.08	0.24	54.1	0.02	0.01	0.45	85.8	Ls.
TC1	XXX	tr	X	–	–	42.7	0.02	1.01	0.55	1.79	0.15	0.38	53.0	0.04	0.01	0.44	52.4	Ls.
TC2	XXX	X	X	–	–	42.1	0.02	2.55	1.12	2.54	0.11	0.72	50.1	0.07	0.02	0.73	19.6	Slightly dolomitic ls.
TC3	XXX	X	X	–	–	42.1	0.03	2.15	0.98	2.44	0.15	0.64	50.7	0.06	0.01	0.70	23.6	Slightly dolomitic ls.
TC4	tr	XXX	X	X	–	43.6	< LOD	16.7	1.25	2.81	0.14	0.61	32.3	0.07	0.13	2.34	1.9	Slightly calcitic dls.
TC5	XX	XXX	X	X	–	42.4	0.02	12.9	1.87	3.52	0.12	0.92	36.0	0.12	0.10	2.01	2.8	Calcitic dls.
TC6	tr	XXX	X	X	–	43.6	0.01	16.7	1.20	2.52	0.17	0.58	32.3	0.09	0.10	2.74	1.9	Slightly calcitic dls.
TC7	XXX	XX	X	–	–	41.8	0.04	4.40	1.16	2.67	0.08	0.56	47.1	0.08	0.08	2.00	10.7	Slightly dolomitic ls.
TC8	tr	XXX	X	X	–	44.9	< LOD	16.9	0.47	1.88	0.10	0.23	33.8	0.03	0.04	1.66	2.0	Slightly calcitic dls.
TC9	tr	XXX	X	X	–	44.7	0.02	17.1	0.60	1.82	0.11	0.24	33.3	0.03	0.14	1.96	1.9	Slightly calcitic dls.
DT1	XXX	–	X	–	–	42.2	0.03	0.88	0.83	2.38	0.08	0.52	52.5	0.04	0.01	0.51	59.7	Ls.
DT2	XX	XXX	X	X	–	45.1	< LOD	15.4	0.39	1.32	0.10	0.17	36.0	0.02	0.06	1.38	2.3	Calcitic dls.
RF1	XXX	tr	X	–	–	42.8	0.04	0.78	0.44	1.37	0.07	0.26	53.5	0.02	0.01	0.64	68.6	Ls.
RF2	tr	XXX	X	X	Phyll (tr)	44.0	0.02	17.0	0.90	2.40	0.19	0.41	32.4	0.06	0.13	2.43	1.9	Slightly calcitic dls.
RF3	XX	XXX	X	X	–	44.4	0.02	12.5	0.62	1.23	0.22	0.25	39.3	0.04	0.07	1.34	3.1	Calcitic dls.
FC1	XXX	–	X	–	–	43.0	0.04	0.61	0.42	1.15	0.06	0.24	53.9	0.02	0.01	0.52	88.4	Ls.
FC2	XXX	tr	X	–	–	42.6	0.04	0.76	0.55	2.09	0.07	0.32	53.2	0.03	0.01	0.36	70.0	Ls.
FB1	XXX	–	X	–	–	41.9	0.03	0.79	1.08	2.62	0.08	0.63	52.3	0.05	0.01	0.60	66.1	Ls.
FT1	XXX	tr	X	–	–	42.5	0.03	0.91	0.61	1.80	0.08	0.35	52.8	0.03	0.02	0.86	58.1	Ls.
FT2	XX	XXX	X	X	–	44.23	0.02	14.99	0.54	2.2	0.07	0.25	35.51	0.03	0.13	2.03	2.4	Calcitic dls.
TR2	XXX	–	X	–	–	43.4	0.02	0.82	0.25	0.77	0.10	0.13	54.1	0.02	0.01	0.37	66.0	Ls.
TR3	XXX	–	X	–	–	41.9	0.04	0.77	1.02	2.62	0.10	0.66	52.3	0.06	0.02	0.56	67.9	Ls.
IG1	XXX	–	X	–	Gp (X)	43.1	0.21	0.59	0.31	1.01	0.11	0.34	54.1	0.02	0.01	0.25	91.6	Ls.
IG2	XXX	–	X	–	Gp (X)	43.2	0.17	0.49	0.27	0.76	0.32	0.26	54.3	0.01	0.01	0.20	110.9	Ls.
IW1	tr	XXX	X	X	–	45.1	0.02	17.4	0.59	1.32	0.13	0.26	33.3	0.03	0.11	1.72	1.9	Slightly calcitic dls.
MT1	XXX	X	X	–	–	42.5	0.06	1.84	0.72	2.17	0.08	0.49	51.6	0.03	0.01	0.49	28.0	Slightly dolomitic ls.
HR1	tr	XXX	X	X	–	43.5	0.04	17.5	1.25	3.31	0.08	0.58	31.1	0.08	0.15	2.37	1.8	Slightly calcitic dls.
MW1	XXX	–	X	–	–	41.8	0.08	0.51	0.84	2.57	0.24	0.33	52.6	0.05	0.02	1.03	103.0	Ls.
NB1	tr	XXX	X	X	–	43.8	< LOD	16.6	1.30	2.59	0.10	0.67	32.8	0.08	0.14	1.94	2.0	Slightly calcitic dls.
CQ1	XX	XXX	X	X	–	44.1	< LOD	12.0	0.65	1.58	0.08	0.31	39.5	0.04	0.04	1.69	3.3	Calcitic dls.
CQ2	XX	XXX	X	X	–	43.8	< LOD	9.92	0.57	1.55	0.08	0.27	42.1	0.03	0.03	1.63	4.2	Dolomitic ls.
TQ1	tr	XXX	X	X	–	40.9	0.02	16.2	2.84	6.46	0.14	1.16	29.6	0.16	0.13	2.34	1.8	Slightly calcitic dls.
TQ2	tr	XXX	X	X	–	43.1	0.01	17.2	1.86	3.84	0.08	0.80	31.1	0.13	0.09	1.83	1.8	Slightly calcitic dls.

Minerals and rocks acronyms: Cal = calcite, Dol = dolomite, Qtz = quartz, Fsp = feldspars, Phyll = phyllosilicates, Gp = gypsum, Ls. = limestone, Dls. = dolostone. XXX = large amounts, XX = medium amounts, X = small amounts, tr = trace, − = not detected. The amount of chemical elements is expressed in weight percentage. L.O.I. = loss on ignition (950 °C); Fe₂O₃ T = total iron expressed as Fe₂O₃; < LOD = under the limit of detection.

limestones (CaO/MgO ratios from 10.7 to 28.0: TC2, TC3, TC7, and MT1).

Concerning the significance of other major elements, usually iron and manganese oxides are directly correlated to the presence of dolomite (Morrow, 1982); effectively, while in samples characterized by medium and high amounts of this mineral Fe_2O_3T ranges from 0.82 to 2.74 wt% (mean: 1.90 ± 0.46 wt%) and MnO from 0.03 to 0.15 wt% (mean: 0.10 ± 0.04 wt%), in limestones Fe_2O_3T ranges from 0.20 to 1.03 wt% (mean: 0.52 ± 0.19 wt%) and MnO from 0.01 to 0.02 wt% (mean: 0.012 ± 0.004 wt%). The compositional differences among the possible sedimentary rocks types identified on the basis of CaO/MgO ratio are also evidenced by trends shown in the binary diagrams reported in Fig. 2b and c.

Concerning elements useful to inspect the conservation state of building materials and, the possible degradation processes of structures, it is noteworthy that IG1 and IG2 show contents of Na₂O one order of magnitude higher than in the other samples: namely 0.21 and 0.17 wt %, respectively. Such a high amount of sodium could be related to the presence of soluble salts responsible for severe decay in buildings (Charola et al., 2007). On the contrary, the low amount of sodium in dolomitic limestones and dolostones, as compared to limestones, could be explained by the diagenesis process of these rocks (Abdel-Rahman and Nader, 2002). On the other hand, it must be noticed that TQ1 is characterized by a high content of SiO₂ (6.46%), although the highest

value was detected in sample RW2 (11.55%), while the stones collected from TQ quarry show high amounts of TiO₂ (TQ1: 0.16% and TQ2: 0.13%).

3.3. Trace elements analysis

Table 3 shows the results of trace element analysis performed through ICP-MS, expressed in μg/g. Regarding the total amount of REE (ΣREE), all the samples contained from 1.2 to 28 μg/g, except limestone samples RW2, MW1 and TR2, which have anomalous high concentrations of lanthanides: 84, 100 and 114 μg/g, respectively. These samples have also high amounts of yttrium (RW2: 9 μg/g, MW: 29 μg/g and TR2: 22 μg/g), while the others contain this element from 0.2 to 3 μg/g. Scandium vary from 0.6 to 16 μg/g. In general, the limestone samples (29 ± 23 μg/g) show averagely higher ΣREE values than the ashlars of the other carbonate rocks (12 ± 6 μg/g) and the quarry samples (6 ± 2 μg/g), also excluding the above-quoted anomalous values. The limestone samples are also characterized by high amounts of strontium ranging from 78 to 3003 μg/g (796 ± 781 μg/g) while the other samples range between 46 and 1211 μg/g for ashlars (184 ± 306 μg/g), and between 37 and 112 μg/g for quarry rock (66 ± 35 μg/g). On the other hand, Cr and Li are higher in dolomite limestone and dolostone samples, both from buildings (39 ± 50 μg/g and 1.4 ± 0.9 μg/g) and quarries (50 ± 28 μg/g and 1.8 ± 0.8 μg/g), than in limestone ones
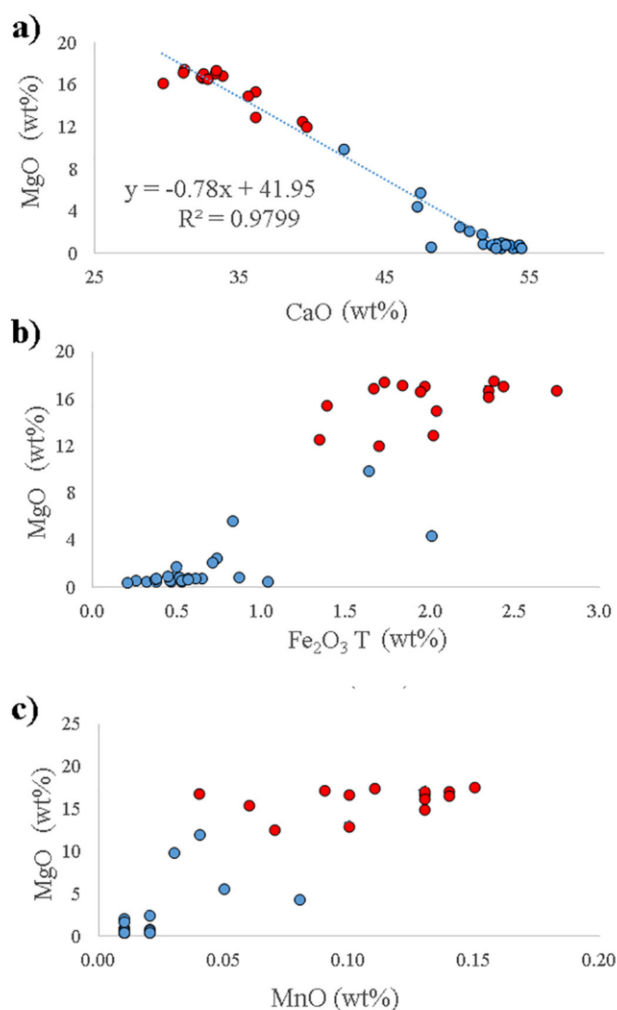
Fig. 2. Binary diagrams (a) CaO vs. MgO; (b) Fe2O3T vs. MgO; (c) MnO vs. MgO. Legenda: red circles = calcitic dolostone; blue circles = limestone and dolomitic limestone.

(16 ± 22 μg/g and 0.9 ± 0.7 μg/g). Furthermore, dolomite limestone-dolostone ashlars and quarry samples have higher levels of Zn (31 ± 28 μg/g and 51 ± 46 μg/g respectively) than limestone ones (21 ± 22 μg/g), and the first ones have higher concentrations of Pb (22 ± 17 μg/g) than limestone and quarry samples (13 ± 12 μg/g and 14 ± 13 μg/g respectively). Other trace elements were found in comparable concentrations in the three types of samples.

3.4. Statistical data processing

Multivariate statistics was carried out to evaluate the similarities and differences among the analyzed samples by applying PCA. In order to reduce the number of variables which could describe appropriately the samples, Na_2O, MgO, CaO, MnO, Fe_2O_3T, REE, Y and Sc of the whole set of samples were used (Fig. 3) due to the important role of these elements on the sedimentary rock composition (Schieber, 1988; Nothdurft et al., 2004; Zhang et al., 2017).

Just two principal components (PC1 and PC2) explain 58.04% and 17.98% of the variance, respectively, and loadings of PC1 and PC2 are correlated with their contribution to the overall model (Fig. 3, bottom). REE data especially contribute on PC1 direction, while PC2 is particularly influenced by major elements (Fig. 3, bottom). Specifically, PC1

accounts La, Ce, Pr, Nd, Sm, Eu, Gd, Dy, Ho, Er, Tm, Yb, Lu and Y variability and higher values of REE mean higher values of PC1. Otherwise, the influence of Na_2O, MgO, CaO, MnO and Fe_2O_3T in discriminating different lithotypes is evidenced by PC2 scores; as can be seen, Na_2O and CaO, and MgO, MnO and Fe_2O_3T inversely contribute to the computation of PC2, meaning that higher values of the first elements, typical of limestone, lead to negative values on y-axis and higher values of the latter ones, typical of magnesian carbonate rocks, lead to positive ones.

The inspection of scores plot shown in the top of Fig. 3 allows to discriminate two main sample populations: in PC2 positive direction, samples exhibiting the presence of dolomite, classified from slightly dolomitic limestones (TC7 and RW7) to calcitic dolostones, are grouped together with the samples taken from both studied local quarries (labeled as TQ and CQ). Conversely, limestone ashlars and most of the slightly dolomitic limestones are grouped on the bottom of the plot. It is noteworthy that dolomitic stones seem to exhibit a more homogenous composition than limestones, which span in a larger area credibly resembling the variability in REE values.

Samples MW1, RW2 and TR2 seem to be outliers as compared with the rest of rocks. It is interesting to note that these limestone ashlars belong to diachronic structures, being correlated only by the high REE levels in the analyzed set. This feature could be related to peculiar sedimentary diagenetic conditions, post-depositional processes or even to restoration works.

3.5. Considerations on provenance of raw materials and construction phases

The chemical and mineralogical results of stones sampled from Sagunto Castle, are showing the five different facies of dolomite and limestone lithologies (calcitic dolostones, slightly calcitic dolostones, dolomitic limestones, slightly dolomitic limestones and limestones) all of them outcropping in the sedimentary sequence of the Sagunto area as indicated by Goy et al. (1972). This discrimination, suggested by chemical and mineralogical data, has been confirmed by the relative amounts of CaO and MgO (Fig. 2) and by the variability in minor and trace elements (Fig. 3).

Concerning provenance issues, the first test seems to indicate a compositional semblance between dolomite-rich ashlars (slightly calcitic dolostone, calcitic dolostone, dolomitic limestone, and slightly dolomitic limestone) and stone samples from local quarries. Furthermore, the representative samples taken from the ancient quarries show a slightly different mineralogical composition, covering the whole range of carbonate rocks: the stones from Theatre Quarry may be classified as slightly calcitic dolostones, while the Calvario Quarry materials may span from calcitic dolostone to dolomitic limestone. In fact, the fortress of Sagunto Castle is built on the rock outcrop of Triassic "Muschelkalk" lithologies, which show different intermediate facies from dolostone to dolomitic limestone. The lithotypes sampled from the Sagunto Castle structures maybe indicate that the stones employed could be from those local quarries. Regarding limestones, until now no local ancient quarries have been identified in the closeness of Sagunto, although the area is interested by the occurrence of this lithotype just few kilometers south-west and north-west of the archaeological site. In this latter area, some Triassic "Buntsandstein" limestones of Lias (Pliensbachiense, Sinemuriense, Hettangiense) also appear, together with dolomites, bioclastic-limestones and carniolas. Within a radius of 5 km from the Castle various limestone facies of Dogger and Lower Malm (Oxfordiense) and marly limestones with nodules were also identified (Goy et al., 1972).

If we try to find a relation between the different lithotypes and the construction phases of the Castle, it can be observed that limestones have been employed in all Imperial buildings (i.e.: Curia, Basilica and Theatre, with the exception of FT2 sample), in the Islamic Gate and in the Modern Wall. Limestone ashlars occur with a non-systematic

Table 3

Trace elements in Sagunto Castle samples determined through ICP-MS analysis.

Sample	Σ REEs	^{209}Bi	^{207}Pb	^{205}Tl	^{138}Ba	^{111}Cd	^{95}Mo	^{89}Y	^{88}Sr	^{64}Zn	^{63}Cu	^{60}Ni	^{59}Co	^{52}Cr	^{51}V	^{45}Sc	^{7}Li
RW1	14	< LOD	4	0.010	5	0.07	3	2	576	16	1.7	140	5	21	< LOD	1.3	0.6
RW2	84	0.07	26	0.04	6	0.09	2	9	2109	2	1.4	12	0.7	11	< LOD	4	1.9
RW3	1.2	< LOD	0.5	< LOD	16	0.006	0.5	0.2	143	26	1.2	420	33	2	11	4	0.6
RW4	9	0.001	5	< LOD	42	0.02	2	1.1	1907	5	0.9	62	2	7	25	1.3	0.8
RW5	3	< LOD	0.3	< LOD	5	0.005	0.3	0.6	364	28	0.2	466	20	3	< LOD	2	0.4
RW6	16	0.02	3	0.06	12	0.03	6	1.9	432	4	1.1	12	0.9	7	7	0.7	0.7
RW7	9	< LOD	3	< LOD	0.4	0.2	3	1.4	49	128	5	1584	93	25	5	6.8	2
RW8	14	< LOD	6	0.02	5	0.04	3	1.9	617	8	1.8	64	2	7	< LOD	1.3	0.9
TC1	29	0.05	46	0.06	2	0.14	2	2	718	45	3	18	1.1	8	4	1.7	3
TC2	28	0.05	44	0.05	6	0.14	2	2	694	43	3	18	1.04	7	3	1.7	3
TC3	1.9	< LOD	0.4	< LOD	5	0.005	0.08	0.3	196	43	1.2	572	37	1.5	< LOD	1.9	0.96
TC4	15	0.003	37	0.015	6	0.03	4	2	61	27	5	27	3	190	< LOD	1.6	1.1
TC5	11	0.012	22	0.03	22	0.10	3	2	62	18	5	9	1.2	7	< LOD	1.2	0.8
TC6	12	0.06	27	0.05	21	0.02	6	2	83	18	4	17	5	52	< LOD	1.3	1.7
TC7	13	0.02	30	0.03	0.8	0.12	12	2	160	36	4	51	1.7	18	20	1.8	1.9
TC8	4	0.007	4.5	0.012	9	0.03	9	0.9	110	39	4	86	4	39	78	1.5	3.8
TC9	8	< LOD	13	< LOD	27	0.05	3	1.5	46	30	1.9	191	7	10	< LOD	2	0.6
DT1	21	0.08	23	0.2	25	0.03	0.2	2	1255	< LOD	1.1	15	0.9	7	< LOD	1.1	1.5
DT2	12	0.02	16	0.04	45	0.05	0.9	1.3	62	9	1.9	24	1.6	24	17	0.7	1.1
RF1	12	0.02	26	0.08	16	0.24	0.8	2	78	19	3	19	1.5	88	22	0.6	0.3
RF2	12	0.03	8	0.03	13	0.03	0.5	2	53	9	2	21	1.6	16	12	1.1	0.7
RF3	7	0.04	65	0.06	18	0.02	0.6	1.1	57	14	2	21	1.1	9	20	1.0	0.5
FC1	18	0.06	6	0.2	7	0.006	0.2	1.7	528	< LOD	0.8	22	1.1	4	< LOD	0.8	0.5
FC2	20	0.03	10	0.04	17	< LOD	0.2	1.3	3003	1.0	2	28	1.5	11	5	1.2	1.6
FB1	25	0.15	14	0.4	8	0.06	0.3	2	577	2	2	20	1.2	10	< LOD	0.8	0.7
FT1	23	0.13	16	0.3	10	0.005	0.5	2	583	8	1.4	23	1.4	10	< LOD	0.7	0.6
FT2	20	0.08	36	0.3	7	0.05	0.99	3	85.7	15	4	22	3.1	31	59	2	1.4
TR2	115	0.09	5	0.07	26	0.09	2	22	287	88	30	46	19	63	82	8	0.03
TR3	14	0.007	0.9	0.007	14	0.02	0.13	3	246	4	< LOD	35	2	< LOD	7	1.1	0.003
IG1	19	0.010	20	0.02	9	0.05	1.1	2	1249	31	2	27	1.3	6	< LOD	1.1	1.6
IG2	12	0.02	28	0.03	23	0.12	11	1.5	150	33	4	48	1.6	16	19	1.7	1.8
IW1	9	0.014	10	0.04	14	0.05	1.1	2	67	33	5	13	1.9	107	49	0.9	2
MT1	18	0.002	26	0.05	16	0.05	0.06	2	1211	27	2	25	1.3	5	< LOD	0.8	0.5
HR1	10	0.04	15	0.09	9	< LOD	0.5	1.5	43.6	3	3	14	2	19	7	1.3	0.96
MW1	101	0.019	17	0.12	26	1.16	0.2	29	305	27	4	28	2	10	< LOD	1.8	0.55
NB1	18	0.03	20	0.04	13	0.07	0.5	2	89	35	4	27	2	103	14	1.7	0.94
CQ1	3	0.008	8	< LOD	47	0.10	14	0.8	76	44	5	389	15	29	135	6	2.47
CQ2	8	0.02	34	0.10	9	0.11	6	1.3	112	18.1	5	39	3	88	5	0.9	1.3
TQ1	6	0.011	12	< LOD	139	0.03	5	2	41	24.2	3	110	5	27	68	4	0.95
TQ2	5	0.003	1.8	< LOD	5	0.08	5.3	1.1	37	119	6	1228	77	55	182	16	2.63

Note: concentrations of elements expressed in µg/g.; the measurement error for each element in all the samples is lower than 1%. < LOD = under the limit of detection.

distribution in some Republican structures, such as the Republican Forum (RF1), Diana Temple (DT1) and the Central Estudiantes Tower (TC1). It is worth noticing that the Republican wall seems to be entirely constructed by using this lithotype (samples labeled as RW), with the sole exception of RW7, which shows an affinity with the Calvario Quarry materials (specifically, CQ2 sample). In the other studied structures, materials were possibly taken from Calvario and Theatre quarries, even if not thoroughly employed.

This first overview could suggest interesting historical and archaeological observations, especially by crossing the present results with the ones of the mortar analysis showed in Gallello et al. (2017) and Ramacciotti et al. (2018). First of all, limestone ashlars were used in most of the samples from buildings dating back to the Roman Ages, suggesting a prevalent use of raw materials from quarries outside the city, being exploited through Republican and Imperial periods. The occurrence of dolomitic-type stones similar to the rocks outcropping in the city quarries in almost all the investigated structures suggests the possible uninterrupted use of construction materials coming from the quarries of Calvario and Theatre. Though the exploitation of the two quarries inside the city during the Roman period would be possible, these cases of urban quarries could find a comparable example in the small quarry of PERI2 in Tarragona (Gutiérrez Garcia-M, 2011). Moreover, the use of these stones in the Republican Forum (FR), in the Republican Wall (RW) and in Diana Temple (DT), whose masonries were dated back to the Roman Republican period through mortar

analysis (Gallello et al., 2017), seems to point out the presence of at least two construction phases during this period or the presence of some architectural intervention on these structures during the following periods. However, it is worth noting that dolomite-rich rocks were used in buildings whose mortars evidenced Islamic (TCE, FT, HR, IW and TM) and Modern (TCE, NP) construction phases (Gallello et al., 2017; Ramacciotti et al., 2018), suggesting a possible heavy exploitation of the city quarries during Medieval and Modern Ages. In conclusion, the occurrence of all the identified stone types in the overall archaeological area supports the considerations, suggested by the previous archaeological and archaeometric studies on Sagunto Castle mortars (Gallello et al., 2017), according to which heavy reworks interested most of the buildings from the Roman period to the Modern Ages.

4. Conclusions

This study have demonstrated the capability of chemical and mineral analyses in discriminating carbonate rocks and supporting archaeological studies, providing information on raw materials provenance and reconstruction of architectural phases, also when just a small amount of sample can be collected.

The results suggest that the dolomitic rock facies (mainly calcitic dolostones and dolomitic limestones) used to erect the Sagunto Castle maybe come from the local "Theatre" and "Calvario" quarries. Trace elements, REE, Y and Sr showed to be good discriminators of these
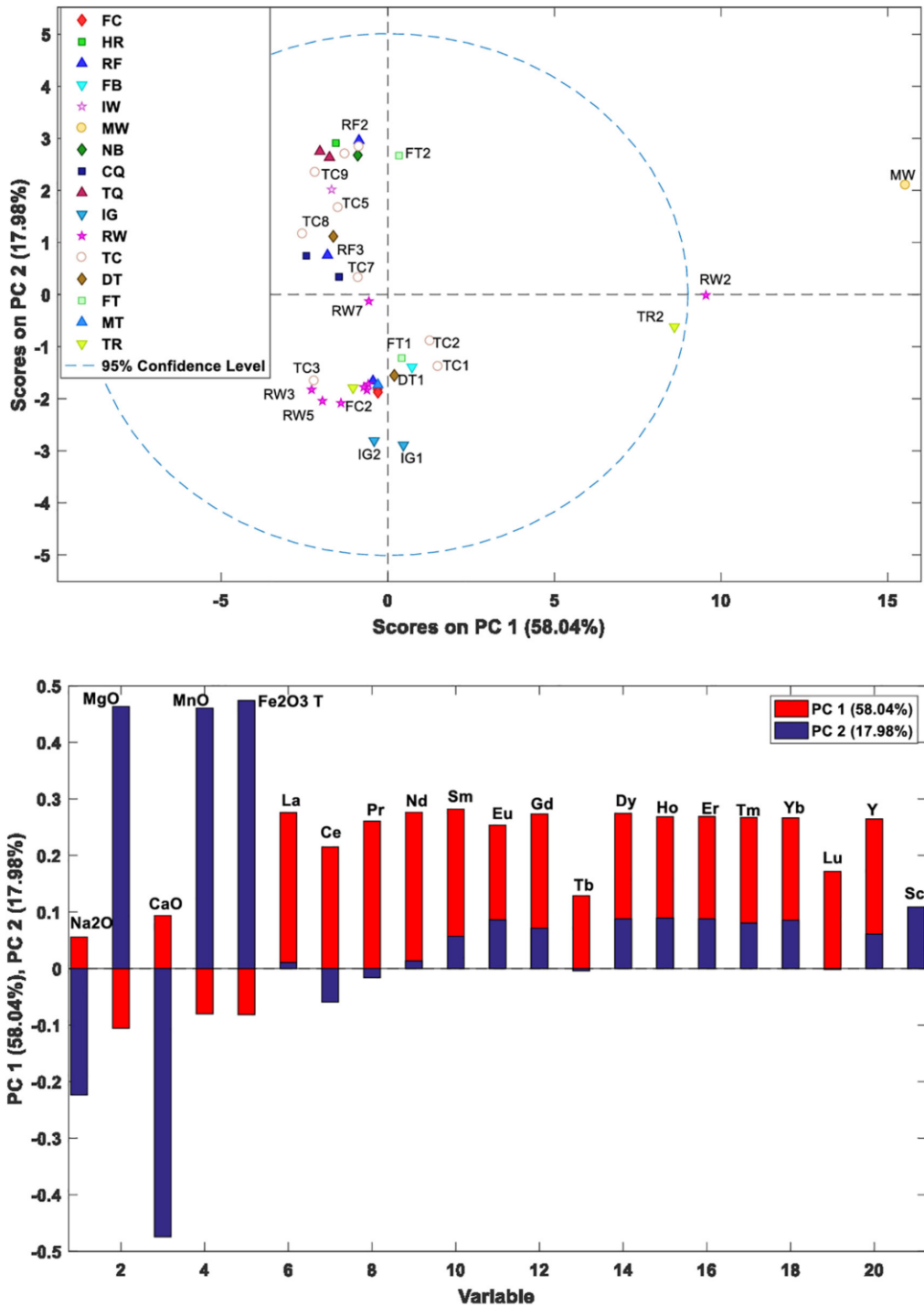
Fig. 3. Principal component analysis through selected oxides and REEs data. Scores biplot (top) and loadings plot (bottom).

rocks from the others. The lower variability in these elements enforces the above-quoted provenance hypothesis of dolomitic limestones and dolostones.

Regarding the limestone facies, although no extraction front or ancient quarry have been recognized near to the archaeological site, it is likely that these stones come from the outcrops located next to the castle (within about 2 km), where lithologies similar to those used in

the castle were found. No conclusions can be inferred by the higher variability of both lanthanides, yttrium and Sr in limestone ashlars due to the impossibility of identifying the ancient quarries and determining the variability of the possible raw materials. However, REE and Y point out the presence of three limestone samples characterized by abnormally high values (RW2, MW1 and TR2).

The results suggest the presence of different construction phases in

RW, RF and FT during the Republican period. Limestone from the unidentified quarries outside the city could have been preferentially used during the Roman Ages, while calcitic dolostone and dolomitic limestone possibly extracted from the urban quarries seems to be especially exploited during the Islamic period and Modern Ages, as suggested by their preferential employment in buildings like TCE, FT, HR, IW, TM and NP.

This study provides a unique opportunity to chemically screen this important site, which is being considerate as a candidate to be declared a UNESCO world heritage. The unsystematic occurrence of the different identified lithotypes in the studied buildings enforces the idea of a complex architectural history of the Sagunto Castle, characterized by reworks and whose complete understanding is probably only at its starting point.

Acknowledgments

References

Aalil, I., Beck, K., Brunetaud, X., Cherkaoui, K., Chaaba, A., Al-Mukhtar, M., 2016. Deterioration analysis of building calcarenite stone in the House of Venus in the archaeological site of Volubilis (Morocco). Const. Build. Mater. 125, 1127–1141.

Abdel-Rahman, A.F.M., Nader, F.H., 2002. Characterization of the Lebanese Jurassic-Cretaceous carbonate stratigraphic sequence: a geochemical approach. Geol. J. 37, 69–91.

Antonelli, F., Columbu, S., Lezzerini, M., Miriello, D., 2014. Petrographic characterization and provenance determination of the white marbles used in the Roman sculptures of Forum Sempronii (Fossombrone, Marche, Italy). Appl. Phys. A Mater. Sci. Process. 115, 1033–1040.

Aranegui, C., Hernández, E., López, M., 1987. El foro de Saguntum: la planta arquitectónica. In: Los foros romanos de las provincias occidentales, Ministerio de Cultural, Madrid, pp. 73–97.

Berthonneau, J., Bromblet, P., Cherblanc, F., Ferrage, E., Vallet, J.M., Grauby, O., 2016. The spalling decay of building bioclastic limestones of Provence (South East of France): from clay minerals swelling to hydric dilation. J. Cult. Heritage 17, 53–60.

Brilli, M., Antonelli, F., Giustini, F., Lazzarini, L., Pensabene, P., 2010. Black limestones used in antiquity: the petrographic, isotopic and EPR database for provenance determination. J. Archaeol. Sci. 37, 994–1005.

Cardell, C., Delalieux, F., Roumpopoulos, K., Moropoulou, A., Auger, F., Van Grieken, R., 2003. Salt-induced decay in calcareous stone monuments and buildings in a marine environment in SW France. Const. Build. Mater. 17, 165–179.

Charola, A.E., Pühringer, J., Steiger, M., 2007. Gypsum: a review of its role in the deterioration of building materials. Environ. Geol. 52, 339–352.

Columbu, S., Antonelli, F., Lezzerini, M., Miriello, D., Adembri, B., Blanco, A., 2014. Provenance of marbles used in the Heliocaminus baths of Hadrian's Villa (Tivoli, Italy). J. Archaeol. Sci. 49, 332–342.

De Kock, T., De Boever, W., Dewanckele, J., Boone, M.A., Jacobs, P., Cnudde, V., 2015. Characterization, performance and replacement stone compatibility of building stone in the 12th century tower of Dudzele (Belgium). Eng. Geol. 184, 43–51.

Dreesen, R., Dusar, M., 2004. Historical building stones in the province of Limburg (NE Belgium): role of petrography in provenance and durability assessment. Mater. Charact. 53, 273–287.

Ferrini, V., De Vito, C., Mignardi, S., Fucinese, D.V., 2012. Archaeological carved slabs of the Langobard art in churches of Peligna Valley and Spoleto (Italy): provenance of the stones. J. Archaeol. Sci. 39, 3505–3515.

Frolova, E.K., 1959. On classification of carbonate rocks of limestone-dolomite-magnesite series. Novosti Neft. Tekhniki (Geology) 3, 34–35.

Gallello, G., Orozco, T., Pastor, A., de la Guardia, M., Bernabeu, G., 2016. Regional provenance of dolerite prehistoric objects through mineral analysis. Microchem. J. 24, 167–174.

Gallello, G., Ramacciotti, M., Lezzerini, M., Hernandez, E., Calvo, M., Morales, A., Pastor, A., de la Guardia, M., 2017. Indirect chronology method employing rare earth elements to identify Sagunto Castle mortar construction periods. Microchem. J. 132, 251–261.

Goy, J.L., Gutiérrez, M., Pedraza, J., Vegas, R., Zazo, C., 1972. Mapa geológico de la Hoja n° 668 (Sagunto), Mapa Geológico de España E. 1:50.000, Segunda Serie (MAGNA), 1ª ed. Instituto Geológico y Minero de España, Madrid.

Gutiérrez Garcia-M, A., 2011. The exploitation of local stone in Roman times: the case of north-eastern Spain. World Archaeol. 43 (2), 318–341.

Hopkinson, L., Rutt, K., Kristova, P., Blows, J., Firth, C., 2015. Sourcing limestone masonry for restoration of historic buildings, a spectroscopic pilot study. J. Cult. Heritage 16, 822–830.

Lezzerini, M., Tamponi, M., Bertoli, M., 2013. Reproducibility, precision and trueness of X-ray fluorescence data for mineralogical and/or petrographic purposes. Atti della Società Toscana di Scienze Naturali, Memorie, Serie A 120, 67–73.

Lezzerini, M., Tamponi, M., Bertoli, M., 2014. Calibration of XRF data on silicate rocks using chemicals as in-house standards. Atti della Società Toscana di Scienze Naturali, Memorie, Serie A 121, 65–70.

Lezzerini, M., Antonelli, F., Columbu, S., Gadducci, R., Marradi, A., Miriello, D., Parodi, L., Secchiari, L., Lazzeri, A., 2016. The documentation and conservation of the cultural heritage: 3D laser scanning and Gis techniques for thematic mapping of the stonework of the Façade of St. Nicholas Church (Pisa, Italy). Int. J. Archit. Heritage 10, 9–19.

Lezzerini, M., Antonelli, F., Gallello, G., Ramacciotti, M., Parodi, L., Alberti, A., Pagnotta, S., Legnaioli, S., Palleschi, V., 2017. Provenance of marbles used for building the internal spiral staircase of the bell tower of St. Nicholas Church (Pisa, Italy). Appl. Phys. A Mater. Sci. Process. 123, 385.

Monserrat, J.M.M., 2007. Dos siglos de destrucción de Patrimonio Histórico de Sagunto (1807–2007). Arse 41, 231–262.

Morrow, D.W., 1982. Diagenesis 1. Dolomite – part 1: the chemistry of dolomitization and dolomite precipitation. Geosci. Can. 9, 5–13.

Nothdurft, L.K., Webb, G.E., Kamber, B.S., 2004. Rare earth element geochemistry of Late Devonian reefal carbonates, Canning Basin, Western Australia: confirmation of a seawater REE proxy in ancient limestones. Geochim. Cosmochim. Acta 68, 263–283.

Ramacciotti, M., Rubio, S., Gallello, G., Lezzerini, M., Columbu, S., Hernandez, E., Morales-Rubio, A., Pastor, A., de la Guardia, M. 2018. Chronological classification of ancient mortars employing spectroscopy and spectrometry techniques: Sagunt (Valencia, Spain) case. J. Spectrosc. (doi:https://doi.org/10.1155/2018/9736547).

Ripollés Alegre, P.P., Llorens Forcada, M.M., 2004. OPVLENTISSIMA SAGVNTVM. Fundación Bancaja, Sagunto.

Sammarco, M., Margiotta, S., Foresi, L.M., Ceraudo, G., 2015. Characterization and provenance of building materials from the Roman Pier at San Cataldo (Lecce, Southern Apulia, Italy): a lithostratigraphical and micropaleonthological approach. Mediterr. Archaeol. Archaeom. 15, 101–112.

Schieber, J., 1988. Redistribution of rare-earth elements during diagenesis of carbonate rocks from the mid-Proterozoic Newland formation, Montana, U.S.A. Chemical Geol 69, 111–126.

Storemyr, P., Degryse, P., King, J.F., 2007. A black Tournai "marble" tombslab from Belgium imported to Trondheim (Norway) in the 12th century: provenance determination based on geological, stylistic and historical evidence. Mater. Charact. 58, 1104–1118.

Török, Á., Přikryl, R., 2010. Current methods and future trends in testing, durability analyses and provenance studies of natural stones used in historical monuments. Eng. Geol. 115, 139–142.

Zhang, K., Li, Q., Yan, L., Zeng, L., Lu, L., Zhang, Y., Hui, J., Jin, X., Tang, X., 2017. Geochemistry of limestones deposited in various plate tectonic settings. Earth-Science Rev 167, 27–46.

Anexo E

Ramacciotti et al. (2020a). An innovative multi-analytical approach based on spectroscopic and electrochemical techniques to study a complex Roman amphorae collection

Contents lists available at ScienceDirect

Applied Clay Science

Research Paper

An innovative multi-analytical approach based on spectroscopic and electrochemical techniques to study a complex Roman amphorae collection

Mirco Ramacciotti[a,b], Gianni Gallello[a,c,*], Daniel Navarro-Martos[a,b], Antonio Doménech-Carbó[b], Clodoaldo Roldán[d], Emilia Hernández[e], Salvador Garrigues[b], Agustín Pastor[b]

[a] Department of Prehistory, Archaeology and Ancient History, University of Valencia, Av. Blasco Ibáñez, 28, 46010 Valencia, Spain
[b] Department of Analytical Chemistry, University of Valencia, C/ Dr. Moliner, 50, 46100 Burjassot, Valencia, Spain
[c] Department of Archaeology, University of York, King's Manor, YO17EP York, UK
[d] Institute of Materials Science, University of Valencia, Av. Catedrático José Beltrán, 2, 46980 Paterna, Valencia, Spain
[e] Sagunto Archaeological Museum, C/ del Castillo, 23, 46500 Sagunto, Valencia, Spain

ARTICLE INFO

ABSTRACT

An innovative multi-analytical approach for the classification of ancient pottery sherds was tested. Twenty Roman amphorae fragments belonging to different known typologies and twenty-seven unclassified ones from a complex Sagunto Archaeological Museum (Spain) collection were studied by multielement analysis (X-ray fluorescence spectroscopy and inductively coupled plasma mass spectrometry), Fourier-transform near infrared spectroscopy and voltammetry of immobilized microparticles employing a minimal amount of sample. Chemometric analysis based on principal component analysis allowed the identification of most of the unclassified samples, proving the importance and reliability of the developed methodological approach for ceramic classification insights.

1. Introduction

Ceramic sherds are frequently recovered in archaeological fieldwork, and the study of pottery artefacts and their manufacturing processes are considered crucial to understand past human activities (Orton and Hughes, 2013).

Amphorae are well known as a particular kind of ceramic containers used to transport different products especially over medium and long distances. In particular, amphorae are linked to the development of trading among the different Mediterranean populations and were widely used for the maritime transport of solid and liquid commodities such as wine, oil, olives and fish (Bevan, 2014). Thus, the recognition of amphorae typologies to identify their provenance and contents is of pivotal importance in order to understand commercial routes and past economic dynamics (Peacock, 1977; Tomber and Williams, 2000; Gupta et al., 2001; Lund, 2011; Rubert and Alonso, 2011; Orengo and Livarda, 2016; Rubio-Campillo et al., 2018).

For this reason, archaeologists have carried out comprehensive typological classifications of these containers based on their morphological features and stamps (Callender, 1965; Keay, 1984; Peacock and Williams, 1991; Opaiţ and Tsaravopoulos, 2011; Carre et al., 2014; Öniz, 2016). However, autoptic analysis of the fragments is in many cases an unviable method of classification since most ceramic remains do not show morphological features which clearly indicate the typology. Therefore, these classic archaeological methods have been complemented by petrographic, mineralogical and chemical analyses to discriminate typologies and thus track amphorae origins (Maniatis et al., 1984; Belfiore et al., 2014; Thierrin-Michael et al., 2018; Tsantini et al., 2019), to investigate aspects such as manufacturing processes, workshops and identification of raw materials (Dias et al., 2010; Barone et al., 2012; Verga et al., 2015; Ferreira et al., 2018). Analytical techniques such as optical microscopy (OM), scanning electron microscopy coupled with energy dispersive X-ray analysis (SEM-EDS) and X-ray diffraction (XRD) have been used to identify petrographic and mineralogical characteristics of ceramic material (Fantuzzi et al., 2016; Finocchiaro et al., 2018; Di Bella et al., 2019). Fourier transform infrared spectroscopy (FT-IR) is commonly employed for the same purpose but most studies have focussed on the mid-IR region (Ostrooumov and Gogichaishvili, 2013; Ceccarelli et al., 2018; Ferri et al., 2019). The near-IR (NIR) has been less used (Bruni et al., 2001, 2018) due to limitations of spectral resolution and to its low sensitivity compared with other techniques, in spite of its capacity to obtain non-destructive direct measurements by using the diffuse reflection technique. Major, minor and trace elements measurement are commonly performed by

---

energy dispersive X-ray fluorescence spectroscopy (ED-XRF) using both portable and non-portable spectrometers. Inductively coupled plasma optical emission spectrometry (ICP-OES) and inductively coupled plasma mass spectrometry (ICP-MS) have been also used to provide insights into the provenance of the studied materials (Aldrabee and Wriekat, 2011; Mannino and Orecchio, 2011; Baklouti et al., 2016; Grau Mira and Gallello, 2017; Raneri et al., 2019). Some studies have used voltammetry of immobilized microparticles (VIMP) in order to characterize the glaze of pottery artefacts (Doménech-Carbó et al., 2000, 2002), but only a few authors employed it to investigate the composition of the ceramic body (Conejo-Barboza et al., 2015; Di Turo et al., 2018; La-Torre-Riveros et al., 2019; Fabrizi et al., 2020).

This study aimed to test the reliability of a multi-analytical approach requiring a very small sample (less than 1 g), employing portable ED-XRF, ICP-MS, VIMP and FT-NIR. These data were combined with chemometric models to classify ancient amphorae sherds from a very complex collection. Furthermore, statistical examination of the results enabled the limitations and advantages of the employed techniques in providing information about different ceramic features to be interrogated. While multielement analysis (XRF and ICP-MS) is a well-established method to determine raw material elemental profiles for provenance studies, VIMP and FT-NIR can provide information about mineralogical and structural aspects often linked to the manufacturing processes such as firing temperature and atmosphere.

2. Materials and methods

2.1. Sampling

Forty-seven different representative amphorae fragments (Fig. 1) dated back to the Roman period (Table 1) were selected from the Sagunto Archaeological Museum, one of the most important museums for pre-Roman and Roman culture in Spain. The city of Sagunto, a few kilometres north of Valencia, was a strategic point for Iberian commerce and from the 6th century B.C. was part of the Mediterranean routes, developing trade with Punic, Italic and Greek peoples (Gascó, 2013). The sampled materials were previously classified, when feasible, following the classic archaeological methods; specifically, the amphora typological classification was based on macroscopic and textural features that define production regions (Peacock, 1977).

Most of the samples of classified provenance were sherds from Ibero-Roman (five samples: IR1-5) and Punic (seven samples: P1-7) amphorae types. Except for P3, which was identified as being from Ibiza, the other Punic samples are from the area near the Gibraltar Strait. These two typologies (Ibero-Roman and Punic) are often found in Sagunto archaeological excavations and are a representative part of the Sagunto Archaeological Museum ceramic collection. Therefore the development of a method to identify and distinguish Ibero-Roman from Punic amphorae types would be particularly useful to tackle one of the main issues related to Sagunto amphorae provenance studies. Two fragments belong to Adriatic amphorae types (A1-2) and two fragments are Campanian (C1-2). Two local Sagunto amphorae (S1-2) were identified and collected. One fragment was classified as Marseilles amphora (M1) and another one as amphora of Tarragona (T1). These twenty samples constituted the reference set for this study.
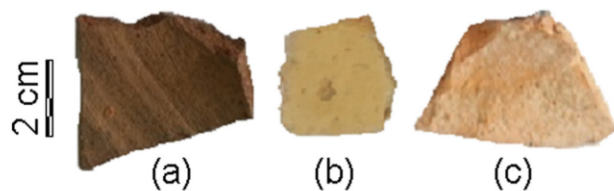

Fig. 1. Three fragments from the collected sample set (see Table 1): a) sample P4; b) sample A2; c) sample U01.

Table 1
The typological classification of samples.

Sample	Type	Sample	Type
A1	Adriatic	P4	Punic
A2	Adriatic	P5	Punic
C1	Campanian	P6	Punic
C2	Campanian	P7	Punic
IR1	Ibero-Roman	S1	Sagunto
IR2	Ibero-Roman	S2	Sagunto
IR3	Ibero-Roman	T1	Tarraconensis
IR4	Ibero-Roman	U01-U15	Unclassified
IR5	Ibero-Roman	U16*	Unclassified
M1	Marseilles	U17-U24	Unclassified
P1	Punic	U25*	Unclassified
P2	Punic	U26-U27	Unclassified
P3[+]	Punic		

Note: [+] P1, P2 and P4-7 are Punic amphorae from the area of the Gibraltar strait and P3 is from Ibiza. *U16 is probably Punic or Campanian, and U25 Ibero-Roman or Punic.

Additionally, twenty-seven fragments of unclassified amphorae (U01-27) were sampled from the same collection as the reference set, so that the archaeological context and chronology were the same. Samples U16 and U25 were of uncertain attribution; the former was classified as Punic or Campanian, and the latter as Punic or Ibero-Roman.

2.2. Portable energy dispersive X-ray fluorescence spectroscopy (pED-XRF)

A small amount (± 1 g) of each amphora fragment was pulverized and homogenized using an agate pestle and mortar andthe concentrations of major elements of the powdered samples were obtained using a S1 Titan pED-XRF Bruker (Kennewick, Washington DC, USA) equipped with a Rh X-ray tube (50 kV) and X-Flash® SDD (resolution: 147 eV; FWHM: 5.9 keV). Geochem-trace application was used to perform the quantitative analyses, and S1 Sync software (Bruker) was employed to measure Al, Si, K, Ca, Ti and Fe concentrations. The accuracy and precision of the analysis were tested by using an appropriate certified reference material (Soil NIM GBW07408) with a matrix similar to the studied material. Portable X-ray fluorescence spectrometers are well established devices in archaeological research (Frahm and Doonan, 2013), being employed to analyse different materials including ceramics.

2.3. Inductively coupled plasma mass spectrometry (ICP-MS)

A total digestion method with hydrofluoric acid was preferred since it dissolves the aluminosilicates which comprise a large part of the ceramic matrix. The applied digestion method was developed to obtain satisfactory recovery results and to avoid the use of fluxes or H_3BO_3 to neutralize HF that involves excessive dilutions (Tsolakidou et al., 2002).

The preparation protocol and digestion method used in this study is the same as that used successfully by Raneri et al. (2019) in their ceramic provenance studies.

A sample of the certified reference material, Soil NIM GBW07408, was prepared in the same way and used to evaluate the analytical quality of the method. Multi-element solutions in HNO_3 (5%,Sharlab) for ICP analysis, containing known concentrations of the analysed elements, were used to prepare calibration standards. Concentrations between 5 and 600 µg/L were used for Ba, Bi, Cd, Cr, Co, Cu, Pb, Li, Mn, Mo, Ni, Sr, Tl, *V*, Zn, La, Ce, Pr and Nd, and between 1 and 120 µg/L for Sm, Eu, Gd, Tb, Dy, Ho, Er, Tm, Yb, Lu, Sc and Y. Rh was employed as internal standard for ICP-MS analyses. The prepared solutions were analysed with an Elan DRCII spectrometer (Perkin Elmer, Concord, Ontario, Canada).

Table 2
Concentrations (%) of major elements.

Sample	Al	Si	K	Ca	Ti	Fe	Sample	Al	Si	K	Ca	Ti	Fe
A1	7.82	19.24	2.20	8.78	0.39	4.29	U01	7.56	24.61	2.12	9.30	0.44	4.61
A2	7.20	21.88	2.37	6.75	0.38	3.23	U02	8.01	24.81	1.99	8.92	0.42	4.26
Mean	*7.51*	*20.56*	*2.29*	*7.77*	*0.39*	*3.76*	U03	6.01	22.32	1.57	7.91	0.36	3.82
SD	*0.44*	*1.87*	*0.12*	*1.44*	*0.01*	*0.75*	U04	5.87	22.42	2.30	8.06	0.35	3.65
C1	8.62	23.52	1.50	6.52	0.49	5.54	U05	5.64	20.00	1.52	3.66	0.51	3.27
C2	8.69	22.41	1.51	7.10	0.32	3.31	U06	8.13	23.23	2.23	6.66	0.42	4.26
Mean	*8.65*	*22.97*	*1.51*	*6.81*	*0.41*	*4.43*	U07	5.96	21.31	1.00	9.86	0.29	4.32
SD	*0.04*	*0.79*	*0.01*	*0.41*	*0.12*	*1.58*	U08	5.42	19.90	1.49	8.16	0.36	3.65
IR1	9.22	21.66	2.09	5.14	0.40	3.60	U09	5.86	27.43	1.20	6.71	0.43	3.78
IR2	9.75	23.40	2.59	3.17	0.42	3.83	U10	8.30	19.50	1.66	1.91	0.43	5.17
IR3	10.12	24.11	2.42	4.22	0.37	3.67	U11	8.04	18.10	1.48	5.83	0.37	4.57
IR4	5.75	17.84	0.77	7.93	0.34	4.16	U12	6.06	23.26	1.21	7.39	0.38	3.75
IR5	8.72	22.23	2.14	5.95	0.36	3.41	U13	6.48	25.15	2.27	6.6	0.39	3.54
Mean	*8.71*	*21.85*	*2.00*	*5.28*	*0.38*	*3.73*	U14	5.51	21.25	2.49	6.73	0.35	3.23
SD	*1.74*	*2.44*	*0.72*	*1.81*	*0.03*	*0.28*	U15	6.02	22.38	1.48	8.36	0.42	4.25
M1	6.11	20.29	1.42	6.23	0.37	4.41	U16	7.30	21.54	1.94	7.26	0.46	5.11
P1	6.57	22.51	1.38	7.86	0.34	3.79	U17	7.37	24.36	1.93	5.87	0.36	4.03
P2	5.12	22.47	1.32	7.45	0.37	3.49	U18	7.15	19.84	1.60	4.65	0.38	3.69
P3	8.63	25.46	2.80	3.41	0.37	3.29	U19	5.40	27.88	1.38	8.63	0.32	2.82
P4	6.67	25.27	1.47	7.72	0.42	3.70	U20	8.65	22.00	1.95	7.99	0.35	4.58
P5	5.54	23.74	1.11	11.08	0.34	3.47	U21	5.77	24.09	1.39	7.84	0.39	3.52
P6	5.79	20.84	1.88	7.35	0.34	3.78	U22	6.31	21.48	1.65	10.96	0.28	2.29
P7	5.69	24.72	1.10	9.28	0.34	3.50	U23	6.87	22.01	2.74	8.74	0.29	3.38
Mean	*6.29*	*23.57*	*1.58*	*7.74*	*0.36*	*3.57*	U24	5.85	24.76	1.67	5.99	0.39	3.65
SD	*1.17*	*1.71*	*0.60*	*2.33*	*0.03*	*0.19*	U25	8.53	21.49	2.66	4.94	0.39	3.45
S1	6.17	23.98	1.31	6.73	0.39	3.85	U26	6.17	18.22	1.98	7.43	0.38	3.66
S2	7.31	25.83	1.61	2.54	0.48	4.95	U27	6.93	20.10	1.81	8.17	0.21	2.70
Mean	*6.74*	*24.90*	*1.46*	*4.64*	*0.44*	*4.40*	*Mean*	*6.71*	*22.35*	*1.80*	*7.20*	*0.37*	*3.82*
SD	*0.81*	*1.31*	*0.21*	*2.96*	*0.06*	*0.78*	*SD*	*1.04*	*2.49*	*0.45*	*1.93*	*0.06*	*0.68*
T1	7.90	21.02	2.64	7.82	0.40	4.58							
*Mean**	*7.37*	*22.62*	*1.78*	*6.65*	*0.38*	*3.89*							
*SD**	*1.53*	*2.10*	*0.59*	*2.13*	*0.05*	*0.60*							

Note: SD: standard deviation. *Mean and SD of all the reference samples.

2.4. Fourier-transform near-infrared spectroscopy (FT-NIR)

A FT-NIR spectrometer, model Multipurpose Analyzer (MPA) (Bruker, Ettlingen, Germany) equipped with an integrating sphere, was employed for diffuse reflectance near infrared spectra acquisition. For instrument control and data acquisition, Bruker OPUS software 6.5 was used. The FT-NIR measuring conditions employed are the same previously employed by Cascant et al. (2017). A small amount of each powdered sample was put inside a vial of clear glass and then in a laboratory oven at 105 °C for 48 h in order to remove absorbed water. The vials were then plugged and placed in a desiccator to cool down and avoid rehydration.

FT-NIR spectra were then directly obtained by diffuse reflectance. Spectra were recorded in Kubelka–Munk units, in the 14,000–4000 cm[1] region, using a nominal resolution of 4 cm^{-1} and cumulating 50 scans per spectrum. Two measurements of each sample were obtained by rotating the sample vial position between replicates to ensure better reliability. The background spectrum was acquired from the closed integrating sphere using the same instrumental conditions as those employed for the samples.

2.5. Voltammetry of immobilized microparticles (VIMP)

The VIMP measurements were performed at 298 K using a CH I660C potentiostat (Cambria Scientific, Llwynhendy, Llanelli UK). Air-saturated aqueous 0.1 M H_2SO_4 solution (Panreac, Barcelona, Spain) was used as a supporting electrolyte; no deaeration was performed in order to mimic operating conditions for in-field analysis using available portable equipment. The three electrodes arrangement used sample-modified graphite bars of 2 mm diameter (Alpino, BH type) as working electrodes, a platinum wire auxiliary electrode and an Ag/AgCl (3 M NaCl) reference electrode. The analysis of the samples was carried out by extracting, with the aid of a scalpel, 2–5 μg of sample from the section of the ceramic fragment and crushing it with an agate mortar and pestle. The material was extended and grouped forming a fine coating on the plane face of the mortar and then was abrasively transferred onto the graphite electrode (La-Torre-Riveros et al., 2019; Fabrizi et al., 2020).

2.6. Statistical data processing

Data analysis was performed with R (version 3.6.2; R Core Team, 2019). Mahalanobis distance was calculated on the whole dataset in order to detect outliers employing a cut-off value of 0.95. This takes into account correlations within the data that allow the identification of outliers that univariate techniques would not detect (De Maesschalck et al., 2000). Outliers detection was made with "OutlierDetection" R package (version 0.1.1; Tiwari and Kashikar, 2019).

Principal Component Analysis (PCA) is a multivariate statistical technique, often used in archaeometric studies, which allows a reduction of dimensionality employing new variables (the principal components) that are uncorrelated linear combinations of the original ones and captures relevant percentages of the overall variance in a dataset (Baxter, 2004). It was used to evaluate differences among the reference samples (classified typologies of ceramics sherds) and to categorize unclassified materials according to the results of multielement analysis (MA) and FT-NIR spectroscopy. For the MA, three PCA models were built. In the first one only the rare earth elements (REE: La, Ce, Pr, Nd, Sm, Eu, Gd, Tb, Dy, Ho, Er, Tm, Yb, Lu, and Sc and Y) were employed as variables, in the second one all the elements were used, while in the third only the REE were excluded. In all the cases the reference sample set of data were first autoscaled and PCA carried out. Then, the unclassified samples scores were calculated in the PCA models. For the PCA of the NIR analysis, each spectrum was initially processed through the Savitzky-Golay filter (Rinnan et al., 2009; filter order: 2nd, filter length: 31, derivative order: 2nd) with the "signal" R package (version 0.7–6; Signal developers,

Table 3
Concentrations (μg/g) of rare earth elements (REE).

Sample	La	Ce	Pr	Nd	Sm	Eu	Gd	Tb	Dy	Ho	Er	Tm	Yb	Lu	TREE	Sc	Y
A1	29.4	58.0	5.81	21.3	3.78	0.748	2.78	0.297	1.48	0.201	0.566	0.062	0.446	0.054	125	11.1	5.81
A2	25.9	51.7	5.38	19.1	3.98	0.839	3.53	0.426	2.25	0.354	0.953	0.119	0.783	0.102	115	9.87	10.7
Mean	*27.7*	*54.9*	*5.59*	*20.2*	*3.88*	*0.794*	*3.16*	*0.361*	*1.87*	*0.277*	*0.759*	*0.091*	*0.615*	*0.078*	*120*	*10.5*	*8.27*
SD	*2.5*	*4.5*	*0.30*	*1.6*	*0.14*	*0.065*	*0.53*	*0.091*	*0.54*	*0.108*	*0.274*	*0.040*	*0.238*	*0.034*	*7*	*0.8*	*3.47*
C1	51.7	101	9.96	40.4	6.67	1.50	6.17	0.707	3.75	0.567	1.55	0.186	1.22	0.162	225	19.6	17.3
C2	42.8	96.6	8.40	34.7	5.78	1.15	5.73	0.665	3.64	0.584	1.63	0.209	1.43	0.188	204	10.1	20.1
Mean	*47.3*	*98.7*	*9.18*	*37.6*	*6.22*	*1.33*	*5.95*	*0.686*	*3.70*	*0.575*	*1.59*	*0.197*	*1.32*	*0.175*	*214*	*14.9*	*18.7*
SD	*6.3*	*2.9*	*1.10*	*4.0*	*0.63*	*0.25*	*0.32*	*0.030*	*0.08*	*0.012*	*0.06*	*0.016*	*0.15*	*0.019*	*15*	*6.7*	*2.0*
IR1	26.3	52.7	5.64	19.9	4.24	0.816	3.60	0.414	2.12	0.337	0.844	0.105	0.686	0.090	118	11.1	9.08
IR2	20.2	43.4	4.55	15.9	3.46	0.708	2.94	0.342	1.72	0.254	0.668	0.080	0.537	0.071	94.9	11.1	6.28
IR3	20.6	42.9	4.60	15.9	3.45	0.712	2.94	0.342	1.73	0.254	0.673	0.083	0.544	0.072	94.8	10.3	7.02
IR4	24.8	48.4	5.12	17.9	3.53	0.717	3.02	0.318	1.57	0.223	0.614	0.073	0.481	0.061	107	6.93	5.42
IR5	27.1	55.9	5.81	20.2	4.26	0.821	3.75	0.423	2.18	0.327	0.880	0.108	0.726	0.096	123	10.9	8.18
Mean	*23.8*	*48.6*	*5.14*	*18.0*	*3.79*	*0.755*	*3.25*	*0.368*	*1.86*	*0.279*	*0.736*	*0.090*	*0.595*	*0.078*	*107*	*10.1*	*7.20*
SD	*3.2*	*5.7*	*0.58*	*2.1*	*0.42*	*0.058*	*0.39*	*0.047*	*0.27*	*0.050*	*0.118*	*0.016*	*0.105*	*0.014*	*13*	*1.8*	*1.46*
M1	26.4	54.2	5.47	19.5	4.10	0.902	3.89	0.506	2.84	0.469	1.30	0.167	1.09	0.142	121	11.7	14.5
P1	39.4	87.2	7.76	31.7	5.24	1.15	5.05	0.613	3.43	0.561	1.57	0.202	1.37	0.177	185	12.6	17.2
P2	30.3	62.1	6.12	21.1	4.17	0.940	4.02	0.465	2.47	0.386	1.05	0.125	0.827	0.106	134	8.34	9.82
P3	24.1	51.6	5.34	18.6	4.05	0.810	3.53	0.430	2.29	0.351	0.957	0.122	0.830	0.108	113	12.3	8.13
P4	33.7	69.5	6.86	23.6	4.72	1.06	4.46	0.526	2.81	0.439	1.18	0.144	0.934	0.121	150	9.66	10.5
P5	27.0	52.8	5.37	18.6	3.82	0.888	3.57	0.417	2.23	0.341	0.909	0.108	0.694	0.090	117	9.20	9.23
P6	18.9	38.0	3.79	13.1	2.78	0.608	2.64	0.303	1.76	0.264	0.719	0.089	0.591	0.077	83.6	6.55	6.09
P7	32.5	65.5	6.58	22.3	4.62	1.08	4.58	0.541	2.98	0.478	1.31	0.164	1.07	0.140	144	10.2	12.3
Mean	*29.0*	*60.1*	*5.91*	*21.1*	*4.19*	*0.931*	*3.97*	*0.475*	*2.60*	*0.411*	*1.12*	*0.140*	*0.926*	*0.120*	*132*	*10.1*	*11.0*
SD	*6.3*	*14.7*	*1.20*	*5.3*	*0.73*	*0.174*	*0.75*	*0.094*	*0.52*	*0.094*	*0.27*	*0.036*	*0.247*	*0.032*	*32*	*2.1*	*3.6*
S1	26.3	52.2	5.16	19.1	3.44	0.784	3.02	0.368	1.94	0.294	0.790	0.093	0.599	0.076	114	9.56	9.06
S2	32.3	64.5	6.45	26.5	4.49	1.01	4.08	0.483	2.54	0.381	0.976	0.112	0.700	0.087	145	15.2	12.1
Mean	*29.3*	*58.4*	*5.80*	*22.8*	*3.97*	*0.898*	*3.55*	*0.425*	*2.24*	*0.338*	*0.883*	*0.103*	*0.649*	*0.081*	*129*	*12.4*	*10.6*
SD	*4.2*	*8.7*	*0.91*	*5.2*	*0.74*	*0.161*	*0.75*	*0.081*	*0.43*	*0.061*	*0.132*	*0.013*	*0.071*	*0.008*	*22*	*4.0*	*2.1*
T1	27.4	55.4	5.49	19.0	3.31	0.597	2.35	0.229	1.17	0.156	0.468	0.050	0.369	0.044	116	8.32	3.76
Mean*	*29.4*	*60.2*	*5.98*	*21.9*	*4.19*	*0.893*	*3.78*	*0.441*	*2.35*	*0.361*	*0.980*	*0.120*	*0.796*	*0.103*	*131*	*10.7*	*10.1*
SD*	*7.9*	*16.9*	*1.42*	*6.7*	*0.90*	*0.219*	*1.01*	*0.126*	*0.72*	*0.124*	*0.344*	*0.045*	*0.302*	*0.041*	*36*	*2.9*	*4.4*
U01	66.0	148	12.71	49.6	7.93	1.65	6.97	0.842	4.49	0.689	1.90	0.226	1.50	0.189	303	14.6	21.1
U02	45.2	95.3	8.33	33.7	5.42	1.12	4.80	0.588	3.16	0.488	1.35	0.164	1.08	0.136	201	11.0	16.1
U03	29.5	56.4	6.09	22.6	4.04	0.899	3.50	0.439	2.41	0.384	1.08	0.131	0.886	0.110	128	11.3	12.0
U04	25.0	47.2	4.86	17.0	3.40	0.747	2.93	0.360	1.95	0.298	0.813	0.094	0.628	0.077	105	10.4	9.9
U05	23.9	46.5	4.78	16.6	3.09	0.634	2.73	0.330	1.76	0.282	0.795	0.102	0.697	0.092	102	8.14	7.96
U06	29.3	57.3	6.09	23.2	4.11	0.889	3.82	0.492	2.77	0.456	1.25	0.157	1.03	0.132	131	12.2	12.8
U07	30.2	52.9	6.16	24.7	4.44	0.994	4.15	0.532	2.99	0.500	1.37	0.169	1.10	0.140	130	7.39	14.5
U08	23.7	46.5	4.71	16.5	3.28	0.702	3.09	0.391	2.20	0.361	0.982	0.123	0.798	0.103	103	8.98	11.0
U09	28.5	57.7	5.77	24.2	3.89	0.869	3.66	0.431	2.28	0.346	0.938	0.112	0.726	0.093	129	8.26	9.56
U10	23.6	50.0	5.13	17.8	3.32	0.612	2.56	0.247	1.20	0.158	0.443	0.049	0.318	0.040	105	9.40	3.04
U11	27.5	55.7	5.71	20.2	3.86	0.784	3.29	0.356	1.84	0.270	0.756	0.094	0.628	0.082	121	9.53	6.56
U12	22.9	45.5	4.58	15.8	3.15	0.724	2.90	0.352	1.86	0.289	0.766	0.090	0.590	0.075	100	9.54	8.45
U13	21.6	42.2	4.45	16.6	3.21	0.659	2.88	0.336	1.73	0.263	0.708	0.085	0.575	0.075	95.4	9.33	8.53
U14	28.1	56.9	5.54	18.7	3.64	0.753	3.23	0.364	1.95	0.290	0.816	0.104	0.718	0.094	121	10.3	7.15
U15	33.0	67.8	6.69	28.4	4.69	1.09	4.47	0.534	2.87	0.452	1.22	0.147	0.969	0.124	152	10.0	14.4
U16	50.1	97.2	9.75	41.3	7.02	1.67	6.58	0.796	4.30	0.692	1.93	0.247	1.62	0.217	223	20.0	22.3
U17	46.3	88.3	8.44	34.2	5.47	1.20	5.15	0.617	3.41	0.552	1.55	0.201	1.33	0.174	197	10.6	15.4
U18	20.4	42.6	4.30	16.0	3.11	0.645	2.64	0.295	1.52	0.233	0.659	0.084	0.577	0.078	93.2	10.3	6.12
U19	20.7	40.7	4.16	14.6	2.99	0.679	2.75	0.349	1.92	0.322	0.902	0.116	0.798	0.104	91.0	7.01	9.08
U20	33.1	66.0	6.70	23.2	4.83	1.06	4.59	0.587	3.29	0.549	1.53	0.198	1.30	0.169	147	14.5	14.8
U21	33.0	66.8	6.64	24.7	4.51	1.04	4.31	0.509	2.74	0.424	1.15	0.140	0.911	0.118	147	8.60	10.3
U22	18.7	39.7	3.91	13.2	2.76	0.587	2.56	0.299	1.59	0.245	0.671	0.084	0.555	0.073	85	7.46	6.42
U23	22.8	47.5	4.70	16.1	3.49	0.741	3.12	0.361	1.93	0.298	0.829	0.103	0.695	0.091	103	7.92	7.52
U24	26.9	52.5	5.30	18.2	3.66	0.846	3.38	0.404	2.17	0.341	0.914	0.113	0.749	0.097	116	11.8	8.79
U25	26.1	55.2	6.01	20.5	4.32	0.878	3.72	0.433	2.22	0.328	0.880	0.107	0.714	0.093	121	12.4	7.37
U26	32.3	65.8	6.57	24.2	4.55	0.906	3.87	0.378	1.89	0.261	0.732	0.084	0.576	0.072	142	9.02	6.56
U27	22.8	46.7	4.66	15.7	3.47	0.758	3.27	0.380	2.03	0.319	0.899	0.111	0.754	0.101	102	8.82	8.52
Mean#	*30.0*	*60.6*	*6.03*	*22.5*	*4.14*	*0.894*	*3.74*	*0.444*	*2.39*	*0.374*	*1.03*	*0.127*	*0.846*	*0.109*	*133*	*10.3*	*10.6*
SD#	*10.6*	*23.3*	*1.93*	*8.6*	*1.21*	*0.276*	*1.13*	*0.144*	*0.81*	*0.134*	*0.37*	*0.048*	*0.311*	*0.040*	*48*	*2.7*	*4.6*
LOD	0.0007	0.0007	0.0002	0.001	0.0003	0.0003	0.002	0.00008	0.0004	0.00005	0.0002	0.0001	0.0003	0.00008	–	0.0009	0.016

Note: TREE: total REE concentration. SD: standard deviation. LOD: limit of detection. * Mean and SD of all the reference samples. # Mean and SD of all the unclassified samples.

2013). The signals from the wavenumbers between 7350 and 4000 cm^{-1} were employed as variables due to the low background level and the presence of major and minor bands. The signals of the reference samples in the selected region interval were mean centred and the PCA model built. Then, the scores of the unclassified samples were calculated on the basis of this PCA model. The PCA diagrams were made using "ggplot2" R package (version 3.2.1; Wickham, 2016).

3. Results and discussion

3.1. Multielement analysis

The results of MA are given in Table 2 (major elements), Table 3 (REE) and in the supplementary materials SM1 (trace elements).

Tarraconensis, Campanian and Ibero-Roman samples have higher

levels of Al (7.90–10.12%, except for IR4, 5.75%) compared to the other typologies (5.12–7.82%, except for P3, 8.63%). Most Punic, Saguntine and Campanian samples have higher concentrations of Si (22.47–25.83%, except for P6, 20.84%) than the other reference samples (17.84–22.23%, except for IR2, 23.40%, and IR3, 24.11%). Ibero-Roman, Adriatic and Tarraconensis amphorae have higher amounts of K (2.09–2.64%), although the highest K concentrations were measured in P3 (2.80%) and the lowest ones in IR4 (0.77%). The reference amphorae have similar concentrations of the other major elements such as Ca (2.54–11.08%), Ti (0.32–0.49%) and Fe (3.23–5.54%). It is worth noting that P3, which was previously classified as a Punic amphora produced in Ibiza (Spain), is slightly higher in Al (8.63%) and K (2.80%) and lower in Ca (3.41%) than the other Punic samples. This could be related to the use of clay characterized by different levels of carbonates. However, previous archaeometric studies of Punic amphorae from the Gibraltar area indicated the addition of calcareous clasts to the ceramic mixture that may explain the different chemical profiles (Maniatis et al., 1984).

With regard to the REE, the Campanian samples have the highest lanthanides and Y levels (lanthanides sum, TREE: 204–225 µg/g; Y: 17.3–20.1 µg/g), while the different groups have similar amounts of Sc (6.55–19.6 µg/g) (Table 3). High REE concentrations in Campanian amphorae maybe related to the use of volcanic rock fragments as temper (Belfiore et al., 2014) as recently high REE contents have been measured in Campania pottery (Grifa et al., 2019).

Results of the trace elements (supplementary material, SM1), show that the different types have comparable concentrations of Ba, Bi, Cd, Cr, Cu, Li, Pb, Sr, Tl and *V*. Sample P3 had a lower Sr concentration (125 µg/g) compared to the Punic samples from the Gilbraltar Strait area (251–564 µg/g), which corresponds with its lower Ca concentration. The sample from the amphora form Marseille had the highest levels of Mo (8.60 µg/g) and Ni (64.6 µg/g). Amphorae from Campania, Marseilles, Sagunto and Tarragona had higher concentrations of Co (24.6–39.6 µg/g) than the other reference samples (11.3–28.0 µg/g). Adriatic, Ibero-Roman and Tarraconensis amphorae had the lowest levels of Zn (40.8–57.0 µg/g). The highest concentrations of Mn were detected in Campanian (C1 and C2) and Marseilles (M1) amphorae (939–1079 µg/g) with C1 concentrations being higher than C2 in almost all trace elements.

The elemental concentrations of Ca and Sr in the Ibero-Roman samples suggest that the amphorae provenance could be limited to the Catalonia area since the use of moderately calcareous raw materials excludes their production in the area of Valencia, while the concentrations of strontium (Sr ≤ 456 µg/g) disallow a provenance from the Alicante area (Tsantini et al., 2019).

From the Mahalanobis distance, none of the unknown samples were revealed as outliers within the whole sample set, although they occasionally showed higher or lower elemental concentrations than those in the reference set.

3.2. FT- NIR spectroscopy

The FT-NIR spectra of the reference samples are shown Fig. 2, while the spectra of the unclassified samples are reported in the supplementary materials (SM2). The bands characterized by the highest intensities were identified in all the samples at about 7080, 5200 and 4525 cm^{-1}. These bands correspond to particular water bands and can be attributed to OH stretch, H-O-H bend and metal-OH bend, respectively (Clark et al., 1990). Previous studies have shown that the intensity of these bands is inversely correlated to the firing temperature, which induces molecular water loss and mineral dehydroxylation (Bruni et al., 2001, 2018). It is worth noting that, among samples which received the same classification, the intensity of these bands varied considerably (e.g. P1 P2 and P4 vs P5-7, Fig. 2), but it is not uncommon that amphorae of the same type have undergone different firing temperatures (e.g.: Sondi and Slovenec, 2003).

Minor bands were found also between 4330 and 4255 cm^{-1}. Combination and overtone bands of carbonate minerals are usually identified in this range (Gaffey, 1987) but also some clay minerals such as muscovite and illite show bands for Al-OH bends at about 4255 cm^{-1} (Clark et al., 1990). However, the heterogeneous ceramic matrix and the relatively low sensitivity of FT-NIR spectroscopy make identification of the mineralogical phases present problematic.

3.3. Electrochemical analysis

Fig. 3 shows the square wave voltammetric response for the Campanian sample C1. The voltammetric response of microparticulate deposits of pottery samples in contact with an acidic solution when the potential is scanned in the negative direction consists of a series of cathodic signals between 0.8 and − 0.8 V vs. Ag/AgCl (labelled C_1 to C_4 in Fig. 3a) confined between the gross extreme currents corresponding to the oxygen evolution reaction (OER) and hydrogen evolution reaction (HER) processes. The signals C_1 to C_3 can be attributed to the reduction of Fe(III) minerals of different composition, crystallinity, degree of hydration and grain size whereas the signal C_4 results from the superposition of the reduction of dissolved oxygen (oxygen reduction reaction, ORR) superimposed on the reduction of hematite (Di Turo et al., 2018; La-Torre-Riveros et al., 2019; Fabrizi et al., 2020). The positive-going potential scan voltammograms (Fig. 3b) display a series of anodic signals (labelled A_1 to A_4) corresponding to the anodic counterparts of the reduction of Fe (III) minerals and/or oxidation of Fe (II) minerals. The relevant point to emphasize is that the relative height of the voltammetric signals varies from one ceramic sample to another as a result of the differences in composition, crystallinity and degree of hydration determining changes in the signals C_1-C_4 and A_1-A_4 but also in the extreme currents for the OER and HER signals due to the catalytic effect exerted by several iron minerals on such processes.

3.4. PCA classification by MA data

The PCA using the results of the REE analysis is shown in Fig. 4.

Fig. 4a shows that the use of REE allows discrimination between Punic and Ibero-Roman amphorae, which are the most numerous of the reference samples. Two main groups can be distinguished: Punic and the Marseilles samples (large rectangle with red border) show lower values of PC2 and are scattered on PC1-axis. On the other hand, the Ibero-Roman amphorae, together with Saguntine and Tarraconensis ones (large rectangle with blue border) have higher values of PC2 and are less dispersed on PC1-axis. Adriatic sample A2 falls within the first group while A1 falls within the second one. The Campanian samples have the lowest values of PC1 due to their high REE concentrations, although C2 shows REE levels close to the Punic samples. The two Campanian samples are wide apart on the PC2-axis. From these results, the two groups are subsequently referred to as P·M·A (Punic, Marseilles, Adriatic) and I·S·T·A (Ibero-Roman, Saguntine, Tarraconensis, Adriatic). PC1 (Fig. 4b) is negatively correlated with all the REE, which indicates that its value is mainly related to the overall content of REE. The PC2 loadings (Fig. 4c) with lanthanides indicates that while light REE (La to Gd) are important variables in the positive direction of PC2, the heavier REE (Tb to Lu) are more important in the negative PC2 direction. PC2 also shows a negative correlation with Y, which behaves as a heavy REE (Bau, 1996), and has the highest positive correlation with Sc. The PCA model employing all measured elemental concentrations as variables (supplementary material SM3) suggests that the correlations of lanthanides with Ca and Sr are higher for the heavy REE than for the light REE, as shown by PC2 loadings (supplementary materials SM3c). Previous studies have shown that the REE-carbonates compatibility increases with increasing atomic number of the REE (Laveuf and Cornu, 2009; Zhaozhou et al., 2012). Thus, the different impact of light and heavy REE in the model could be linked to REE fractionation processes that are influenced by the amount of carbonate minerals present in the
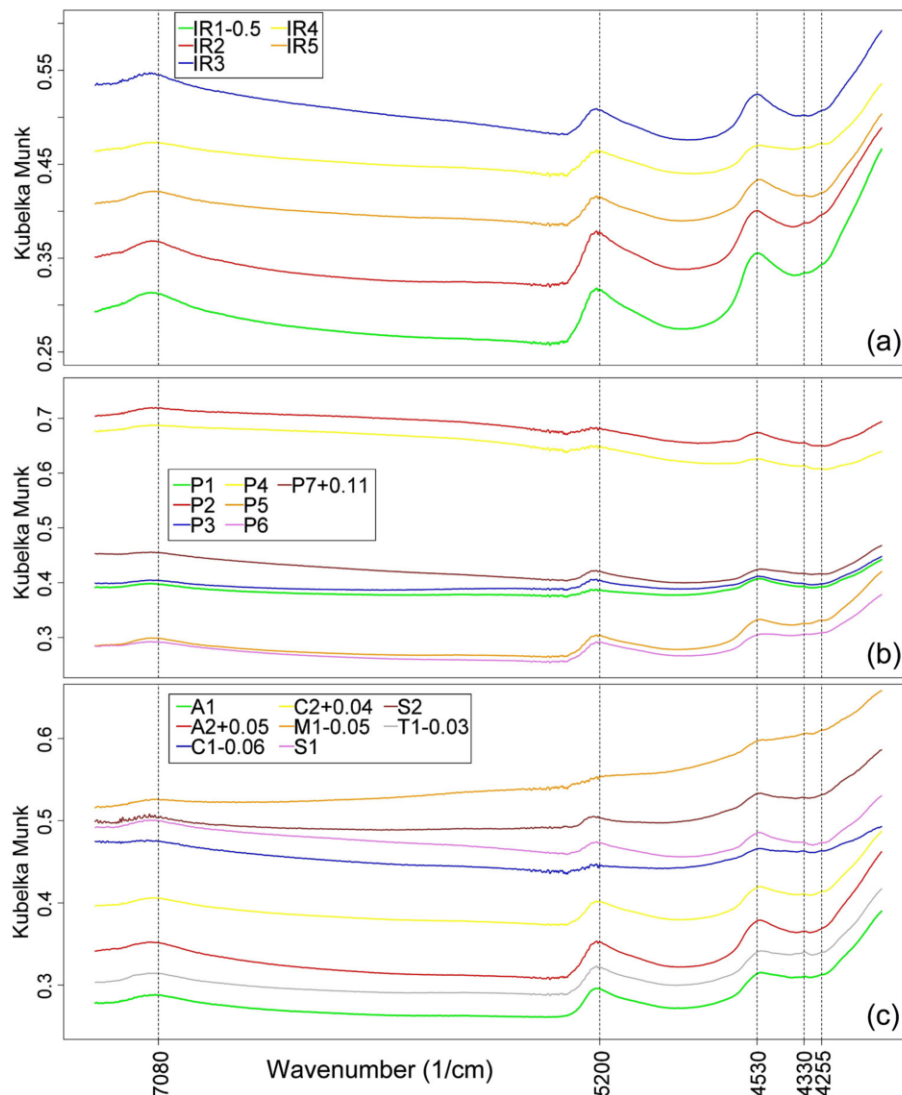
Fig. 2. FT-NIR spectra for the (a) Ibero-Roman (IR), (b) Punic (P), and (c) Adriatic (A), Campanian (C), Marseilles (M), Saguntine (S) and Tarraconensis (T) reference samples between 7350 and 4000 cm^{-1}. Spectra were offset on the y-axis to avoid overlapping by the value indicated in the legend.

raw materials employed to make the studied amphorae.

Most of the unclassified samples (Table 4), fall within the P·M·A group, while U11, U14, U25 and U26 are in the I·S·T·A group. U01 and U16 have high PC1 scores, due to their REE levels, which suggest that they could be fragments of Campanian amphorae. U04, U09, U18 and U24 as well as U02 fall between the two main groups and cannot be readily placed in either group. U10 is located near the I·S·T·A samples, while U02, U07, U17, U19 and U22 are closer to the P·M·A group.

Distinguishing between Punic and Ibero-Roman amphorae was one of the main goals of this work due to the importance that these two typologies of amphorae have in the Sagunto Archaeological Museum ceramic collection. However the PCA model employing only major and trace elements (supplementary materials, SM3d-f) does not allow these two groups to be separated since P3 falls among the Ibero-Roman samples and IR4 among the Punic ones. Furthermore, Campanian sample C2 falls between the two groups. Many unclassified samples could not be identified according to the results of this PCA since they do not fall within any group. The PCA employing REE, major and trace elements (supplementary materials, SM3a-c) slightly improves the

typological grouping of the samples. However, Punic sample P3 from the Ibiza amphora is located with the Ibero-Roman ones (supplementary materials SM3a) and Ibero-Roman samples are scattered on PC2 with IR4 falling closer to P6 and not with the other Ibero-Roman amphorae. The REE concentrations were shown to be the pivotal variables for discriminating the different main amphora typologies. This capability of REE to allow discrimination between geologic samples from different provenances has been shown for both rocks (Gallello et al., 2016; Orozco-Köhler and Gallello, 2017; Ramacciotti et al., 2019) and artificial materials such as mortars (Gallello et al., 2017) and ceramics (González et al., 2018; Saiano et al., 2019).

Finally, the variability in REE concentrations observed in some samples from the same morphological typologies could be explained by the different production locations and, consequently, the use of different raw materials.

3.5. PCA classification by FT-NIR spectra

Fig. 5 a and b shows the Samples/Scores Plot of the PCA for FT-NIR
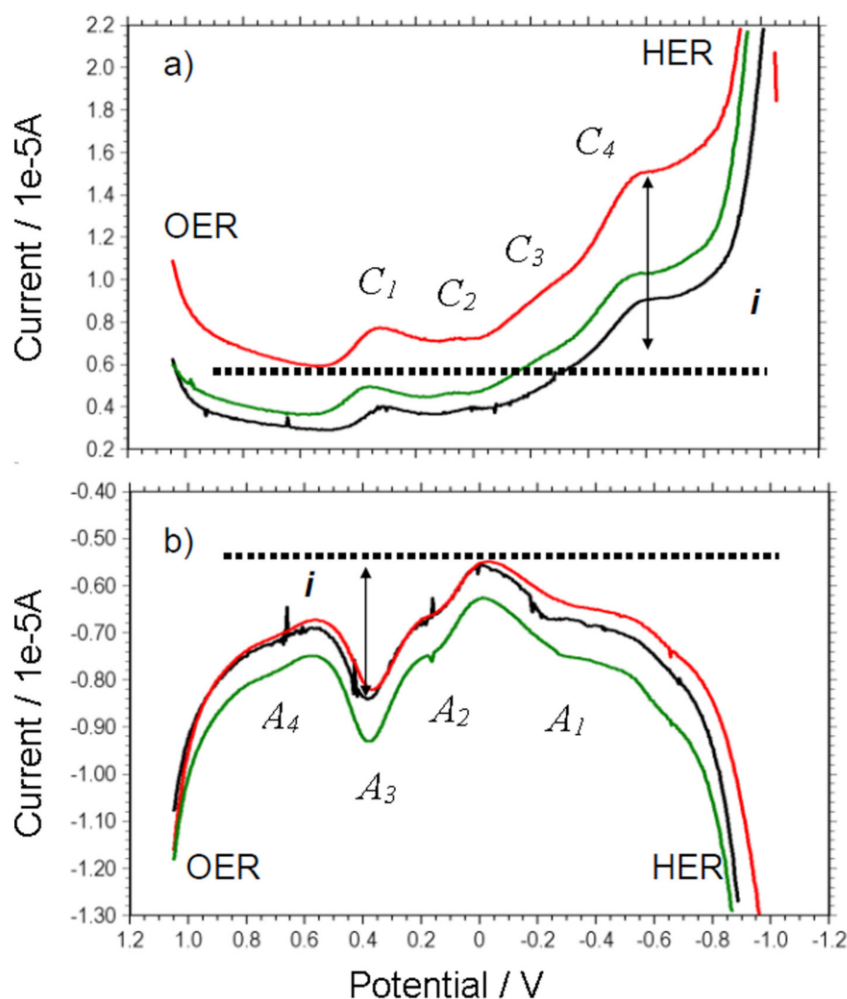
Fig. 3. Square wave voltammograms of Campanian sample C1 (three replicate measurements are superimposed). Potential scan initiated at a) +1.25 V in the negative direction; b) -0.85 V in the positive direction; potential step increment 4 mV; square wave amplitude 25 mv; frequency of 5 Hz. C_1-C_4 denote the cathodic signals and A_1-A_4 the anodic signals recorded in negative-going and positive-going potential scans, respectively. OER: oxygen evolution reaction; HER: hydrogen evolution reaction. The arrowed lines mark the base lines used for peak current (*i*) measurements used to analyse voltammetric data.

spectroscopy. PC1 (51.5%) and PC2 (17.5%) account for 69% of the variance, however, PC3 that explained 7.1% of the variance, was also taken into consideration.

Both Ibero-Roman and Punic samples are scattered on PC1, although Ibero-Roman samples have lower scores than Punic ones, except for P5 and P6 which fall on the negative PC1-axis. However, the discrimination is further improved on PC3 since P5 and P6 have negative scores while Ibero-Roman samples have positive scores, except for IR5 (Fig. 5b). Adriatic and Tarraconensis samples are plotted among the Ibero-Roman samples in Fig. 5a but have lower PC3 scores (Fig. 5b). The other Punic samples fall along the positive PC1-axis and are scattered on the PC2 (Fig. 5a) and PC3 (Fig. 5b) axes with Adriatic, Tarraconensis, Saguntine and Marseilles samples. The Campanian samples, C2 falls between Ibero-Roman and Punic samples and C1 with Punic and Marseilles amphorae. Thus, according to these PCA data, two main groups are distinguished: Group I (Ibero-Roman), characterized by low PC1 scores and higher PC3 scores, and Group P·C·M·S (Punic, Campanian, Marseilles and Sagunto), characterized by positive PC1 scores and scattered on PC2 and PC3 axes. A third group could possibly be separated with P5-6, and the Adriatic and Tarraconensis samples, characterized by negative values of PC1 like Group I but discriminated by

negative values for PC3.

Fig. 6 shows four representative reference samples, raw (Fig. 6a) and processed (Fig. 6b) FT-NIR spectra and PCA loadings for the first three principal components (Fig. 6c) which explain 51.5%, 17.5% and 7.1% of the total variance in the identified samples set, respectively. All three PCs (Fig. 6c) show the highest correlations with the second derivative values of the signal (Fig. 6b) between 7350 and 7030 cm^{-1}, 5500 and 5120 cm^{-1}, and 4720 and 4460 cm^{-1}. These regions correspond to water combination and overtone bands at 7080, 5200 and 4525 cm^{-1} in the original spectra (Fig. 6a). PC1 loadings peak (Fig. 6c) between 4385 and 4220 cm^{-1} are related to the feature of the spectra in proximity of the bands at 4330 and 4255 cm^{-1} of the original spectra, and are probably linked to the presence of carbonate (Gaffey, 1987) or clay minerals (Clark et al., 1990). However, the very low loadings values (within ± 0.05) indicate a poor correlation with PC1. The samples characterized by high PC1 scores (e.g. P4) are characterized by less intense bands than IR1 for example, which suggest higher firing temperatures (Bruni et al., 2001, 2018).

Concerning PC2 and PC3, it is worth noting that loading values indicate fluctuations within the main bands, evidencing their composite nature. For example, PC2 loadings with the second derivative around
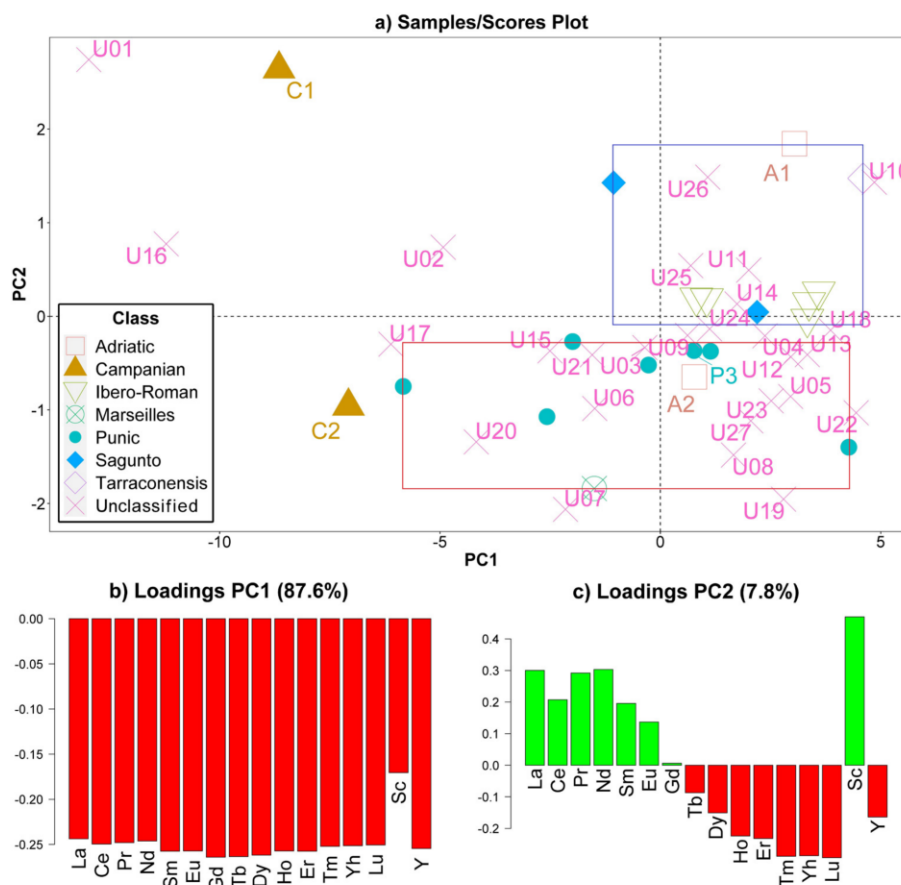
Fig. 4. Samples/Scores PCA diagram using rare earth elements as variables, and Variables/Loadings barplots for (b) PC1 and (c) PC2.

the 5200 cm^{-1} band of molecular water vary considerably between 5500 and 5120 cm^{-1}. Similarly, loadings fluctuate between 4720 and 4460 cm^{-1}, the spectral range of the metal-OH bend at about 4525 cm^{-1}. Both PC2 and PC3 show loadings fluctuations in the region between 7350 and 7030 cm^{-1}. PC3 has its strongest peak at about 4575 cm^{-1}, which corresponds to a small bump in the second derivative line plot. Strong peaks also occur between 4460 and 4220 cm^{-1}, which are probably linked to carbonate and perhaps clay minerals.

According to previous literature, spectra of pure minerals show

bands which allow a classification based on characteristic wavenumbers. As observed by some authors the position of carbonate bands slightly change when calcite or dolomite are analysed (Gaffey, 1987) and, similarly, the position of metal-OH bend changes according to the cations linked to the hydroxyl group and to mineral structure (Clark et al., 1990). However, bands of composite materials like pottery are combinations of different minerals which can determine the presence of asymmetric features, such as the shoulder at about 4575 cm^{-1} in the four example spectra (Fig. 6b), as well as shift after Savitzky-Golay

Table 4

Typologies of the unclassified samples according to multielement analysis (MA), FT-NIR and VIMP, and their final attribution.

Sample	MA	FT-NIR	VIMP	Final attribution	Sample	MA	FT-NIR	VIMP	Final attribution
U01	C	Uncertain	A·P·C·S	C?	U15	P·M·A	Uncertain	S·M	M?
U02	Uncertain	P·C·M·S	S·M	S or M	U16	C	P·C·M·S	S·M	C?
U03	P·M·A	P·C·M·S	A·P·C·S	P	U17	Uncertain	P·C·M·S	I	Not classified
U04	Uncertain	I	I	I	U18	Uncertain	P·C·M·S	A·P·C·S	P or S
U05	P·M·A	P·C·M·S	A·P·C·S	P	U19	Uncertain	P·C·M·S	I	Not classified
U06	P·M·A	P·C·M·S	I	Not classified	U20	P·M·A	P·C·M·S	A·P·C·S	P
U07	Uncertain	P·C·M·S	A·P·C·S	P or S	U21	P·M·A	P·C·M·S	S·M	M?
U08	P·M·A	P·C·M·S	S·M	M?	U22	Uncertain	P·C·M·S	S·M	S or M
U09	Uncertain	P·C·M·S	A·P·C·S	P or S	U23	P·M·A	Uncertain	A·P·C·S	P or A
U10	Uncertain	Uncertain	S·M	S?	U24	Uncertain	I	I	I
U11	I·S·T·A	P·C·M·S	S·M	S	U25	I·S·T·A	P·C·M·S	A·P·C·S	Not classified*
U12	P·M·A	P·C·M·S	S·M	M?	U26	I·S·T·A	Uncertain	A·P·C·S	S or A
U13	P·M·A	Uncertain	A·P·C·S	P or A	U27	P·M·A	Uncertain	A·P·C·S	P or A
U14	I·S·T·A	P·C·M·S	I	Not classified					

Note: A = Adriatic, C = Campanian, I = Ibero-Roman, M = Marseilles, P = Punic, S = Saguntine, T = Tarraconensis. *U25 was not classified since the analytical classification is in contradiction with the typological one.
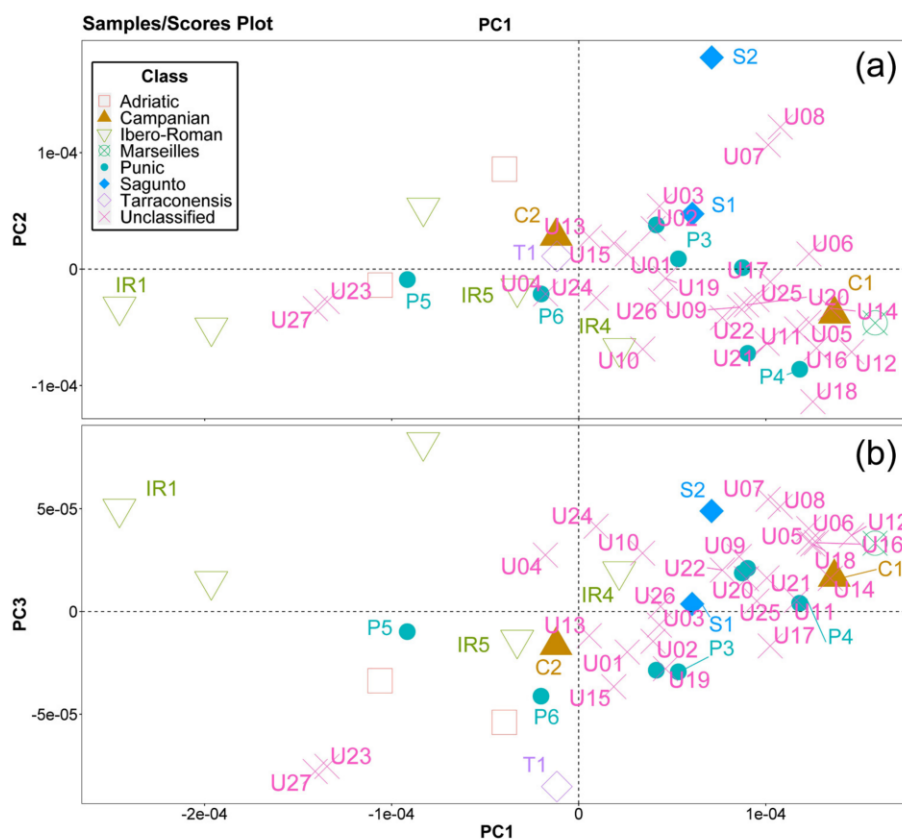
Fig. 5. Samples/Scores diagrams for PCA of FT-NIR spectroscopy employing the signals from the region between 7350 and 4000 cm^{-1} as variables: a) PC2 vs PC1, b) PC3 vs PC1.

filter processing (McClure, 2007). Thus, while slope changes and consequent fluctuation of PC loadings (Fig. 6b-c) likely indicate differences in the ceramic matrix structures, the identification of the exact mineralogical phases is problematic and needs more appropriate analyses. Most of the unclassified fragments plot within the P·C·M·S group, while only samples U04 and U25 appear related to the Ibero-Roman samples. U01, U10, U13, U15 and U26 fall between the two main groups. Finally, U23 and U27 are closer to Punic and Adriatic samples but they have lower PC1 and PC3 scores.

3.6. Grouping of samples by VIMP peaks

Absolute peak values were not used for sample comparison because the single measurements are not comparable since the absolute amount of powder transferred onto the electrode surface cannot be exactly controlled. Accordingly, replicate experiments for the same sample display different absolute values of the peak currents. However, the plots of one peak current vs another peak current fall within a common tendency curve for each specimen, thus allowing the grouping of ceramic samples (Di Turo et al., 2018; La-Torre-Riveros et al., 2019; Fabrizi et al., 2020). Plotting $I(C_3)$ vs. $I(C_1)$ (supplementary materials, SM4) does not allow different groups of samples to be distinguished, thus denoting that these signals have no discriminating ability. In contrast, plots of $I(C_1)$ vs. I(OER) allowed the separation of the data points for the reference samples into different tendency lines. This can be seen in Fig. 7a for samples from Ibero-Roman, Adriatic, and Saguntum, and Fig. 7b for samples of Punic, Campanian and Marseille provenance. Considered together, voltammetric data permit discrimination between three groups: the first group (I) reflects Ibero-

Roman production, the second includes the Saguntum (S2) and Marseille samples (S·M), and the third Adriatic, Punic, Campanian and Saguntine (S1) ceramics (A·P·C·S). However, the data points of samples P2 and T1 do not fall in any of these groups. In general, the first group of samples is characterized by relatively higher concentration of Al and K, whereas the samples of the second group are rich in Si. However differences in voltammetric response arise not only as a result of differences in raw materials, but also to those in firing temperature and reductive/oxidative atmosphere, among other factors (La-Torre-Riveros, 2019; Fabrizi et al., 2020).

All the unclassified samples were able to be classified according to VIMP results (Table 4). U04, U06, U014, U17, U19 and U24 are related to Group I (Fig. 7c), and U02, U08, U10-12, U15, U16 and U21 and U22 to the Group S·M (Fig. 7c). The remaining samples are in Group A·P·C·S (Fig. 7d).

3.7. Identification of the unclassified samples according to the three methods

The results obtained for the identification of the unclassified samples according to PCA (employing MA and FT-NIR data) and VIMP results are given in Table 4.

The classification of the samples by these techniques depends on different ceramic features. Elemental concentrations are mainly a result of the raw materials employed for the production of the amphorae, while FT-NIR and VIMP results are also influenced by manufacturing conditions such as firing atmosphere and temperature. The possibility of cross-checking the statistical results of the three approaches allowed the reduction of the possible classifications to one or two typologies of
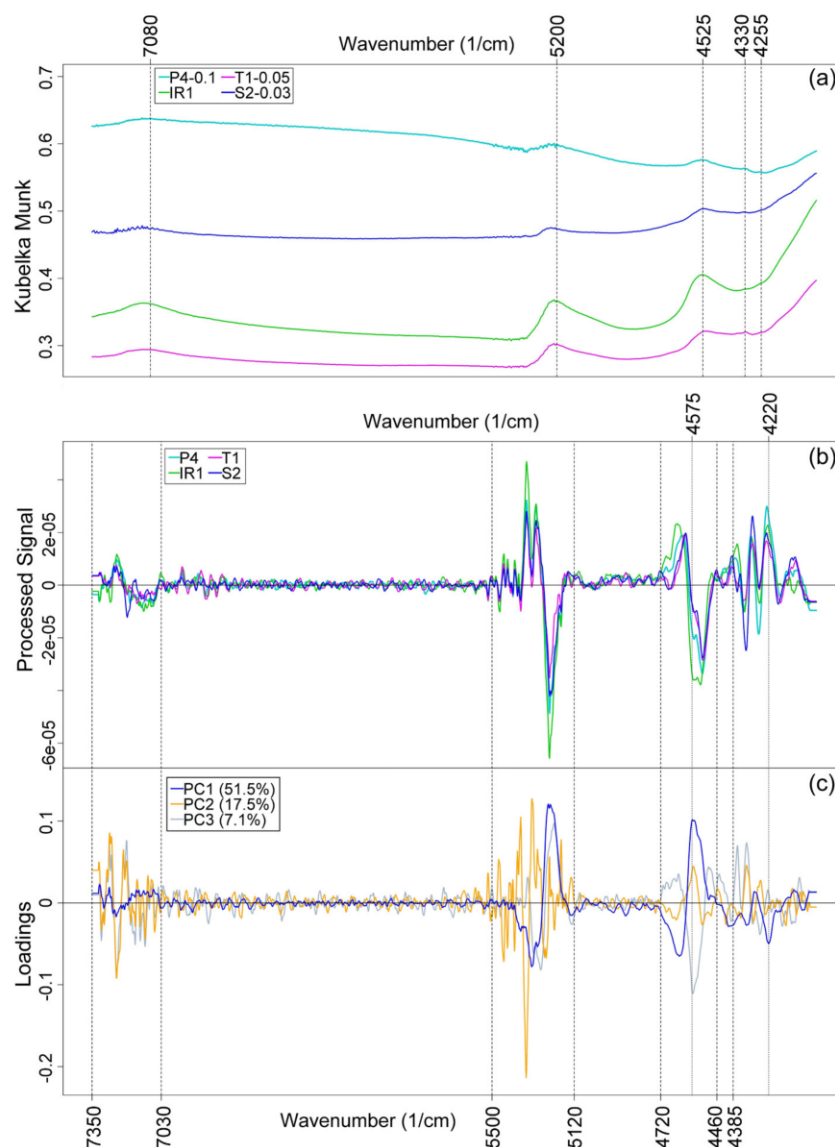
Fig. 6. Comparison of a) raw FT-NIR data between 7350 and 4000 cm^{-1} of four representative reference samples (spectra were offset on the y-axis by the value indicated in the legend to avoid overlapping); b) the same spectra processed through Savitzky-Golay filter; c) PC1, PC2 and PC3 variables/loadings plot.

amphora for most of the studied samples (Fig. 8a). However, some samples could not be classified because the different methods gave inconclusive results (Fig. 8b), although, in some cases, multielement analysis results permitted the first classification to be improved based on the statistical results (Fig. 8c).

The PCA using REE as variables allowed the classification of seventeen of the twenty-seven unclassified samples, while twenty were able to be classified using FT-NIR. On the other hand, all of the unclassified samples received a classification using VIMP.

Therefore, while some samples were classified just by cross-checking PCA results, as previously stated, some classifications need to be better explained. Samples U04, U09, U18 and U24 were between the I·S·T·A and P·M·A groups in the REE PCA (Fig. 4a) but FT-NIR and VIMP results limited their possible classification. U04 and U24 were classified as Ibero-Roman according to both the latter techniques. U09 and U18 are possibly fragments from Punic or Saguntine amphorae; a Campanian classification was excluded for these samples, and U07, due to low

TREE amounts. U01 and U16 were classified as Campanian due to their high amount of REE (TREE is 303 μg/g and 223 μg/g, respectively, see also Fig. 4a) and high levels of Mn (1327 μg/g and 1044 μg/g, respectively). In case of U16, morphological features also suggested this origin (Table 1). PCA cross-checking suggests a Punic, Saguntine or Campanian classification for sample U07 but low TREE levels excluded a Campanian provenance. U10 was classified as S·M only through VIMP results, however, both REE and FT-NIR PCA (Figs. 4 and 5) suggest a Saguntine origin. Four samples were classified as Marseilles amphora fragments (U08, U12, U15, and U21) but since only one reference sample of this typology was analysed, the classifications are uncertain. However, the high concentration of Mo in U08 (8 μg/g) and U12 (10 μg/g) together with their FT-NIR spectra may support the classification since the Marseilles sample M1 showed similar features (Fig. 5).

Samples U06, U14, U17, U19 and U25 were unable to be classified due to the inconclusive results of the methods employed. This could be caused by anomalous chemical features or by their belonging to
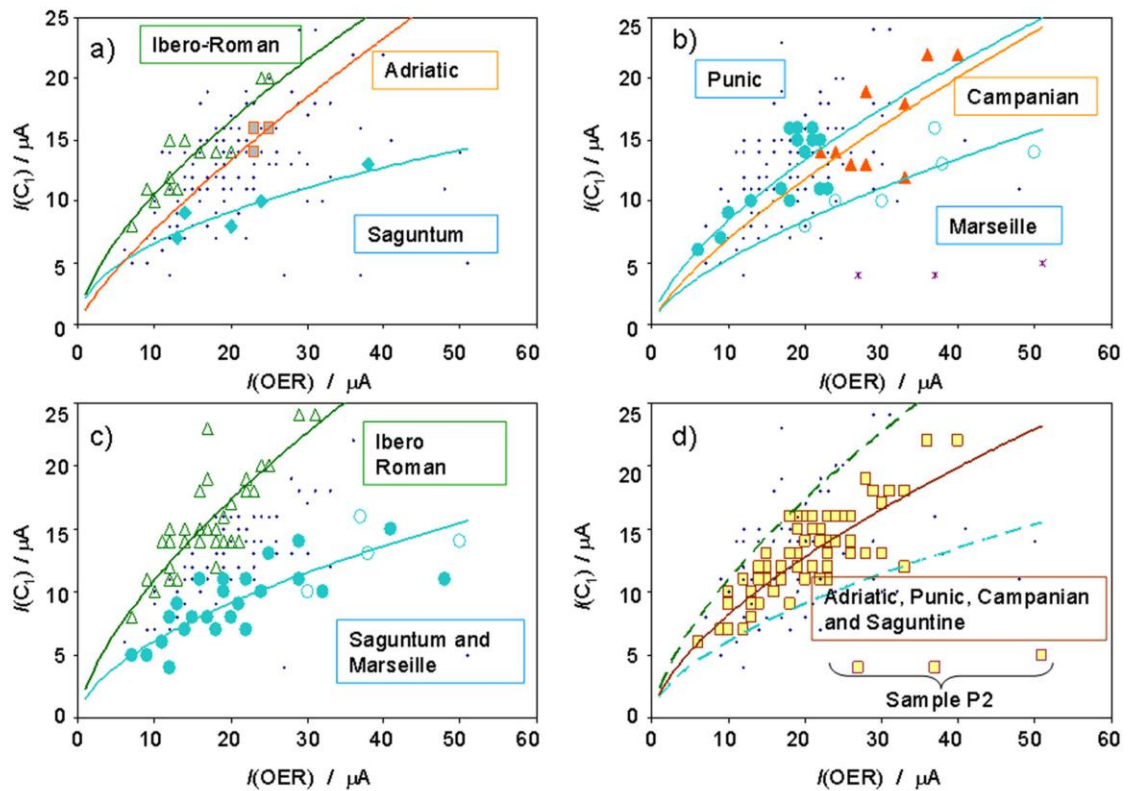
Fig. 7. Plots of I(C_1) vs. I(OER) recorded in square wave measurements (as in Fig. 3a) for reference samples from (a) Ibero-Roman, Adriatic, and Saguntum, and (b) Punic, Campanian and Marseille productions; grouping of all samples, including unclassified ones; (c) Ibero-Roman (Group I), and Saguntum, S2, plus Marseilles samples (Group S·M); and (d) Adriatic, Punic, Campanian and Saguntine, S1, (Group A·P·C·S). The entire dataset is represented as small points; large symbols denote each one of the different sub-sets of reference and unclassified samples grouped according to their tendency lines.
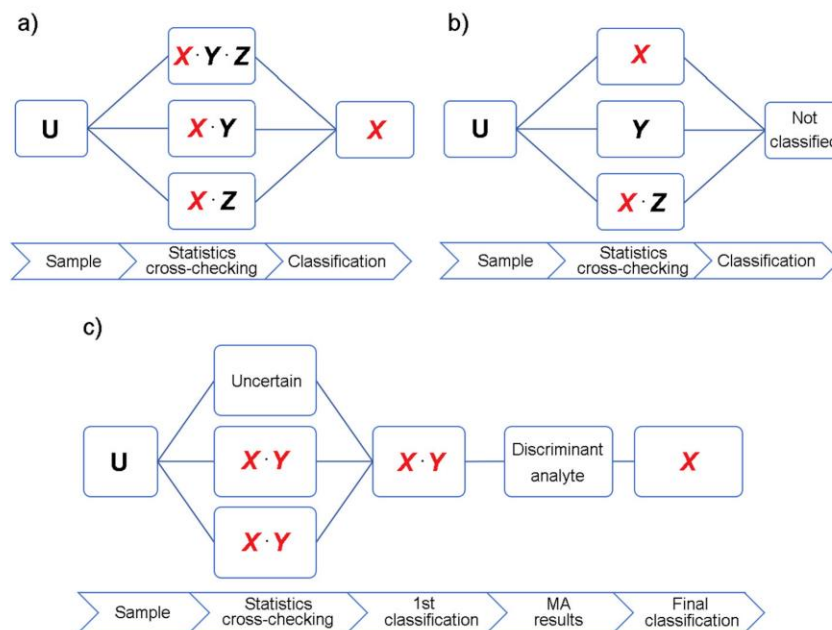
Fig. 8. Examples of the cognitive paths leading to classification of unclassified amphora samples: a) classification through statistical results cross-checking, b) impossibility of classification due to inconclusive results of the three techniques, c) two-step classification through statistical results cross-checking and multielement analysis results.

amphora typologies that were not included in the reference samples set. However, our proposed methodology represents just a starting point and future studies analysing several amphorae samples including a large number of typologies should be carried out to construct a significant database that will allow the classification of more unclassified materials. In order to optimize our proposed approach, complementary

information on petrographic and mineralogical features could be obtained by using traditional techniques such as optical microscopy, scanning electron microscopy - energy dispersive X-ray spectroscopy, X-ray diffraction and mid-infrared spectroscopy.

4. Conclusions

An innovative multi-analytical approach was successfully developed to classify Roman amphorae types using less than 1 g.

Twenty reference samples were analysed by MA, FT-NIR and VIMP and data were statistically processed in order to identify the features related to their classification to be recognized. Then, the unclassified samples were grouped in relation to the reference classes found. The MA (employing REE) and FT-NIR spectroscopy permitted the classification of most of the samples, while VIMP allowed the classification of all the samples. However, since these techniques measure different ceramic features that provide information about raw material provenance and production technology, cross-referencing the results allowed greater refinement of the classification than if only one technique had been used. An origin from the Catalonia region of the Ibero-Roman fragments was suggested following earlier literature, and features that distinguish Punic Gibraltar and Ibiza production area were proposed for the first time. This is probably due to the presence of calcareous raw material in the Gibraltar type (Maniatis et al., 1984) as confirmed by the present data. However, more samples should be analysed in order to confirm this hypothesis. Furthermore, the high REE concentration of Campanian amphorae allowed their discrimination from other western Mediterranean types.

Finally, the REE variability observed for some typologies suggested their manufacture at different production locations. This finding is of importance as it shows the limits of morphological identification and regional classifications, and enforces the need to develop multi-analytical approaches for understanding the provenance of ceramic assemblages.

Declaration of Competing Interest

None.

Acknowledgements

Declaration of Competing Interest

The authors declare that they have no known competing financial interests or personal relationships that could have appeared to influence the work reported in this paper.

Appendix A. Supplementary data

Supplementary data to this article can be found online at https://doi.org/10.1016/j.clay.2020.105857.

References

Aldrabee, A., Wriekat, A.H., 2011. Archaeometric characterization of ancient glazed pottery sherds from Khirbet Faris, Jordan by inductively coupled plasma mass spectrometry (ICP-MS). Microchem. J. 99, 289–295. https://doi.org/10.1016/j.microc.2011.05.018.

Baklouti, S., Maritan, L., Casas, L., Ouazaa, N.L., Jàrrega, R., Prevosti, M., Mazzoli, C., Fouzaï, B., Larabi Kassaa, S., Fantar, M., 2016. Establishing a new reference group of Keay 25.2 amphorae from Sidi Zahruni (Nabeul, Tunisia). App. Clay Sci. 132, 140–154. https://doi.org/10.1016/j.clay.2016.05.027.

Barone, G., Mazzoleni, P., Spagnolo, G., Aquilia, E., 2012. The transport amphorae of Gela: a multidisciplinary study on provenance and technological aspects. J. Archaeol. Sci. 39, 11–22. https://doi.org/10.1016/j.jas.2011.06.018.

Bau, M., 1996. Controls on the fractionation of isovalent trace elements in magmatic and aqueous systems: evidence from Y/Ho, Zr/Hf, and lanthanide tetrad effect. Contrib. Mineral. Petrol. 123, 323–333. https://doi.org/10.1007/s004100050159.

Baxter, M.J., 2004. Distance and transformation in the multivariate analysis of archaeometric data. In: Martini, M., Milazzo, M., Piacentini, M. (Eds.), Physics Methods in Archaeometry, Proceedings of the International School of Physics "Enrico Fermi". IOS PRESS, Amsterdam, pp. 17–36. https://doi.org/10.3254/978-1-61499-010-9-17.

Belfiore, C.M., La Russa, M.F., Barca, D., Galli, G., Pezzino, A., Ruffolo, S.A., Viccaro, M., Fichera, G.V., 2014. A trace element study for the provenance attribution of ceramic artefacts: the case of Dressel 1 amphorae from a late-republican ship. J. Archaeol. Sci. 43, 91–104. https://doi.org/10.1016/j.jas.2013.12.015.

Bevan, A., 2014. Mediterranean containerization. Curr. Anthropol. 55, 387–418. https://doi.org/10.1086/677034.

Bruni, S., Cariati, F., Bagnasco Gianni, G., Bonghi Jovino, M., Artioli, G., Russo, U., 2001. Spectroscopic characterization of Etruscan depurata and impasto pottery from the excavation at Pian di Civita in Tarquinia (Italy): a comparison with local clay. In: Druc, I.C. (Ed.), Archaeology and Clays. 942. British Archaeological Reports Ltd, Oxford, pp. 27–38.

Bruni, S., Guglielmi, V., Della Foglia, E., Castoldi, M., Gianni, G.B., 2018. A non-destructive spectroscopic study of the decoration of archaeological pottery: from matt-painted bichrome ceramic sherds (southern Italy, VIII-VII BC) to an intact Etruscan cinerary urn. Spectrochim. Acta Part A 191, 88–97. https://doi.org/10.1016/j.saa.2017.10.010.

Callender, M.H., 1965. Roman Amphorae: With Index of Stamps. Oxford University Press, Oxford.

Carre, M.B., Monsieur, P., Mattioli, S.P., 2014. Transport amphorae Lamboglia 2 and Dressel 6A: Italy and/or Dalmatia? Some clarifications. J. Rom. Archaeol. 27, 417–428. https://doi.org/10.1017/S1047759414001329.

Cascant, M.M., Rubio, S., Gallello, G., Pastor, A., Garrigues, S., de la Guardia, M., 2017. Prediction of alkaline earth elements in bone remains by near infrared spectroscopy. Talanta 162, 428–434. https://doi.org/10.1016/j.talanta.2016.10.071.

Ceccarelli, L., Bellotto, M.P., Caruso, M., Cristiani, C., Dotelli, G., Gallo Stampino, P., Gasti, G., Primavesi, L., 2018. Characterization of clays and the technology of Roman ceramics production. Clay Miner. 53, 413–429. https://doi.org/10.1180/clm.2018.30.

Clark, R.N., King, T.V., Klejwa, M., Swayze, G.A., Vergo, N., 1990. High spectral resolution reflectance spectroscopy of minerals. J. Geophys. Res. Solid Earth 95, 12653–12680. https://doi.org/10.1029/JB095iB08p12653.

Conejo-Barboza, G., Sanabria-Chinchilla, J., Ulloa, F.C., Villalobos, M.M., 2015. Characterization of Costa Rican archaeological ceramics from the formative period: preliminary electrochemical studies. STAR 22–29. https://doi.org/10.1080/20548923.2015.1133122.

De Maesschalck, R., Jouan-Rimbaud, D., Massart, D.L., 2000. The Mahalanobis Distance. Chemom. Intell. Lab. Syst. 50, 1–18. https://doi.org/10.1016/S0169-7439(99)00047-7.

Di Bella, M., Mastelloni, M.A., Baldanza, A., Quartieri, S., Italiano, F., Tripodo, A., Romano, D., Leonetti, F., Sabatino, G., 2019. Archaeometric constraints by multidisciplinary study of Richborough 527 amphorae and yellow clays from the C. da Portinenti pottery workshop (Lipari Island, Italy). Archaeol. Anthropol. Sci. 11, 2957–2970. https://doi.org/10.1007/s12520-018-0727-2.

Di Turo, F., Montoya, N., Piquero-Cilla, J., De Vito, C., Coletti, F., De Luca, I., Doménech-Carbó, A., 2018. Electrochemical discrimination of manufacturing types of pottery from Magna Mater Temple and Fora of Nerva and Caesar (Rome, Italy). Appl. Clay Sci. 162, 305–310. https://doi.org/10.1016/j.clay.2018.06.024.

Dias, M.I., Prudêncio, M.I., Gouveia, M.A., Trindade, M.J., Marques, R., Franco, D., Raposo, J., Fabião, C.S., Guerra, A., 2010. Chemical tracers of Lusitanian amphorae kilns from the Tagus estuary (Portugal). J. Archaeol. Sci. 37, 784–798. https://doi.org/10.1016/j.jas.2009.11.008.

Doménech-Carbó, A., Doménech-Carbó, M.T., Gimeno-Adelantado, J.V., Moya-Moreno, M., Bosch-Reig, F., 2000. Voltammetric Identification of Lead (II) and (IV) in mediaeval glazes in abrasion-modified carbon paste and polymer film electrodes. Application to the study of alterations in archaeological ceramic. Electroanal. 12, 120–127. https://doi.org/10.1002/(SICI)1521-4109(200002)12:2 < 120::AID-ELAN120 > 3.0.CO;2-E.

Doménech-Carbó, A., Doménech-Carbó, M.T., Osete-Cortina, L., Gimeno-Adelantado, J.V., Bosch-Reig, F., Mateo-Castro, R., 2002. Electrochemical identification of metal ions in archaeological ceramic glazes by stripping voltammetry at graphite/polyester composite electrodes. Talanta 56, 161–174. https://doi.org/10.1016/S0039-9140(01)00552-5.

Fabrizi, L., Nigro, L., Cappella, F., Spagnoli, F., Guirguis, M., Niveau de Villedary y Mariñas, A.M., Doménech-Carbó, M.T., De Vito, C., Doménech-Carbó, A., 2020. Discrimination and provenances of phoenician red slip ware using both the solid state

electrochemistry and petrographic analyses. Electroanal. 32, 258–270. doi:https://doi.org/10.1002/elan.201900515.

Fantuzzi, L., Cau Ontiveros, M.A., Aquilué, X., 2016. Archaeometric characterization of amphorae from the late antique city of Emporiae (Catalonia, Spain). Archaeom. 58, 1–22. https://doi.org/10.1111/arcm.12176.

Ferreira, L.V., Barros, L., Machado, I.F., Gonzalez, A., Pereira, M.F.C., Casimiro, T.M., 2018. Spectroscopic characterization of amphorae from the 8th to the 7th c. BCE found at the Almaraz settlement in Almada, Portugal. J. Archaeol. Sci. Rep. 21, 166–174. https://doi.org/10.1016/j.jasrep.2018.07.005.

Ferri, T.Z., Rončević, S., Vrkljan, G.L., Konestra, A., 2019. Post-depositional alterations of terrestrial and marine finds of Roman ceramics from Crikvenica production Centre (NE Adriatic, Croatia)–a contribution towards chemometric classification. J. Cultur. Heritage. https://doi.org/10.1016/j.culher.2019.10.005. in press.

Finocchiaro, C., Barone, G., Mazzoleni, P., Spagnolo, G., 2018. New Insights on the Archaic 'Corinthian B' Amphorae from Gela (Sicily): the Contribution of the analyses of Corfu Raw Materials. Mediterr. Archaeol. Archaeom. 18, 179–189. https://doi.org/10.5281/zenodo.1285908.

Frahm, E., Doonan, R.C.P., 2013. The technological versus methodological revolution of portable XRF in archaeology. J. Archaeol. Sci. 40 (2), 1425–1434. https://doi.org/10.1016/j.jas.2012.10.013.

Gaffey, S.J., 1987. Spectral reflectance of carbonate minerals in the visible and near infrared (0.35–2.55 um): Anhydrous carbonate minerals. J. Geophysic. Res.: Solid Earth 92, 1429–1440. https://doi.org/10.1029/JB092iB02p01429.

Gallello, G., Orozco, T., Pastor, A., de la Guardia, M., Bernabeu, J., 2016. Regional provenance of dolerite prehistoric objects through mineral analysis. Microchem. J. 124, 167–174. https://doi.org/10.1016/j.microc.2015.08.018.

Gallello, G., Ramacciotti, M., Lezzerini, M., Hernandez, E., Calvo, M., Morales, A., Pastor, A., de la Guardia, M., 2017. Indirect chronology method employing rare earth elements to identify Sagunto Castle mortar construction periods. Microchem. J. 132, 251–261. https://doi.org/10.1016/j.microc.2017.02.009.

Gascó, C.A., 2013. Saguntum (Sagunto). In: The Encyclopedia of Ancient History, https://doi.org/10.1002/9781444338386.wbeah16130.

González, I., Romero-Baena, A., Galán, E., Miras, A., Castilla-Alcántara, J.C., Campos, P., 2018. Ceramic materials from Cuatrovitas archaeological site (Spain). A mineralogical and chemical study for determining the provenance and the firing temperature. Appl. Clay Sci. 166, 38–48. https://doi.org/10.1016/j.clay.2018.09.003.

Grau Mira, I., Gallello, G., 2017. Assessing the territorial influence of an Iberian worship site. The chemical characterisation of the terracotta from the Iron Age sanctuary of La Serreta. J. Archaeol. Sci. Rep. 13, 142–150. https://doi.org/10.1016/j.jasrep.2017.03.045.

Grifa, C., Germinario, C., De Bonis, A., Langella, A., Mercurio, M., Izzo, F., Smiljanic, D., Guarino, V., Di Mauro, S., Soricelli, G., 2019. Comparing ceramic technologies: the production of Terra Sigillata in Puteoli and in the Bay of Naples. J. Archaeol. Sci. Rep. 23, 291–303. https://doi.org/10.1016/j.jasrep.2018.10.014.

Gupta, S., Williams, D., Peacock, D., 2001. Dressel 2–4 amphorae and Roman trade with India: the evidence from Nevasa. South Asian Stud. 17, 7–18. https://doi.org/10.1080/02666030.2001.9628589.

Keay, S.J., 1984. Late Roman Amphorae in the Western Mediterranean: A Typology and Economic Study: The Catalan Evidence, Volume 196. BAR International Series, London.

La-Torre-Riveros, L., Doménech-Carbó, A., Cabrera, C.R., Doménech-Carbó, M.T., Huahuasoncco-Condori, W., Guzmán, D.Q., Gutiérrez-Castillo, M.C., Carmona-Ochoa, K., Pérez-Trujillo, A., 2019. Solid-state electrochemical analysis of Inka pottery from Qotakalli archeological site in the Cusco (Perú) area. J. Solid State Electrochem. 23, 1541–1552. https://doi.org/10.1007/s10008-019-04243-3.

Laveuf, C., Cornu, S., 2009. A review on the potentiality of rare earth elements to trace pedogenetic processes. Geoderma 154, 1–12. https://doi.org/10.1016/j.geoderma.2009.10.002.

Lund, J., 2011. Rhodian transport amphorae as a source for economic ebbs and flows in the eastern Mediterranean in the second century BC. In: Archibald, Z., Davies, J.K., Gabrielsen, V. (Eds.), The economies of Hellenistic societies, third to first centuries BC. Oxford Scholarship Online, pp. 280–295. https://doi.org/10.1093/acprof:osobl/9780199587926.003.0013.

Maniatis, Y., Jones, R.E., Whitbread, I.K., Kostikas, A., Simopoulos, A., Karakalos, C., Williams, C.K., 1984. Punic amphoras found at Corinth, Greece: an investigation of their origin and technology. J. Field Archaeol. 11, 205–222. https://doi.org/10.1179/jfa.1984.11.2.205.

Mannino, M.R., Orecchio, S., 2011. Chemical characterization of ancient potteries from Himera and Pestavecchia necropolis (Sicily, Italy) by inductively coupled plasma–optical emission spectrometry (ICP–OES). Microchem. J. 97, 165–172. https://doi.org/10.1016/j.microc.2010.08.010.

McClure, W.F., 2007. Analysis using fourier transforms. In: Burns, D.A., Ciurczak, E.W. (Eds.), Handbook of Near-Infrared Analysis (Third Edition), Practical Spectroscopy Series. vol. 15. CRC Press, Boca Raton, Florida, USA, pp. 93–122. (Chapter 6). https://doi.org/10.1201/9781420007374.

Öniz, H., 2016. Amphorae in the Eastern Mediterranean. Archaeopress Publishing Ltd, Oxford.

Opaiţ, A., Tsaravopoulos, A., 2011. Amphorae of Dressel 24 similis type in the Central Aegean area (Chios–Erythrai–Kyme). Ann. Br. Sch. Athens 106, 275–323. https://doi.org/10.1017/S0068245411000050.

Orengo, H.A., Livarda, A., 2016. The seeds of commerce: a network analysis-based approach to the Romano-British transport system. J. Archaeol. Sci. 66, 21–35. https://doi.org/10.1016/j.jas.2015.12.003.

Orozco-Köhler, T., Gallello, G., 2017. Testing a new methodological approach to define the use of dolerite outcrops for prehistoric tool production in Mediterranean Iberia. In: Pereira, T., Terradas, X., Bicho, N. (Eds.), Raw Materials Exploitation in Prehistory: Sourcing, Processing and Distribution. Cambridge Scholars Publishing, Newcastle upon Tyne, pp. 193–205.

Orton, C., Hughes, M., 2013. Pottery in Archaeology. Cambridge University Press, Cambridge. https://doi.org/10.1017/CBO9780511920066.

Ostrooumov, M., Gogichaishvili, A., 2013. Raman and infrared reflection spectroscopic study of pre-Columbian Mesoamerican pottery. Eur. J. Mineralogy 25, 895–905. https://doi.org/10.1127/0935-1221/2013/0025-2304.

Peacock, D., 1977. Roman amphorae: typology, fabric and origins. Publ. École Fr. Rome 32, 261–278.

Peacock, D., Williams, D.F. (Eds.), 1991. Amphorae and the Roman Economy: An Introductory Guide. Longman, London and New York (1991).

R Core Team, 2019. R: A Language and Environment for Statistical Computing. R Foundation for Statistical Computing, Wien URL. https://www.R-project.org/.

Ramacciotti, M., Gallello, G., Pastor, A., Diez Castillo, A., García Puchol, O., 2019. Chert Nucleus and Cortex Characterization for Archaeological Provenance Study Tested in the Prebaetic System Region (Valencian Community, Spain). Lithic Technol. 44, 166–180. https://doi.org/10.1080/01977261.2019.1618043.

Raneri, S., Venturi, F., Palleschi, V., Legnaioli, S., Lezzerini, M., Pagnotta, S., Ramacciotti, M., Gallello, G., 2019. Social and technological changes in the ceramic production of the Northern Levant during the LBA/IA transition: New evidence about the Sea People issue through archaeometry. J. Anthropol. Archaeol. 56, 101087. https://doi.org/10.1016/j.jaa.2019.101087.

Rinnan, Å., van den Berg, F., Balling Engelsen, S., 2009. Review of the most common preprocessing techniques for near- infrared spectra. TrAC 28, 1201–1222. https://doi.org/10.1016/j.trac.2009.07.007.

Rubert, D.G.I., Alonso, F.G., 2011. Phoenician Trade in the North-East of the Iberian Peninsula: a Historiographical Problem. Oxf. J. Archaeol. 30, 33–56. https://doi.org/10.1111/j.1468-0092.2010.00358.x.

Rubio-Campillo, X., Montanier, J.M., Rull, G., Lorenzo, J.M.B., Díaz, J.M., González, J.P., Rodríguez, J.R., 2018. The ecology of Roman trade. Reconstructing provincial connectivity with similarity measures. J. Archaeol. Sci. 92, 37–47. https://doi.org/10.1016/j.jas.2018.02.010.

Saiano, F., Pantani, O.L., Scalenghe, R., 2019. A rapid method of screening ceramic artefacts to reject unlikely hypotheses of provenance. Geoarchaeol. 34, 759–767. https://doi.org/10.1002/gea.21749.

Signal developers, 2013. Signal: Signal Processing. URL. http://r-forge.r-project.org/projects/signal/.

Sondi, I., Slovenec, D., 2003. The Mineralogical Characteristics of the Lamboglia 2 Roman-Age Amphorae from the Central Adriatic (Croatia). Archaeom. 45, 251–262. https://doi.org/10.1111/1475-4754.00107.

Thierrin-Michael, G., Martinez, D.T., Serneels, V., 2018. Assessment of the amphora spectrum in a rural late La Tène settlement at Reinach-Nord, Basel region, Switzerland. J. Archaeol. Sci. Rep. 21, 1055–1063. https://doi.org/10.1016/j.jasrep.2017.11.039.

Tiwari, V., Kashikar, A., 2019. OutlierDetection: Outlier Detection. R Package Version 0.1.1. https://CRAN.R-project.org/package=OutlierDetection.

Tomber, R., Williams, D., 2000. Egyptian amphorae in Britain and the western provinces. Britannia 31, 41–54. https://doi.org/10.2307/526918.

Tsantini, E., Quintana, C., Albero, D., Ontiveros, M.Á.C., 2019. Iberian amphorae beyond the mainland: imports in southwestern Mallorca (Balearic Islands, Spain). Archaeol. Anthropol. Sci. 11, 1793–1812. https://doi.org/10.1007/s12520-018-0630-x.

Tsolakidou, A., Buxeda, i, Garrigós, J., Kilikoglou, V., 2002. Assessment of dissolution techniques for the analysis of ceramic samples by plasma spectrometry. Anal. Chim. Acta 474, 177–188. https://doi.org/10.1016/S0003-2670(02)01029-2.

Verga, F., Conti, L., Di Luzio, E., Lentini, A., 2015. Late republican transport amphorae of the Tiber Valley (Rieti–Italy): preliminary study on their composition and archaeometrical characterization. J. Cultur. Herit. 16, 106–112. https://doi.org/10.1016/j.culher.2014.02.003.

Wickham, H., 2016. ggplot2: Elegant Graphics for Data Analysis. Springer-Verlag, New York. https://doi.org/10.1007/978-3-319-24277-4.

Zhaozhou, Z., Zhongliang, W., Jun, L., Yong, L.I., Zhang, Z., Zhang, P., 2012. Distribution of rare earth elements in sewage-irrigated soil profiles in Tianjin, China. J. Rare Earths 30 (6), 609–613. https://doi.org/10.1016/S1002-0721(12) 60099-4.

Supplementary Materials 1 (SM1)

Table of trace element concentrations (expressed as µg/g) measured by ICP-MS.

Sample	Ba	Bi	Cd	Cr	Co	Cu	Li	Mn	Mo	Ni	Pb	Sr	Tl	V	Zn
A1	390	0.034	0.004	85.1	22.8	25	39.8	481	0.851	37.5	11.5	251	0.236	106	53.4
A2	418	0.378	0.088	70.3	14.4	14	35.4	243	0.264	26.2	42.3	292	0.542	86.1	56.6
Mean	*404*	*0.206*	*0.046*	*77.7*	*18.6*	*19*	*37.6*	*362*	*0.558*	*31.8*	*26.9*	*272*	*0.389*	*96.2*	*55.0*
SD	*19*	*0.243*	*0.059*	*10.5*	*6.0*	*8*	*3.1*	*168*	*0.415*	*8.0*	*21.8*	*30*	*0.216*	*14.3*	*2.2*
C1	532	0.216	0.304	173	37.0	28	25.2	1079	7.6	55.5	31.1	381	0.481	232	137
C2	413	0.081	0.198	79.7	25.1	12	26.4	1027	0.612	27.2	20.5	355	0.769	99.7	86.4
Mean	*473*	*0.149*	*0.251*	*126*	*31.1*	*20*	*25.8*	*1053*	*4.1*	*41.4*	*25.8*	*368*	*0.625*	*166*	*112*
SD	*84*	*0.096*	*0.075*	*66*	*8.4*	*11*	*0.9*	*36*	*5.0*	*20.0*	*7.5*	*18*	*0.204*	*94*	*36*
IR1	602	0.395	0.090	80.9	12.3	14	42.2	340	0.496	29.3	16.4	384	0.603	84.9	56.0
IR2	460	0.476	0.079	72.0	17.1	15	59.0	375	0.360	33.0	17.7	346	0.783	86.7	53.9
IR3	513	0.280	0.087	72.7	14.8	15	46.9	358	0.417	29.0	17.9	454	0.708	86.5	57.0
IR4	260	0.056	0.054	68.8	18.1	6	77.0	370	0.627	30.7	7.50	271	0.147	90.3	47.7
IR5	469	0.303	0.091	79.3	17.7	14	52.5	317	0.611	27.3	16.0	456	0.711	96.3	56.1
Mean	*461*	*0.302*	*0.080*	*74.7*	*16.0*	*13*	*55.5*	*352*	*0.503*	*29.9*	*15.1*	*382*	*0.590*	*88.9*	*54.1*
SD	*126*	*0.158*	*0.015*	*5.1*	*2.4*	*4*	*13.5*	*24*	*0.117*	*2.1*	*4.3*	*78*	*0.256*	*4.6*	*3.8*
M1	368	0.290	0.181	126	39.6	26	34.2	939	8.6	64.6	16.4	352	0.469	117	113
P1	374	0.011	0.091	111	28.0	24	49.1	589	0.638	41.5	11.4	438	0.056	142	88.0
P2	247	0.116	0.171	88.5	17.4	10	28.6	175	0.908	21.8	11.5	435	0.247	111	76.2
P3	467	0.013	0.047	80.2	23.7	15	48.6	207	0.251	29.1	17.9	125	0.490	102	63.3
P4	283	0.112	0.190	91.7	21.2	11	30.8	206	0.978	23.7	13.0	453	0.248	119	86.2
P5	489	0.099	0.199	104	11.8	10	27.9	160	2.02	22.8	30.2	564	0.225	114	86.6

P6	263	0.126	0.077	56.6	11.3	18	19.9	330	0.371	25.7	13.2	251	0.253	78.0	48.9
P7	311	0.110	0.218	83.5	17.6	9	31.4	280	1.57	23.7	12.1	315	0.250	116	66.4
Mean	*350*	*0.110*	*0.147*	*92.6*	*21.3*	*15*	*33.8*	*361*	*1.92*	*31.6*	*15.7*	*367*	*0.280*	*112*	*78.6*
SD	*91*	*0.086*	*0.065*	*21.1*	*9.3*	*7*	*10.2*	*271*	*2.76*	*14.8*	*6.3*	*137*	*0.140*	*18*	*19.5*
S1	216	0.116	0.103	111	24.6	15.9	26.1	321	0.833	28.6	17.9	370	0.267	145	88.8
S2	503	0.174	0.152	119	34.3	28.8	40.1	623	3.05	42.6	13.8	141	0.420	162	127
Mean	*360*	*0.145*	*0.128*	*115*	*29.4*	*22.4*	*33.1*	*472*	*1.94*	*35.6*	*15.8*	*256*	*0.344*	*154*	*108*
SD	*203*	*0.041*	*0.035*	*6*	*6.8*	*9.2*	*9.9*	*214*	*1.57*	*9.9*	*2.9*	*162*	*0.108*	*12*	*27*
T1	412	<LOD	<LOD	77.1	26.6	22.4	49.4	461	1.42	36.0	8.72	219	0.241	102	40.8
Mean*	*399*	*0.178*	*0.128*	*92.3*	*21.5*	*16.3*	*39.0*	*443*	*1.64*	*32.6*	*17.8*	*349*	*0.416*	*114*	*76.2*
SD*	*111*	*0.138*	*0.074*	*27.0*	*8.4*	*6.8*	*14.1*	*284*	*2.39*	*11.4*	*8.39*	*111*	*0.223*	*36.3*	*26.4*
U01	662	0.257	0.314	146	41.2	42.8	29.4	1327	1.53	63.6	38.4	572	0.993	213	157
U02	427	0.178	0.187	100	25.6	23.8	26.4	941	0.893	41.5	65.5	400	0.639	143	133
U03	633	0.027	0.058	91.7	25.4	26.5	26.0	545	0.413	41.2	11.9	335	<LOD	114	83.4
U04	367	0.066	0.069	71.7	18.9	44.1	20.6	560	0.645	36.2	19.1	266	0.224	98.2	66.5
U05	170	0.035	0.075	61.3	15.1	16.8	46.4	268	6.33	25.3	10.9	141	0.318	88.4	54.6
U06	381	0.296	0.132	127	20.8	24.4	30.8	465	3.63	60.1	22.9	311	0.534	127	109
U07	381	0.221	0.215	79.4	23.0	29.7	27.2	943	2.41	54.5	16.6	581	0.409	97.6	84.6
U08	233	0.147	0.107	86.6	20.8	20.6	24.6	568	8.19	46.7	14.6	320	0.456	108	78.9
U09	151	0.108	0.190	91.1	25.2	10.6	24.5	259	4.92	24.7	10.0	345	0.242	117	109
U10	261	0.304	0.061	67.6	27.7	16.9	73.8	572	1.91	36.6	12.1	113	0.268	109	60.1
U11	300	0.054	0.052	93.1	26.6	13.0	56.1	390	1.13	40.2	12.7	184	0.247	125	57.1
U12	193	0.004	0.058	89.7	22.1	13.3	25.7	380	10.3	26.1	17.3	381	0.285	130	72.9
U13	357	0.015	0.029	54.9	14.0	10.6	34.9	179	0.293	21.5	14.7	385	0.448	77.3	47.5
U14	248	0.030	0.073	77.8	20.9	17.4	24.5	151	1.04	20.4	15.1	929	0.086	126	54.8

|															
U15	324	0.103	0.203	88.9	24.8	12.1	33.9	439	0.713	25.4	13.4	299	0.270	104	84.0
U16	843	0.031	0.222	157	39.9	26.1	31.2	1044	1.13	47.3	26.2	511	0.295	211	134
U17	510	0.038	0.117	146	31.3	23.0	34.9	349	0.874	186	31.9	303	0.132	109	87.3
U18	342	0.217	0.062	72.8	12.9	11.6	42.6	246	7.01	26.8	11.4	202	0.49	98.4	60.0
U19	305	0.096	0.103	61.8	16.4	11.7	25.8	296	0.724	21.2	12.5	322	0.064	62.2	52.0
U20	633	0.021	0.051	105	22.6	22.4	92.1	509	0.876	36.9	44.7	399	0.065	152	175
U21	252	0.110	0.179	90.6	20.1	10.2	32.3	189	1.02	23.0	11.6	503	0.276	121	80.8
U22	366	0.063	0.049	53.0	12.2	11.8	32.8	169	0.367	19.8	15.3	365	0.468	71.9	53.0
U23	595	0.017	0.052	59.7	14.7	14.8	25.8	275	0.484	22.1	18.4	467	0.481	85.6	50.1
U24	357	0.087	0.104	104	24.8	14.1	42.5	342	0.425	28.9	36.7	419	0.325	130	75.1
U25	440	0.512	0.101	85.1	24.9	14.6	63.5	280	0.600	29.2	23.9	310	1.07	104	75.0
U26	540	0.072	0.097	80.3	16.9	15.2	87.4	288	0.774	31.8	30.4	428	0.423	104	55.4
U27	549	0.018	0.056	55.4	12.8	13.7	27.9	277	0.564	22.0	17.3	537	0.494	86.5	157
Mean[#]	401	0.116	0.112	88.8	22.3	18.9	38.7	454	2.19	39.2	21.3	383	0.384	115	85.4
SD[#]	170	0.12	0.071	28.0	7.3	9.0	19.4	294	2.72	31.9	12.9	163	0.242	35	36.4
LOD	0.001	0.003	0.002	0.205	0.004	0.005	0.001	0.086	0.007	0.008	0.060	0.006	0.001	0.615	0.101

Note: LOD: limit of detection. < LOD: under the limit of detection. SD: standard deviation. * Mean and SD for all the classified samples. [#] Mean and SD for all the unclassified samples.
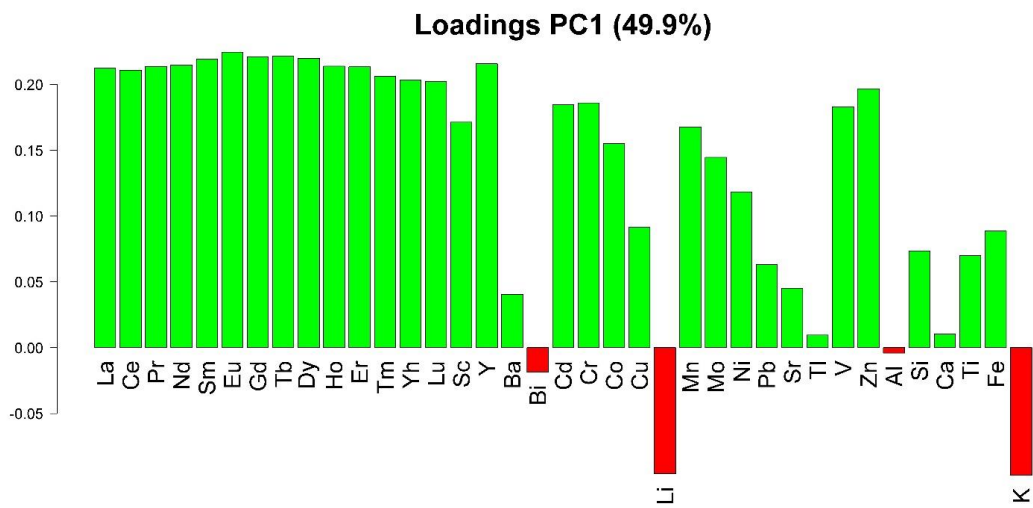
Supplementary Materials 2 (SM2)

FT-NIR spectra of the unclassified samples between 7350 and 4000 cm^{-1}, spectra were offset on the y-axis of the value indicated in the legend to avoid overlapping.
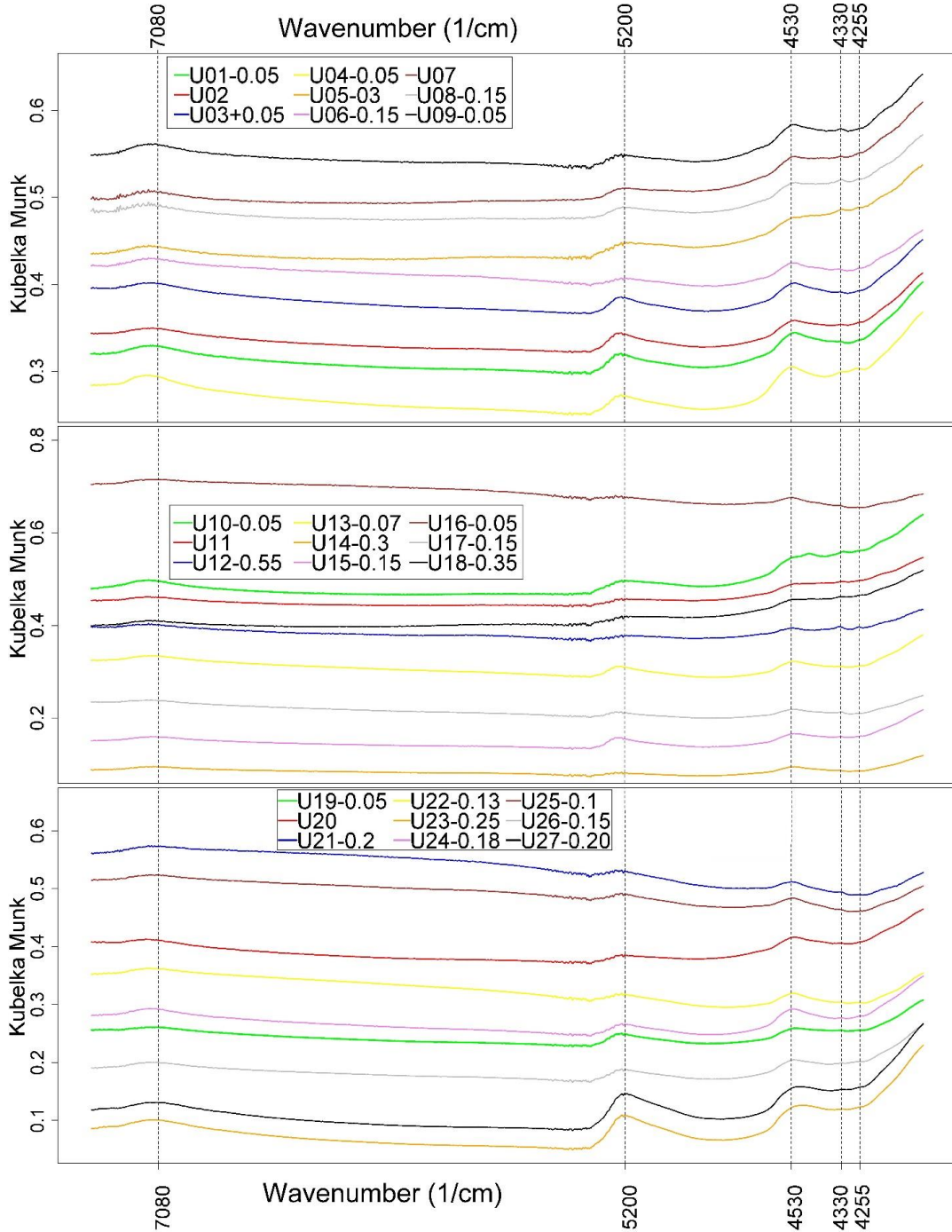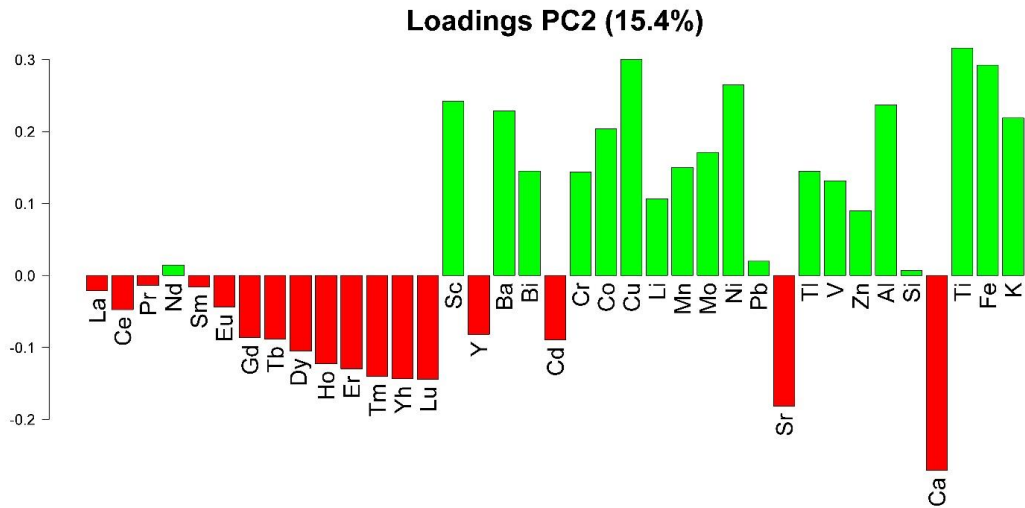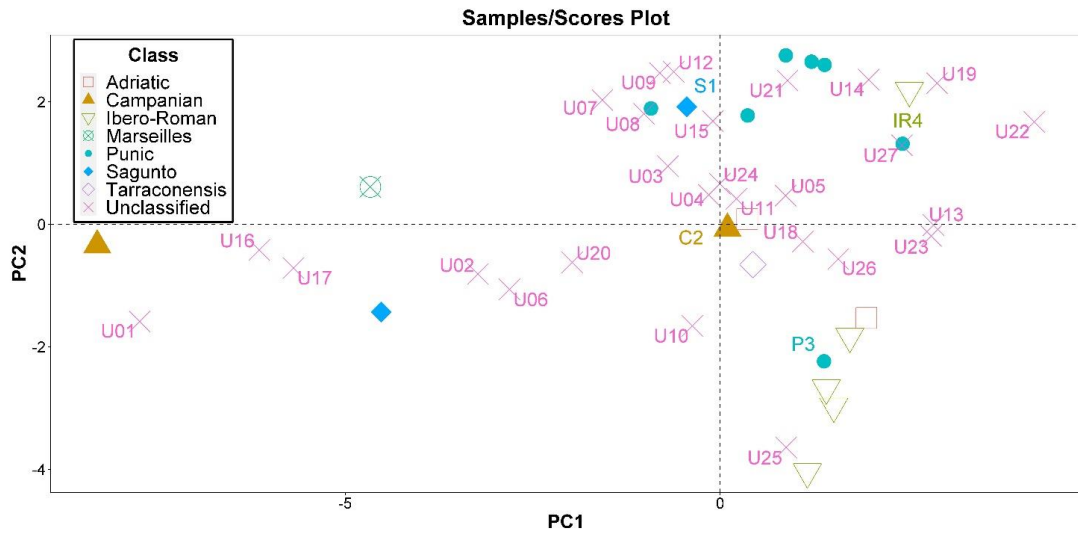
Supplementary Materials 3 (SM3)
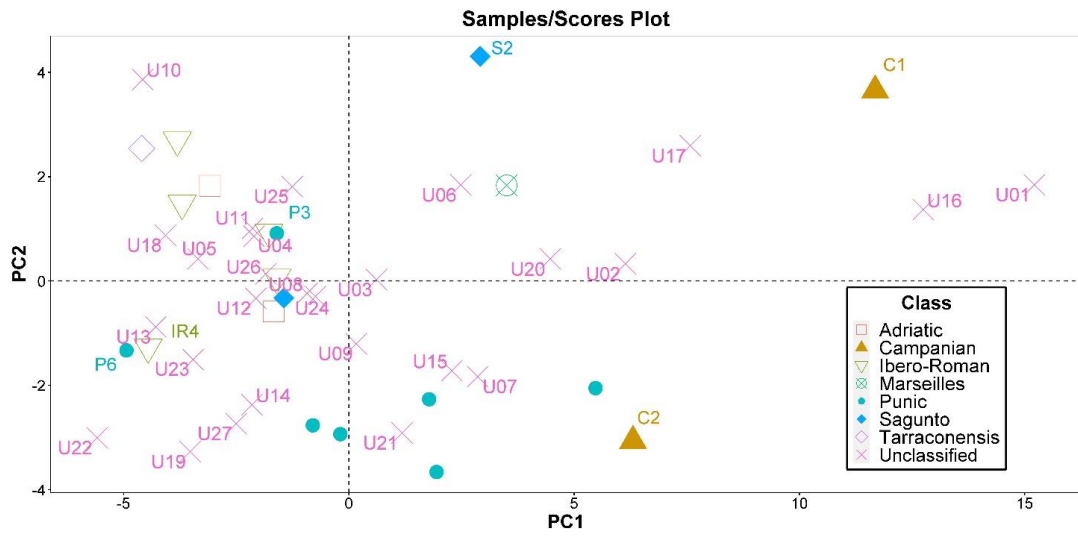
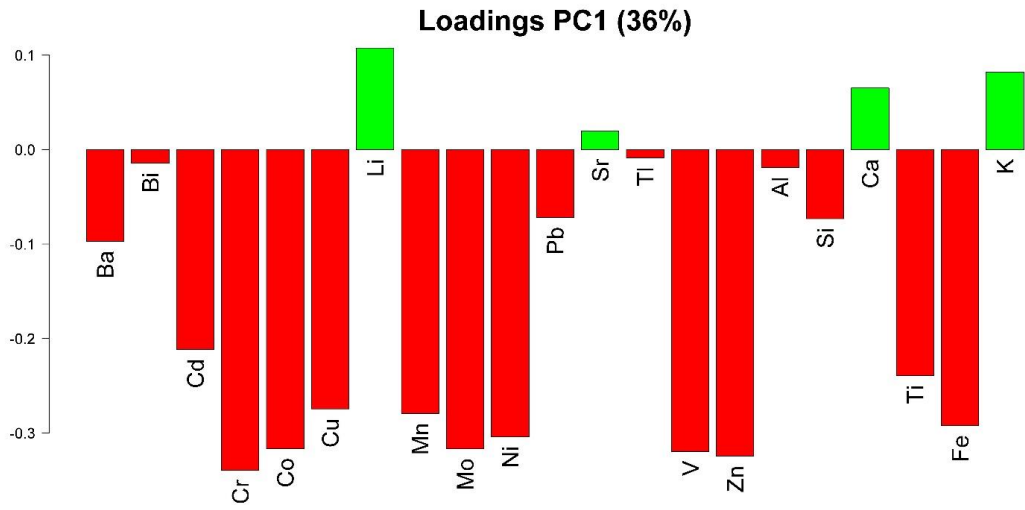a) Samples/Scores diagram of PCA for identified samples employing all the elements as variables.

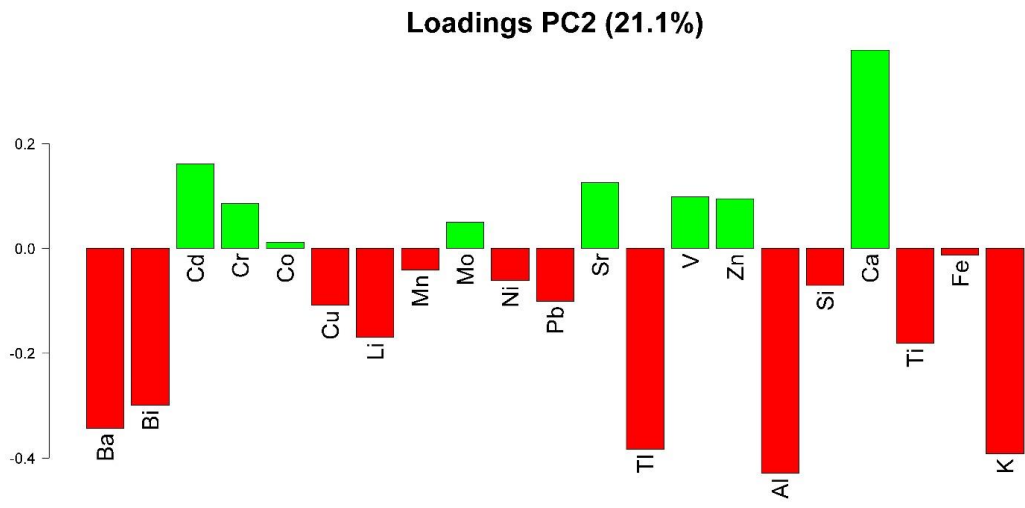b) Variables/Loadings barplot for PC1.

c) Variables/Loadings barplot for PC2.

d) Samples/Scores diagram of PCA for identified samples employing major and trace elements as variables.
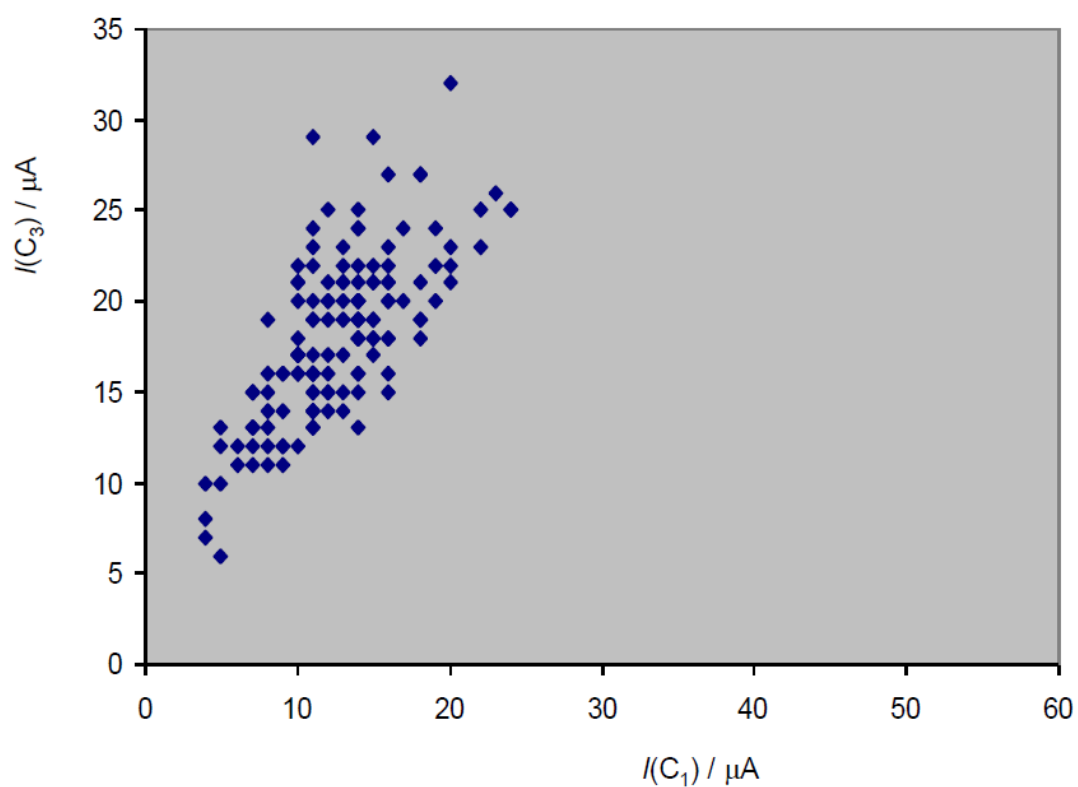
Loadings PC1 (36%)

e) Variables/Loadings barplot for PC1.

Loadings PC2 (21.1%)

f) Variables/Loadings barplot for PC2.

Supplementary Materials 4 (SM4)

Representation of $I(C_3)$ vs $I(C_1)$ for pottery samples in this study from square wave voltammograms in conditions such as in Figure 3: three replicate measurements of samples attached to graphite electrode in contact with air-saturated 1.0 M H_2SO_4. Potential scan initiated at +1.25 V in the negative direction; -0.85 V in the positive direction; potential step increment 4 mV; square wave amplitude 25 mv; frequency of 5 Hz.